Probabilistic Models of Design Wind Loads in South Africa

by

Jacques Botha

Dissertation presented for the degree of Doctor of Philosophy in the Faculty of Engineering at Stellenbosch University

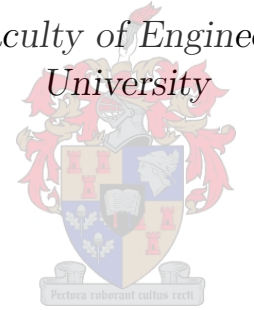

Department of Civil Engineering,
University of Stellenbosch,
Private Bag X1, Matieland 7602, South Africa.

Promoters:

Dr C. Viljoen	Prof J.V. Retief
Civil Engineering	Civil Engineering
University of Stellenbosch	University of Stellenbosch

December 2016

Declaration

By submitting this dissertation electronically, I declare that the entirety of the work contained therein is my own, original work, that I am the sole author thereof (save to the extent explicitly otherwise stated), that reproduction and publication thereof by Stellenbosch University will not infringe any third party rights and that I have not previously in its entirety or in part submitted it for obtaining any qualification.

Signature: .....

J. Botha

Date: December, 2016

Summary

The formulation of design wind loads on structures is subject to multiple sources of uncertainties, both inherent in the physical process itself and due to the engineering models used in the formulation. Accurate reliability modelling of this process is required to ensure that the desired reliability performance of structures is achieved when using wind loading standards. This dissertation presents an investigation of wind load uncertainties and the development of a probabilistic wind load model based on a rational and transparent reliability basis.

A background investigation of the wind load formulation and relevant wind engineering models was performed in order to identify sources of uncertainties. Through this process the primary wind load components relevant to the South African wind load formulation were identified. These components are the time variant free-field wind pressure, and the time invariant pressure coefficients and terrain roughness factors.

The traditional approach to probabilistic modelling of wind loads was investigated. Relevant existing probabilistic models were investigated and compared. The lack of substantiating background information relating to the existing models calls into question the trustworthiness of results obtained using those models. This serves as the primary motivation for the research presented in this dissertation. The reliability basis of the investigation was therefore developed in a rational and transparent manner. To this end the traditional reliability approach was extended through the use of hierarchical Bayesian models to quantify wind load uncertainties on the component level.

The three primary wind load components were investigated independently. This investigation follows the investigation by Kruger (2011) of the South African strong wind climatology and the development of a new characteristic wind speed map. The results from that investigation were used to quantify the free-field wind pressure uncertainties due to the inherent variability of the strong wind climate and the conservative bias introduced through the use of a wind speed map. Lacking sufficient sources of information to quantify the time invariant component uncertainties, a rational reliability method for the use of comparison of wind loads standards as an indicator of wind load uncertainties was developed. This methodology was used in conjunction with direct sampling of limited available observed data to quantify the uncertainties inherent in pressure coefficients and terrain roughness factors.

The new component models were compared to the corresponding distributions in the existing models. In all cases the new models resulted in higher reliability requirements than the existing models. Full probabilistic wind load models which include secondary factors were then developed using engineering judgement and Bayesian updating of the existing models. Multiple reliability assessments were performed using the new models to investigate the reliability performance of the South African wind load formulation. The results conclusively show that the current wind load partial factor of 1.3 does not provide adequate reliability performance. Finally, the effect on the average design wind load across the country due to the combined implementation of the new characteristic wind speed map and a potentially updated wind load partial factor was quantified.

Opsomming

Die formulering van ontwerp windlaste op strukture is onderhewig aan verskeie bronne van onsekerheid, beide inherent in die fisiese proses self en as gevolg van die ingenieursmodelle wat gebruik word in die formulering. Akkurate betroubaarheids modellering van hierdie proses is nodig om te verseker dat die gewenste vlak van betroubaarheid van strukture bereik word wanneer windlas standaarde gebruik word. 'n Ondersoek van windlas onsekerhede en die ontwikkeling van 'n probabilistiese windlas model wat gebaseer is op 'n rasionele en deursigtige betroubaarheids basis, word in hierdie verhandeling aangebied.

'n Agtergrond ondersoek van die windlas formulering en relevante windingenieurswese modelle is uitgevoer om bronne van onsekerheid te identifiseer. Deur hierdie proses is die primêre windlas komponente relevant aan die Suid-Afrikaanse windlas formulering geïdentifiseer. Hierdie kom-ponente is die tyd-afhanklike vryveld winddruk, en die tyd-onafhanklike druk koëffisiënte en terrein ruheid faktore.

Die tradisionele benadering tot probabilistiese modellering van windlaste is ondersoek. Relevante bestaande probabilistiese modelle is ondersoek en vergelyk. Die gebrek aan stawende agtergrond inligting wat verband hou met die bestaande modelle bring die geloofwaardigheid van die resultate verkry deur die modelle in gedrang. Dit dien as die primêre motivering vir die navorsing wat in hierdie verhandeling aangebied word. Die betroubaarheids basis van die ondersoek is dus op 'n rasionele en deursigtige wyse ontwikkel. Met die oog hierop is die tradisionele betroubaarheids benadering uitgebrei met gebruik van hiërargiese Bayesiese modelle om windlas onsekerhede op die komponent vlak te kwantifiseer.

Die drie primêre windlas komponente is onafhanklik ondersoek. Hierdie ondersoek volg die ondersoek deur Kruger (2011) van die Suid-Afrikaanse sterk-wind klimatologie en die ontwikkeling van 'n nuwe karakteristieke windspoed kaart. Die resultate van daardie ondersoek is gebruik om die vryveld winddruk onsekerhede, as gevolg van die inherente variasie van die sterk-wind klimaat asook die konserwatisme weens die gebruik van 'n windspoed kaart, te kwantifiseer. Weens 'n gebrek aan voldoende bronne van inligting om die onsekerhede van die tyd-onafhanklike komponente te kwantifiseer is 'n rasionele betroubaarheids metode vir die gebruik van vergelyking van windlas standaarde as 'n aanduiding van windlas onsekerhede ontwikkel. Hierdie metode is in samewerking met direkte steekproefneming van beperkte beskikbare waargenome data gebruik om die onsekerhede inherent in druk koëffisiënte en terrein ruheid faktore te kwantifiseer.

Die nuwe komponent modelle is vergelyk met die ooreenstemmende statistiese verdelings in die bestaande modelle. In alle gevalle het die nuwe modelle gelei tot hoër betroubaarheids vereistes as die bestaande modelle. Volle probabilistiese windlas modelle wat sekondêre faktore insluit is daarna ontwikkel met gebruik van ingenieurs oordeel en Bayesiese opdatering van die bestaande modelle. Betroubaarheid assesserings is uitgevoer met die nuwe modelle om die betroubaarheid van die Suid-Afrikaanse windlas formulering te ondersoek. Die resultate wys onweerlegbaar dat die huidige windlas parsiële faktor van 1.3 onvoldoende betroubaarheid voorsien. Ten slotte is die effek op die gemiddelde ontwerp windbelasting regoor die land as gevolg van die gekombineerde implementering van die nuwe karakteristieke windspoed kaart en 'n potensieel opgedateerde windlas parsiële faktor gekwantifiseer.

Acknowledgements

I would like to express my sincere gratitude to my promoters, Dr. Celeste Viljoen and Prof. Johan Retief, for their invaluable advice and guidance. You have been tremendous role models to me. I would also like to thank Dr. Adam Goliger and Prof. Milan Holický for their willingness to share their vast knowledge and experience in the fields of wind engineering and structural reliability, respectively.

This study would not have been possible without funding from the Wilhelm Frank Trust scholarship program, for which I am immensely grateful. I am also thankful for the opportunities I received to attend international conferences and workshops, which was only possible due to funding from the Wilhelm Frank Trust and Stellenbosch University Subcommittee B.

Finally, I would like to thank my family. Your unwavering support has allowed me grow both personally and professionally. I could not have achieved any of my goals without you.

Dedications

This thesis is dedicated to my brilliant wife, Maxine, for her endless love and support.

Contents

Declaration i

Summary ii

Opsomming iii

Acknowledgements iv

Dedications v

Contents vi

List of Figures x

List of Tables xv

1 Introduction 1

1.1 Motivation and problem statement 2

1.2 Research objectives 3

1.3 Scope 4

1.4 Structure of the dissertation 5

2 Background 8

2.1 Overview of wind loading on structures 8

2.2 Wind load components 12

2.2.1 Reference wind pressure 12

2.2.2 Gust factor 14

2.2.3 Terrain and topographical effects 17

2.2.3.1 Surface roughness 17

2.2.3.2 Topographical features and surrounding built environment . . . 20
2.2.4 Aerodynamic factors . . . 22
2.2.4.1 Pressure coefficient overview and codification process . . . 22
2.2.4.2 Pressure coefficient uncertainties . . . 27
2.2.5 Thunderstorm winds . . . 29
2.2.6 Wind directionality . . . 32

3 Wind Load Probability Modeling 35
3.1 Overview of structural reliability . . . 36
3.2 Uncertainty characterization . . . 39
3.3 Overview of probabilistic modeling of wind loads . . . 41
3.3.1 Existing wind load probability models . . . 42
3.3.1.1 JCSS model . . . 43
3.3.1.2 Holický/Eurocode models . . . 44
3.3.1.3 ASCE 7-95 model . . . 45
3.3.1.4 Milford/SANS models . . . 46
3.3.2 Comparison of existing models . . . 48
3.4 Reliability basis of investigation . . . 52
3.4.1 Comparison of codified values and observed values . . . 54
3.4.2 Comparative studies of wind load standards . . . 55
3.4.3 Methodology summary . . . 60
3.5 Bayesian hierarchical models and Monte Carlo method . . . 61

4 Free-Field Wind 66
4.1 Statistical models of strong winds . . . 67
4.1.1 Wind data reliability . . . 67
4.1.2 Estimation methods . . . 70
4.1.2.1 Extreme Value methods . . . 70
4.1.2.2 Peak-Over-Threshold methods . . . 72
4.1.2.3 Mixed climate distribution method . . . 73
4.1.3 Design quantiles . . . 75
4.2 South African wind speed map . . . 78
4.3 Statistical parameters of representative design free-field wind pressure . . . 82

4.3.1 Systematic bias . . . 82
4.3.2 Variability . . . 83
4.3.2.1 Envelope method . . . 84
4.3.2.2 Equivalent Gumbel distribution parameters for EXP models . . 89
4.3.2.3 Envelope method results . . . 92
4.3.3 Final representative distribution . . . 95

5 Pressure Coefficients 97
5.1 Wind tunnel and full-scale test result comparison . . . 97
5.1.1 Texas Tech University experiment . . . 98
5.1.2 Jan Smuts Airport hanger experiment . . . 102
5.1.3 Holmes low-rise building wind tunnel experiment . . . 103
5.1.4 Silsoe Research Institute portal frame experiment . . . 105
5.1.5 Fredericton low-rise building experiment . . . 107
5.1.6 Sainte-Foy light-frame wood building experiment . . . 108
5.1.7 Uematsu and Isyumov comparison of wind engineering studies . . . 110
5.1.8 Summary of results . . . 111
5.1.9 Discussion . . . 114
5.2 Wind load standard pressure coefficient comparison . . . 115
5.2.1 Pressure Coefficient Calculation Program . . . 115
5.2.2 Sampling space definition . . . 122
5.2.3 Parameter study results . . . 125
5.2.3.1 SANS bias . . . 125
5.2.3.2 Variability . . . 129
5.2.3.3 Combined distribution . . . 132
5.3 Summary and discussion . . . 133

6 Terrain Roughness Factors 135
6.1 Baseline model . . . 136
6.2 Systematic bias . . . 139
6.3 Variability . . . 143
6.4 Combined Distribution . . . 147

7 Preliminary Reliability Assessment of SANS 10160 **149**

7.1 Summary of wind load component models 150

7.1.1 Free-field wind pressure model 151

7.1.2 Pressure coefficient model 154

7.1.3 Terrain roughness factor model 157

7.2 Full probabilistic wind load model 158

7.2.1 Engineering judgement based model 159

7.2.2 Bayesian updating of existing models 161

7.2.3 Full model comparison 162

7.3 Reliability assessment 168

7.4 Influence of changes to SANS 10160 173

8 Conclusions **179**

8.1 Assessment of the reliability basis and methodology of the investigation 179

8.1.1 Hierarchical Bayesian models 180

8.1.2 Comparative algorithm for wind load standards 181

8.2 Achievement of research objectives 182

8.2.1 Wind load uncertainties 183

8.2.2 Probabilistic wind load models 184

8.2.3 Reliability implications for South African wind loads 187

8.2.4 Secondary objectives 187

8.3 Future research 188

List of References **190**

Appendices **198**

A Design Wind Speed Quantiles **A1**

B Free-Field Wind Pressure Systematic Bias **B1**

C Regional Total Wind Load Systematic Bias **C1**

List of Figures

2.1 The Davenport wind load chain. (Reproduced from Dyrbye and Hansen (1996)) . . 9
2.2 Strong wind generating mechanisms across South Africa, taken from Kruger (2011). 14
2.3 SANS Terrain roughness factors $c_r(z)$ for Terrain Categories A-D. 19
2.4 Comparison of roughness lengths for ISO, Eurocode and SANS values. (Reproduced from Retief and Dunaiski (2009)) 20
2.5 Typical variation of pressure coefficient on low-rise building roof taken from Holmes (2015). 23
2.6 Experimental results of area averaged pressure coefficients for four zones of a gable roof and NBCC 1995 provisions taken from Stathopoulos *et al.* (2000). 25
2.7 Instantaneous and equivalent static wind load distributions on low-rise building taken from Holmes and Syme (1994). 26
2.8 Pressure zones used in different wind load standards. 29
2.9 Outflow gust front caused by thunderstorm downburst, taken from Chay (2001). . . 30
2.10 Thunderstorm terrain roughness factor profile using ISO 4354:2009 stipulations. . . 31
2.11 Prevailing movement of air masses across Southern Africa during summer and winter months. (Reproduced from Szewczuk and Prinsloo (2010)) 34

3.1 Probability distributions of structural resistance, load effect and the safety margin, reproduced from Nowak and Collins (2000). 37
3.2 Davenport reliability model, reproduced from Davenport (1983). 42
3.3 Results from multivariate FORM analysis of existing models. 50
3.4 General reliability investigation approach followed. 54
3.5 Algorithm for using comparison of design standards to estimate uncertainties. . . . 58

3.6 Summary of methodologies used to investigate time invariant wind load components in this investigation. 60
3.7 Three level hierarchical model. 62
3.8 Sensitivity analysis on number of simulations used in Monte Carlo method. 64
3.9 Extended reliability modeling framework used in the investigation. 65

4.1 Annual number of daily maximum wind gust readings available in the SAWS climate database, taken from Kruger (2011). 68
4.2 Spatial distribution of weather stations considered in this investigation. 69
4.3 Number (percentage) of stations with one to four strong wind mechanisms, taken from Kruger (2011). 74
4.4 Spatial distribution of stations and selected extreme wind prediction methods for each. 78
4.5 Spatial distribution of weather stations used to develop current wind map (left) and new wind map (right), taken from Kruger (2011). 79
4.6 Current characteristic wind speed map in South African wind loading code including 1.4 conversion factor. 81
4.7 Proposed new map for South African wind loading code, from Retief *et al.* (2015). . 81
4.8 Histogram and probability density function of free-field wind systematic bias. 84
4.9 Normalized predictive models for each of the three model sets showing results disaggregated by dominant strong wind generating mechanisms. 86
4.10 Design wind speed for given return period for the EXP and equivalent Gumbel distributions for George weather station. 92
4.11 Histogram and fitted log-normal probability distribution for each of the three model sets showing results disaggregated by dominant strong wind generating mechanisms. 93
4.12 Monte Carlo histogram and probability density function of representative probability distribution of South African design wind pressure. 96

5.1 Photo of the WERFL test building at TTU taken from Website (2015). 99
5.2 Central frame of TTU building as shown in Chen and Zhou (2007). 100
5.3 Mean point pressure coefficient results from wind tunnel and full-scale tests on central frame of TTU building. 100

5.4 Mean area-averaged pressure coefficient results from full-scale test on central frame of TTU building. . . . 101
5.5 Jan Smuts experiment: (a) Hangar geometry, and (b) layout of roof pressure taps (taken from Milford *et al.* (1992)). . . . 103
5.6 Mean point pressure coefficient results from wind tunnel and full-scale tests on Jan Smuts hangar. . . . 104
5.7 Holmes low-rise building experiment geometry and pressure tap panels (taken from Holmes and Best (1981)). . . . 105
5.8 Mean area-averaged pressure coefficient results from Holmes wind tunnel test on low-rise building. . . . 106
5.9 Mean point pressure coefficient results from full-scale tests on central frame of Silsoe Structures Building. . . . 107
5.10 Mean point pressure coefficient results from full-scale and wind tunnel tests on Fredericton building. . . . 108
5.11 Position and numbers of pressure taps on Sainte-Foy building (taken from Doudak *et al.* (2009)). . . . 109
5.12 Mean point pressure coefficient results from full-scale and wind tunnel tests on Fredericton building on Sainte-Foy building. . . . 110
5.13 Mean pressure coefficient results from Uematsu and Isyumov comparison of wind engineering studies for roof pressure zones F, G and J. . . . 111
5.14 Algorithm for using comparison of design standards to estimate uncertainties. . . . 116
5.15 Pressure Coefficient Calculation Program structure. . . . 117
5.16 Structural and wind related parameters used in PCCP calculation process. . . . 119
5.17 SANS and AS/NZS pressure coefficients on windward roof of example structure. . . . 120
5.18 Simplified summary of PCCP calculation procedure. . . . 121
5.19 Combinations of wind direction and roof type considered in the parameter study. . 125
5.20 SANS bias values calculated in parameter study. . . . 126
5.21 Coefficient of variation of wind load standard pressure coefficients calculated in the parameter study. . . . 130
5.22 Monte Carlo histogram and probability density function of representative probability distribution of SANS pressure coefficients. . . . 133

6.1 Schematic boundary layer above a fetch with two roughness changes using Wang-Stathopoulos model. (Taken from Wang and Stathopoulos (2007)) 137
6.2 Wang-Stathopoulos wind velocity profiles for OC, Suburban and Urban terrain categories with wind tunnel and full-scale test results. 138
6.3 Wang-Stathopoulos and SANS terrain roughness factor profiles. 139
6.4 Bounded parameter space and subdivided zones for terrain roughness factor systematic bias investigation. 141
6.5 Functions used to determine mean and variance of systematic bias for a given zone. 142
6.6 Wind load standard terrain roughness factors for equivalent terrain categories. . . . 146
6.7 Monte Carlo histogram and probability density function of representative probability distribution of terrain roughness factors. 148

7.1 Summary of new free-field wind pressure probabilistic model. 151
7.2 Comparison of new free-field wind pressure probabilistic model with existing models. 153
7.3 Summary of pressure coefficient probabilistic model. 154
7.4 Comparison of new pressure coefficient probabilistic model with existing models. . . 156
7.5 Summary of terrain roughness factor probabilistic model. 157
7.6 Comparison of new terrain roughness factor probabilistic model with existing models. 158
7.7 Summary of the development of full probabilistic models. 159
7.8 Fitting of Gumbel distributions to tail-end of FORM analysis results for full probabilistic models. 164
7.9 Results from multivariate FORM analysis of new models. 165
7.10 Sensitivity obtained from multivariate FORM analysis of the engineering judgement based model. 166
7.11 Reliability requirement for $\beta = 3.0$ for different models using a coefficient of variation of resistance $w_R = 0.15$. 170
7.12 Reliability performance of SANS 10160 design function for $\beta = 3.0$ across parametric range of resistances. 172
7.13 Old (left) and new (right) characteristic gust wind speed maps for South Africa. . . 173
7.14 South Africa elevation map from GeoCommunity (2016) (left) and region averaged elevation map (right). 174

7.15 Average gust wind pressure across South Africa calculated using the old wind map. 176

7.16 Average gust wind pressure across South Africa calculated using the new wind map. 176

7.17 Regional systematic bias of total design wind loads across South Africa. 177

7.18 Area-averaged systematic bias of South African wind loads with new wind map and an updated wind load partial factor. 178

8.1 Envelope of reliability models of design wind pressure developed in the investigation. 186

List of Tables

2.1 SANS wind profile parameters. 19

3.1 JCSS (2001-2002) probabilistic model. 43
3.2 Eurocode probabilistic model by Gulvanessian and Holický (2005). 44
3.3 Holický (2009) probabilistic model. 45
3.4 ASCE 7-95 probabilistic model as presented by Ellingwood and Tekie (1999). 45
3.5 Milford probabilistic model (1985 technical report). 47
3.6 SANS model by Kemp *et al.* (1987). 47
3.7 Milford design wind load statistics (1985 report) Milford (1985*a*). 48
3.8 Milford design wind load statistics (1987 article) Kemp *et al.* (1987). 48
3.9 Required normalized design wind pressure (partial factor) to achieve target reliability indices using existing probabilistic models. 51

4.1 Final selected stations and 50 year return period quantile values for each of the extreme wind prediction methods investigated, excluding exposure correction factors. 75
4.2 Ranges of calculated skewness values for wind pressure models. 88
4.3 EXP distribution parameters and design quantiles for George weather station. . . . 91
4.4 Equivalent Gumbel distribution parameters and design quantiles for George weather station. 91
4.5 Statistical parameters of free-field wind variability for different model sets. 94
4.6 Monte Carlo input distributions and resulting representative distribution of terrain roughness factors. 95

5.1 External mean point pressure coefficient from TTU experiment for nominally sealed and 2% opening in windward wall cases. 102

5.2 Mean (μ) and standard deviation (σ) of SANS pressure coefficient systematic bias for each study considered in the investigation. . . . 113
5.3 Example parameter space of SANS scope. . . . 122
5.4 Reference structures' dimensions and parameter ranges. . . . 124
5.5 Mean and standard deviation of SANS bias values calculated in parameter study. . 127
5.6 Bias sensitivity factors of parameters used to determine pressure coefficients. . . . 127
5.7 Mean and standard deviation of the pressure coefficient variability calculated in parameter study. . . . 131
5.8 Variability sensitivity factors of parameters used to determine pressure coefficients. 131
5.9 Monte Carlo input distributions and resulting representative distribution of SANS pressure coefficients. . . . 133
5.10 Summary of representative distributions of SANS pressure coefficients 134

6.1 Wang-Stathopoulos terrain roughness classification and power law parameters. . . . 137
6.2 Equivalent SANS and Wang-Stathopoulos terrain categories and roughness lengths as given by Retief and Dunaiski (2009) and Wang and Stathopoulos (2007). . . . 140
6.3 Terrain roughness factor systematic bias statistical parameters. . . . 143
6.4 Representative exposure categories used in comparative study of terrain roughness factors. . . . 144
6.5 Equivalent terrain categories for each wind load standard considered in the terrain roughness factor variability investigation 144
6.6 Terrain roughness factor epistemic variability statistical parameters. . . . 147
6.7 Monte Carlo input distributions and resulting representative distribution of terrain roughness factors. . . . 148

7.1 New and existing free-field wind pressure probabilistic models. . . . 153
7.2 New and existing pressure coefficient probabilistic models. . . . 155
7.3 New and existing terrain roughness factor probabilistic models. . . . 158
7.4 Engineering judgement based full probabilistic wind load model. . . . 160
7.5 Updated Eurocode full probabilistic wind load model. . . . 163
7.6 Updated Holický full probabilistic wind load model. . . . 163
7.7 Updated Milford full probabilistic wind load model. . . . 164

7.8 Required normalized design wind pressure (partial factor) to achieve target reliability indices using new models. . . . 165
7.9 Probability models for representative basic variables. . . . 169
7.10 SANS (2011*a*) basic variable partial factors 171
7.11 Air density as a function of altitude as specified in SANS (2011*b*). . . . 174
7.12 Area-averaged bias values of total wind load across South Africa for different partial wind load factors γ_W. . . . 177

8.1 Sources of uncertainty identified in the formulation of the primary wind load components. . . . 183
8.2 Representative probability distributions for primary wind load components. . . . 184
8.3 Average sensitivity factors calculated using combined component uncertainty distributions. . . . 185
8.4 Upper and lower limits of representative probabilistic model of design wind pressure for South Africa. . . . 185

A.1 Design wind speed quantiles calculated using the selected extreme wind estimation model shown for stations across South Africa. . . . A1

B.1 Exposure corrected design wind speed 2% quantiles from Kruger (2011) and new wind map converted to pressure values and used to calculate the free-field wind systematic bias. . . . B1

C.1 Regional properties used to calculate the total wind load systematic bias across South Africa. . . . C1

Chapter 1

Introduction

All physical processes are inherently variable and uncertain. Structural engineers are specifically interested not only in the physical processes which relate to how materials react when subjected to forces, but also the processes which cause those forces. Accurate modelling of these intrinsically uncertain physical processes is paramount, as the buildings and structures used by society are designed based upon the adequacy of the predictions of structural engineering models. The purpose of reliability investigations such as the one presented in this dissertation is to understand and quantify the uncertainties inherent in both the physical process itself and the engineering formulation of the process in order to statistically assess these predictions.

Environmental actions are prime examples of physical processes which cause loads on structures. Due to the temperate climate in South Africa, environmental actions such as snow loads and extreme temperature loads are not commonplace. Certain regions in the country are prone to moderate seismic activity, however significant seismic actions are not prevalent across most of the country. South Africa is however host to a complex strong wind climatology, and wind actions represent the most critical environmental loading for the built environment.

The variable and uncertain nature of wind is evidenced simply by inspection on a windy day. Wind characteristics at a specific location are dependent on multiple factors such as the type strong wind generating mechanism, the gustiness and turbulence of the wind, the influence of upstream topography and surrounding obstacles, the wind directionality, and surface roughness of the terrain. Furthermore, the conversion of wind pressure to structural loads also requires the influence of the aerodynamic properties and the dynamic response of the structure to be considered. Each of these factors is subject to their own uncertainties. Wind loading on

structures is therefore not defined by a single physical process, but rather by the combined effects of multiple processes.

In addition to the uncertainties inherent in the physical wind loading process, additional uncertainties are introduced as a result of the engineering formulation of the process. By definition an engineering model requires the simplification of a complex process to allow for convenient calculation of the outcomes of that process. As such it stands to reason that there is a certain measure of uncertainty inherent in the models themselves due to this simplification, or simply due to the lack of information required to formulate a better model. The wind load formulation as used in structural engineering design standards across the world is not exempt from these uncertainties.

Identifying and understanding the various sources of uncertainties in the wind load formulation allows for the quantification of the uncertainties through the development of a probabilistic wind load model. Such a probabilistic model allows assessments of the wind load formulation to be performed in order to obtain the reliability requirements for a given target level of reliability. It may then be possible to calibrate the partial load factors in the semi-probabilistic limit states design stipulations of the South African loading code to ensure that the level of reliability specified by the standard is achieved. The ultimate goal of the research presented in this dissertation is the development of a probabilistic model of the South African wind load formulation, not the reliability assessment and calibration of the South African loading code. Nonetheless, the natural outcome of the development of such a model would be reliability calibration of the standard using the available new information. As such the underlying motivation behind the development of the model is that it may serve as a valuable resource for the reliability assessment and calibration of the standard.

1.1 Motivation and problem statement

During the updating process of the South African loading code from SABS 0160:1989 to the current SANS 10160:2010 (republished in 2011), a deficiency in the available information regarding wind load uncertainties was identified by Retief and Dunaiski (2009). The existing South African probabilistic wind load model as presented by Kemp *et al.* (1987) resulted in anomalously low reliability requirements for wind loads, as evidenced by comparison with Eu-

ropean wind load models such as the Holický (2009) model. Furthermore, investigation of international wind load models revealed scant background information and details regarding the development of those models, calling into question the trustworthiness of results obtained using those models. The need was therefore clear for an investigation of the uncertainties inherent in the wind load formulation and the probabilistic models used to quantify them.

Accurate reliability assessment of wind loading is critical to ensure that desired levels of reliability are achieved for structures for which wind loading is the dominant action. In view of this, three questions may be asked which concisely define the problem statement of this research:

1. What are the uncertainties inherent in the South African wind load formulation?
2. How can these uncertainties be quantified?
3. What influence do these uncertainties have on the reliability performance of the South African wind load standard?

To answer these questions requires a comprehensive investigation of wind loads. The scope of the problem and limited available experimental instrumentation means that no new data is measured throughout the investigation. A rational methodology is therefore required in which all readily available statistical data and supporting information are used to develop a probabilistic wind load model in a systematic and transparent manner.

1.2 Research objectives

In response to the three research questions posed in the problem statement, the desired objectives of this research are summarized as follows:

- To characterize and quantify the uncertainties, both inherent in the processes themselves and introduced through engineering modeling of the processes, in the primary wind load components relevant to the South African design wind load formulation.
- To develop an accurate and transparent representative probability model of the global wind loads on structures as calculated using the current South African wind load standard (SANS 10160-3:2011).

- To determine the influence that the new probability model would have on the reliability performance of the South African loading code design functions.

Through the pursuit of these primary objectives it is expected that the following secondary goals will be achieved:

- A comprehensive study of the relevant existing probabilistic wind load models.
- The identification of readily available sources of data and information relating to wind load uncertainties.
- The identification and potential development of a methodology in which all readily available data is used to quantify uncertainties as accurately as possible.
- An investigation of available statistical and reliability techniques for the treatment of processes subject to multiple sources of uncertainty.
- An investigation of the influence of changes to the South African wind load standard on design wind loads across the country.

1.3 Scope

The purpose of a wind load probability model is to represent the uncertainties inherent in the majority of design situations which may be designed using the loading standard being considered. As the ultimate outcome of this research is the development of a probability model of the South African wind load standard, the scope of the South African standard is a useful reference to delineate the boundaries of the research. As such, the wind load components investigated are those which are relevant to the South African wind load formulation, namely free-field wind pressure, pressure coefficients and terrain roughness factors.

The research presented in this dissertation exclusively relates to the reliability of wind loads resulting in global failure of a structure. Local peak wind loads, or element and cladding loads, are not considered. The structures which fall within the scope of the investigation are limited to regular, low-rise structures which are sufficiently rigid that dynamic effects of the structures may be neglected. Furthermore, only external pressures on structures are investigated.

1.4 Structure of the dissertation

This dissertation has been organized into eight chapters that follow a logical sequence in order to achieve the primary objectives as laid out above. Each chapter represents an independent study within the overarching investigation, with the results obtained in individual chapters serving as inputs to subsequent chapters. A synopsis of each chapter is presented below.

Chapter 2 presents a general background investigation of the individual physical processes which make up the structural wind loading process - referred to as wind load components - and the wind engineering models used to describe those processes. Each wind load component is described and the sources of uncertainty inherent in the components are reviewed. Through this process the primary wind load components which are investigated in this dissertation are identified based on which components contribute most to the uncertainty of the total design wind load formulation.

Chapter 3 presents the reliability and probabilistic modeling basis of the investigation. Probabilistic modeling of wind loads is discussed in a general sense, after which the relevant existing probabilistic wind load models are investigated and compared. The conclusions drawn from the comparison of existing wind load models and the detailed investigation of the background information used to develop the models, specifically the South African model, serve as further motivation for the current research. The general investigative methodology used in this dissertation is then presented. This methodology consists of two approaches: the direct sampling of available reliability data and observations to quantify uncertainties, and the use of comparison of wind load standards as an indicator of uncertainties. Finally, a reliability method is developed for the treatment of wind load components subject to multiple sources of uncertainty through the use of hierarchical Bayesian models. This extension of the traditional system level reliability modeling approach is used as a framework for the investigations conducted in the following chapters.

Chapter 4 presents the investigation of the uncertainties in the free-field wind pressure formulation. Statistical modeling of extreme wind is discussed, followed by a summary of the investigation by Kruger (2011) regarding the South African strong wind climatology and the development of the new wind map of characteristic wind speeds for South Africa. The results from those investigations are used as inputs to the quantification of free-field wind pressure

uncertainties. The conservative bias caused by the use of wind speed intervals in the wind map is quantified, and a reliability method is presented in which the inherent free-field wind variability values for different regions across the country are combined into a single probability distribution. The inherent variability of winds caused by different strong wind generating mechanisms is also investigated.

Chapter 5 presents the investigation of the uncertainties in the pressure coefficient formulation. The methodologies presented in Chapter 3 are applied in a two-part investigation of pressure coefficient uncertainties. The first part of the study sampled observed values from numerous full-scale and wind tunnel test to directly quantify pressure coefficient uncertainties. The second part was the comparison of major international wind load standards as an indicator of pressure coefficient uncertainties. The comparison of wind load standards as a reliability method is based on an expert opinion analysis approach in which the wind load standards are considered as an expression of the combined expert judgment used in the development of the standards. The two approaches resulted in upper and lower limit approximation of the pressure coefficient uncertainties, defining an envelope of possible values from which a single representative model could be selected.

Chapter 6 presents the investigation of the uncertainties in the terrain roughness factor formulation. An experimentally validated baseline model of terrain roughness factors is selected and described. This model is used in conjunction with comparison of international standards, as mentioned above, to quantify terrain roughness factor uncertainties. As in the previous two chapters, the hierarchical Bayesian model framework developed in Chapter 3 is used to quantify the different sources of uncertainty within the component independently and combine them into a single component probability distribution.

Chapter 7 presents a preliminary reliability analysis of the South African loading code using information about wind load uncertainties obtained from the preceding investigations. A critical evaluation of the component models developed in Chapters 4, 5 and 6 is done, including comparison with component models from the existing probabilistic models investigated in Chapter 3. Full probabilistic wind load models which include secondary factors not investigated in this dissertation are then developed using engineering judgement and Bayesian updating of the existing probabilistic models. Subsequent preliminary reliability assessments of wind loads using the new models are presented to investigate the influence that the new models may have

on the reliability performance of the South African loading code. Finally, the changes to the design wind loads in South Africa due to implementation of the new wind map as developed by Kruger *et al.* (2013) in combination with potential implementation of an updated partial factor for wind loads is quantified.

Chapter 8 presents the conclusions of the research. The underlying theme of the investigation as the efficient use of limited information is highlighted. A critical evaluation of the reliability basis and methodology used in the investigation is then presented. The three research questions posed in the Problem Statement above are answered with a discussion of how the primary and secondary research objectives were achieved through the application of rational and transparent reliability methods. Finally, aspects that have been identified for further investigation are presented, and recommendations based on the outcomes of the research are made.

Chapter 2

Background

Before an investigation into the reliability of the wind load design process can commence, the formulation of wind loads should be studied to understand the factors that affect wind loading on structures. Although this dissertation is predominantly a reliability investigation which deals with the probabilistic treatment of wind load component uncertainties, such an investigation requires a foundational knowledge of the underlying technical wind engineering expertise related to wind load components. The aim in this chapter is therefore to outline the wind engineering models used in the formulation of design wind loads on structures for the purpose of identifying sources of uncertainties inherent in the process. To this end the general wind load formation, the primary design wind load components and other major factors which influence wind loading are discussed in the following sections.

2.1 Overview of wind loading on structures

The physical process which results in wind loading on structures can be divided into three broad topics: description of the free-field wind at the location of the structure, the effect of the local environment on the free-field wind, and the interface between the wind and the structure. The field of study of these topics is called wind engineering. As outlined by Baker (2007), the history of wind engineering can be traced back to the 18th century with the development of the first empirical formulations of fluid mechanics. Wind engineering was formally developed in the "establishment period" from 1900 to 1960 and the general formulation of wind loading on structures, specifically wind loading on regular, rigid structures as considered in this disser-

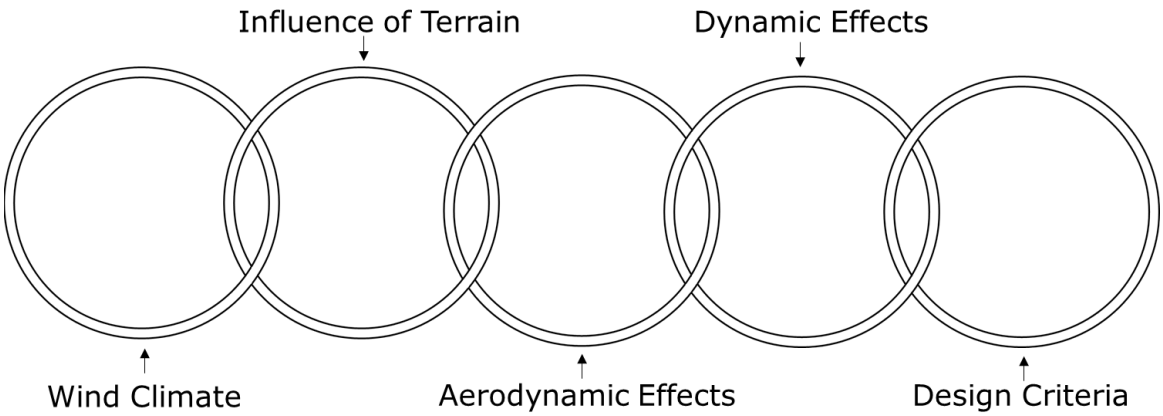

Figure 2.1: The Davenport wind load chain. (Reproduced from Dyrbye and Hansen (1996))

tation, was developed in the "period of growth" from 1960 to 1980. The "modern era" of wind engineering following this period has been characterized by investigations of the dynamic and nonlinear effects of wind loading, specifically on tall, slender structures. As such, much of the research used for the codification of wind loading on regular low-rise structures as considered in this dissertation is from or based upon research done more than three decades ago.

The foundation of the general design wind load process is the concept of the wind loading chain as introduced by Davenport (1961) (see Figure 2.1). Davenport's chain effectively represents the components which make up the standard wind load formulation. The formulation of the design wind pressure is given mathematically as the product of the wind load components considered, as shown in Equation 2.1.1. As reported by Dyrbye and Hansen (1996) and Holmes (2015), this equation, or some permutation of it, is used for the calculation of wind loads on rigid structures in all major international standards. In addition to a general description of the wind load components, Davenport (1983) also emphasized the importance of reliability treatment of wind loads when using the wind loading chain. The reliability treatment of wind loading is described in Chapter 3.

$$q = c_r \, c_a \, c_g \, c_d \, Q_{ref} \tag{2.1.1}$$

where, q is the design wind pressure

c_r is the roughness factor

c_a is the aerodynamic shape factor

c_g is the gust factor

c_d is the dynamic response factor

Q_{ref} is the reference free-field wind pressure at the location of the structure

Each component in the wind loading chain may be characterized by its time dependance. The description of the free-field wind at the location of the structure is a time dependent process which is subject to the stochastic nature of strong wind conditions. The conversion of the free-field wind into wind pressure loading on the structure is primarily a function of the aerodynamic and terrain roughness effects. While the free-field wind is time dependent, these factors are time independent since the physical conditions which influence them, namely the geometry of the structure and the surrounding terrain, remain relatively constant over time.

Referring back to the three broad topics which describe wind engineering, the description of the free-field wind at the location of the structure is represented in the wind loading chain by the reference free-field wind pressure (Q_{ref}) and the gust factor (c_g). As described by Holmes (2015), the calculation of the free-field wind requires a description of the strong wind (also referred to as extreme wind) climatology of the region considered. The free-field wind is therefore not only time dependent, but location dependent. Goliger (2016) explains that the primary input to the development of a strong wind climatology is observed wind data which is analysed through the application of relevant statistical techniques. Most of these statistical techniques are based on extreme value theory as described by De Haan and Ferreira (2007). Extreme wind speed modeling techniques have been the object of multiple investigations, some notable examples being the research by Gomes and Vickery (1978), Ellingwood *et al.* (1980), and Milford (1985*b*) in South Africa. However, this investigation directly follows the completion of an investigation of the South African strong wind climatology by Kruger (2011) which is based on the most recent wind speed observations available at time of writing, and as such the study by Kruger serves as the primary reference for the treatment of free-field wind uncertainties as presented in this dissertation.

The second topic considered, namely the effect of the local environment on the free-field wind, is commonly subdivided further into two effects. As explained by Holmes (2015), the first is the reduction of wind speed due to the surface roughness. This is represented in the basic wind loading chain by the terrain roughness factor (c_r). In most wind engineering models, and subsequently in most design wind load standards, the effects of terrain roughness factors are taken into account through the establishment of boundary layer wind velocity profiles for given representative terrain types, referred to as terrain categories. Davenport (1960) proposed

a set of terrain categories and qualitative descriptions of representative boundary layer profiles. The Davenport roughness classification has been updated through the use of experimental studies by Wieringa (1992), Wieringa (2001) and Wang and Stathopoulos (2007), however the fundamental principles proposed by Davenport remain mostly unchanged. The second effect of the local environment is the acceleration or reduction of wind speed due to large topographical features such as hills, embankments, cliffs, or surrounding structures. Most wind load standards provide basic provisions for incorporating the effects of topography, however as stated by Goliger (2012) the influence of topographical effects are too complex to be reduced to simple operational models. As such, topographical effects are often treated in specialist studies such as the investigations by Ho *et al.* (1991) and Goliger (2005).

The final topic to consider is the interface between the wind and the structure as a result of the aerodynamic properties of the structure. As described by Davenport (2002) and Baker (2007), this has been a critical topic of investigation in wind engineering since the 1980s. In the basic wind loading chain, this interface is described by the aerodynamic shape factor (c_a), also referred to as the pressure coefficient, and the dynamic response factor (c_d). Pressure coefficients are developed using wind tunnel and full-scale test results. The pressure coefficients used in Eurocode and the South African wind load standard for typical design situations were first published by Cook (1985). As stated by Baker (2007), several major full scale tests on low-rise structures have been conducted since such as the studies by Milford *et al.* (1992), Hoxey (1991) and Levitan *et al.* (1991). There have also been multiple pressure coefficient studies, several of which are discussed in Chapter 5 of this dissertation. Unfortunately, the pressure coefficients observed in these tests cannot be used directly for the development of design pressure coefficients. As described by Holmes (2015), it is preferable for typical structural design purposes to apply the design wind pressure as a static load. The design pressure should be calculated in such a way that the maximum load effects are obtained. The wind load is therefore applied as an effective peak static load distribution rather than a dynamic load. The advantage of this approach is that for typical structures dynamic effects do not need to be taken into account. However, this makes development of design pressure coefficients more complicated. There are several approaches which may be followed to develop design wind load standards. The approach followed in this investigation is discussed in Section 2.2.4.1.

2.2 Wind load components

This investigation aims to investigate the general reliability model for standardized wind load design. The design space is therefore defined accordingly. This general case should then serve as norm for provisions for special cases, such as structures subject to dynamic loading effects as mentioned above. Special cases should be calibrated to provide reliability performance consistent with the general case, considering that specific uncertainties and consequences of failure are not considered here. This framework should ensure that selection of situations to be investigated is not made on an ad hoc basis or simply to exclude difficult cases. In keeping with this investigative philosophy, the following sections provide a description and discussion of each of the primary wind load components and factors which influence wind loading on structures in greater detail than the overview provided above. The relative importance of each component for this investigation is discussed, with clear explanations provided to justify decisions where components and factors have been excluded from this investigation. In doing so the scope of this dissertation as laid out in the introductory chapter is clarified.

2.2.1 Reference wind pressure

The first step in the formulation of design wind loads is the determination of the characteristic free-field wind pressure at the location of the structure. Free-field wind describes the wind before it has been affected by the local environment. The free-field wind characteristics are determined by the wind climate, which describes the general behaviour of wind on a macroscopic scale. Each country or region has a unique wind climate and different factors which influence it, which makes it impractical to discuss free-field wind in a generalized way. Therefore, the discussion and investigation of the free-field wind which follows in this document are strictly related to the South African free-field wind and strong wind climate.

The South African strong wind climate consists of multiple wind generating mechanisms. Chief among these are synoptic scale weather events such as cold fronts which dominate along the coast, and meso-scale events such as thunderstorms which are more prevalent in the internal parts of the country. It stands to reason that different strong wind mechanisms generate winds with different characteristics. Meso-scale convective wind conditions such as thunderstorms, for example, create relatively brief periods of strong winds with erratic gusts, whereas synoptic

scale mechanisms such as cold fronts generate more consistent winds. It is therefore important to understand and consider the strong wind climate when developing design wind maps.

A recent study by Kruger (2011) characterised the South African strong wind climatology. There have been numerous studies in the past in which South Africa was divided into climatic zones based primarily on rainfall data, however the study by Kruger was the first which attempted to delineate different zones based on wind data. Kruger gathered wind data from 209 Automatic Weather Stations (AWS) across the country. After a rigourous quality control audit to ensure the homogeneity and reliability of the data, 91 stations were selected for the final analysis of the strong wind climatology. The details of the quality audit are discussed in Section 4.1.1.

Kruger identified six strong wind generating mechanisms in South Africa: cold fronts, thunderstorms, ridging, trough to the west with strong ridging to the east, troughs on the West Coast of the country, and isolated low-pressure systems. By analysis of the wind and climatic data from the selected weather stations Kruger determined which sources caused strong winds at each station. Most stations had more than one strong wind source, with one station having four separate mechanisms which contribute to annual extreme winds. Cold fronts and convective wind events such as thunderstorms were the most common sources, with one of these mechanisms contributing to the annual extremes of every station considered. Using cluster analysis, Kruger delineated the country into zones based on the dominant strong wind mechanisms, as shown in Figure 2.2

Although understanding the wind climate and knowing which strong wind generating mechanism is the source of wind loads is required in order to predict strong winds, this information is not directly used in the formulation of design wind pressure. The most important characteristic of the free-field wind for design purposes is the design velocity of the wind at the location of the structure being considered. In most national standards, the variation of wind velocity over a geographical region is represented using a wind map. Wind maps show contours of reference wind velocities with a certain probability of occurrence as determined using statistical analysis on observed wind data. In the study by Kruger an extreme wind prediction analysis was done wherein statistical models were developed for 76 wind stations across the country and used to develop a design wind map for South Africa. This is discussed in detail in Chapter 4.

Once the wind velocity has been obtained from a wind map, the design reference pressure,

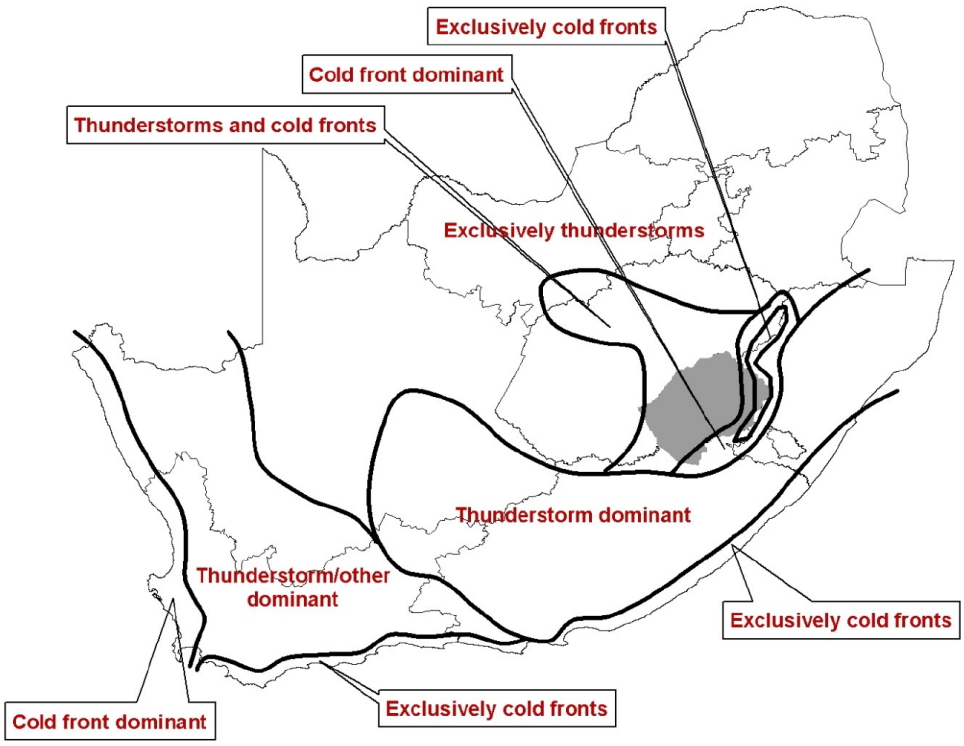

Figure 2.2: Strong wind generating mechanisms across South Africa, taken from Kruger (2011).

as used in Equation 2.1.1, may be obtained using Equation 2.2.1.

$$Q_{ref} = 0.5 \times \rho \times v^2 \tag{2.2.1}$$

where, ρ is the air density

v is the free-field wind velocity

An important aspect to consider in the description of free-field wind is the averaging period of the wind velocity. This is described in detail in the following section.

2.2.2 Gust factor

National wind loading codes provide wind maps for their countries which show the mean free-field wind speed averaged over a given period of time. The averaging period used is dependant on the wind climate of the region. The European wind climate, for example, is dominated by synoptic wind generating mechanisms which generally result in steady and mature conditions in terms of the turbulence of the wind, and as such EN-1991-1-4 uses a basic wind speed derived for an averaging period of 10 minutes. However, the peak gust wind speed, usually averaged

over 2-3 seconds, is required to obtain the effective peak static load distribution as used for structural design. A gust factor, which is the ratio of the expected peak wind speed to the average wind speed, is used to convert the mean wind speed to the peak gust wind speed.

$$G = \frac{\hat{U}}{\bar{U}} \tag{2.2.2}$$

where, $\hat{U}$ is the expected peak gust wind speed

$\bar{U}$ is the mean wind speed

Due to the nature of wind as a random process, the expected peak gust wind speed is itself also a random variable. Various formulations for the gust factor have been developed, however there are two methods which are predominantly used, as given by Choi and Hidayat (2002). Using the first method, ratios of gust wind speeds with the same gust period to mean wind speeds with different averaging periods are investigated. Linear functions are then used to represent the gust factor values and a regression slope of the fitted data is used to calculate the rate of the drop in wind speed for different averaging periods. The second method follows the same procedure, however the ratios of hourly mean wind speeds to gust wind speeds with different gust periods are used.

The gust factor is often expressed as a function of the turbulence intensity of the wind. Turbulence intensity is a measure of how laminar or turbulent the wind profile is, and is calculated using Equation 2.2.3, given in the book by Cook (1985).

$$T_i = \frac{\sigma}{\bar{U}} \tag{2.2.3}$$

where, T_i is the turbulence intensity

σ is the standard deviation of the wind speed

$\bar{U}$ is the mean wind speed

Note: Values used in Equation 2.2.3 should be based on 1 minute averaged data sampled at 1 Hz

Equation 2.2.4 is used to calculate the gust factor for gust winds of period t and a mean wind averaging time of T.

$$G_{t,T} = 1 + C_g T_i ln(T/t) \tag{2.2.4}$$

where, C_g is the gust factor coefficient

T_i is the turbulence intensity

T is the mean wind speed averaging period

t is the gust period

The latest version of the South African loading code, SANS 10160:2011, was developed using Eurocode as a technology base. However, as the climatic conditions of Europe and Southern Africa differ, it stands to reason that certain aspects of the wind load calculation procedure will differ. As stated above, the Eurocode wind load calculation procedure uses a fundamental basic wind speed velocity based on a 10 minute averaging period. In South Africa, where a mixed strong wind climate is found in which meso-scale events such as thunderstorms are a dominant source of extreme wind speeds, an averaging time of 3 seconds or less is required for a meaningful determination of the extreme value design wind speeds. Therefore, SANS 10160-3 uses a basic wind speed derived from gust wind speed observations with averaging times of 2-3 seconds. However, to adopt the Eurocode format the SANS wind map needed to be presented with 10 minute averaged wind speeds. Goliger (2012) explains that in order to overcome this difficulty, the wind map used in the previous version of the loading code, SABS 0160:1989, was retained. This wind map was based on wind speeds averaged over a 3 second period. The map was augmented by a factor of 1.4 to convert the gust values into 10 minute averaged values. The new gust wind map which will be used in future editions of the South African loading code as developed by Kruger is also based on the 2-3 second gust wind speed values. The development of the new wind map is discussed in detail in Chapter 4.

The use of a wind map based on gust wind speeds effectively negates the necessity for gust factors in the wind load design process. Therefore, gust factors are not used in the SANS wind load stipulations. Further investigation into gust factors is therefore not done in this investigation.

2.2.3 Terrain and topographical effects

The influence of the surrounding terrain on the wind load acting on a structure is one of the most variable and uncertain aspects of the design wind load process. This is due to the difficulty in quantifying the effects of complex topography or rough terrain on the wind load without specialist studies or wind tunnel tests. When considering local effects there are two primary factors that need to be considered: surface roughness of the terrain and topography of the terrain.

2.2.3.1 Surface roughness

When considering the effects of surface roughness, structures are assumed to be isolated on a level plane. The quantified effect is therefore not affected by any surrounding buildings or topographical features, but only by regular obstacles on the ground surface upwind of the structure. These obstacles cause turbulence in air flow, which causes a reduction in wind speed near the ground. The variation of wind velocity with height above ground level is called the boundary layer wind profile. The wind load design process uses a terrain roughness factor, c_r in Equation 2.1.1, to take the reduction of wind speed due to surface roughness into account. The roughness factor is a function of the height above the terrain and the surface roughness length. As explained by Dyrbye and Hansen (1996), the roughness length can be interpreted as the characteristic size of the vortices created by the obstacles on the ground surface.

Roughness factors as used in wind load standards are derived from wind velocity profiles. There are two primary methods used to model velocity boundary layer profiles. The first is the logarithmic law, which is given in Equation 2.2.5. Eurocode, AS/NZS and ISO use the logarithmic law to determine roughness factors. The second velocity profile which is commonly used is the power law, given in Equation 2.2.6. SANS, ASCE and NBCC use the power law to describe the boundary layer profile.

$$\bar{U}(z) = u_* \frac{1}{k} ln \frac{z}{z_0} \tag{2.2.5}$$

where, $\bar{U}$ is wind velocity

z is the height above ground level

u_* is the friction velocity

k is von Karman's constant ≈ 0.4

z_0 is the surface roughness length

$$\bar{U}(z) = \bar{U}_{ref} \left(\frac{z}{z_{ref}} \right)^{\alpha} \tag{2.2.6}$$

$$\alpha = \frac{1}{ln(z_{ref}/z_0)} \tag{2.2.7}$$

where, $\bar{U}$ is wind velocity

z is the height above ground level

z_{ref} is the reference height

$\bar{U}_{ref}$ is the mean wind speed at the reference height

z_0 is the surface roughness length

Using established velocity profiles for the representative terrain categories, terrain roughness or exposure factor equations are set up as a function of the reference velocity pressure for the standard terrain category. For SANS, the reference velocity is taken at the standard reference elevation of 10 m in Terrain Category B. Normalizing all velocity profiles with respect to this value, a constant roughness factor coefficient of 1.36 may be calculated. The general formula for terrain roughness factors in SANS is given in Equation 2.2.8 and the wind profile parameters are given in Table 2.1. The SANS terrain roughness profiles are shown in Figure 2.3.

$$c_r = 1.36 \left(\frac{z - z_0}{z_g - z_0} \right)^{\alpha} \tag{2.2.8}$$

where, z_0 is the reference plane height

z_g is the gradient height

z_c is the height below which no further reduction in wind speed is allowed

α is the power law exponent

The most significant problem with using these laws to model wind behavior is the un-

Table 2.1: SANS wind profile parameters.

Terrain Category	z_g	z_0	z_c	α
A	250	0	1	0.070
B	300	0	2	0.095
C	350	3	5	0.120
D	400	5	10	0.150

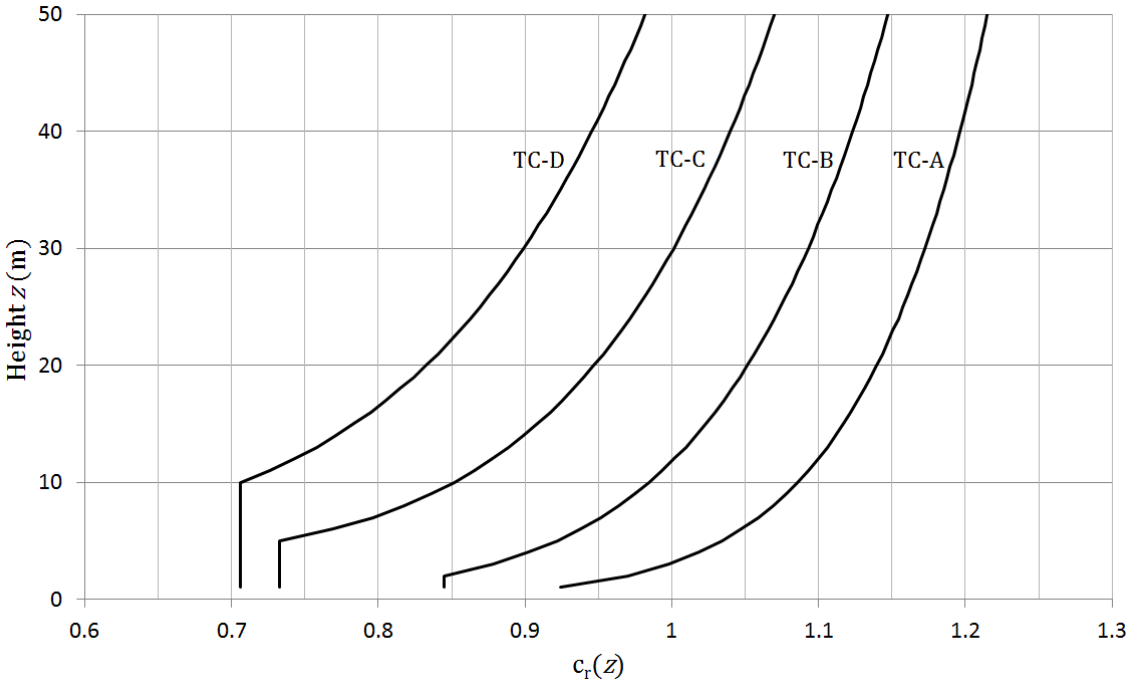

Figure 2.3: SANS Terrain roughness factors $c_r(z)$ for Terrain Categories A-D.

certainty of the roughness length. To solve this problem wind load standards provide terrain categories which describe different environments using generalized descriptions. Representative values for the roughness length and other related parameters to be used in the logarithmic or power laws are given for each terrain category. The designer may then choose which terrain category is most applicable to the building site. It stands to reason that in most cases the terrain roughness will fall somewhere between two categories. In these cases it is advised that the upper limit value be used. Therefore, the use of terrain category roughness factors is inherently conservative.

Unfortunately, these is no consensus between international standards on wind velocity profiles laws and terrain category parameters. This is a clear indication of the uncertainty inherent in terrain roughness factors. To illustrate this point, Figure 2.4 compares the roughness lengths used for the terrain categories in ISO, Eurocode and SANS. From the figure it may be seen that there is a general correspondence between the roughness lengths used for Terrain Category 2,

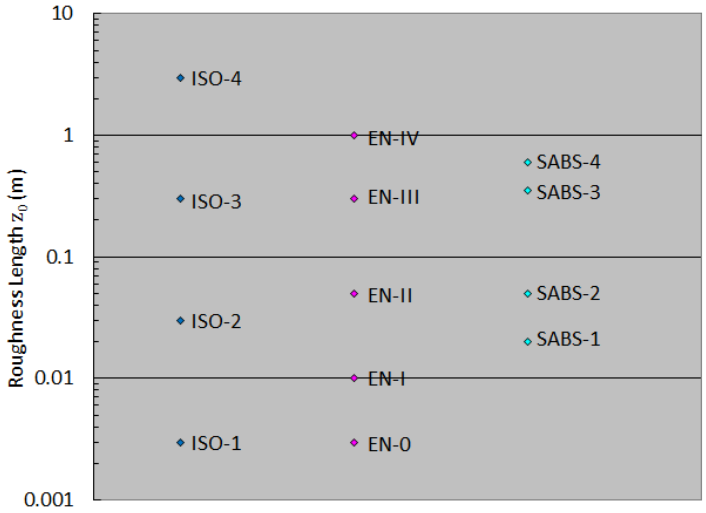

Figure 2.4: Comparison of roughness lengths for ISO, Eurocode and SANS values. (Reproduced from Retief and Dunaiski (2009))

which is used as the reference terrain category, but there is significant dispersion around the reference case.

The uncertainties which need to be considered for terrain roughness factors are primarily modelling uncertainties due to the subjective way in which terrain categories are defined. A baseline model is required to serve as an objective reference against which terrain roughness factor stipulations may be measured. The selection of such a baseline model is discussed further and the uncertainties inherent in terrain roughness factors are quantitatively estimated in Chapter 6.

2.2.3.2 Topographical features and surrounding built environment

Topographical features refer to natural obstacles such as hills or cliffs, however other large scale obstructions in wind flow such as surrounding buildings also need to be considered when determining the design wind load on structures. These features significantly influence the design wind pressure, but in most cases these effects are difficult to establish. The surrounding topography and built environment may decrease the wind speed in some cases or accelerate it in others. In some cases vortices generated by hills or cliffs may cause complex pressure distributions due to uplift on the structure, and in others the topography may cause extreme downward pressure acting on the structure. There are as many different influences caused by topography as there are different configurations of a structure and surrounding topography.

Most wind load standards, including SANS 10160-3, provide basic provisions to account for

the effects of generic topographical features such as hills and cliffs, as well as the influence of surrounding buildings. In many cases it is unclear, however, when these provisions are applicable and when the effects of these features are beyond the scope of the provisions given. Basic procedures are also provided to determine the effects of the surrounding build environment, however Goliger (2012) states that the only reliable way to predict these effects is by using wind tunnel technology.

It is the responsibility of the design engineer to establish whether the topography of a given site falls within the limits of the scope of the wind load standard used or requires specialist studies. This presents a significant challenge when trying to quantify uncertainties related to topography. As there are no clear boundaries delineating the scope of the standard when considering topographical effects, subjective "soft" boundaries can only be established through engineering judgement and assessment of typical design procedures. In this investigation these boundaries are defined as the design situations where specialist studies are first conducted in order to quantify the effects of the topography. When specialist studies are conducted, the topographical effects are no longer within the scope of the standard, and as such the uncertainties beyond those boundaries do not need to be quantified in a probabilistic model of the design standard.

For economic reasons, it stands to reason that more often than not specialist studies are not conducted for low-rise buildings. It is reasonable to assume that responsible engineers will err on the side of caution and are therefore more likely to conduct specialist studies in cases where there is potential for wind acceleration due to the surrounding topography, and less likely to request specialist input in cases where the surrounding topography has a shielding effect on the specific site. The implication of this in terms of wind load reliability is that topographical effects which fall within the considered "soft" boundaries are more likely to be on the conservative side.

Due to the complexity involved, the influence of large scale topographical features is not a topic which is covered in more detail within this investigation. It is still important that the topography and surrounding built environment be kept in mind, however, as it makes it clear that even the most sophisticated probabilistic models may be useless if such influences can change the characteristics of the physical problem being modeled.

2.2.4 Aerodynamic factors

A critical step in the wind load design process is describing the interface between the free-field wind and the structure. A structure is not subjected to a constant pressure distribution across its entirety, but different areas are subject to different loads due to the aerodynamic properties of the building. When calculating wind loads, these aerodynamic effects are accounted for through the use of pressure coefficients, also known as aerodynamic shape factors.

The determination of pressure coefficients for the purposes of structural design is a complex wind engineering problem which is a research field in itself. For the purposes of this investigation, only a superficial overview of pressure coefficients is given for the sole purpose of identifying the dominant sources of uncertainty which may affect the uncertainty of design wind loads. Due to the complexity of pressure coefficients it is impractical to provide an overview of pressure coefficient formulation and discuss sources of uncertainty simultaneously, unlike the other wind load factors considered in this investigation. Therefore, this section is divided into two subsections. First, a brief summary of pressure coefficients and the related codification process is given, which is followed by a discussion of the primary sources of uncertainty inherent in pressure coefficients.

2.2.4.1 Pressure coefficient overview and codification process

Pressure coefficients are defined as the ratio of the fluctuating dynamic pressure at a point to the reference pressure of the surrounding air. Due to the turbulent nature of free-field wind air flow, pressure coefficients are generally not constant values but fluctuate with time. The general formula for pressure coefficients, which is derived from Bernoulli's equation, is given in Equation 2.2.9 as a function of time.

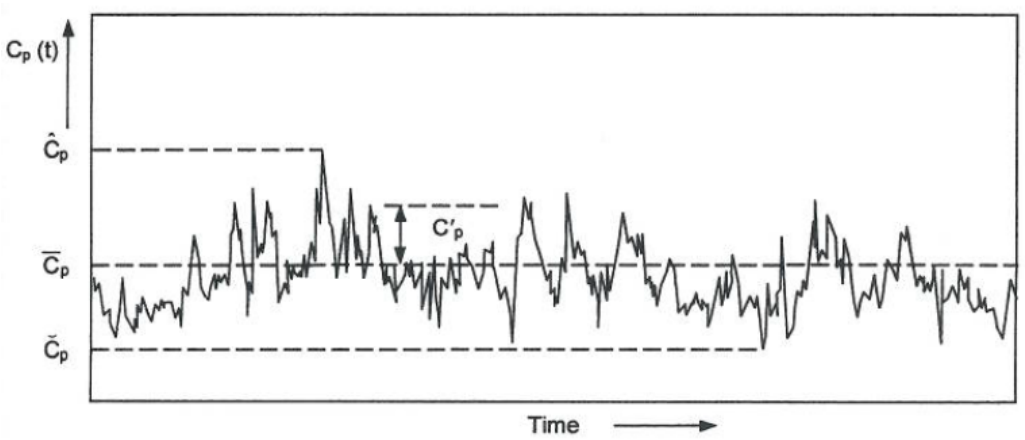

Figure 2.5: Typical variation of pressure coefficient on low-rise building roof taken from Holmes (2015).

$$c_p(t) = \frac{p(t) - p_0}{p_{ref}(t)} = \frac{p(t) - p_0}{\frac{1}{2}\rho U(t)^2} \tag{2.2.9}$$

where, $c_p(t)$ is the pressure coefficient at time t

$p(t)$ is the pressure at time t

p_0 is the static reference pressure (normally atmospheric pressure)

$p_{ref}(t)$ is the reference wind pressure at time t

ρ is the air density

$U(t)$ is the wind velocity at time t

Pressure coefficients are most commonly measured using boundary layer wind tunnel tests. A scale model of the structure under consideration is made and pressures are measured on the model for different wind directions. Figure 2.5 shows the typical fluctuation of the pressure coefficient over time at a position on the roof of a low-rise building measured in a wind tunnel. The figure also shows the mean ($\bar{C}_p$), peak ($\hat{C}_p$), minimum ($\check{C}_p$) and root-mean-square (C'_p) pressure coefficients as calculated from the measured time series.

As stated in the introduction to this chapter, for most structural design purposes it is preferable to apply the design wind pressure as a static load instead of a dynamic load. There are a few issues which need to be considered in order to convert dynamic wind loads into static loads. These are the method used to determine static design pressures at a given point, area-averaging of pressure coefficients and the equivalent static load distribution pattern, or pressure zone pattern, across the structure.

Design loads may be based on mean pressure coefficients or peak pressure coefficients,

depending on the design criteria. As described by Cook (1985), there are several approaches which may be used, although the most commonly used methods are the quasi-steady approach, the peak factor approach and the method developed by Cook and Mayne (1979). For global structural loads used to design primary structural elements, the quasi-steady assumption which is based on the use of mean values pressure coefficient values is typically used. Wind loads on specific elements or cladding are usually designed using peak local pressures which are based on peak pressure coefficient values using any of the three methods, however the Cook-Mayne method is most commonly used as described by Hansen *et al.* (2015). As this investigation is focused on the global reliability of structures, only the quasi-steady approach is considered.

As stated by Holmes (2015), most wind load standard pressure coefficient stipulations are based on the quasi-steady approach. This approach is based on the assumption that fluctuating wind pressures measured at a position on a structure are due to variations in longitudinal wind velocity upstream of the structure and not due to dynamic fluctuations of the structure itself. A number of studies, such as the investigations by Tamura *et al.* (2001) and Mendis *et al.* (2007), have stated that for the majority of low-rise buildings the rigidity of the structure is high enough that the resonant movement of the building may be neglected, thus the assumption holds true. By dividing the wind velocity into its mean and fluctuating components, it may be shown that for small turbulence intensities the quasi-static pressure coefficient is approximately equal to the mean pressure coefficient. The result is that the peak design wind pressures (maxima and minima) may be predicted by using mean pressure coefficients with the peak gust wind velocity, as shown in Equation 2.2.10. A full derivation of this formula may be found in the book by Holmes (2015).

$$\hat{p}, \check{p} = c_{po}(0.5)\rho\hat{U}^2 = \bar{c}_p(0.5)\rho\hat{U}^2 \tag{2.2.10}$$

where, $\hat{p}, \check{p}$ are the maximum and minimum design wind pressures

c_{po} is the quasi-steady pressure coefficient

$\bar{c}_p$ is the mean pressure coefficient

$\hat{U}$ is the peak wind velocity

Using pressure coefficients measured at a single point is not an accurate representation of the pressure which occurs over the entirety of a structural element. Therefore, pressure coefficients

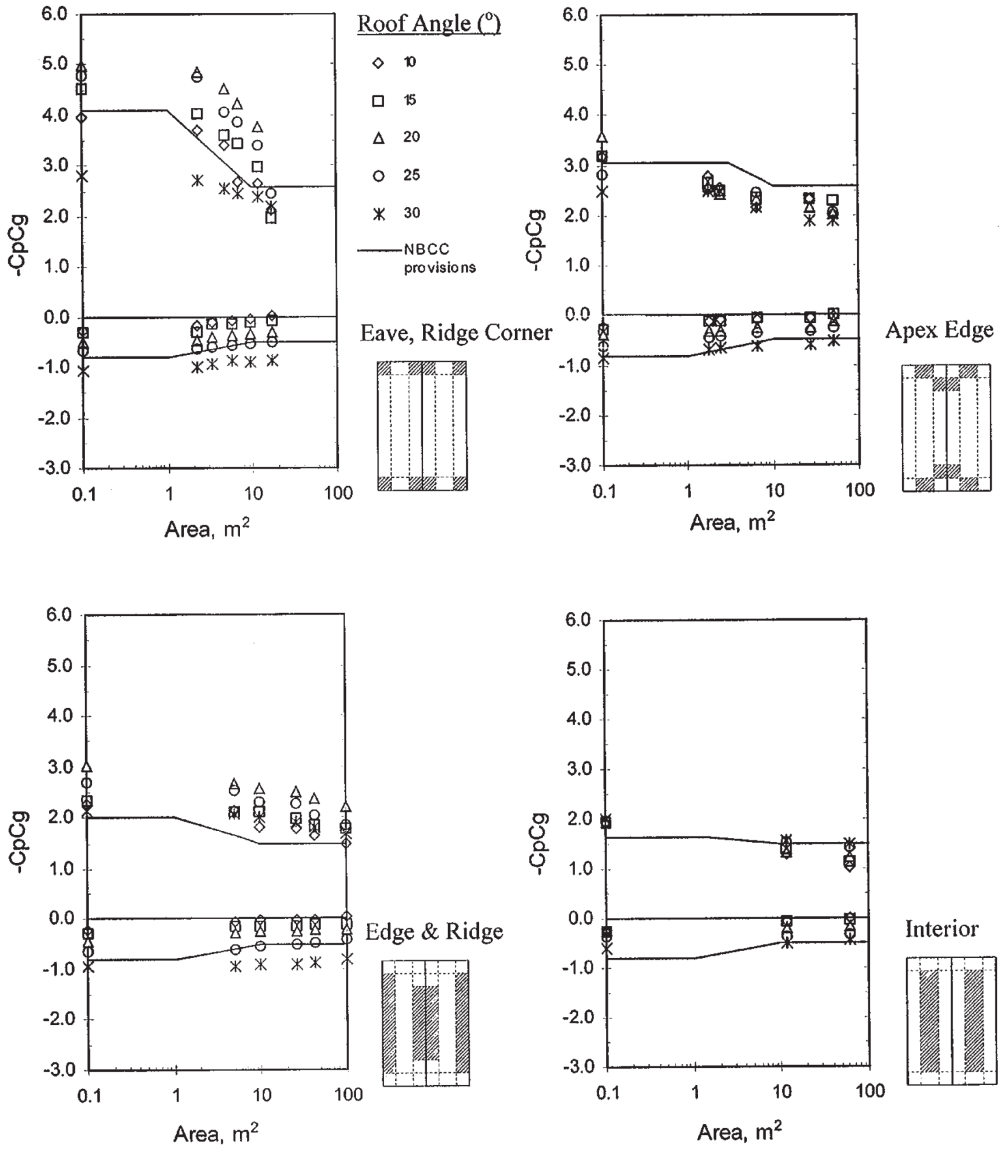

Figure 2.6: Experimental results of area averaged pressure coefficients for four zones of a gable roof and NBCC 1995 provisions taken from Stathopoulos *et al.* (2000).

need to be modified by averaging the measurements of multiple points over a tributary area. The standard areas over which pressure coefficients are averaged are 1 m^2 and 10 m^2. Average pressure coefficients decrease as the area over which they are averaged increases. Wind load standards typically provide design pressure coefficients for these two areas ($c_{p,1}$ and $c_{p,10}$) used as upper and lower limit values and allow for interpolation of values between the limits. Figure 2.6 taken from an investigation by Stathopoulos *et al.* (2000) shows wind tunnel test results and the provisions given in a previous Canadian wind load standard NBCC 1995 for area-averaged pressure coefficients of four critical pressures zones on gable roofs.

The final step in determining static design wind loads is to define an equivalent static wind load distribution in such a way that the correct expected values of load effects such as bending

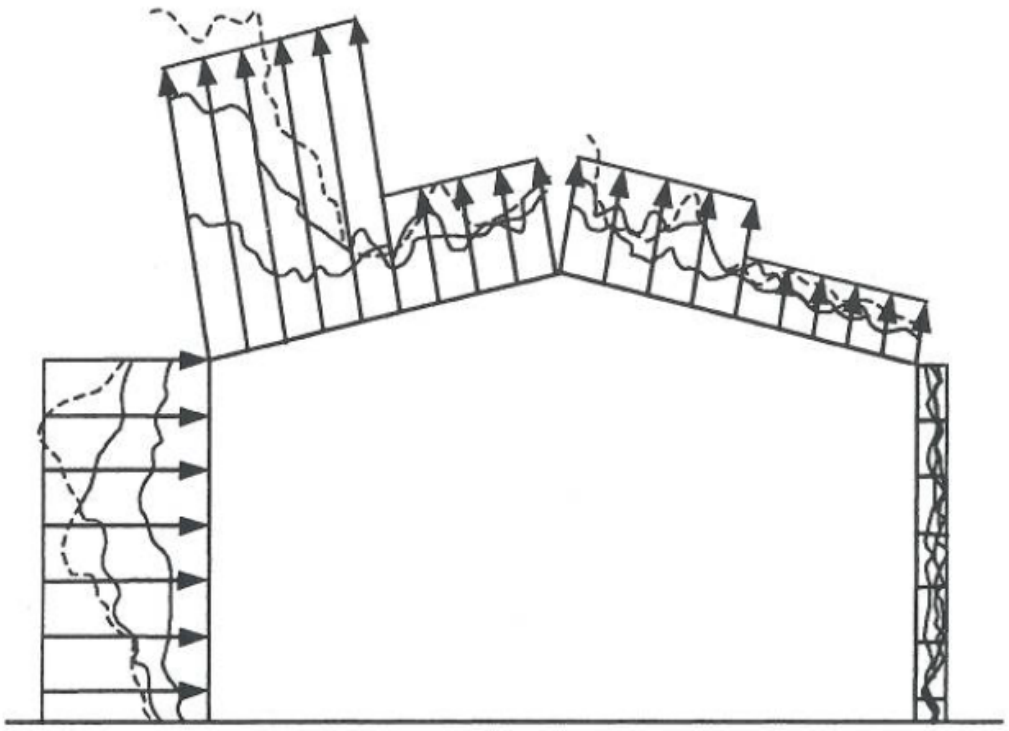

Figure 2.7: Instantaneous and equivalent static wind load distributions on low-rise building taken from Holmes and Syme (1994).

moments and forces in structural members and deflections are obtained. The effective design wind loads are dependent on the correlation between the fluctuating pressures on different parts of the structure, which is an area-averaging effect. The primary purpose of equivalent static wind loads is to represent a "worst case scenario" in terms of the wind pressure acting on the structure simultaneously. This is illustrated in Figure 2.7 which was taken from an investigation by Holmes and Syme (1994), which shows the instantaneous pressure distributions on a portal frame structure as well as the simplified equivalent static load.

Equivalent static wind load distributions used in wind load standards are usually determined using an "envelope" loading procedure with the maximum observed pressure in a given pre-defined zone uniformly distributed over that zone. Chen and Zhou (2007) found that this procedure is generally considered to provide conservative estimates of wind load effects, but cited a number of investigations by Ginger and Holmes (2003), Simiu *et al.* (2003) and Stathopoulos (2003) which found that such simple wind loading models may lead to inconsistent and even underestimated values of load effects in low-rise buildings.

As structures are not solid bluff bodies but rather hollow shells, it is important to note that all structures have an internal pressure. Unlike the external pressure, internal pressure is assumed to be constant across the entire structure assuming that the structure consists

of a single internal opening. If the structure has several fully enclosed rooms, the internal pressure for each room is assumed to be constant and different rooms may have different internal pressures. The internal pressure is dependent on the external pressure at any openings in the structure. If an opening exists in the windward face of the structure the internal pressure will be positive, whereas openings on the side or leeward faces of the structure will result in a negative internal pressure. The resultant design load acting on the structural members is taken as the combination of both internal and external pressures. In cases when no openings are present, wind load standards typically provide upper and lower limit values for the internal pressure and the pressure which provides the most conservative load is to be used. As internal pressures are entirely dependent on the openings in the structures and there are numerous combinations which need to be considered for each structure depending on which openings are present, this investigation excludes internal pressure coefficients and only considers external pressure coefficients.

2.2.4.2 Pressure coefficient uncertainties

The first and arguably largest source of uncertainty in pressure coefficient values is the tool which is used to measure them, namely boundary layer wind tunnel tests. Comparison of more than 200 research papers on low-rise buildings by Uematsu and Isyumov (1999) found significant variation in the results obtained from wind tunnel tests investigating the same structures. Uematsu and Isyumov attributed this variability primarily to the determination of geometric scale and correct boundary layer modeling. The scale of wind tunnel flows generated by using naturally grown boundary layers typically ranges from $1:200$ to $1:500$. At these scales, most models are too small to accurately model architectural details which may influence the pressure coefficients and setting up instrumentation which is too large becomes an issue.

According to Goliger (2015) the variability in wind tunnel test results is a result of different wind tunnel configurations. The positions at which the static reference pressure and the reference wind pressures (see Equation 2.2.9) are measured in the wind tunnel have a significant influence on the measured pressure coefficients, yet there are no standard measuring positions which are used consistently throughout all wind tunnel tests. Goliger added that negligent pressure tap placement may be a contributing factor to the pressure coefficient measurement uncertainty, as it is imperative that the pressure taps are placed flush with the surface of the

model. If the pressure taps protrude even slightly they affect the wind flow and result in unreliable measurements.

Another issue to consider is how well wind tunnel tests simulate full-scale wind behaviour. This has been the subject of much research by the wind engineering community, and a number of full-scale experiments such as the Aylesbury experiment, the Texas Tech Building experiment and full-scale measurements on a large hangar at Jan Smuts Airport, South Africa have been carried out over the last 40 years in order to answer this question. Results from these experiments as published by Hansen and Sørensen (1986), Milford *et al.* (1992), Endo *et al.* (2006) and numerous others have found inconsistencies between the results obtained from wind tunnel and full-scale tests. This is investigated in detail in Section 5.1.

The inherent uncertainty of the quasi-static approach used to determine peak static pressures should also be considered. According to Holmes (2015), the quasi-static approach is conservative when applied over large areas as full correlation of the pressure peaks at different positions is implied. Unfortunately it is impossible to quantify this conservatism without a dynamic analysis of the element forces and moments in a structure during fluctuating peak wind loads. This falls outside the scope of this investigation, however it is important to take note of this additional conservatism when critically assessing the representative probability distributions of pressure coefficients which is determined in this investigation.

Finally, it stands to reason that the equivalent static wind load distributions selected for the purposes of codification will contribute to the uncertainty of pressure coefficients. Throughout this investigation the comparison of wind load calculation procedures given by different wind load standards will be used as a tool to determine the uncertainty of wind load components, as discussed in Section 3.4.2. The differences between the equivalent static wind load distributions used in the different standards is a good example of why this method is effective for determining wind load component uncertainties. Figure 2.8 shows the three primary zoning systems used in the seven wind load standards considered in this investigation for wind acting from two directions on a gable roof structure. Although there are certain similarities in the three zoning systems, such as peak pressure zones on the roof near the windward eaves and large low pressure zones toward the leeward side of the structure, the systems are clearly inconsistent. Even if the absolute magnitude of the pressure coefficients used in these wind load standards were theoretically identical, which is not the case, the design forces obtained would differ

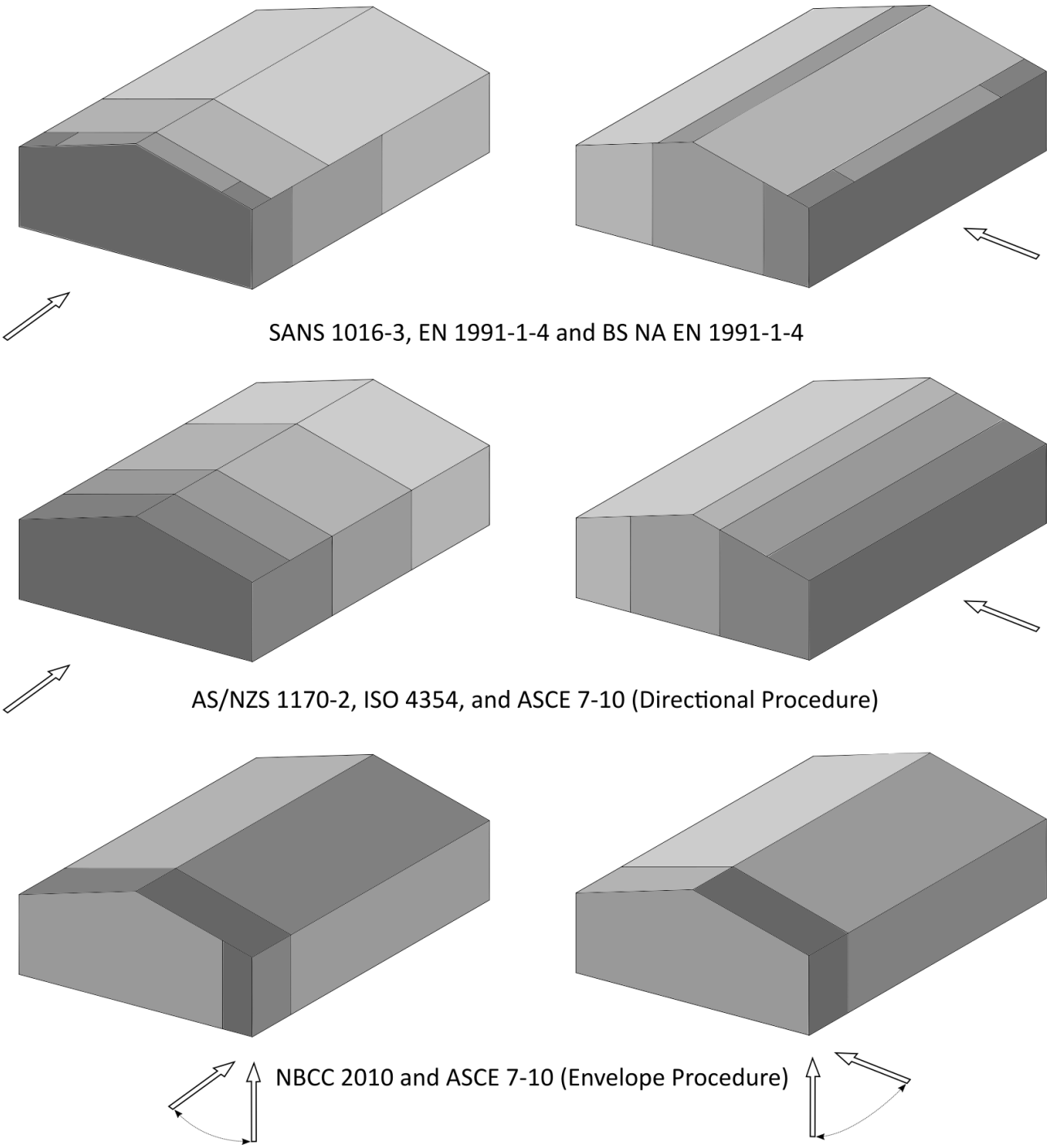

Figure 2.8: Pressure zones used in different wind load standards.

significantly as the distribution of wind pressure across the structures vary significantly. This is a clear indicator of the uncertainty of pressure coefficients as there is no universal consensus regarding the correct equivalent static wind load distributions to be used.

2.2.5 Thunderstorm winds

As stated in the discussion of free-field wind pressures earlier in this chapter, South Africa plays host to a complex strong wind environment with multiple wind generating mechanisms.

It stands to reason that winds generated by different mechanisms have different characteristics. However, the South African wind load standard and most other international wind load standards only provide a single method for calculation of wind loads, regardless of the type of wind. The differences in the characteristics of winds generated by different mechanisms therefore need to be considered.

Due to the complex nature of thunderstorms, a number of different extreme wind events may occur due to different mechanisms within the storm. Letchford *et al.* (2002) described the development of thunderstorms and the different wind characteristics which are observed throughout the life cycle of a storm. During the formative stage of the storm, convection of warm air causes an updraft, which in certain cases may lead to tornado formation. As the storm matures and dissipates, the warm air cools and creates a downdraft, which may cause downbursts. A downburst can be best visualized as a jet of air acting vertically downwards. Once this jet reaches the ground it dissipates outward creating an outflow gust front as shown in Figure 2.9.

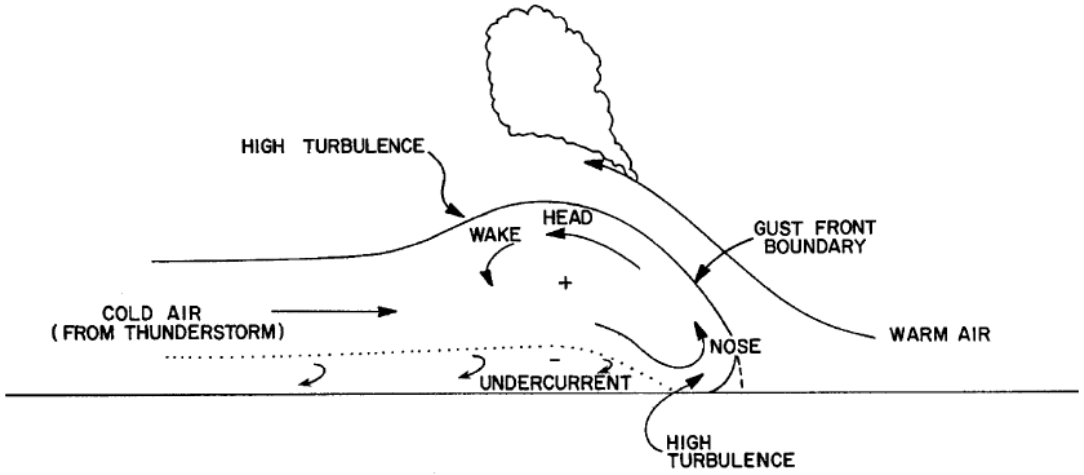

Figure 2.9: Outflow gust front caused by thunderstorm downburst, taken from Chay (2001).

The wind profile created by downbursts is not a normal boundary layer profile as caused by frontal or synoptic winds. Synoptic winds are usually mature and have a well-developed boundary layer profile. Downburst wind profiles cause peak wind speeds closer to the ground due to the increased pressure. ISO 4354:2009 provides an equation which may be used to calculate the profile of the peak wind speeds for thunderstorms, which is given in Equation 2.2.11 and plotted in Figure 2.10. As reported by Choi (2004), this profile is typically only applicable

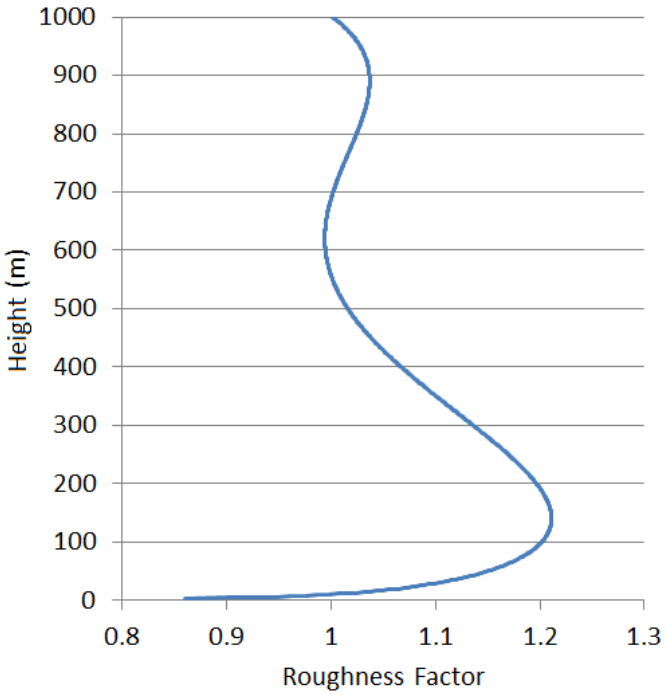

Figure 2.10: Thunderstorm terrain roughness factor profile using ISO 4354:2009 stipulations.

near the source of the downburst as the surface roughness has little effect on the profile. As the gust front moves away from the source, the surface roughness has a greater effect and the profile gradually develops into a boundary layer profile.

$$k_{tr} = 0.821 + 7.55 \times 10^{-4} \times z - 6.75 \times 10^{-6} \times z^2 + 1.06 \times 10^{-8} \times z^3 - 4.97 \times 10^{-12} \times z^4 + 0.079 ln(z - 1.4) \tag{2.2.11}$$

where, k_{tr} is the peak wind speed normalized by the wind speed at 10m above ground level

z is the height above ground level

It is clear from Figure 2.10 above that the thunderstorm profile is significantly different to the typical boundary layer profile across most of the height range shown. However, at lower heights which are considered for typical low-rise buildings the profile has a similar form to that of a typical boundary layer profile. The primary concern regarding thunderstorm winds is therefore not the use of boundary layer profiles, but rather the nullification of terrain categories. As terrain roughness has limited effect on the wind speed near the source of a thunderstorm downburst, the reduction in wind speed for rough terrain such as urban environments may not be justified where thunderstorms are the primary wind generating mechanism. This is especially relevant to structures of higher reliability classes as the return periods for design

loads used to design such structures are longer. This increases the probability that an extreme event such as a downburst will occur within the lifetime of the structure.

Along with the temporal uncertainty of thunderstorm downbursts, an important factor to consider is their spatial uncertainty. Although thunderstorm weather systems may be very large, downbursts are typically smaller and cause localized extreme winds, as reported by Goliger (2002). This further reduces the probability of a downburst affecting a specific structure being designed. Due to this small probability, it has historically been assumed that the provisions given by wind load standards for synoptic winds are adequate enough to incorporate both thunderstorm winds and synoptic winds. It is unclear, however, whether this approach is applicable in a wind climate such as South Africa's where thunderstorms dominate over a significant part of the country.

The effects of thunderstorms on wind load uncertainties is not investigated further in this study. It is however important to note that thunderstorms may have a significant influence on the wind load formulation, especially in South Africa. Further research is required in order to determine how to treat thunderstorm winds in terms of wind load reliability.

2.2.6 Wind directionality

Wind directionality is a broad term that relates to the various influences that a change in wind direction may have on the wind loading on a structure. There are two primary types of wind directionality effects. The first is the influence of small changes in wind direction and variation of wind direction from orthogonal to the building faces, and the second is the influence of the macro-climatic wind conditions at the site of the structure.

In most wind load standards, including SANS 10160-3, wind loading on structures is calculated using multiple load cases in which the wind is considered in each as blowing orthogonally onto one of the faces of the structure. It is assumed that the maximum load effect will be obtained when the wind blows in this orthogonal direction. This holds true for most regular structures, as indicated by results from wind tunnel and full-scale investigations such as those done by Zisis and Stathopoulos (2009) and Doudak *et al.* (2009), which is discussed in further detail in Section 5.1. However, it should be noted that surrounding topography may have a significant influence as it is possible that wind acceleration may occur for some oblique wind

directions or shielding may occur for the orthogonal wind directions. Such effects are not a factor of wind directionality, but rather of topography, as discussed in Section 2.2.3.2 above, but it should be remembered that these components are closely linked.

The problem with designing structures for orthogonal wind directions is that due to the intrinsic variability of wind the direction is very rarely constant. Even in locations where the predominant wind direction is orthogonal to the building, the wind direction will still fluctuate rapidly. Considering this fluctuation in addition to the temporal wind speed fluctuation due to wind gusts, it is clear that the occurrence of peak extreme wind loads acting perfectly orthogonally is highly unlikely. As such, the base assumption of orthogonal wind loads is inherently conservative.

The macro-climatic wind conditions at the site of the structure also have a significant influence on the wind loading on the structure. Most areas have one or two prevailing wind directions due to the wind climate in that area. It therefore stands to reason that the wind speed exceeded for a specified probability can differ for different directions. As such, designing the structure for peak wind speeds from all orthogonal directions will result in an inherently conservative design.

Although the South African wind load standard does not address wind directionality directly, other wind load standards do account for the conservatism due to wind directionality. As stated by Isyumov *et al.* (2014) there are two approaches to incorporating wind directionality factors. The first is to specify a reduction in the design speed for a particular azimuth sector, based on the analysis of extreme wind speeds for the different wind directions done on a sector by sector basis. This approach is used in the British National Annex to Eurocode, BS-NA-EN (2010), and the Australian and New Zealand standards, AS-NZS (2011). This approach is entirely dependent on the wind climate of the specific region, and as such comparison of the wind directionality stipulations in those standards does not yield any noteworthy results which may be applied to the South African wind load standard.

Using an azimuth reduction scheme for wind directionality in South Africa would be challenging due to the strong wind climate and the size of the country. Figure 2.11 shows the movement of air masses and the prevailing wind directions across Southern Africa during summer and winter months. As seen from the figure, there are multiple different wind directions at different locations, with no single dominant wind direction across the country. Furthermore,

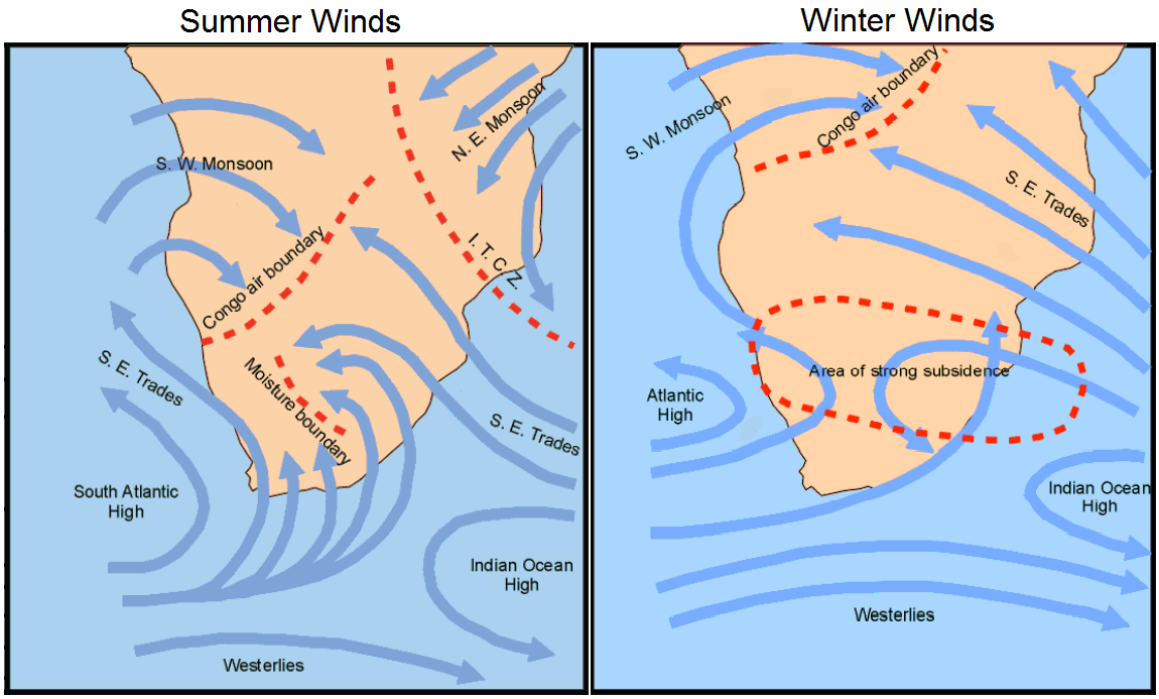

Figure 2.11: Prevailing movement of air masses across Southern Africa during summer and winter months. (Reproduced from Szewczuk and Prinsloo (2010))

there is a significant difference in the prevailing wind directions during summer and winter months. As such, a single set of azimuth wind directionality reduction factors would not be sufficient. For this reason, this approach is disregarded for the remainder of this investigation.

The second approach to incorporating wind directionality factors is to use an across-the-board reduction of wind loads using a single wind directionality factor. The United States wind load standard, ASCE (2010), stipulates that all wind loads be modified with a factor of 0.85 to account for wind directionality effects. Various studies have been done to investigate the ASCE wind directionality factor. Ellingwood and Tekie (1999) performed an expert opinion analysis and found a wind directionality factor of 0.86 for wind loads on main wind force-resisting systems, although it was recommended that allowances for wind directionality should be made on a case-by-case basis. Rigato *et al.* (2001) used a database-assisted design method and found that wind directionality reduction factors are dependant upon mean recurrence interval. They recommended a blanket wind directionality factor of 0.86 for a 50-year mean recurrence interval and 0.95 for a 500-year mean recurrence interval.

The uncertainties due to wind directionality is not considered in further detail in this investigation. However, the use of wind directionality in a final probability model of wind loading is essential as exclusion of the factor may lead to significantly overconservative design stipulations.

Chapter 3

Wind Load Probability Modeling

Reliability investigations are a dual process composed of the technical knowledge of the system being investigated and the reliability treatment of the variables which make up that system. Where the groundwork for the technical wind engineering expertise relating to the general wind load formulation was laid in the previous chapter, this chapter discusses the reliability and probabilistic modeling basis of this investigation. For the ultimate results of this investigation to be of any value, it is not enough that the data and information upon which the results are based be trustworthy. It is also imperative that the treatment of that data and information be logically sound and done in such a way that the results truly reflect the uncertainties in the system being investigated. The discussions in this chapter aim to show that this is indeed the case in this investigation.

Firstly, an overview of structural reliability is provided. The nature of uncertainties and the characterization of different types of uncertainties are then discussed. The general procedure followed for reliability modeling of the wind load formulation is presented and existing probabilistic wind load models are outlined and compared. The general treatment of data and reliability information in this investigation is then detailed. Finally, the reliability and statistical techniques which are used throughout the following investigation are developed and presented in an abstract sense, with the specific implementations of these methods described in the dissertation where appropriate.

3.1 Overview of structural reliability

As described by Melchers (1999), structural reliability is concerned with the prediction of the probability of a given condition, typically defined as a limit state, being exceeded for a structural system. These limit states may describe the serviceability condition of the structure or the ultimate limit state which relates to the structural safety. In this investigation only the ultimate limit state will be considered. The basis of structural design is defined by the performance function or simple limit state function ($g(R, Q)$) shown in Equation 3.1.1. The function describes the structural performance using two variables, the structural resistance (R) and the load effect (Q). Nowak and Collins (2000) explains that the limit state is defined as the boundary between adequate performance and failure when $g = 0$. In terms of structural safety, if $g \geq 0$ the structure is safe, whereas $g < 0$ results in structural failure. The probability of failure of the structure (p_f) may be calculated mathematically using Equation 3.1.2.

$$g(R, Q) = R - Q \tag{3.1.1}$$

$$p_f = P(R - Q < 0) = P(g < 0) \tag{3.1.2}$$

In order to calculate the probability of failure according to the limit state, it is necessary to treat the variables in the limit state function probabilistically. As stated by Nowak and Collins (2000), the variables R and Q may be treated as continuous random variables, with the uncertainty of each variable described by a probability distribution. This results in the residual, $R - Q$, which is referred to as the safety margin, being a random variable described by its own distribution. By determining the area of the safety margin distribution which is less than zero the probability of failure may be calculated. This is shown graphically in Figure 3.1.

Structural reliability is closely linked with codification of structural design procedures. The ultimate goal of structural reliability is to develop design standards in such a way that the probability of failure of structures designed using those standards is limited to an acceptable value. This limiting probability of failure is referred to as the target level of reliability, and is commonly expressed in terms of the reliability index β. Holický (2009) formally defines β as a negative value of the standardized normal random variable corresponding to the probability of failure. As described by Melchers (1999), several design formats have been used for ensuring structural safety in standards, including the safety factor or allowable stress method, the load

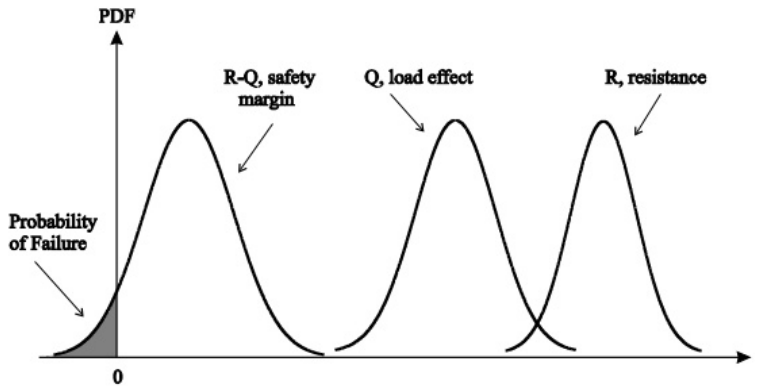

Figure 3.1: Probability distributions of structural resistance, load effect and the safety margin, reproduced from Nowak and Collins (2000).

factor method, and the load and resistance factor design or partial factor method. The partial factor method forms the basis of design for most modern design standards. The Probabilistic Model Code by JCSS (2001-2002) describes the general approach to the basis of structural design using the partial factor method. The partial factor method also forms the basis of design for Eurocode and the South African structural design standard, SANS 10160-1. As this investigation is specifically related to the South African environment, only the implementation of the partial factor method in South Africa is considered.

The partial factor method is based on the design value approach. As described by Holický (2009), the design value approach states that if a structural design is verified such that no limit state is exceeded when the design values of structural resistance R_d and load effect E_d are used, the structure is considered reliable. The design values of basic variables are not expressed directly in the design standards. Instead, characteristic or nominal values are specified which are converted to design values by factoring them with partial factors (γ). The formulation of structural design verification of the ultimate limit state in SANS 10160-1 as well as the relevant factors in the formulation are shown in Equations 3.1.3 to 3.1.5. In typical design situations the design verification is performed for individual elements in the structural system as opposed to verification of the system as a whole.

$$E_d < R_d \tag{3.1.3}$$

$$E_d = E(\Sigma\gamma_{F,i} \times \psi_i \times F_{k,i}) \tag{3.1.4}$$

where, $E()$ is the function defining action effects

$\gamma_{F,i}$ is the partial factor for the action effect

ψ_i is the combination factor to account for the probability of simultaneous actions

$F_{k,i}$ is the characteristic value of the action effect

$$R_d = \frac{1}{\gamma_R} R\left(\frac{x_{k,i}}{\gamma_m}\right) \tag{3.1.5}$$

where, γ_R is the partial factor for the resistance model

$R()$ is the function defining structural resistance

$x_{k,i}$ is the characteristic value of the material property

γ_m is the partial factor factor for the material property

By converting characteristic and nominal values to design values, the partial factors in these equations account for uncertainties in the basic variables. Calibration of partial factors is the primary method by which the target reliability level of the design formulation is attained. The first step toward reliability calibration is reliability assessment of a given design situation. There are several methods which may be used for such assessments, including basic Monte Carlo simulation methods or more sophisticated reliability methods such as First Order Reliability Method. These methods are well established and clearly documented by authors such as Nowak and Collins (2000) and Schneider (2006). To calibrate partial factors, these methods are used to assess multiple design situations with varying parameters such as different structural configurations, material types, and load ratios. Partial factors are then developed in such a way that the design stipulations result in adequate reliability performance across the scope of the design standard being considered.

It is clear from the general overview of structural reliability that the calibration of structural design standards, and by extension the levels of safety achieved by those standards, is dependent on the initial reliability treatment of basic variables as random variables. In order to enable accurate calibration of partial factors, accurate models of the uncertainties inherent in the basic variables are required. The research presented in this dissertation aims to develop such a model, namely a probabilistic model of wind load effects. A overview of the general sources of uncertainties in the design wind load formulation was given in Chapter 2. This Chapter

presents the information required to quantify those uncertainties.

3.2 Uncertainty characterization

In order to develop a probabilistic wind load model, it is important to consider what such a model represents. The uncertainties quantified by a model are as much dependent on the variable being quantified as the purpose for which the model is to be used. In the case of the design wind load formulation, the purpose of the wind load model is not only to represent the uncertainty of the wind loads in general, but rather to represent the uncertainty of the wind loading on any structure calculated using the specific wind load standard which that model represents, which in this investigation is the South African wind load standard. This is required so that the model may be used for reliability assessment and calibration of the standard. The uncertainties which need to be considered are therefore not only those inherent in the physical process of wind loading, but also the uncertainties introduced in modeling of the wind load in the wind load standard. It is therefore important that the nature of the uncertainties and how those uncertainties are represented are understood.

Der Kiureghian and Ditlevsen (2009) discussed the nature of uncertainties and the manner of dealing with them within the risk and reliability context. They identified seven sources of uncertainty which may exist in engineering problems, namely:

1. Uncertainty inherent in the basic random variables which can be directly measured.
2. Uncertain model error resulting from selection of the form of the probabilistic model used to describe the distribution of basic variables.
3. Uncertain modeling errors resulting from selection of the physical models used to describe the derived variables.
4. Statistical uncertainty in the estimation of the parameters of the probabilistic models.
5. Statistical uncertainty in the estimation of the parameters of the physical models.
6. Uncertain errors involved in measuring of observations, based on which the parameters of both the probabilistic and physical models are estimated.

7. Uncertainty modeled by random variables corresponding to derived variables, which may include, in addition to all the above uncertainties, uncertain errors resulting from computational errors, numerical approximations or truncations.

It is the aim of any reliability investigation to identify these sources of uncertainty and to determine the extent to which they influence the model. It is not computationally possible to consider every single source of uncertainty for any variable. Computational effort must therefore only be expended on those uncertainties which have the greatest total influence on the model. In this investigation the primary sources of uncertainty in each of the wind load components under consideration have already briefly been outlined in Chapter 2. In the following chapters the reliability treatment of the wind load components is discussed in greater detail and the sources of uncertainty which are considered in this investigation are identified.

Although these sources of uncertainty are vastly different, they may all broadly be divided into two categories, aleatoric uncertainties and epistemic uncertainties. Aleatoric uncertainty, also referred to as statistical uncertainty, represents the intrinsic uncertainty of a physical process which cannot be altered. In other words, aleatoric uncertainties are representative of unknowns that differ each time the same experiment is run. Epistemic or model uncertainty refers to the uncertainty introduced by the imperfect modeling of a process. Epistemic uncertainty is unavoidable in most cases as it is nigh on impossible to perfectly model any system, however these uncertainties may be reduced by improving the model. By categorizing the uncertainties being considered, appropriate action may be taken as to how the uncertainties are to be treated probabilistically.

In addition to understanding the different types of uncertainties, it is also important to understand the influence of different uncertainties of the variable being considered. To this end it is necessary to subdivide the term "uncertainty" into two different concepts, namely systematic bias and variability. Together, the bias and variability compose the total uncertainty of a variable.

Systematic bias, which is quantified by the mean value of a probability distribution, represents the systematic shift between the observed "real world" values and the values predicted by the model. The bias is defined as the ratio of the observed values to the predicted values. As such, when considering loading a bias value of less than unity implies that the model gives

conservative predictions, whereas a bias value of greater than unity implies an unconservative model. The bias has the greater effect on the reliability of a variable as it effectively shifts the entire probability distribution toward overestimating or underestimating the process.

The variability, quantified by the variance or standard deviation of a probability distribution, is a measure of the spread of values around the mean. Although the variability may not have such a readily apparent influence on the total uncertainty of a variable, it should not be ignored. A high variability significantly influences the reliability of a component as the likelihood of extreme values (both above and below the mean value) is increased. Fractile values required to obtain a given reliability are therefore significantly higher for variables with high variability than for those with low variability.

3.3 Overview of probabilistic modeling of wind loads

As stated in the research objectives given in Section 1.2, the final output of this investigation is a new probabilistic wind load model for South Africa. The term "probabilistic model" has been used throughout the introductory sections of this dissertation, however it may be valuable to define what is meant by the term before continuing. Probabilistic models describe the uncertainty of a given system or process through the use of representative probability distributions of the components which make up that system. The model itself is not the final outcome of a reliability investigation of such a system, but rather a conglomerate of the information about that system which may be used in reliability analyses to draw conclusions and make decisions about the system.

Effectively, wind load probabilistic models are simply a collection of probability distributions, each of which represents the inherent uncertainty of a wind load component. It therefore stands to reason that the probabilistic model is directly related to the wind load formulation and the level of approximation considered. Not all probabilistic models have the same form as the number and complexity of the components of the formulation considered may differ. In order to clarify what is meant by this, consider the following: as already stated Chapter 2, gust factors are not investigated in this study as the South African free-field wind data is already based on gust values. The European free-field wind data is based on ten minute mean wind speeds, and as such gust factors are an integral part of the Eurocode wind load formulation.

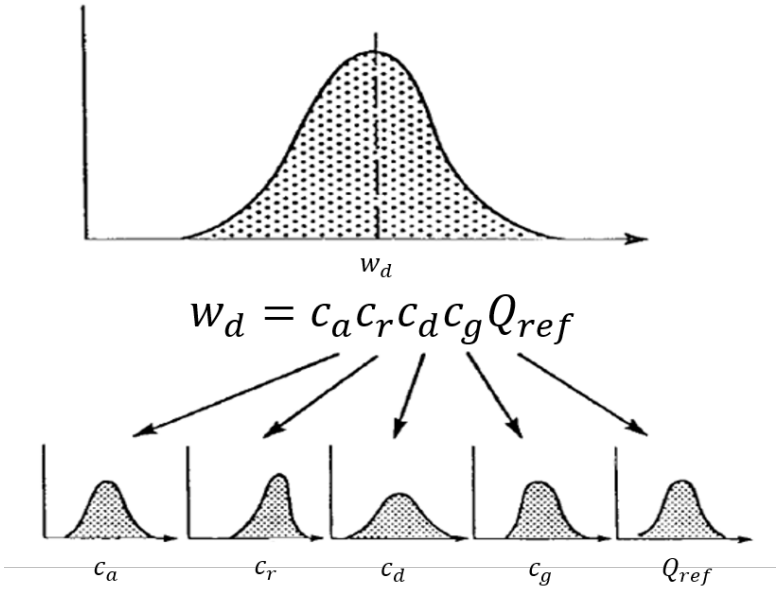

Figure 3.2: Davenport reliability model, reproduced from Davenport (1983).

The Eurocode probabilistic model therefore includes this additional component, whereas the model developed in this study does not.

Probabilistic models of wind loads are based upon the wind engineering formulation of the loads. As such, the probabilistic models used for assessment of wind load standards are based upon the wind loading chain developed by Davenport (1961). The wind engineering basis of this formulations is described in Section 2.1 and Equation 2.1.1. Davenport (1983) stated that within the wind loading chain, each wind load component should be regarded as an independent random variable, subject to its own uncertainties. Each component is therefore defined by a probability distribution which represents the uncertainties of that component. Davenport (1983) further showed that these uncertainties could be combined using standard reliability techniques such as Monte Carlo simulation or First-Order Reliability Method into a single representative distribution of design wind load uncertainties. This is shown visually in Figure 3.2. This framework describes the system level treatment of wind load uncertainties used in all the probabilistic models discussed in the following sections.

3.3.1 Existing wind load probability models

There are several existing probabilistic models for wind loads which have been used in the past for reliability assessment and calibration of wind load standards. As this study is specifically focused on the South African wind load formulation, the models related to the South African loading code were investigated in order to determine the state of affairs with regard to wind

load probability modeling at the time of writing. The latest South African loading code, SANS 10160:2011, uses Eurocode as a technology base. It was therefore decided to investigate the European probabilistic wind load models as well as the South African model. Furthermore, the probabilistic model used for reliability assessment of a previous version of the United States wind loading code, ASCE 7-95, was included in order to compare how the European and South African models compare with other international models. These models are discussed in more detail in the following sections. The analysis and comparison of these models serve as the primary motivation for the need to develop a new probabilistic model for South African design wind loads.

3.3.1.1 JCSS model

The JCSS model was developed by the Joint Committee on Structural Safety (JCSS) and is given in the JCSS (2001-2002) Probabilistic Model Code. The probabilistic model represents the design wind load formulation at the most basic level of approximation. The statistical parameters of the wind load factors are shown in Table 3.1. Note that the statistical parameters given in the table are normalized with respect to the characteristic value of the variable (X_k).

The JCSS model does not provide specific values for the wind load parameters, but rather intervals of suggested values. The derivation of these values is unclear, however, and it was reported by Holický (2009) that the indications provided in literature are inconclusive. Holický also suggested that any results obtained from reliability analyses using the the JCSS model be regarded as indicative findings only.

Table 3.1: JCSS (2001-2002) probabilistic model.

Variable	Symbol	Distribution	Relative Mean $[\mu_X/X_k]$	Standard Deviation $[\sigma_X/X_k]$	Coefficient of Variation $[w_X]$
50-year extremes of wind pressure	$q_{b,ref}$	Log-normal	0.80	0.16 - 0.24	0.20 - 0.30
Pressure coefficient	c_p	Log-normal	1.00	0.10 - 0.30	0.10 - 0.30
Gust factor	c_g	Log-normal	1.00	0.10 - 0.15	0.10 - 0.15
Roughness factor	c_r	Log-normal	0.80	0.08 - 0.16	0.10 - 0.20
Design wind pressure	W_{ref}	Log-normal	0.64	0.17 - 0.31	0.26 - 0.48

3.3.1.2 Holický/Eurocode models

The Holický/Eurocode models were primarily developed by Holický (2009). The models are refinements of the JCSS model with specific values chosen from within the intervals provided by the JCSS model. No motivation or data to substantiate the choices of values which were selected has been found. The distribution types were also altered. The free-field as well as the design wind are distributed using the conventional Type I Extreme Value distribution, also known as the Gumbel distribution, whereas the other wind load factors are distributed using normal distributions.

The Eurocode model has been used for reliability assessment of the Eurocode by Gulvanessian and Holický (2005). This model also takes the uncertainties inherent in the statistical modeling of a physical process into account by introducing a model coefficient, m_q. The statistical parameters of the wind load factors are shown in Table 3.2. It is interesting to note that in the Eurocode model a fairly high systematic bias value was assumed for the basic wind pressure, unlike the value provided in the JCSS model. The influence of this is however negated to some extent by the addition of the model uncertainty factor which has a low systematic bias value.

Table 3.2: Eurocode probabilistic model by Gulvanessian and Holický (2005).

Variable	Symbol	Distribution	Relative Mean $[\mu_X/X_k]$	Standard Deviation $[\sigma_X/X_k]$	Coefficient of Variation $[w_X]$
50-year extremes of wind pressure	$q_{b,ref}$	Gumbel	1.10	0.20	0.18
Pressure coefficient	c_p	Normal	1.00	0.10	0.10
Gust factor	c_g	Normal	1.00	0.10	0.10
Roughness factor	c_r	Normal	0.80	0.08	0.10
Model coefficient	m_q	Normal	0.80	0.16	0.20
Design wind pressure	W_{ref}	Gumbel	0.70	0.21	0.33

Holický (2009) also presented an alternative model with different parameter values and without the model coefficient, as shown in Table 3.3. This model was used to show that the Eurocode wind load partial factor of $\gamma_Q = 1.5$ is reasonable.

Table 3.3: Holický (2009) probabilistic model.

Variable	Symbol	Distribution	Relative Mean $[\mu_X/X_k]$	Standard Deviation $[\sigma_X/X_k]$	Coefficient of Variation $[w_X]$
50-year extremes of wind pressure	$q_{b,ref}$	Gumbel	0.80	0.20	0.25
Pressure coefficient	c_p	Normal	1.00	0.20	0.20
Gust factor	c_g	Normal	1.00	0.15	0.15
Roughness factor	c_r	Normal	0.80	0.12	0.15
Design wind pressure	W_{ref}	Gumbel	0.64	0.24	0.38

3.3.1.3 ASCE 7-95 model

The ASCE 7-95 model was presented by Ellingwood and Tekie (1999) and used for the reliability assessment of a previous version of the United States wind load standard, ASCE (1995). This model has the most complete background references detailing the sources used to determine statistical distributions to represent wind load components. These components are summarised in Table 3.4 below.

Table 3.4: ASCE 7-95 probabilistic model as presented by Ellingwood and Tekie (1999).

Variable	Symbol	Distribution	Relative Mean $[\mu_X/X_k]$	Standard Deviation $[\sigma_X/X_k]$	Coefficient of Variation $[w_X]$
50-year extremes of wind speed	v	Gumbel	1.00*	0.12*	0.12*
Pressure coefficient	c_p	Normal	1.00	0.12	0.12
Gust factor	c_g	Normal	1.00	0.11	0.11
Exposure factor	k_z	Normal	1.00	0.16	0.16
Directional factor	d	Deterministic	0.85	-	-
Design wind pressure	W_{ref}	Gumbel	0.78	0.29	0.37

The first thing to notice regarding the ASCE model is that wind pressure is not used as a basic variable, but rather the wind speed itself. As such the variable, and by extension the statistical distribution which describes the variable, needs to be squared in order to obtain the reference free-field wind pressure. Furthermore, Ellingwood and Tekie (1999) made the distinction that the wind speed is strictly site dependent, and did not attempt to determine a single representative distribution for the wind speed. The distribution parameters for this

variable presented in Table 3.4 are therefore purely indicative and denoted as such with "*". This distinction is important to note when considering other probabilistic models, as the free-field wind climate of every region will almost certainly be different, and as such it is never feasible to directly adopt the probabilistic model for free-field wind developed for a different region.

The distribution parameters for pressure coefficients were determined from four studies which included both wind tunnel and full-scale tests. These studies by Peterka and Cermak (1975), Marshall (1977), Cook and Mayne (1979) and Stathopoulos (1980), and the techniques used in them are fairly dated, however they still serve as a valuable reference point when starting the investigation of pressure coefficient uncertainties. According to Ellingwood and Tekie (1999), information on the gust and exposure factors relied on engineering judgement.

Finally, the distribution of the design wind pressure W_{ref} for this model was not calculated using the product of means to determine the systematic bias and the square root of the sum of the squares of the coefficients of variation to determine the variability, as done in the other probabilistic models. As mentioned above, Ellingwood and Tekie (1999) determined that the free-field wind distributions should remain site specific. Seven stations were used to determine typical statistics, all of which were situated in non-hurricane prone regions. The locations of these stations are not specified. The distribution of W_{ref} was determined by numerical integration for each station and a Type I Extreme Value (Gumbel) distribution was fitted to the largest values in the 90th percentile and above for all the stations, the region that is significant for structural reliability analysis.

3.3.1.4 Milford/SANS models

The probabilistic model of the South African wind load process was developed by Milford in the 1980's. This model is similar to the Holický model, however there are a few differences with regard to the level of approximation of the models. The first difference is the combination of the pressure coefficient and gust factor into a single factor, referred to as the exposure factor. The Milford model also includes an additional level of approximation by the addition of a directionality factor, which is used to represent the variability of the direction of the wind. Milford (1985*a*) used Monte Carlo simulation to determine the statistical parameters for the representative design wind distribution.

The values for the statistical parameters of the individual wind load factors and the final representative distribution were obtained from a technical report written by Milford (1985*a*), and are shown in Table 3.5. A journal article was later published in the *Civil Engineer in South Africa* by Kemp *et al.* (1987) in which the statistical parameters of loads to be used in the South African loading code were published. The parameters of the lifetime maximum design wind load published in this article were different from those given in the 1985 report. The article parameters are given in Table 3.6 and were used for reliability calibration of the latest version of the South African Loading Code, SANS 10160. To avoid ambiguity, the distribution given in the article is referred to as the SANS model from here onwards.

Table 3.5: Milford probabilistic model (1985 technical report).

Variable	Symbol	Distribution	Relative Mean $[\mu_X/X_k]$	Standard Deviation $[\sigma_X/X_k]$	Coefficient of Variation $[w_X]$
50-year extremes of wind pressure	$q_{b,ref}$	Gumbel	1.02	0.17	0.16
Exposure factor	c_e	Normal	0.70	0.14	0.20
Roughness factor	c_r	Normal	0.80	0.16	0.20
Model coefficient	m_q	Normal	1.00	0.15	0.15
Directional factor	θ	Normal	0.90	0.09	0.10
Design wind pressure	W_{ref}	Gumbel	0.52	0.25	0.48

Table 3.6: SANS model by Kemp *et al.* (1987).

Variable	Symbol	Distribution	Relative Mean $[\mu_X/X_k]$	Standard Deviation $[\sigma_X/X_k]$	Coefficient of Variation $[w_X]$
Design wind pressure	W_{ref}	Gumbel	0.41	0.21	0.52

One explanation for the discrepancy between these two sources may be that a simple a data transfer mistake occurred. Tables 3.8 and 3.7 were taken directly from the 1987 article and 1985 report respectively. Considering the arbitrary point-in-time wind statistics, it can be seen that the nominal mean (W/W_n) and coefficient of variation (v_w) values of the two tables correspond. However, for the lifetime maximum wind statistics, it appears that the nominal mean value used in the article was taken from the value for the mode (u) in the report, and

the value for the coefficient of variation in the article taken from the nominal mean value in the report.

Table 3.7: Milford design wind load statistics (1985 report) Milford (1985*a*).

ARBITRARY POINT-IN-TIME	
α	0,034
k	0,923
$\bar{W}/W_n$	0,050
V_W	1,08
CDF	WEIBULL
LIFETIME MAXIMUM	
u	0,406
a	5,230
W/W_n	0,52
V_Q	0,475
CDF	TYPE I

Table 3.8: Milford design wind load statistics (1987 article) Kemp *et al.* (1987).

Type of load	*Code*	*Mean nominal*	*Coefficient of variation (v)*	*Type of distribution*
Dead (permanent) load	ANSI A58.1 Australian SABS 0160	1,05 1,05 1,05	0,10 0,10 0,10	Normal Log-normal Log-normal
Live (office): lifetime maximum	ANSI A58.1 Australian SABS 0160	1,0 0,7 0,96	0,25 0,26 0,25	Type I Type I Type I
Live (office): 'point-in-time'	ANSI A58.1 Australian SABS 0160	0,25 0,19 0,25	0,71 0,79 0,60	Gamma Weibull Gamma
Wind: lifetime maximum	ANSI A58.1 Australian SABS 0160	0,78 0,30 0,41	0,37 0,43 0,52	Type I Log-normal Type I
Wind: 'point-in-time'	ANSI A58.1 Australian SABS 0160	0,0097 0,022 0,05	6,95 0,94 1,08	Type I Weibull Weibull

3.3.2 Comparison of existing models

In order to compare the probabilistic models discussed in the previous section, First-Order Reliability Method (FORM) analyses were performed. FORM is a reliability method used

to calculate the highest probability of a given limit state function being true. The variables in the limit state function are considered as independent statistical variables, each with its own statistical parameters. This makes FORM a powerful tool for analysing multivariate probabilistic models, such as the wind load models. The basic FORM implementation as described by Holický (2009) was used in this investigation.

The FORM analyses were performed using the multivariate representation of each model. The limit state functions used in this analysis follow directly from the basic wind load equation (Equation 2.1.1) and the level of approximation of each model. A different limit state function was set up for each model using the given statistical parameters for each factor. For the JCSS model, which does not provide specific values for the statistical parameters of the factors used, the upper and lower bound values were used. These functions are given in Equations 3.3.1 to 3.3.4. For the ASCE model, a multivariate model using the indicative parameters given in Table 3.4 was used as well as a single variable model using the final distribution parameters for the design wind speed. The single variable model resulted from a Gumbel distribution fitted to results from the seven stations used in the study, as discussed in Section 3.3.1.3. Finally, for the SANS model, it was impossible to establish a multivariate model and as such only a single variable analysis was done.

JCSS and Holický Models Limit State Function:

$$q_{b,ref}\, c_p\, c_g\, c_r - w_d = 0 \tag{3.3.1}$$

Eurocode Model Limit State Function:

$$q_{b,ref}\, c_p\, c_g\, c_r\, m_q - w_d = 0 \tag{3.3.2}$$

ASCE Model Limit State Function:

$$v^2\, c_p\, c_g\, k_z\, d - w_d = 0 \tag{3.3.3}$$

Milford Model Limit State Function:

$$q_{b,ref}\, c_e\, c_r\, m_q\, \theta - w_d = 0 \tag{3.3.4}$$

In these functions, w_d is not a statistical variable used to model the representative distribution of values for the design wind pressure, but rather a deterministic variable representing a

specific value. It should be noted that all parameters in the probabilistic models are normalized with respect to their characteristic values which are based on the return period of the characteristic wind speed. Therefore, w_d is the design wind pressure normalized with respect to the characteristic wind pressure. Furthermore, due to the normalization, w_d can be interpreted as the partial factor that will achieve the corresponding reliability index according to the relevant probability model, denoted as γ_w.

The deterministic variable was varied parametrically in order to determine the highest probability of the limit state function being true for different design wind pressures. A FORM analysis was performed for each limit state function for values of w_d (or γ_w) ranging from 0.5 to 2.5 using an interval size of 0.1. This effectively produces the tail-end of the cumulative probability distributions for the different models. The results are shown in Figure 3.3.

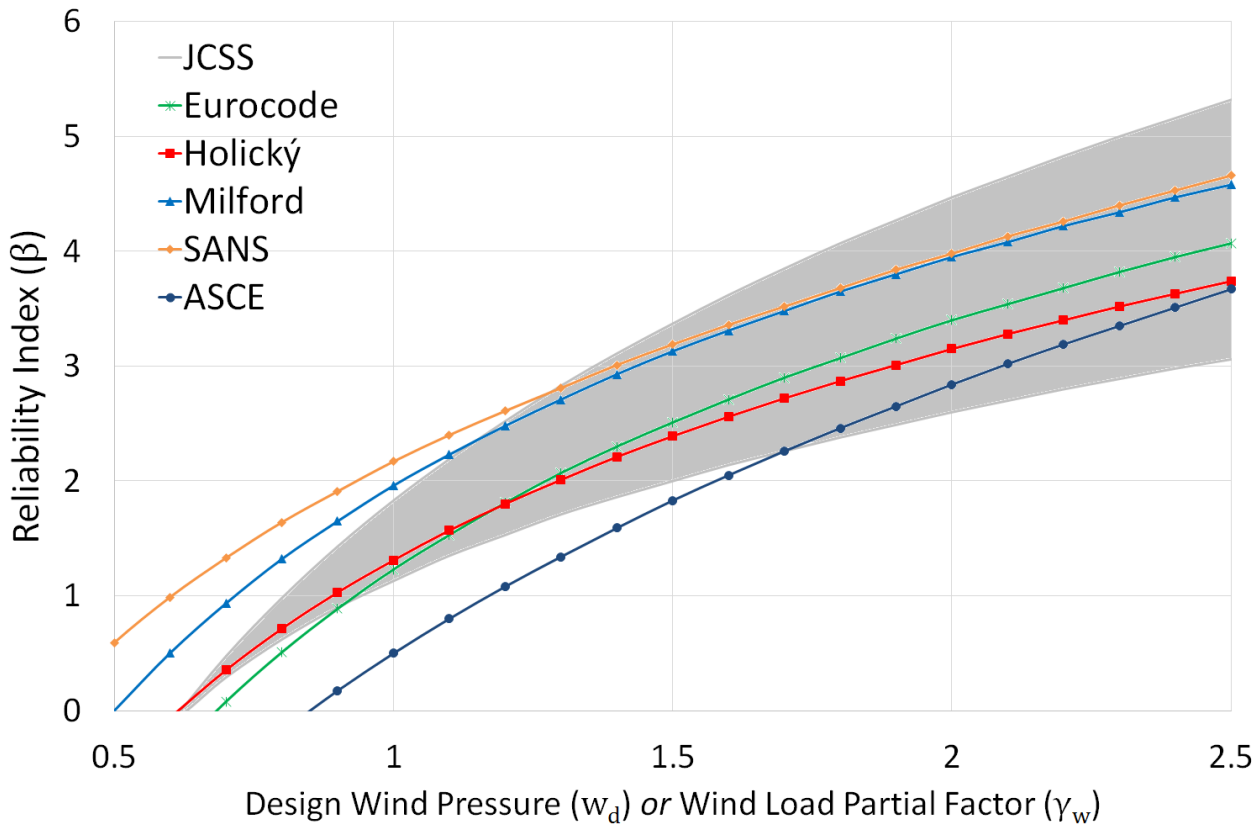

Figure 3.3: Results from multivariate FORM analysis of existing models.

The results show the significance of the difference between the probabilistic models. It is illustrated most clearly when considering specific reliability index values. The baseline target reliability index values (β_T) for Eurocode and South African loading codes, which are 3.8 and 3.0 respectively, were multiplied by the standard sensitivity factor for action effects (α_E) of 0.7

as stipulated in Eurocode. The Eurocode stipulations regarding this sensitivity factor state that it is applicable for typical design situations where the ratio of the standard deviations of loading and structural resistance (σ_E/σ_R) is between 0.16 and 7.6. As the scope of this investigation is limited to the global loading of typical structures, it may safely be assumed that this condition holds. The resultant target reliability ($\alpha_E\beta_T$) values associated with the loading component of a structural reliability assessment are 2.66 and 2.10, and are shown on Figure 3.3. The normalized design wind pressure or partial factor required to obtain the reliability indices was then found for each of the models. These values are summarised in Table 3.9.

Table 3.9: Required normalized design wind pressure (partial factor) to achieve target reliability indices using existing probabilistic models.

Model	w_d ($\alpha\beta = 2.10$)	w_d ($\alpha\beta = 2.66$)
JCSS (lower limit)	1.08	1.25
JCSS (upper limit)	1.57	2.05
Eurocode	1.31	1.57
Holický	1.35	1.66
ASCE (Indicative)	1.63	1.91
ASCE (Fitted)	1.55	1.91
Milford	1.05	1.28
SANS	0.97	1.22

A number of observations and conclusions may be drawn from these results. The first observation serves as a clarification of the differences in partial factor between Eurocode and the South African loading code. Where Eurocode uses a partial factor of $\gamma = 1.5$, SANS uses a value of $\gamma = 1.3$. Retief and Dunaiski (2009) explained that the lower South African partial factor derives from the anomalously low design wind pressure systematic bias in the South African wind load probability model. These results clearly illustrate this, as the design wind pressures required to achieve a target reliability level using the Eurocode and Holický models are consistently greater than the values required to reach the same target reliability level when using the Milford and SANS models.

Another significant conclusion is the importance of developing reliability models of wind loads based on transparent and reliable information. Consider the JCSS model which provides an envelope of possible values, as shown by the shaded area in Figure 3.3. By comparing the design wind pressures required to achieve the same target reliability level using the upper and lower limits of this model, we find that the values differ by as much as a factor of 1.64 when

using the Eurocode reliability index. Simply looking at these models serves as an indication of the uncertainties inherent in the modelling of design wind loads. The fact that the JCSS model was developed using unclear background information simply adds to this uncertainty.

This investigation of the existing wind load probability models reveals a number of factors which call the trustworthiness and accuracy of the existing wind load probability models into question. These include:

- the discrepancies between the South African and European probability models;
- the discrepancy between the Milford model and the SANS model used for reliability calibration of SANS 10160;
- the overall lack of consensus on wind load uncertainties, illustrated by the wide range of values obtained using the different models; and
- the lack of background data and information used to develop these models.

These points serve as the primary motivation behind this investigation. The problem statement, already discussed at length in the introductory chapters of this dissertation, is reinforced by the conclusions drawn from this section. The necessity of a new wind load probability model based on transparent data and information is therefore made abundantly clear within the context of reliability assessment and calibration of the design wind load formulation, specifically within the South African environment.

3.4 Reliability basis of investigation

Arguably the most critical part of any reliability investigation is the data and information upon which the investigation is based and how that data is used to represent the uncertainties inherent in the system under investigation. As discussed in the previous section, a probability model which is not based on reliable sources is in itself unreliable, and the use of such a model effectively negates the purpose of any reliability assessment. Obtaining reliable data and information may be challenging, however, particularly when considering complex systems such as the design wind load formulation. This section outlines the reliability basis of this investigation.

One of the greatest challenges faced in this investigation was the enormity of the scope of design situations which needed to be considered. The final probabilistic model of design wind loads for a specific wind load standard, in this case SANS 10160, should effectively be representative of all the uncertainties inherent in the calculation of wind loads for any basic design situation that falls within the scope of applicability of that standard. The implication is that, when incorporating all the restrictions of the scope of this investigation, the final probabilistic wind load component models developed in this dissertation aim to represent the uncertainty of those components for any basic structure anywhere in South Africa as accurately as possible. The primary challenge then was to use as much information and data as practically possible which describe the uncertainties of as many design situations as possible. Therefore, as with most reliability investigations, this investigation was based not only on pure data extracted from observations, but also on supporting information and metadata.

In order to systematically and effectively use all available data to obtain the most accurate estimates of the wind load component uncertainties, two complementary methodologies were used to process the available information. The first method was the direct use of statistical data where available, such as comparison of codified values with data obtained from observations. The second method was an indirect use of the available information through the comparison of the codified values stipulated in different major international wind load standards. This two-pronged approach is visually represented in Figure 3.4. The methodologies are described in greater detail in the following sections.

An important consideration in any reliability investigation, regardless of whether it is based on pure data or supporting information, is to ensure that the observations which are used are predominantly statistically independent. This is necessary to effectively represent the entire sample space under consideration whilst avoiding results which are biased towards specific points in the sample space where more data is available. Throughout this investigation care was taken to ensure unbiased sampling, and the specific procedures employed to achieve this are described where applicable.

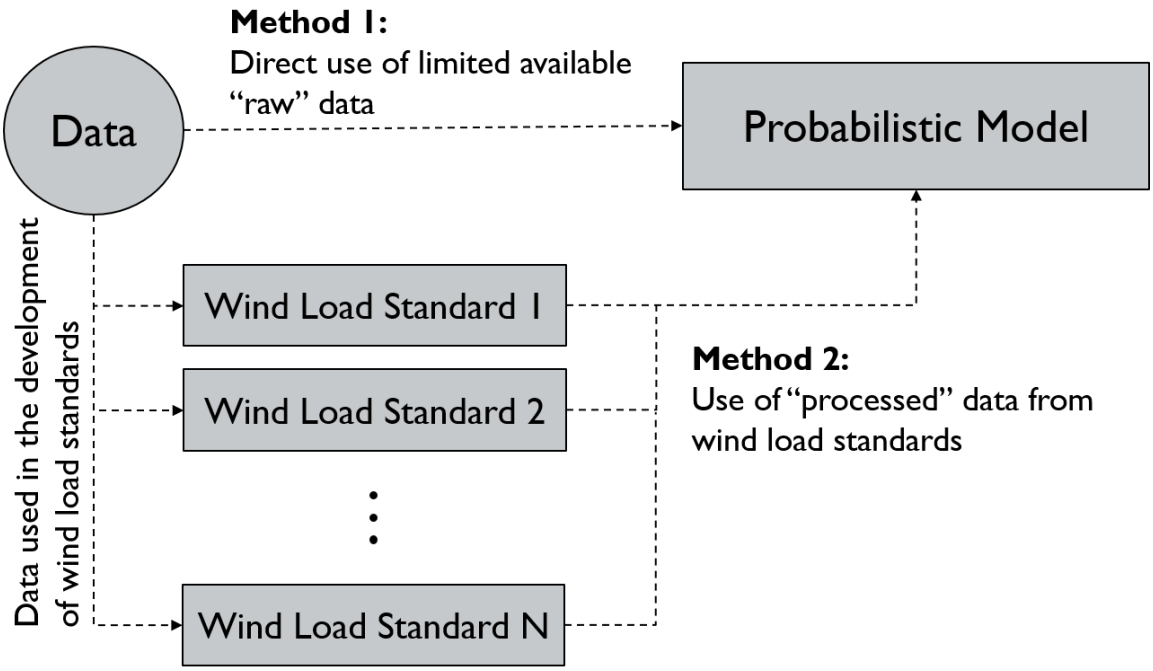

Figure 3.4: General reliability investigation approach followed.

3.4.1 Comparison of codified values and observed values

Direct comparison of observed values is a standard statistical technique and is the most effective way of quantifying uncertainties in a given variable. By this method the codified values of a given standard are compared to data obtained from wind tunnel and full-scale tests. The statistical parameters estimated by this method reflect the true aleatoric uncertainties in the variable.

Although the direct comparison of codified values with observed values does allow for a reasonable estimation of the wind load component uncertainties to be made, this estimation is not entirely accurate due to the differences between the sources and the epistemic uncertainties inherent in measuring data. Consider pressure coefficients as an example. Pressure coefficients from wind tunnel and full-scale tests are typically calculated using measurements from pressure taps across the structure. As the measurements are taken simultaneously, the correlation between pressures across the structure may be calculated. It has been shown that due to wind gusts the peak design pressure does not occur at all points across the structure simultaneously. However, the pressure coefficients given in wind load standards represent equivalent static load distributions of the design wind pressure on a structure, which implies that the design loading does act across the entire structure simultaneously. There is therefore a certain measure of conservatism built into the codified pressure coefficients as the true pressure distributions are

not fully correlated, both spatially and temporally. This conservatism is not reflected in a direct comparison with observed values.

Another source of uncertainty which needs to be considered when using this method is the lack of standardized testing methods and the consideration of tests of various types, which may reflect greater variability than the true variability of the pressure coefficients. Furthermore, as this study aims to investigate a large portion of the scope of applicability of most wind load standards, this method requires a large number of observations from multiple tests as each observation only provides information regarding a specific design situation. It is not possible to obtain information about every design situation within the sample space of this investigation, and therefore the statistical parameters estimated by this method will be based on a fairly limited set of observations. It should however be noted that an effort was made to ensure that the selected situations should be representative of the basic case of codified design which is investigated. Taking these factors into consideration it may be assumed that this method provides an upper bound approximation of the true uncertainties of the wind load components.

3.4.2 Comparative studies of wind load standards

The comparison of wind load standards has been used in the wind engineering community by researchers such as Bashor *et al.* (2009) as means of illustrating the large discrepancies between different wind load formulations. In this investigation the comparison of standards is used as a reliability technique to estimate the statistical parameters of wind load component probability models. It is not a statistical method applied using pure data, but one that is based on the use of supporting information. The primary advantage of this method is that all design situations which fall within the scope of applicability of the wind load standards may be investigated and a truly representative statistical model of wind load uncertainties may be developed.

In order to understand how the comparison of wind load standards may be used as a method for estimating wind load component uncertainties, the wind load standard development process should be considered. Firstly, background information and research regarding wind load components are converted into operational models to describe design wind loads. These models are then modified and adapted into practical design procedures which systematically cover the scope of the required design situations. The background operational models are the closest

representations of the wind load components, and comparison of those models would provide the closest approximation of the wind load component uncertainties. However, without clear background documentation detailing the development of the standards, as is often the case, these models are not readily accessible. The wind load standards themselves are accessible, and may serve as a representative source of information in order to estimate the uncertainties inherent in the wind load components.

Wind load standards were compared in this study using an analysis in which each wind load standard is regarded as an independent expert opinion. Expert opinion analysis as a tool for determining statistical parameters for wind load components is a well established reliability technique. An example which has already been cited in this investigation is the study by Ellingwood and Tekie (1999) which used the Delphi methodology to determine wind load component statistics from wind engineering experts. Another example is the study done by De Wit (1999) which investigated uncertainty in pressure coefficients on low-rise buildings using expert opinions. In this study however individual people were not used. Instead, the collective knowledge used to develop wind load standards allows the standards to be considered as "experts".

A method was developed for the comparison of wind load standards as expert opinions. Although applied to a very specific case here, the method may be abstracted to be used in any situation where independent secondary sources of information are used to find reliability information. When considering wind load components, the method relies on two critical assumptions: first, the independence and reliability of wind load standards, and second, a lack of measured data or any way to determine the "true" wind load component values.

The independence and reliability of wind load standards requires that wind load component stipulations given in each wind load standard considered be developed using different sources, all of which are assumed to be trustworthy sources of information. The implication of this assumption is that any difference between the codified values of two standards when considering the same design situation reflects the epistemic uncertainties which exist due to the codification process. Furthermore, this assumption also requires that each wind load standard be regarded as equally reliable, i.e. no standard is assumed to be more correct than another.

The assumption regarding the lack of measured data is clearly not true as the other methodology used in this study is the direct comparison of codified values with observed values. How-

ever, the assumption is required in order to establish how theoretically correct answers are defined. Consider a case in which a wind load component needs to be determined for a given design situation. If it is possible to get measured data of the component for the specific design situation there would be no need for any further investigation. Unfortunately, as stated in the section above, there is a limited amount of measured data which is readily available and as such the available data is only applicable for cases which fall within a limited scope. Assuming the design situation falls outside the scope of the available data, an alternative method needs to be used to calculate the "correct" value of the wind load component. Using the first assumption of independence and reliability of wind load standards, it stands to reason that the closest approximation to the true value would be the average of the values stipulated by the different standards. The true value is therefore estimated using the pooled information and body of knowledge used to develop the respective wind load standards. By comparing the values stipulated by different standards, the statistical parameters of the wind load component for the specific design situation may be estimated. By varying the design situation parametrically and repeating the process statistical parameters for a wide range of design situations may be estimated. This process is the basis which was used to determine representative statistical parameters for the wind load components.

An algorithm was developed to implement the method described above. The algorithm is generic and may be used to determine the statistical parameters for a given sample space in any system where there is limited measured data but multiple models or alternate sources of information are available. The algorithm is shown graphically in Figure 3.5.

The first step is to define the target variable which is to be investigated (v) which is a function of a number (L) of parameters (z_i). Once the parameters have been defined, a sampling space (S) is defined by specifying discrete sets of possible values for each of the parameters ($z_{i,1},...,z_{i,M}$). Each parameter's sampling set may have a different size (M_i). A set of the sources of information (C) consisting of a number (N) of independent sources (c_k) is then defined. In this investigation design standards are the sources of information. A reference case (R) is then defined by selecting specific values ($z_{i,ref},...,z_{L,ref}$) for each of the parameters from within the sampling sets.

Each parameter is varied parametrically across its sampling set in turn as the other parameters remain at their respective reference values. The value of the target variable is calculated

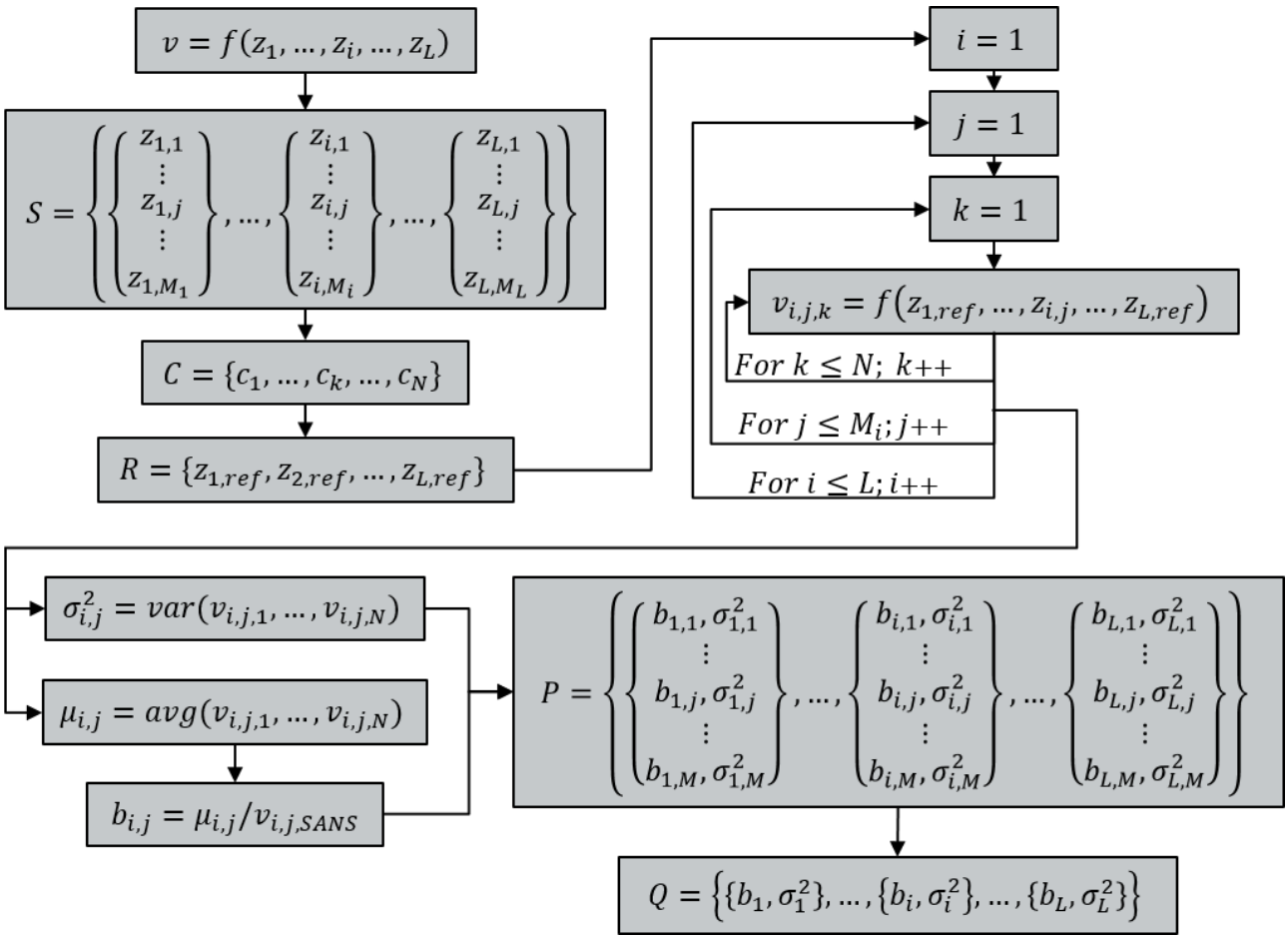

Figure 3.5: Algorithm for using comparison of design standards to estimate uncertainties.

for each case using the selected design standards, i.e. using the stipulations given in k-th design standard, the j-th sampling value of the i-th parameter is used in conjunction with the reference value of the other parameters to calculate the target variable value ($v_{i,j,k}$).

Once the target variable value for a specific case (i,j) has been calculated according to all the design standards, an estimate of the "true" value for that case may be made. As discussed above, the average value ($\mu_{i,j}$) for the specific case is taken as the closest approximation to the true value. The systematic bias ($b_{i,j}$) for a given code may then be calculated as the ratio of the average value to the target variable value specified by the code for the specific case. In this study the bias is calculated relative to the SANS code ($v_{i,j,SANS}$), but this calculation can be applied for any of the standards. The variance ($\sigma_{i,j}^2$) for the specific case is also calculated using the target variable values stipulated by all the standards. Both the bias and the variance for each case are then stored in a set of results (P).

The final step of the algorithm is to ensure unbiased sampling by reducing the results from all cases to a set of statistically independent values (Q). It is not reasonable to assume that

two specific cases (i,j and i,$j+1$), where one of the parameters was only slightly different in the second case, are statistically independent. As the sampling set sizes for each parameter may be different, sampling every value in the full set of results P would result in a bias toward the values obtained for the parameters which have bigger sampling set sizes. It may however be assumed that the full set of results obtained from the parametric varying of one of the parameters is independent of the set of results obtained for another parameter. The bias and variance values for each parameter are therefore sampled and used to determine a single bias (b_i) and variance (σ_i^2) value which represents the total uncertainty of the cases in which a specific parameter z_i was varied. This final set of statistically independent values may then be used to determine representative statistical parameters for the target variable across the entire sampling space.

The algorithm may be summarised in three distinct steps:

1. the definition of the sampling space;

2. the sampling process based on varying design variables parametrically one-by-one and calculating parameters using the different wind load standard stipulations; and

3. the statistical treatment of the generated data by aggregating data into independent subsets.

It is important to remember that this method is not based on statistical data but rather on sampling reliability information in the form of codified wind load parameters. The wind load standard development process may result in additional levels of conservatism being added or simplification of the background models. As the basic data from specific physical cases are used to formulate generalized loading stipulations for a wide range of design situations, the simplification and generalization reduces the variability of the codified values. Furthermore, one must consider that the wind load standards which are being compared have different formulations of the same wind load components. Effectively comparison of wind load standard stipulations provides an estimation of the epistemic uncertainties related to modelling wind load components. Considering these factors it may be assumed that this method will result in lower bound approximations of the systematic bias and variability values for the wind load components.

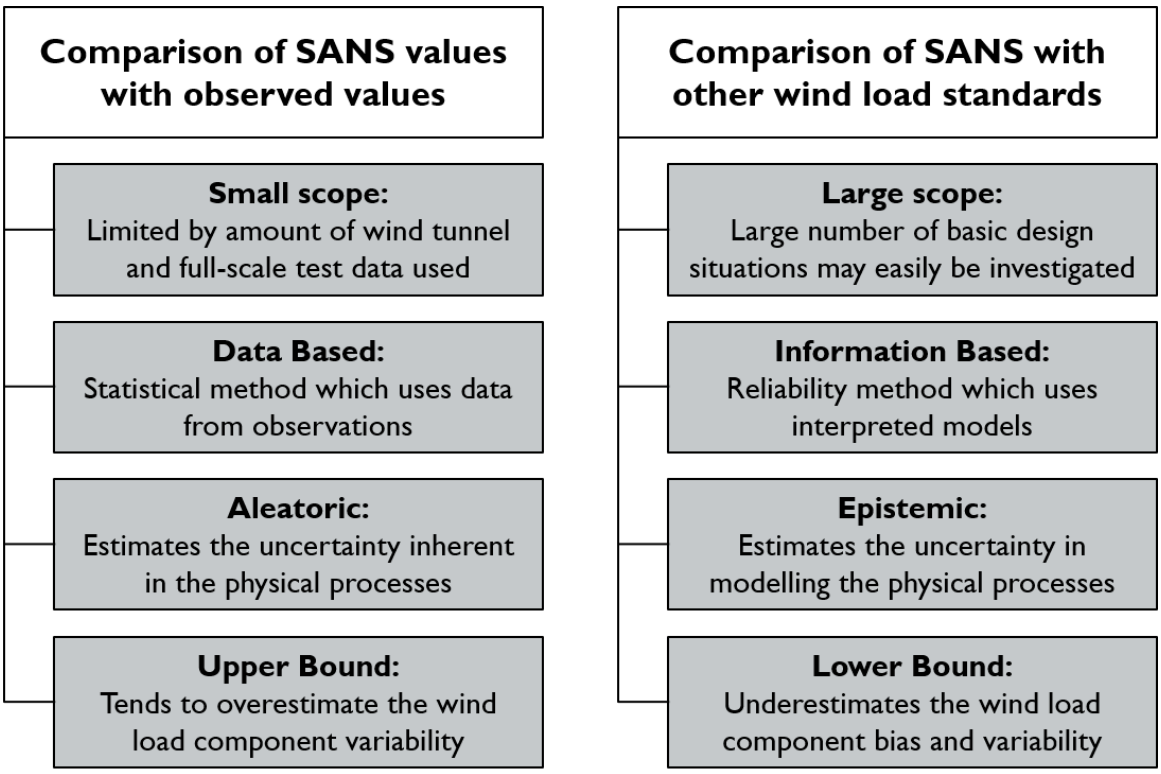

Figure 3.6: Summary of methodologies used to investigate time invariant wind load components in this investigation.

3.4.3 Methodology summary

Each of the methods described above has its own strengths and weaknesses, as summarised in Figure 3.6. The purpose of using two supplementary methods is to make the best use of all available data and information in order to estimate the wind load component uncertainties. By approaching the problem from two sides and using these methods the closest approximation of the true wind load component uncertainty may be found by using an approximation which falls within the limits of the statistical parameters obtained. In this investigation the geometric average of the values between the upper and lower bound was selected as the closest approximation of the true value.

These methods were only used for the investigation of the time invariant wind load components in this investigation. As time variant uncertainties are location specific, the comparison with the free-field wind parameters given in other wind load standards would be nonsensical. As such, the free-field wind investigation is based directly on the use of local South African wind data.

3.5 Bayesian hierarchical models and Monte Carlo method

The wind load components investigated in this study are all subject to multiple sources of uncertainty, both aleatoric and epistemic. Although there are many well established reliability methods dealing with the reliability treatment of systems subject to multiple variables, quantifying the uncertainty of a single variable subject to multiple sources of uncertainty becomes challenging. To aid with this problem the statistical treatment of unknowns in general and the reliability approach followed needed to be assessed.

As summarized by Ang and Tang (1984), the classical statistical approach, also called the frequentist approach, is based on the assumption that the parameters of any system are constant, albeit unknown. The frequentist approach uses sample statistics as estimators of these parameters and confidence intervals to express the degree to which these estimations are believed to be incorrect. A drawback to using this approach is that accurate estimates of parameters require large amounts of data. In engineering problems, secondary information often supersedes the available data. As has been clearly established in this chapter, this is certainly the case when considering wind load components. Unfortunately the classical approach makes no provision for combining secondary sources of information with observed data.

One solution to this drawback of the classical statistical approach is to use the Bayesian approach. The Bayesian approach is based on the assumption that the parameters of a system are not constant, but rather random variables. This provides a natural platform for combining multiple data sources, be they observational data, secondary information or judgmental expert opinions, while managing their uncertainties. The Bayesian approach allows modelling of systems with multiple levels of complexity. These models are referred to as multilevel or hierarchical models. A three level hierarchical model of a single component forms the basis of the probability method used throughout this investigation. Such a model is shown in Figure 3.7.

In the model presented above, the highest level of the model θ represents one of the wind load components. The distribution of θ is the model of the underlying system. The distribution parameters of θ, namely μ and σ, are regarded as random variables. This implies that different sources of uncertainty affect the different distribution parameters of the underlying system. These probability distributions describing μ and σ are prior distributions of θ. The distribution

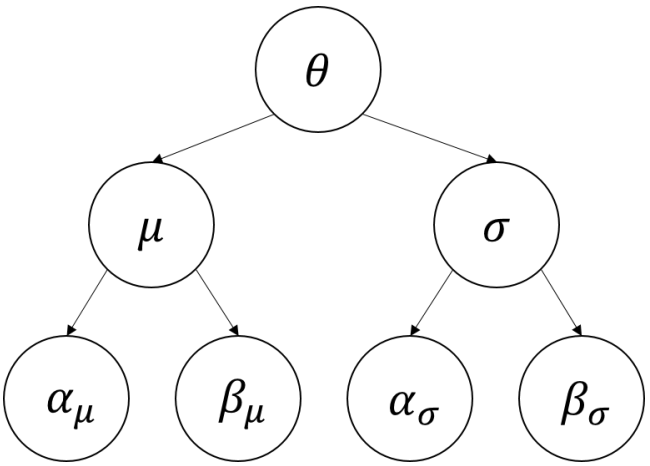

Figure 3.7: Three level hierarchical model.

parameters of the prior distributions, namely α_μ, β_μ, α_σ and β_σ, are referred to as hyperparameters. In theory the model may be extended further by considering the hyperparameters as priors to μ and σ, thus becoming hyperpriors which are described by hyperhyperparameters, and so forth. However, for the purposes of this investigation the three level model is sufficient.

Fink (1997) described the process whereby the posterior distribution for this model may be obtained using Bayes theorem, given as:

$$p(\theta|\mu,\sigma) = \frac{\pi(\theta)L(\theta|\mu,\sigma)}{\int \pi(\theta)L(\theta|\mu,\sigma)d\theta} \tag{3.5.1}$$

Inference is made on the unknown parameter θ based on existing knowledge of θ and the priors μ and σ. The existing knowledge of θ is described by the probability distribution $\pi(\theta)$. The likelihood function $L(\theta|\mu,\sigma)$ combines the available data about the prior. The normalized product of these functions yields the posterior probability distribution of θ which is conditional on the information available about the priors.

Although Bayes theorem is mathematically simple, finding analytical solutions may be challenging depending on the distribution types used in the model. In certain cases where the prior, likelihood and posterior distributions all belong to the same class of distributions the calculation becomes simpler due to conjugacy. A simple example is the case where the mean is unknown and the variance is known. If the mean has a normal distribution, the posterior distribution will also have a normal distribution, resulting in a normal-normal hierarchical model. Conjugacy is defined by Gamerman and Lopes (2006) as the preservation of the distribution after updating in the same class, whereby passage from the prior to the posterior involves a change in the hyperparameters with no additional calculation.

The calculation of the posterior predictive parameters using conjugate functions simplifies the analysis of hierarchical models, however it does limit the flexibility of the models as only certain distributions can be used together. Therefore, a numerical solution such as using the Monte Carlo method often proves to be more useful. The general Monte Carlo method is fairly familiar to most engineers due its flexibility and simplicity. Fishman (2013) formally defined the Monte Carlo method as the method whereby approximate solutions to mathematical problems are found through the use of random statistical sampling experiments.

The use of the Monte Carlo method for posterior predictive model checking in hierarchical models was presented by Sinharay and Stern (2003). Their method was adapted slightly in this investigation to be used to estimate the posterior predictive model distribution parameters for the wind load components under consideration. Consider the hierarchical model shown in Figure 3.7 once again. The method is summarized as follows:

1. Select appropriate distribution types for the prior distributions of μ and σ as well as for the posterior predictive distribution of θ, denoted as $p(\mu|\alpha_\mu, \beta_\mu)$, $p(\sigma|\alpha_\sigma, \beta_\sigma)$, and $p(\theta|\mu, \sigma)$.

2. Generate a random sample μ_i from $p(\mu|\alpha_\mu, \beta_\mu)$.

3. Generate a random sample σ_i from $p(\sigma|\alpha_\sigma, \beta_\sigma)$.

4. Generate a random sample θ_i from $p(\theta|\mu, \sigma)$ using the distribution parameters μ_i and σ_i.

5. Repeat steps 2-4 N times to establish a set of random samples.

6. Fit a distribution to the samples $\theta_1, \theta_2, ..., \theta_N$ which is representative of the posterior predictive distribution $p(\theta|\mu, \sigma)$.

To illustrate how the Monte Carlo method results compare with results obtained using conjugate functions, consider a simple example of a normal-normal hierarchical model discussed above. Let θ be an unknown variable which is normally distributed with a fixed prior standard deviation $\sigma = 0.8$ and a variable mean which is also normally distributed. The hyperparameters of the mean prior distribution are mean $\alpha_\mu = 3.0$ and standard deviation $\beta_\mu = 0.5$. Using the conjugate function solution for normal-normal models given by Murphy (2007), the posterior predictive distribution parameters may be found as $\mu' = \alpha_\mu = 3.0$ and $\sigma' = (\sigma^2 + \beta_\mu^2)^{0.5} = 0.943$.

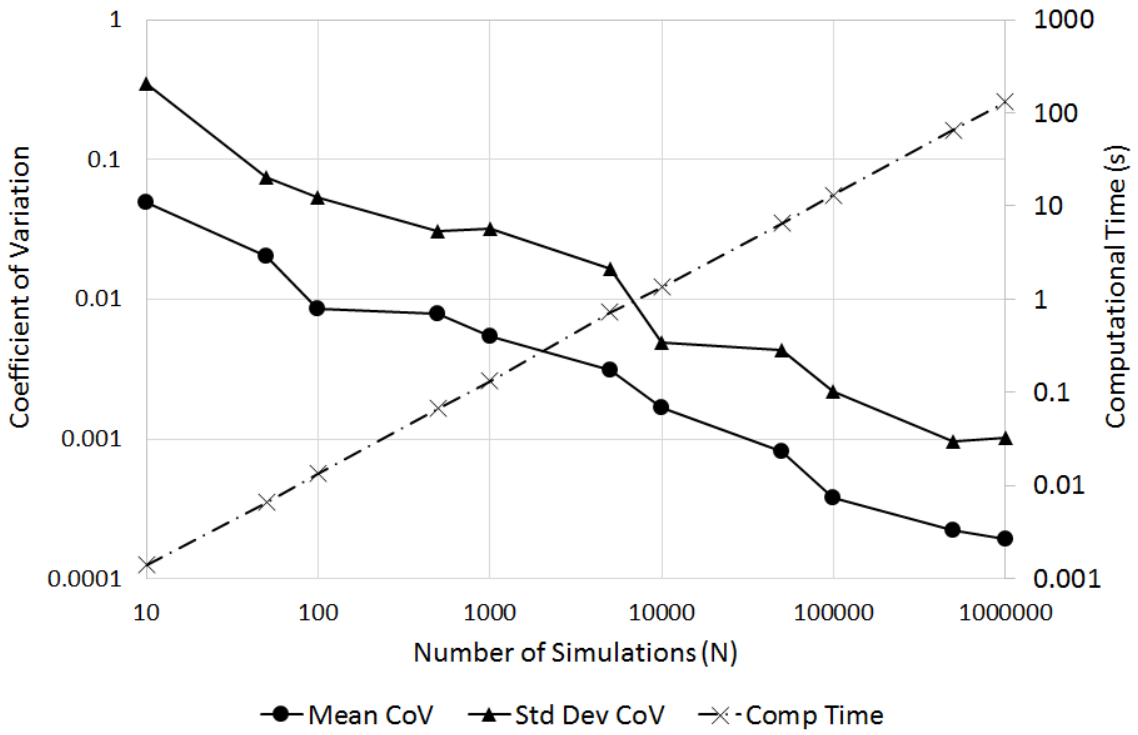

Figure 3.8: Sensitivity analysis on number of simulations used in Monte Carlo method.

The Monte Carlo method above may be modified to accommodate a constant prior standard deviation by simply removing step 3 and using the fixed standard deviation in step 4. The posterior predictive distribution parameters found using 100,000 samples are $\mu' = 3.0$ and $\sigma' = 0.944$.

The accuracy of the method is directly related to the number of simulations used. To illustrate this an example hierarchical model with a variable mean and variable standard deviation was used. A sensitivity analysis was done by varying the number of simulations used. For each number of simulations tested the Monte Carlo method was run ten times and the results recorded. The coefficients of variation of the calculated posterior predictive mean and standard deviation values were computed and the average computational time for each run was recorded. The results of this analysis are shown in Figure 3.8.

As expected, the accuracy of the method is inversely proportional to the number of simulations used, while directly proportional to the computational time. What is interesting to note is that the standard deviation results are consistently more variable than those of the mean. Using 100,000 simulations resulted in coefficients of variation of less than 0.002 for both the mean and the standard deviation, with a computational time of only 13 seconds on a mid-range computer. However, as the method would only be used once for every wind load

component considered, it was decided that 1,000,000 simulations would be used throughout the investigation to determine the posterior distribution parameters.

The use of hierarchical Bayesian models to quantify wind load component uncertainties is an extension of the traditional Davenport reliability method described in Section 3.3 and shown in Figure 3.2. In the traditional method, as the design wind load (w_d) is the product of a number (N) of independent wind load components (θ_i) as discussed in Chapter 2, the total uncertainty of the design wind load is obtained by combining the uncertainties of the individual components on the system level. By treating the sources of uncertainty in the components independently through the use of prior distributions (μ_{θ_i}, σ_{θ_i}), the same rational methodology applied at the system level is extended to the component level. This extended framework, as represented in Figure 3.9, allows for a more detailed level of approximation of wind load uncertainties and serves as the basis for the component investigations in the following chapters.

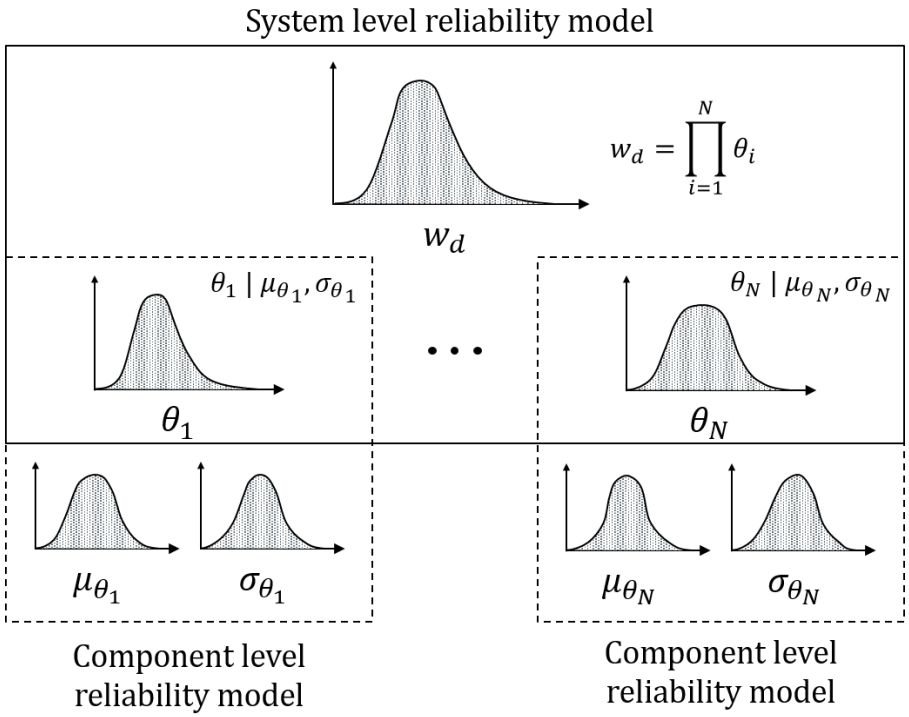

Figure 3.9: Extended reliability modeling framework used in the investigation.

Chapter 4

Free-Field Wind

The first of the primary wind load components to be investigated is the time variant free-field wind pressure. It has already been mentioned in Section 2.2.1 that a recent study was done by Kruger *et al.* (2013) which investigated the strong wind climatology of South Africa. This study used wind data from weather stations across the country to investigate the strong wind climate and delineate the country into zones based on the dominant strong wind generating mechanisms. This process and the results thereof were discussed in Section 2.2.1. The wind data was further used to develop statistical models of strong winds for each weather station considered, which finally led to the development of a new design wind map of the South African free-field wind. This data and the work done by Kruger provides the ideal framework to quantify the uncertainties of the annual extreme wind pressures used as free-field wind pressure in SANS 10160-3.

The development of a probabilistic free-field wind pressure model is outlined in this chapter. Firstly, Kruger's work is discussed in greater detail, with a focus on how the extreme wind prediction models were developed by Kruger. Of particular interest in this investigation are the quality control measures taken in order to ensure the trustworthiness of the results. The new South African design wind map is then discussed. Finally, the use of the data and results from the Kruger study as well as the new wind map to determine a representative probability distribution of the SANS reference wind pressure is presented.

4.1 Statistical models of strong winds

Extreme wind prediction relies on statistical models which are fitted to observed wind speed data. There are numerous strong wind estimation methods which may be used, each having its own advantages and disadvantages. The purpose of the investigation by Kruger (2011) was to determine the most appropriate of these methods and to apply them to the available wind speed data in order to develop predictive models. This section provides a brief overview of how these models were developed. First, the quality of the data used in the analysis by Kruger is discussed. This is followed by a description of each of the estimation methods which were used in the study. Finally, a comparison of the quantiles predicted by each of the methods and the final design quantiles selected by Kruger are given.

4.1.1 Wind data reliability

As stated in Section 2.2.1, Kruger (2011) gathered wind data from 209 Automatic Weather Stations (AWS) across the country. Before this raw data could be used, a quality audit was required in order to ensure the reliability of the wind data.

The first consideration of the quality audit was the homogeneity of the wind data. As stated by Kruger, it is expected that quality issues will arise in any dataset that is continuously updated due to the modernisation of measuring equipment through the years. Kruger listed a number of factors which cause these homogeneity issues, namely:

- Change in location of the measuring station;
- Change in measuring units;
- Change in instrumentation;
- Change in the exposure of the instrumentation:
- Faulty or damaged instrumentation;
- Incorrect digitization of data; and
- Problems due to electronic transfer of data between databases.

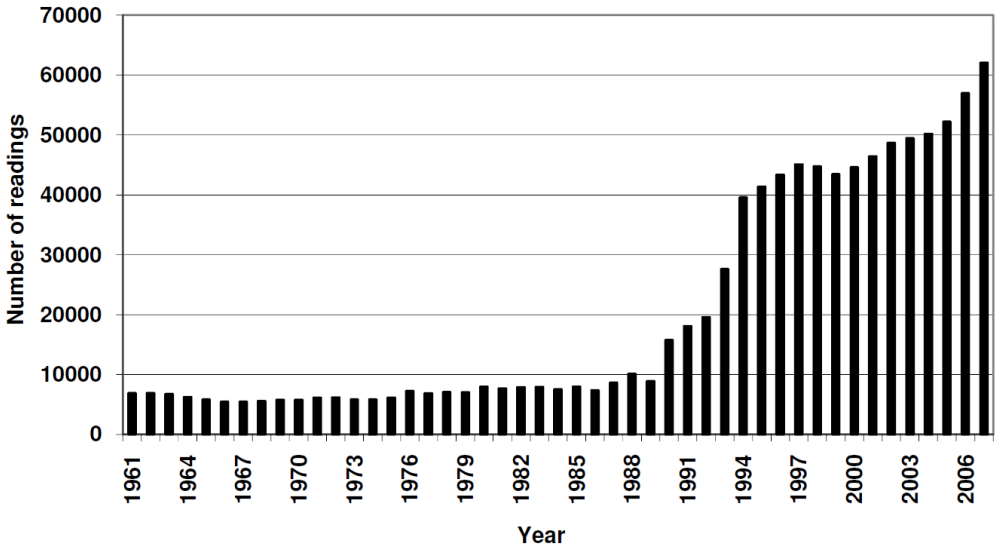

Figure 4.1: Annual number of daily maximum wind gust readings available in the SAWS climate database, taken from Kruger (2011).

Each station's data were investigated for data inhomogeneities such as individual outliers, shifts in mean observed values and gaps in the data. A comparison was also done between the wind data and other supporting climatic data to determine the validity of measured extremes and general trends. Any station in which the utilised time series contained at least 90% reliable data was selected for further investigation.

A significant issue which needed to be addressed was the length of the record periods available. In the early 1990's the South African Weather Service upgraded its wind measuring network with the installation of numerous AWSs across the country. This provided a good spatial distribution of the final AWS records which were used, but as most of the stations were installed relatively recently the wind records were short. Figure 4.1 shows the wind gust readings available for the years from 1961 to 2007. A significant rise in recorded values is seen starting in 1990. It was decided that each AWS needed to have at least 10 years of reliable records. Any stations which did not meet this criterion was excluded from the investigation.

The final consideration regarding the quality of the wind data was the terrain exposures of the weather stations. In order to obtain consistent results it is imperative that wind information be standardized. The requirement of all international wind load standards is that wind data be measured at a standard elevation of 10 m above the ground level in open terrain, equivalent to SANS Terrain Category B. It is also required that the general topography surrounding the measuring station be flat. Kruger therefore assessed the positioning and the influence

Figure 4.2: Spatial distribution of weather stations considered in this investigation.

of the surrounding surface roughness, obstructions and topography of each station in order to estimate the influence of the exposure on the measured data. Correction factors were calculated for each station as required. It should be noted that exposure problems are related to specific wind directions. The correction factors were therefore not determined for all the wind data at a wind station, but the 16 primary wind directions were considered independently and a different correction factor calculated and applied to the wind data from each direction.

After the initial quality audit which considered the homogeneity and record length of the data, 91 stations were selected. These stations were used to investigate the South African strong wind climatology as discussed in Section 2.2.1. After further investigation of the exposure of the stations, a further 15 stations were removed and 76 stations were finally selected and extreme wind prediction methods were developed using the data from these stations. The spatial distribution of the stations across the county is shown in Figure 4.2. Due to the thorough nature of the quality audit done by Kruger it may safely be assumed that the data from these stations are reliable. Therefore, these stations and their wind data are used throughout this investigation to determine the representative statistical parameters of the South African design free-field wind pressure.

4.1.2 Estimation methods

The application of the estimation methods used for extreme wind prediction is an important step in the development of a representative probability distribution of the South African free-field wind. The extreme wind prediction models of each station are used as the basis for the free-field wind uncertainty investigation. This section provides a brief description of the extreme value estimation methods used by Kruger (2011) to develop predictive strong wind models. It should be noted that this is simply a summary of the work done by Kruger and only serves as background information which is required in the current investigation.

4.1.2.1 Extreme Value methods

The most widely used estimation methods for extreme winds are based on the Generalized Extreme Value (GEV) theory. This method is described by Palutikof *et al.* (1999). The GEV distribution, also known as the Fisher-Tippett distribution, is based on using only the extreme values from a given population. In the case of wind speed, the GEV distribution is usually fitted to the annual maximum wind speed values. The cumulative distribution functions of the GEV distribution are given in Equations 4.1.1 and 4.1.2.

$$F(x) = e^{-(1-\kappa y)^{1/\kappa}} \qquad \kappa \neq 0 \tag{4.1.1}$$

$$F(x) = e^{-e^{y}} \qquad \kappa = 0 \tag{4.1.2}$$

where, κ is the shape parameter

y is the standardised or reduced variate, as given in Equation 4.1.3

$$y = \frac{x - \beta}{\alpha} \tag{4.1.3}$$

where, x is the extreme value variable

α is the scale or dispersion parameter

β is the mode of the distribution

The GEV distribution is heavily dependent on the shape parameter κ, which results in three variations of the extreme value distribution depending on its value. Fisher-Tippett Type I, also known as the Gumbel distribution, has $\kappa = 0$. The Type II distribution has a negative value of κ, and Type III has a positive value of κ. Type I and II are bounded on the lower end, and

Type III is bounded on the higher end.

As stated by Cook (1985), it is widely accepted that the Gumbel distribution is a suitable model for wind speed distributions. Although there has recently been speculation by Holický *et al.* (2015) regarding the suitability of the use of the Gumbel distribution for modeling extreme winds, this investigation will continue to regard the Gumbel distribution as a suitable option. One of the advantages of the Gumbel distribution is the ease with which its parameters may be estimated. Equations 4.1.4 and 4.1.5 give the equations used to estimate the scale parameter and mode of a Gumbel distribution based on the mean and standard deviation of a sample. Using these parameters the design quantile for a given return period may be calculated using Equation 4.1.6.

$$\alpha = \frac{s\sqrt{6}}{\pi} \tag{4.1.4}$$

$$\beta = \bar{x} - \gamma\alpha \tag{4.1.5}$$

where, s is the standard deviation of the sample

$\bar{x}$ is the mean of the sample

γ is Euler's constant, $\gamma = 0.57721...$

$$X_T = \beta - \alpha ln[-ln(1 - \frac{1}{T})] \tag{4.1.6}$$

where, X_T is the quantile

T is the return period

Another approach to fitting predictive models to observed wind speeds is to assume that the shape parameter κ is not equal to zero and to fit the GEV distribution. This approach does generally result in a better fit to the data, however it makes estimating distribution parameters significantly more complicated. It also means that a Type III distribution may be fitted if the shape factor is calculated to be positive. Many authors criticize this method as the Type III distribution is bounded on the higher end, which implies an upper bound for the wind speed. Nonetheless, Kruger fitted GEV distributions to wind station data using a software package to estimate parameters through an iterative process. Using an interval of κ between -0.05 and 0.05 as being equivalent to zero, the analysis by Kruger found that 18.7% of the stations showed a Type I form, 28.6% showed a Type II form and 52.7% showed a Type III form.

The biggest drawback of the GEV/Gumbel method is that only one value is used from each

year of available data. Cook (1985) stated that at least 20 years of data should be used to obtain reliable results and that the method should not be applied to a data series with less than 10 years of data, hence this restriction on the data length was used by Kruger. All stations used in the investigation by Kruger had less than 20 years of reliable data available. This calls the reliability of results from the GEV/Gumbel method into question.

4.1.2.2 Peak-Over-Threshold methods

Due to the limitations of the record length of the dataset, extreme wind prediction methods that specifically account for short record periods needed to be considered. The typically used methods for estimating extreme winds for short time series were summarised by Palutikof *et al.* (1999). These methods involve selecting a threshold value above which wind speed values are selected and used to estimate the distribution parameters of the predictive models. There are two primary methods used, the Method of Independent Storms (MIS), and the Peak-Over-Threshold (POT) method. Using MIS requires only that a threshold value be selected and all values greater than that threshold are used. The more commonly used POT method requires that a threshold value and a separation distance be chosen, which eliminates the possibility of a single storm with a lull in wind speeds being regarded as two independent storms. The POT method was employed by Kruger.

A General Pareto Distribution (GPD) is typically fitted to selected values when the POT method is used. Its cumulative distribution function is given in Equation 4.1.7. Similar to the GEV distribution simplifying to a Gumbel distribution when the shape factor κ is zero, the GPD simplifies to the Exponential (EXP) distribution, as shown in Equation 4.1.8.

$$F(x) = 1 - [1 - (\frac{\kappa}{\alpha})(x - \xi)]^{-\frac{x-\xi}{\alpha}} \qquad \kappa \neq 0 \qquad (4.1.7)$$

$$F(x) = 1 - e^{-\frac{x-\xi}{\alpha}} \qquad \kappa = 0 \qquad (4.1.8)$$

where, κ is the shape parameter

α is the scale or dispersion parameter

ξ is the threshold value

In order to calculate quantile values for the GPD and EXP distributions the average crossing rate of the threshold needs to be calculated. This is shown in Equation 4.1.9. Once this value

is known design quantiles for a given return period may be calculated using Equations 4.1.10 and 4.1.11. The shape factor and scale parameter may be estimated using probability weighted moments and maximum likelihood solutions as described by Palutikof *et al.* (1999), however these methods are not described in this investigation.

$$\lambda = \frac{n}{M} \tag{4.1.9}$$

where, λ is the crossing rate

n is the total number of exceedances over the selected threshold ξ

M is the number of years of record

$$X_T = \xi + \frac{\alpha}{\kappa}[1 - (\lambda T)^{-\kappa}] \qquad \kappa \neq 0 \tag{4.1.10}$$

$$X_T = \xi + \alpha ln(\lambda T) \qquad \kappa = 0 \tag{4.1.11}$$

where, X_T is the quantile

T is the return period

Kruger analysed the wind data using a range of threshold values in 2.5 m/s increments. The data sets to be used to fit predictive models were selected based on the largest number of wind speed values with at least 80% of the values being from independent storms. This method was used to determine design quantiles using both the GPD and EXP distributions. It was found that for gust values the EXP distribution resulted in a better fit to the data.

One characteristic of the EXP distribution which should be noted as it has significant bearing on the investigation to follow is the shape of the distribution. As the distribution is undefined for any values below the selected threshold, the distribution is bounded at the threshold and is only effective for estimating tail end values. Furthermore, the distribution maintains a constant shape and the mean and standard deviation values are always equal to each other. This results in a coefficient of variation of unity for all EXP distributions.

4.1.2.3 Mixed climate distribution method

The different strong wind generating mechanisms across South Africa needed to be considered during the application of extreme wind prediction methods. Most methods assume all observed wind speeds to be caused by the same phenomena. However, as discussed in Section 2.2.1,

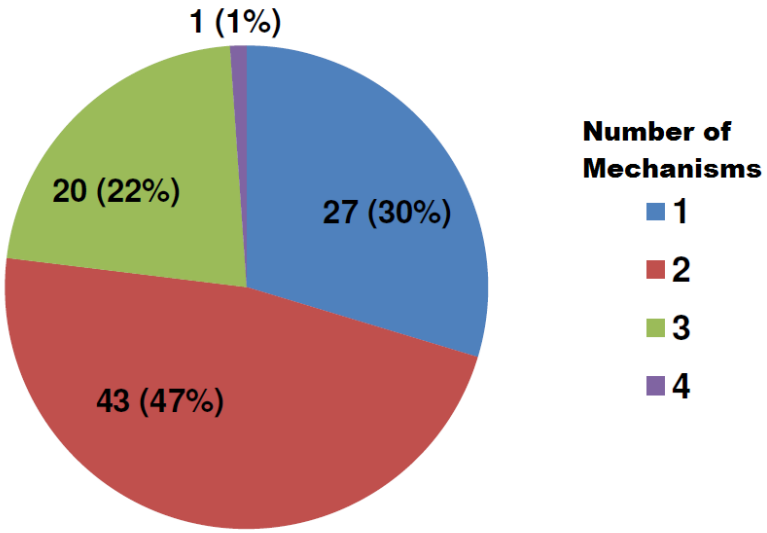

Figure 4.3: Number (percentage) of stations with one to four strong wind mechanisms, taken from Kruger (2011).

Kruger used wind records and other climatic conditions to determine the dominant strong wind generating mechanisms at every station and found that 70% of the stations had at least two mechanisms contributing to the annual extreme winds, as shown in Figure 4.3. Therefore Kruger considered strong wind estimation methods that explicitly account for a mixed strong wind climatology.

The technique developed by Gomes and Vickery (1978) is the most commonly used method for the fitting of mixed wind speed distributions and was used by Kruger on the South African wind data. In this method the wind speed data from each station were disaggregated by the mechanisms which caused them and a separate population of wind speed values was established for each strong wind generating mechanism. The method requires the use of the Gumbel distribution as discussed in Section 4.1.2.1. Therefore, only the annual extremes of each population are considered. It should be noted that this treatment has the advantage of increasing the number of observations to a full set of annual extremes for each independent mechanism. The Gumbel distribution parameters are estimated for each dataset and a distribution is fitted to the data. The mixed climate distribution which represents the combined contribution from each independent strong wind generating mechanism may then be calculated as the sum of the individual risks of exceedance for each mechanism as given in Equation 4.1.12. The return period for a specific wind speed is calculated using Equation 4.1.13, which was used to determine the design wind speed quantiles.

$$F(x) = 1 - \sum_{i=1}^{n}(1 - e^{-e^{-y_i}}) \tag{4.1.12}$$

where, n is the total number of independent strong wind generating mechanisms

y_i is the reduced variate for the ith strong wind generating mechanisms

$$T = \frac{1}{\sum_{i=1}^{n} e^{\frac{\alpha_i - V_T}{\beta_i}}} \tag{4.1.13}$$

where, T is the return period

α_i is the scale parameter for the ith strong wind generating mechanisms

β_i is the mode of the distribution for the ith strong wind generating mechanisms

V_T is the wind speed associated with the return period T

4.1.3 Design quantiles

Using the extreme wind prediction methods described above, Kruger (2011) established models for each of the stations and calculated the 50, 100 and 500 year return period quantiles of the gust wind speed. For the purposes of structural design the 50 year return period quantile represents the characteristic value, on which wind maps are based. Those values are presented here in Table 4.1, along with which extreme wind prediction method was selected as the most appropriate for each station. The other design wind speed quantile values (100 year, 500 year) are given in Appendix A. All the design quantiles are used in the following investigation.

Table 4.1: Final selected stations and 50 year return period quantile values for each of the extreme wind prediction methods investigated, excluding exposure correction factors.

Station Name	Wind Gust X_{50} (m/s)					Selected Distribution
	GEV	Gumbel	GPD	EXP	Mixed	
Struisbaai	45.2	40.6	43.2	**41.3**	-	EXP
Strand	36.5	36.4	37.2	33.6	**36.6**	Mixed
Hermanus	31.8	33.6	35.2	**36.6**	-	EXP
Tygerhoek	39.1	37.3	40.4	**37.3**	-	EXP
Stilbaai	30.4	30.1	30.8	**30.3**	-	EXP
George	31.4	32.2	31.3	**33.3**	-	EXP
Knysna	27.7	**28.5**	26.9	30.8	-	Gumbel
Plettenbergbaai	28.3	**31.1**	28.0	30.6	-	Gumbel
Tsitsikamma	31.7	31.1	31.8	**31.6**	-	EXP

Station Name	Wind Gust X_{50} (m/s)					Selected Distribution
	GEV	Gumbel	GPD	EXP	Mixed	
Robbeneiland	28.7	28.4	27.2	**28.7**	29.7	EXP
Cape Town	39.9	38.3	42.7	36.7	**38.7**	Mixed
Paarl	24.6	25.1	24.5	25.7	**26.1**	Mixed
Worcester	39.5	37.6	35.9	**41.5**	-	EXP
Patensie	28.4	26.0	31.1	27.3	**30.5**	Mixed
Uitenhage	32.1	31.7	32.1	32.1	**33.8**	Mixed
Port Elizabeth	39.6	38.1	35.2	**40.4**	-	EXP
Geelbek	30.1	28.2	29.0	**28.8**	28.6	EXP
Malmesbury	28.8	28.4	29.7	27.1	**28.8**	Mixed
Porterville	32.5	32.8	30.4	**32.9**	32.8	EXP
Grahamstown	31.7	32.2	33.2	31.5	**34.0**	Mixed
East London	37.3	31.8	32.3	**36.1**	-	EXP
Langebaanweg	37.7	33.2	36.6	29.4	**33.1**	Mixed
Fort Beaufort	40.3	36.4	39.1	35.4	**37.2**	Mixed
Lambertsbaai	23.2	24.9	25.6	**27.9**	26.0	EXP
Beaufort-Wes	38.9	38.6	38.0	**39.0**	38.8	EXP
Graaff-Reinet	30.8	31.2	32.3	31.1	**31.9**	Mixed
Queenstown	30.8	31.9	31.1	**37.1**	33.1	EXP
Umtata	44.4	40.5	38.3	39.0	**41.9**	Mixed
Calvinia	32.2	32.4	32.7	**33.4**	32.4	EXP
Noupoort	33.9	33.2	37.2	**37.4**	33.8	EXP
Jamestown	35.6	28.2	28.9	**31.9**	30.2	EXP
Elliot	37.2	38.8	44.5	**44.2**	41.8	EXP
Port Edward	32.2	30.8	31.9	**32.6**	-	EXP
De Aar	41.2	39.7	43.2	**42.3**	41.2	EXP
Paddock	30.6	30.8	30.5	30.3	**30.5**	Mixed
Margate	30.7	**30.6**	30.8	33.3	-	Gumbel
Koingnaas	26.1	26.6	26.4	26.3	**27.6**	Mixed
Brandvlei	30.6	31.9	30.9	**35.2**	35.0	EXP
Prieska	33.8	33.3	32.8	**33.9**	33.4	EXP
Pietermaritzburg	29.2	27.0	28.8	**29.1**	28.6	EXP
Oribi Airport	39.0	35.0	33.1	33.6	**35.4**	Mixed
Durban	35.0	**33.3**	34.3	32.6	-	Gumbel
Virginia	27.3	**31.1**	31.7	29.1	-	Gumbel
Bloemfontein	37.1	34.5	35.1	**36.3**	-	EXP
Alexanderbaai	31.3	31.3	30.3	**32.1**	32.2	EXP
Kimberley	35.6	36.4	38.0	**37.7**	-	EXP
Ladysmith	40.8	37.4	33.4	36.4	**37.3**	Mixed
Mtunzini	29.4	29.8	31.4	31.6	**32.3**	Mixed
Upington	40.5	**37.5**	35.1	36.0	-	Gumbel
Postmasburg	30.1	32.2	34.3	**32.7**	-	EXP
Bethlehem	30.1	29.2	29.6	29.9	**30.7**	Mixed

Station Name	Wind Gust X_{50} (m/s)					Selected Distribution
	GEV	Gumbel	GPD	EXP	Mixed	
Ulundi	30.5	30.1	30.2	**32.9**	30.7	EXP
Charters Creek	27.2	25.9	26.4	23.3	**26.5**	Mixed
Kathu	32.4	32.1	32.4	**33.3**	-	EXP
Taung	31.5	32.9	34.5	**36.9**	-	EXP
Bloemhof	40.9	36.7	38.9	30.9	**36.0**	Mixed
Welkom	40.9	39.3	38.0	**40.0**	39.3	EXP
Newcastle	32.2	35.0	33.1	**38.2**	34.6	EXP
Pongola	29.1	29.7	31.5	**31.2**	30.0	EXP
Vereeniging	31.5	33.2	32.4	**33.4**	33.2	EXP
Standerton	33.0	**34.4**	38.5	32.9	34.3	Gumbel
Lichtenburg	32.5	**33.1**	33.2	33.0	32.6	Gumbel
Johannesburg	36.1	**34.0**	34.3	33.4	34.6	Gumbel
Ermelo	27.4	28.9	27.2	**32.1**	28.8	EXP
Mafikeng	31.4	31.9	33.3	**33.0**	31.8	EXP
Rustenburg	28.9	**29.2**	31.3	28.2	29.7	Gumbel
Irene	33.5	32.9	30.7	**33.6**	33.3	EXP
Witbank	30.6	30.7	31.5	**31.5**	31.0	EXP
Komatidraai	30.4	**31.0**	31.1	28.9	-	Gumbel
Pilanesberg	33.1	24.2	34.8	**32.4**	32.3	EXP
Graskop	27.1	**31.2**	37.3	29.6	29.7	Gumbel
Hoedspruit	32.0	30.9	30.9	30.6	**31.9**	Mixed
Ellisras	30.1	28.6	29.1	27.9	**28.7**	Mixed
Marken	31.2	29.5	28.2	27.2	**30.6**	Mixed
Pietersburg	30.5	32.4	30.7	**35.0**	-	EXP
Thohoyandou	27.4	27.2	25.9	**29.0**	28.3	EXP

The final distributions selected were based on which method resulted in the highest quantiles as well as which distributions provided the best fit to the available data. When considering gust wind speeds, Kruger found that in most cases the POT method using an EXP distribution provided the best fit. However, for locations with multiple strong wind generating mechanics it was found that the Gumbel or Mixed distributions gave better results. Figure 4.4 shows the spatial distribution of the stations and which distribution was selected at each. It may be seen that there is no clear grouping for any one distribution and in some places, such as the southernmost point of KwaZulu Natal, all three distributions were used on three different stations in close proximity to one another.

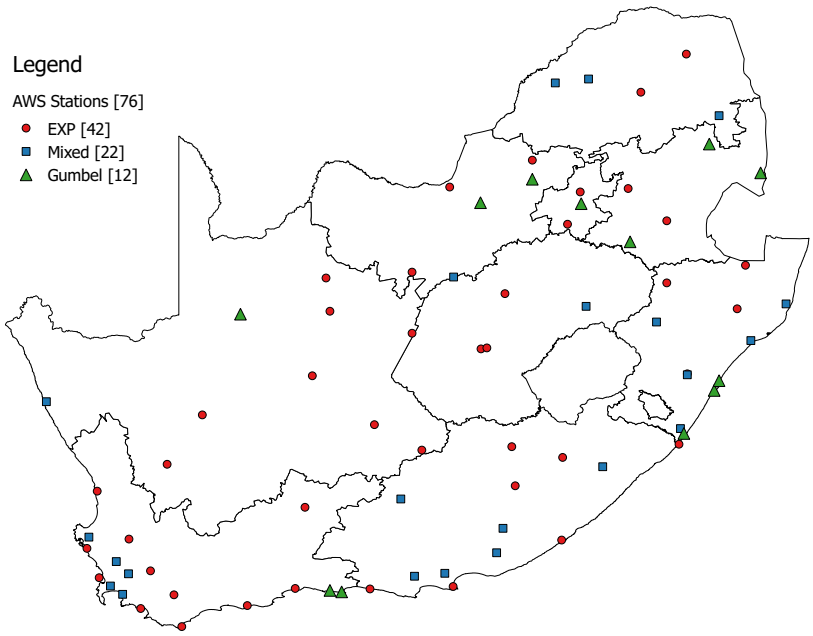

Figure 4.4: Spatial distribution of stations and selected extreme wind prediction methods for each.

The study by Kruger *et al.* (2013) forms the foundation of this investigation into the uncertainties of the South African free-field wind. The predictive models and design quantiles calculated provide the best representation of the free-field wind at specific locations. The challenge now arises of how to describe the representative uncertainty across the entire country for the purposes of calibration of the South African wind load standard. A solution to this problem is presented in Section 4.3, but first the development of the new South African design wind speed map is discussed as it too has an influence on the free-field wind uncertainty.

4.2 South African wind speed map

The research done by Kruger *et al.* (2013) led to the development of a new design wind map for SANS 10160-3. At the time of writing the map had been completed but not yet incorporated into the wind load standard. This section briefly discusses the development of the wind map presently used in the South African loading code as well as the new wind map, presents the provisional new wind map, and compares the new map quantiles to those given in the present map.

The present design wind map is based on research done by Milford (1985*b*). The map was based on wind data from 14 weather stations across the country. As already stated, the new

Figure 4.5: Spatial distribution of weather stations used to develop current wind map (left) and new wind map (right), taken from Kruger (2011).

wind map was developed based on the available data from 209 weather stations of which 76 stations were selected for the final analysis after a rigorous quality audit. Figure 4.5 shows the spatial distribution of these stations. It is clear that the quantiles from the new wind map is more accurate and has a finer spatial resolution than the present wind map.

Although the selected stations do represent a significant improvement to the spatial resolution of the wind map, due to the size of the country there are still large areas which were not covered. The development of a wind map therefore requires spatial interpolation of wind data between stations, which implies that design strong wind values need to be estimated for areas where no wind measurements were made. This proves particularly challenging in areas with complex terrain. Furthermore, it should be noted that the wind data is biased towards areas with dense populations as weather stations are typically located close to main centres such as towns and cities. It was therefore decided by Retief *et al.* (2015), that the new wind map be developed based on municipal zones with weather stations within those zones regarded as being representative of the entire zone. This approach had two advantages. Firstly, municipal boundaries often follow local topography and natural features which may also influence the free-field wind. Secondly, it becomes convenient for the users of the loading code to identify the design free-field wind speed at the location of the structure.

Another important criterion of the wind map which required careful consideration was the wind speed intervals used. The interval needed to be selected in such a way that the increments were not too large as that would lead to a significant overestimation of the design wind speed

in areas that are on the lower end of the interval. However, too small an increment would result in fragmentation of the wind map. It was decided that four intervals of 4 m/s starting from 32 m/s would be used.

The current map used in SANS is shown in Figure 4.6. It should be noted that the values in the map need to be multiplied with a factor of 1.4 to obtain gust wind speed values, as explained in 2.2.1. As expected from the low spatial resolution of the weather stations used in its development, the map provides large zones which are not well defined. Most of the country is in the lowest wind speed zone corresponding to a gust wind speed of 39.2 m/s, with the central part of the country showing higher gust wind speeds of 44.8 m/s and 50.4 m/s.

The proposed new gust wind map is shown in Figure 4.7. There are several distinct differences which are immediately apparent. Firstly, the general shape of the high wind speed zones are significantly different, with the highest wind speed zones now being in the Western Cape and the Eastern Cape, with a lower wind speed area in the South Coast separating them. It is also interesting to note that in general the characteristic wind speed decreases further North. Furthermore, by providing wind speeds based on municipal boundaries, wind speed areas are defined logically and the characteristic free-field wind at any location may be obtained easily. There is very limited fragmentation, or multiple small regions with different wind speeds, and the country seems to be divided into seven primary zones. This indicates an appropriate choice of wind speed interval. Finally, the overall gust wind speeds are significantly lower than in the current map, with the highest having a 44 m/s gust wind speed.

The representative parameters of the free-field wind probability distribution were determined using the design quantiles given in the proposed new wind map, not the current wind map. As the probability model developed in this investigation may be used for future calibration of the South African wind load standard, it stands to reason that the wind map which will be in the standard at that time should be used to develop the model. Furthermore, as the extreme wind predictive models developed by Kruger will be used in the investigation of the free-field wind and not the models developed by Milford, and the new map is also based on the Kruger predictive models, it is the most consistent approach.

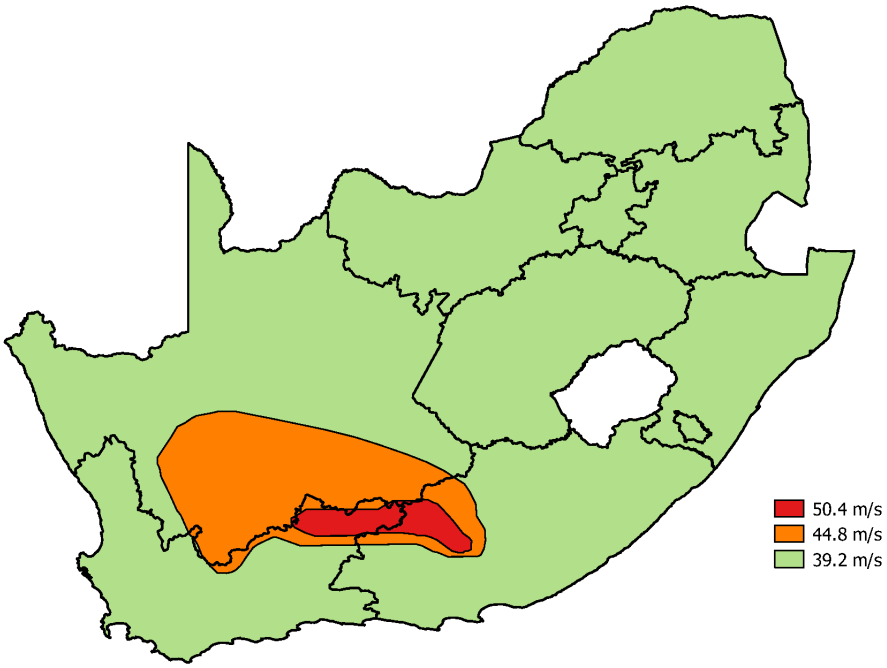

Figure 4.6: Current characteristic wind speed map in South African wind loading code including 1.4 conversion factor.

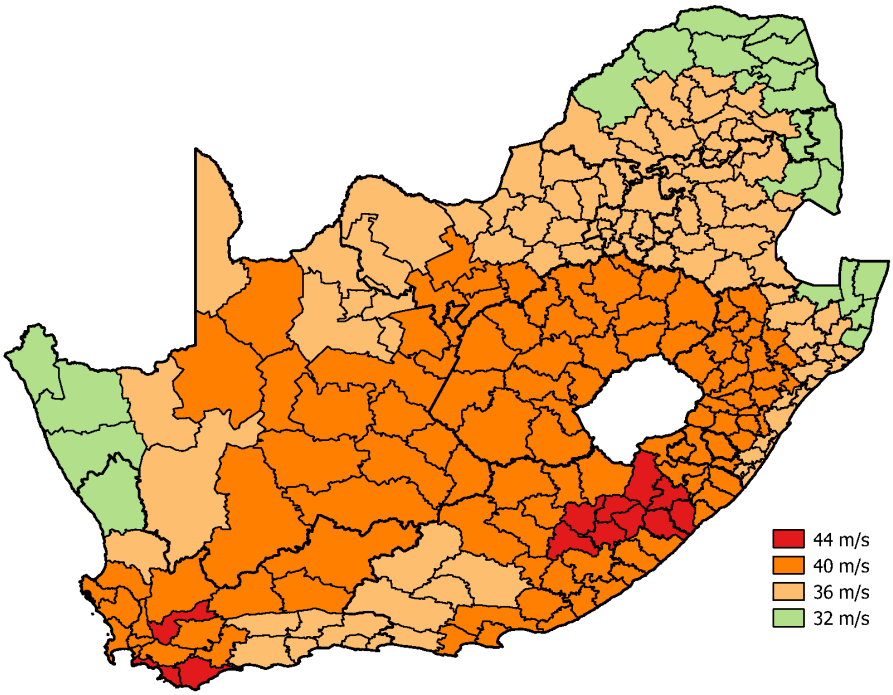

Figure 4.7: Proposed new map for South African wind loading code, from Retief *et al.* (2015).

4.3 Statistical parameters of representative design free-field wind pressure

The purpose of the representative distribution of the free-field wind is not to describe the uncertainty of the free-field wind pressure at a given position, but rather to describe the uncertainty of the characteristic free-field wind pressure selected at any position in the country using the South African wind loading standard. This means that not only do the aleatoric uncertainties of the free-field wind itself need to be considered, but the epistemic uncertainties which are introduced by the way in which the characteristic free-field wind is presented in the standard also need to be taken into account. The following investigation which aims to quantify these uncertainties is therefore done in two parts.

Following the approach discussed in Section 3.5, the free-field wind component was modeled as a hierarchical Bayesian model. Using this method the systematic bias and the variability of the free-field wind were regarded as independent random variables and investigated separately. A prior probability distribution was defined for each and these distributions were then combined into a posterior predictive representative distribution of the free-field wind using the Monte Carlo simulation method.

4.3.1 Systematic bias

The systematic bias as defined in JCSS (2001-2002) is the ratio of the expected "real" or measured value to the value computed using a theoretical model. There are two factors which influence the systematic bias of free-field wind pressure, however they do not influence the systematic bias in the same way. An important distinction should be made between effects of these factors, as explained below.

The first factor to consider is the predictive model used to determine the characteristic extreme wind speed. The predictive models affect the "characteristic bias" as conventionally used and defined by JCSS (2001-2002), which is the ratio of the measured value to the theoretical model. As the predictive models developed by Kruger are based on observed wind speed data, it may be assumed that the characteristic bias value of these models is equal to unity.

This only leaves the influence of the design wind speed map, which does not influence

the characteristic bias but rather introduces a bias of estimating the characteristic value. As discussed in the previous sections, wind maps use wind speed intervals to delineate an area into contiguous zones which share the same characteristic design wind speed. The implication of this is that there is an overestimation of the wind speed in areas with a wind speed which falls on the lower end of the interval, which leads to a systematic bias in the calculation of the characteristic free-field wind speed. It is not possible to calculate the systematic bias at every position across the country. The best approximation of the free-field wind pressure bias is therefore to determine the bias at the positions where there is observed data and to sample those values, effectively regarding the bias as a random variable and fitting a probability distribution to the available data.

The characteristic 50 year wind speed $v_{k,i}$ was determined at each of the 76 weather stations. As mentioned in Section 4.1.1, exposure correction was done by Kruger (2011) during the development of the new wind map to account for the local terrain at each station. As such, the $v_{k,i}$ values used in this investigation were the exposure corrected values as calculated by Kruger, not the values as calculated directly from the extreme wind predictive models. The mapped characteristic wind speed $v_{m,i}$ was then read off from the new wind map. The free-field wind pressure bias b_i could then be calculated at each station by converting the wind speeds to pressures and calculating the ratio of the predicted and mapped values using $b_i = (v_{k,i}/v_{m,i})^2$. These values are given in Appendix B. The values $b_1, b_2, ..., b_{76}$ were then sampled to determine the statistical parameters of the free-field wind pressure bias distribution. The mean and standard deviation of the systematic pressure bias were calculated as 0.92 and 0.13 respectively. A normal distribution was fitted to the data and is shown in Figure 4.8.

4.3.2 Variability

As mentioned in the introduction to the section, the purpose of the probabilistic model of free-field wind pressure is to represent the uncertainty of the free-field wind pressure at any position in the country when the SANS wind load formulation is used. This becomes a significant challenge when considering the variability of the free-field wind, as it is clear from the predictive models developed by Kruger that the variability of the free-field wind is different at each location considered. A method needed to be developed in order to combine the variability of all the

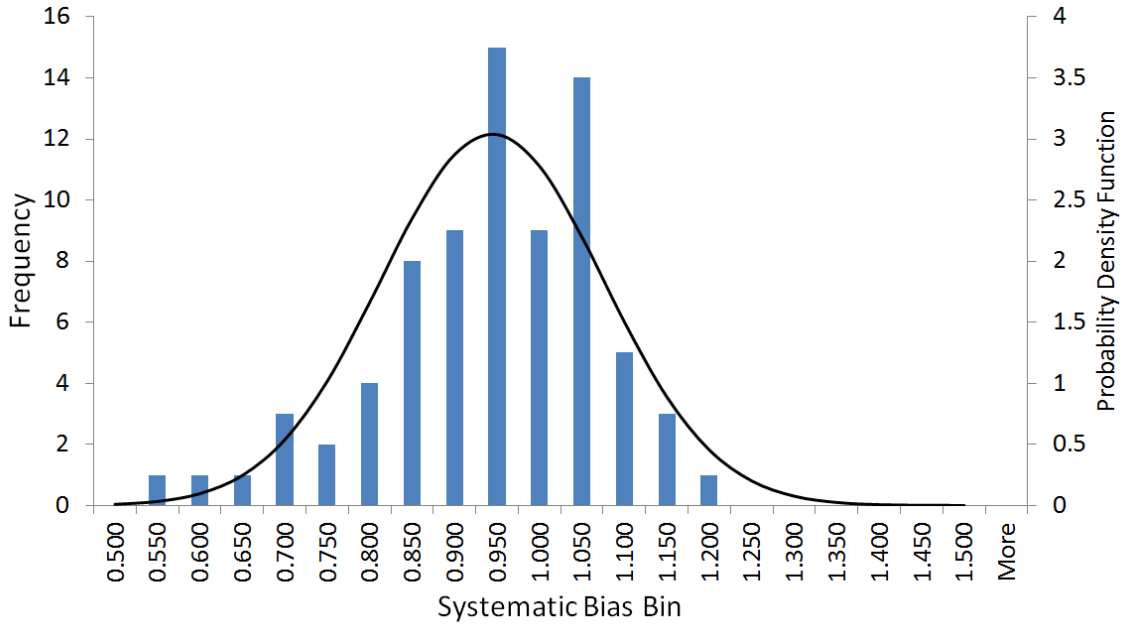

Figure 4.8: Histogram and probability density function of free-field wind systematic bias.

predictive models effectively.

4.3.2.1 Envelope method

A method was presented by Retief *et al.* (2013) for determining an envelope of free-field wind speed variability when considering the extreme wind prediction models of weather stations in close proximity. This method was expanded by Botha *et al.* (2014) to determine an envelope of the free-field wind variability when considering stations across the entire country. For the sake of clarity this method is referred to as the envelope method. The envelope method is based on the assumption that the Gumbel distribution is used for the extreme wind prediction models. Using this method, all models are normalized with respect to the characteristic value at each station, converting the distributions to standard form as used in probabilistic investigations. The wind speed models are then converted to wind pressure models and the upper and lower limit values of the coefficients of variation are used to define the envelope of possible values of the variability. The method is expanded further in this section by sampling the coefficients of variation to determine a probability distribution of the design free-field wind pressure variability.

The first issue that needed to be addressed in order to effectively use the envelope method was the assumption that a Gumbel distribution is fitted to the tail end of observed wind speeds (consisting of wind speed exceeding the characteristic value) when considering extreme wind predictive models. From Table 4.1 it may be seen that for the 76 stations used in this

investigation, the most commonly selected predictive model was the EXP model and not the Gumbel model. The envelope method relies upon comparison of coefficients of variation, and as the EXP model has a constant coefficient of variation equal to unity it is not suitable for use with the method.

A solution was found by performing the envelope method analysis with three different model sets simultaneously and comparing the results. The first model set was formed by simply using the Gumbel distribution parameters determined for each station instead of using the distribution model selected by Kruger. The second model set was formed by excluding all stations where the EXP distribution was selected. As the quantiles from the Gumbel and Mixed distributions correspond well, which is expected considering that the Mixed distribution is based on the combination of Gumbel distributions, the Gumbel distribution parameters were selected for the remaining stations. This resulted in only 34 stations being considered which significantly reduced the spatial distribution of stations across the country, as seen from Figure 4.4. It still provided a point of comparison with the other model sets, however, and would indicate whether the results of the analysis changed significantly if a large portion of the stations were excluded. The final model set was formed by determining equivalent Gumbel distribution parameters for the stations where the EXP and Mixed models were selected by using a regression function on the tail end of the distribution. The procedure followed to calculate the equivalent distributions is described in Section 4.3.2.2 below.

Another issue which needed to be considered was the effect of the different strong wind generating mechanisms on the free-field wind variability. Therefore, in addition to using the three model sets consisting of different predictive models, the stations used were disaggregated according to the most dominant strong wind generating mechanism at each station. Only synoptic scale events and meso-scale convective wind events (thunderstorms) were considered as they are the most widespread of the mechanisms and represent the two most dissimilar mechanisms in terms of wind characteristics. The aim of this was to find out if the strong wind generating mechanisms have different influences on the variability of the free-field wind and to investigate whether the envelope method could be applied to all stations regardless of the dominant mechanism. The models were normalized with respect to the their characteristic 50 year return period design quantiles. Figure 4.9 shows the normalized wind speed plotted against the corresponding probability for all the stations in all three model sets disaggregated

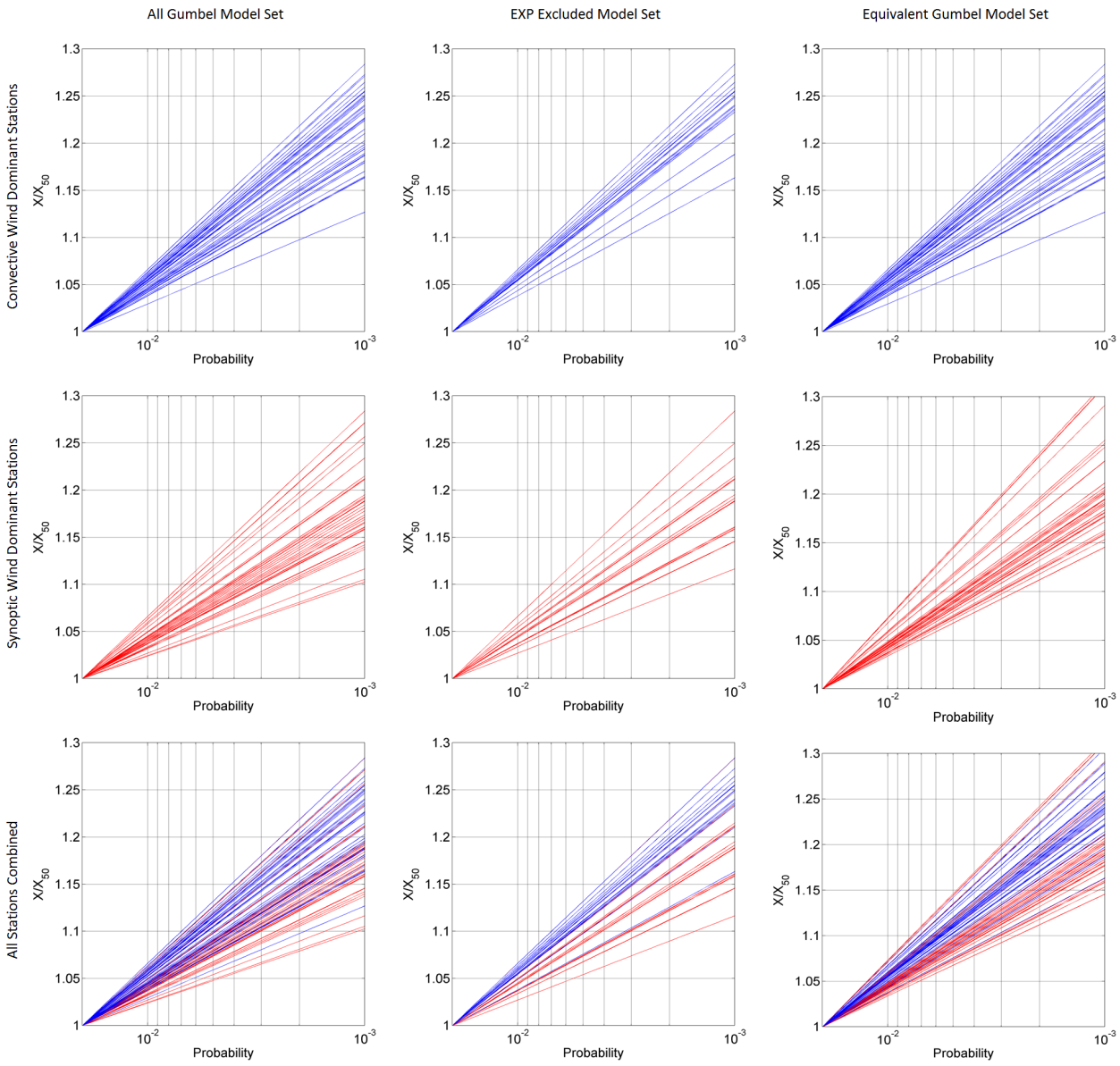

Figure 4.9: Normalized predictive models for each of the three model sets showing results disaggregated by dominant strong wind generating mechanisms.

by dominant strong wind generating mechanisms.

For each of the three model sets the upper and lower limits of the distribution models were selected to determine a range of extreme wind speed model variability for the two strong wind mechanisms. The overlapping areas of these two envelopes were calculated by evaluating the integrals of the distribution functions on the probability interval $[0.001, 0.020]$. The calculation was performed using the following steps:

1. The models were disaggregated according to strong wind generating mechanism and the upper and lower bound models for each mechanism were identified.

2. The areas between the curves for each mechanism as well as between the absolute upper

and lower models were calculated by integrating the difference between the two curves over the probability interval [0.001, 0.020].

3. The overlapping area for the two mechanisms was calculated in the same manner as step 2, and was then converted into a percentage by comparing it with the areas obtained in step 2.

For the first model set which consisted of the Gumbel models for each of the stations an 86.7% overlap of the envelopes was found. The second model set which excluded all stations where the EXP model had been selected showed a 72.0% overlap. Finally, the third model set consisting of equivalent Gumbel models showed a 94.5% overlap. The large difference between the second model set overlap and first and third model sets is explained by the removal of stations on the lower end of the convective wind envelope, as is seen in Figure 4.9. As the percentage overlap of the synoptic and convective wind envelopes is significant for each of the three model sets, these results indicate that the difference between the average wind speed models of the two wind generating mechanisms is insignificant when compared to the difference between the upper and lower bounds of each range.

The probabilistic free-field wind model requires annual extreme wind pressure models as opposed to annual extreme wind speed models. From Equation 2.2.1 it may be seen that a quadratic relationship exists between wind speed and pressure. The wind speed models were therefore transformed into wind pressure models by determining the mean and standard deviation of the wind pressure models using Equations 4.3.1 and 4.3.2. A value of unity was assumed for air density.

$$\mu_{Q,Ref} = 0.5\rho\mu_{V^2} \tag{4.3.1}$$

$$\sigma_{Q,Ref} = 0.5\rho\sigma_{V^2} \tag{4.3.2}$$

where, $\mu_{Q,Ref}$ is the mean of the wind pressure

$\sigma_{Q,Ref}$ is the standard deviation of the wind pressure

ρ is the air density

μ_{V^2} is the mean of the squared wind speed

σ_{V^2} is the standard deviation of the squared wind speed

The mean and standard deviation of the squared wind speed were calculated using standard moment identities (Holický (2009)) as given in Equations 4.3.3 and 4.3.4. It was assumed that the pressure distribution would be the same as the velocity distribution, i.e. a Gumbel model. However, this was not strictly the case as shown by calculation of the skewness of the squared wind speed, which was done using Equation 4.3.5. The Gumbel distribution has a constant skewness of 1.14. The skewness of the pressure models were calculated for each of the three model sets and the ranges of values obtained are given in Table 4.2. It is clear that the calculated skewness of the pressure distribution is greater than 1.14, and it should be noted that underestimating skewness by assuming a Gumbel distribution is unconservative. However, as the assumption to use the Gumbel distribution for the free-field wind pressure model for the sake of consistency had been made at the start of the investigation, it was decided that the disparity was within acceptable limits and that the Gumbel model would continue to be used.

$$\mu_{V^2} = \mu_V^2 + \sigma_V^2 \tag{4.3.3}$$

$$\sigma_{V^2} = 2\sigma_V\sqrt{\mu_V^2 + \mu_V\sigma_V\alpha_V} \tag{4.3.4}$$

$$\alpha_{V^2} = \frac{8\mu_V^3\sigma_V^3(\alpha_V + 3w_V)}{\sigma_{V^2}^3} \tag{4.3.5}$$

where, μ_V is the wind speed model mean

σ_V is the wind speed model standard deviation

α_V is the wind speed model skewness

α_{V^2} is the wind pressure model skewness

Table 4.2: Ranges of calculated skewness values for wind pressure models.

Model Set	Max α_{V^2}	Average α_{V^2}	Min α_{V^2}
All Gumbel	1.27	1.23	1.19
EXP Excluded	1.27	1.24	1.19
Equivalent Gumbel	1.28	1.24	1.21

The final step of the envelope method was to sample the coefficients of variation of the pressure model of each station for the three model sets, continuing to keep the results disaggregated by strong wind generating mechanism. These values were used to determine the distribution parameters of the free-field wind variability. By sampling the stations across the entire country, this distribution effectively encapsulates the variability which is inherent in the selection

of free-field wind speed at any location in the country when using the new South African design wind map. The results from the envelope process and the distribution calculated for the free-field wind variability are given in Section 4.3.2.3 below.

4.3.2.2 Equivalent Gumbel distribution parameters for EXP models

Equivalent Gumbel parameters were found for stations where the EXP model had been selected using a regression function on the tail end of the distribution. As the envelope method normalizes the distributions with respect to the characteristic or 50 year return period design value, the tail end of the distribution is where the greatest accuracy is required. Therefore the three standard design quantiles corresponding to 50, 100 and 500 year return periods as calculated by Kruger for the EXP stations were used as observations for the regression function. These quantile values for all stations used in this investigation are given in Appendix A. The matrix approach to multiple linear regression using the least square estimate method as described in Montgomery and Runger (2010) was used, however instead of using a linear regression function the logarithmic reduced variate of the Gumbel distribution was used. The method is described in detail below.

When using regression functions with multiple observations and regressor variables it is typically most convenient to express mathematical operations using matrix notation. For a model with k regressor values and n observations related by Equation 4.3.6, the model may be represented as a system of n equations which are expressed in matrix notation as shown in Equation 4.3.7.

$$y_i = N_0 + N_1 x_{i1} + N_2 x_{i2} + \cdots + N_k x_{ik} + \epsilon_i \qquad i = 1, 2, \ldots, n \tag{4.3.6}$$

$$\boldsymbol{y} = \boldsymbol{X}\boldsymbol{N} + \boldsymbol{\epsilon} \tag{4.3.7}$$

where

$$\boldsymbol{y} = \begin{bmatrix} y_1 \\ y_2 \\ \vdots \\ y_n \end{bmatrix} \quad \boldsymbol{X} = \begin{bmatrix} 1 & x_{11} & x_{12} & \cdots & x_{1k} \\ 1 & x_{21} & x_{22} & \cdots & x_{2k} \\ \vdots & \vdots & & \vdots & \\ 1 & x_{n1} & x_{n2} & \cdots & x_{nk} \end{bmatrix} \quad \boldsymbol{N} = \begin{bmatrix} N_0 \\ N_1 \\ \vdots \\ N_k \end{bmatrix} \quad \boldsymbol{\epsilon} = \begin{bmatrix} \epsilon_1 \\ \epsilon_2 \\ \vdots \\ \epsilon_n \end{bmatrix}$$

In this equation, $\boldsymbol{y}$ is a $(n \times 1)$ vector which contains the observations, $\boldsymbol{X}$ is a $(n \times p)$ matrix of the levels of the independent variables with $p = k+1$, $\boldsymbol{N}$ is a $(p \times 1)$ vector of the regression coefficients, and $\boldsymbol{\epsilon}$ is a $(n \times 1)$ vector of random errors.

Using the method of least squares estimators requires that the dot product of the error vector with itself as given in Equation 4.3.8 be minimized and effectively reduced to zero. The least square estimate of the regression coefficients $\hat{\boldsymbol{N}}$ is therefore found by equating the derivative of the function equal to zero as shown in Equation 4.3.9.

$$L = \sum_{i=1}^{n} \epsilon_i^2 = \boldsymbol{\epsilon'\epsilon} = (\boldsymbol{y - XN})'(\boldsymbol{y - XN}) \tag{4.3.8}$$

$$\begin{aligned} \frac{\partial L}{\partial \boldsymbol{N}} &= \boldsymbol{0} \\ \boldsymbol{X'X\hat{N}} &= \boldsymbol{X'y} \\ \hat{\boldsymbol{N}} &= \boldsymbol{(X'X)^{-1}X'y} \end{aligned} \tag{4.3.9}$$

This method may be applied to estimate Gumbel distribution parameters. The equation used to calculate design quantiles for the Gumbel distribution as given in Equation 4.1.6 is used as the basic model. However, in order to use the method described above a linear function is required. Therefore the matrix representing the levels of the independent variables $\boldsymbol{X}$ is reduced as shown in Equation 4.3.10 by taking the natural logarithm of the negative natural logarithm of the probabilities associated with the given return periods.

$$\boldsymbol{X} = \begin{bmatrix} \boldsymbol{1} & \boldsymbol{J} \end{bmatrix} \tag{4.3.10}$$

where

$$\boldsymbol{1} = \begin{bmatrix} 1 \\ 1 \\ \vdots \\ 1 \end{bmatrix} \qquad \boldsymbol{J} = -ln[-ln(\boldsymbol{P})] \qquad \boldsymbol{P} = \begin{bmatrix} 1 - \frac{1}{T_1} \\ 1 - \frac{1}{T_2} \\ \vdots \\ 1 - \frac{1}{T_n} \end{bmatrix}$$

The Gumbel distribution parameters α and β are used as the regression coefficients and the design quantiles for the 50, 100 and 500 (X_{50}, X_{100}, X_{500}) year return periods as calculated using the EXP model are used as the observations. The set of simultaneous equations can

then be represented in matrix notation as shown in Equation 4.3.11 and solved using the least square estimate method.

$$\begin{bmatrix} X_{50} \\ X_{100} \\ X_{500} \end{bmatrix} = \begin{bmatrix} 1 & -3.9019 \\ 1 & -4.6001 \\ 1 & -6.2136 \end{bmatrix} \begin{bmatrix} \beta \\ \alpha \end{bmatrix} + \begin{bmatrix} \epsilon_1 \\ \epsilon_2 \\ \epsilon_3 \end{bmatrix} \tag{4.3.11}$$

The method is demonstrated using the distribution parameters of the weather station at George. In the study by Kruger the EXP model was selected as the most appropriate model for the station based on the available data. The EXP distribution parameters and design quantiles as calculated by Kruger for the station are given in Table 4.3. The method described above was used to determine an equivalent Gumbel distribution. The calculated distribution parameters and design quantiles are given in Table 4.4. The differences between the three EXP design quantiles and the design quantiles calculated using the equivalent Gumbel distribution were calculated and the average residual was found to be 4.48×10^{-2}. Figure 4.10 shows the design wind speed plotted against return period for the two distributions. At the lower end the distributions diverge, however at the tail end, which is the significant part of the distribution when considering extreme wind prediction, the two models correspond well.

Table 4.3: EXP distribution parameters and design quantiles for George weather station.

α	β	n	λ	ξ	X_{50}	X_{100}	X_{500}
2.00	22.60	62.00	3.88	22.80	33.34	34.72	37.94

Table 4.4: Equivalent Gumbel distribution parameters and design quantiles for George weather station.

α	β	μ	σ	X_{50}	X_{100}	X_{500}
2.04	25.35	26.52	2.61	33.29	34.71	38.00

This method was applied to all stations where the EXP distribution had been selected and the equivalent Gumbel distribution parameters were calculated. The design quantiles for the selected return periods were calculated using these equivalent distributions and residual values were determined. Across the 42 stations considered the average residual was calculated to be 1.31×10^{-2} m/s, which was deemed acceptable. The equivalent Gumbel distributions in

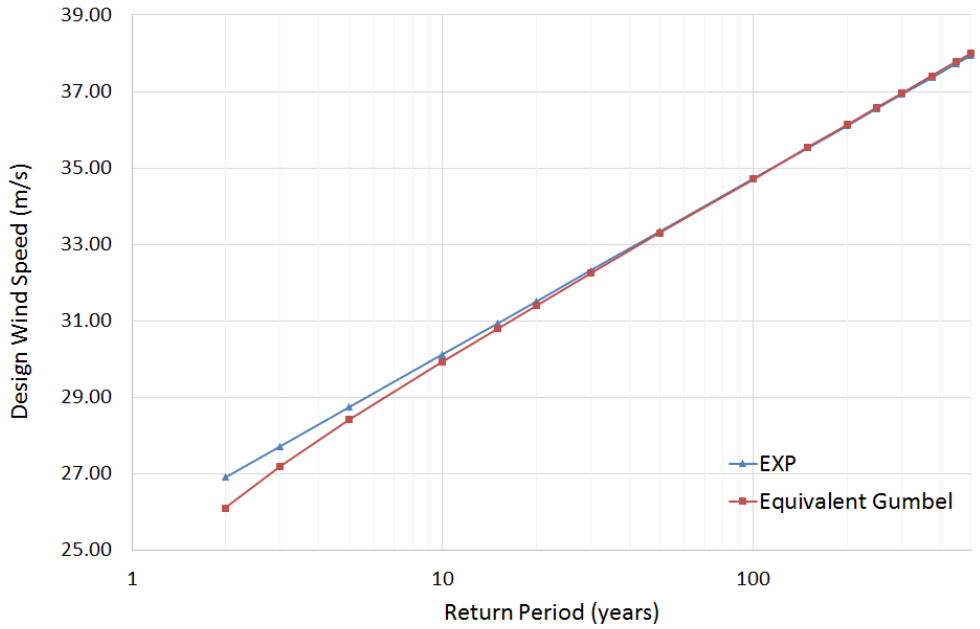

Figure 4.10: Design wind speed for given return period for the EXP and equivalent Gumbel distributions for George weather station.

addition to the stations where the Gumbel or Mixed distributions had already been selected were used as the third model set to be used for the envelope method analysis.

4.3.2.3 Envelope method results

The coefficients of variation of the extreme wind prediction models for the three model sets disaggregated by strong wind mechanism were sampled and a probability distribution was fitted to values from each set. As the standard form of probabilistic models requires that the model be normalised with respect to the expected value, and as already discussed in Section 4.3.1, the systematic bias of the predictive models is equal to unity because the models are based on observed values. It is therefore clear that the coefficient of variation of these models is equal to the standard deviation of the overall probabilistic model.

As the stations are independent of each other it may be assumed by the central limit theorem that the coefficients of variation are normally distributed. However, as the standard deviation cannot be negative, the normal distribution is undesirable. Therefore, the log-normal distribution which is bounded on the lower end was used. The fitted log-normal distributions for the three models sets as well as the disaggregated and combined stations are shown in Figure 4.11, and the calculated statistical parameters are given in Table 4.5.

The results from this investigation of the free-field wind variability need to assessed in

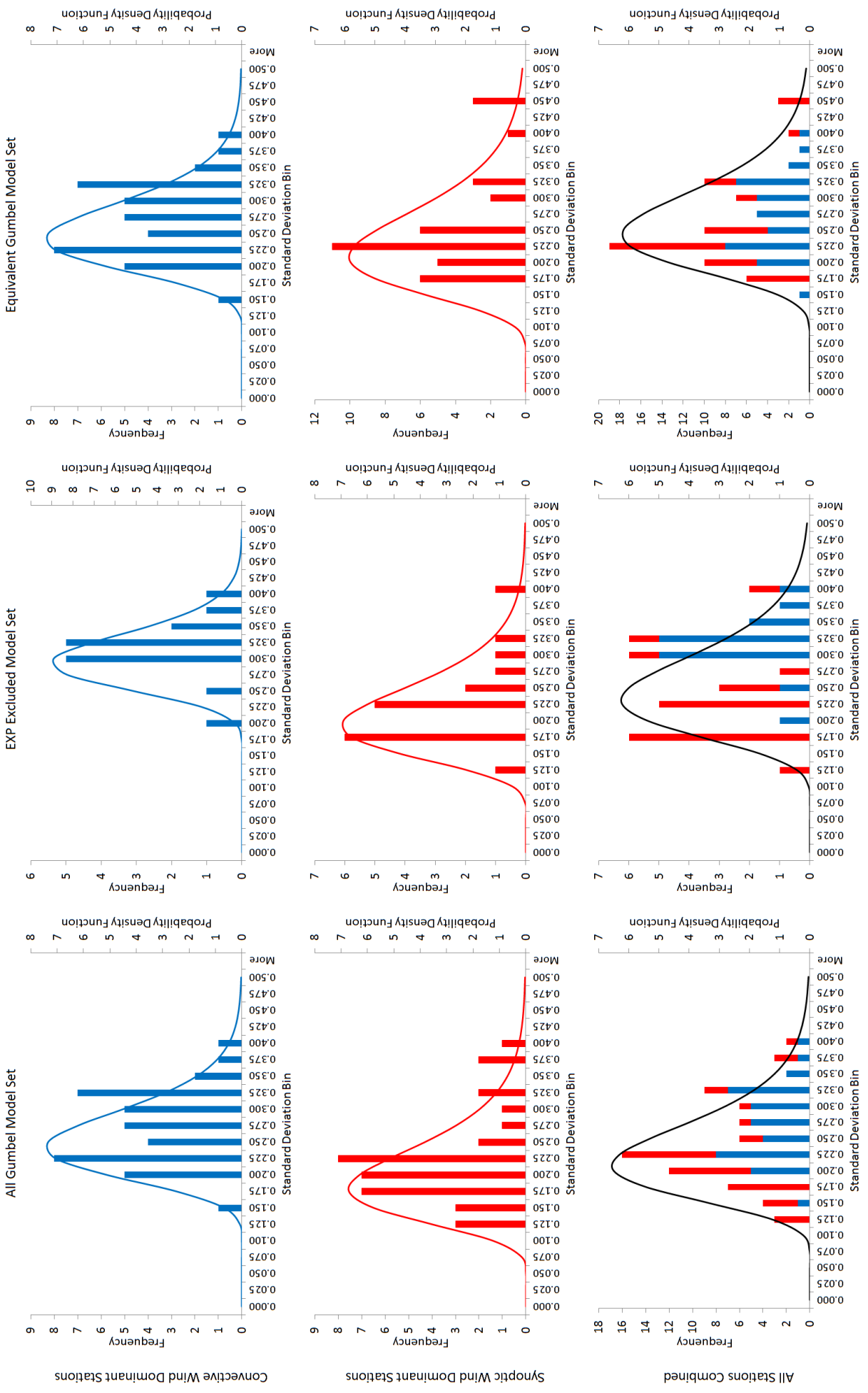

Figure 4.11: Histogram and fitted log-normal probability distribution for each of the three model sets showing results disaggregated by dominant strong wind generating mechanisms.

Table 4.5: Statistical parameters of free-field wind variability for different model sets.

Model Set	Convective			Synoptic			Combined		
	μ_X	σ_X	CoV	μ_X	σ_X	CoV	μ_X	σ_X	CoV
All Gumbel	0.26	0.06	0.22	0.21	0.07	0.33	0.23	0.07	0.29
EXP Excluded	0.30	0.05	0.15	0.22	0.06	0.29	0.26	0.07	0.27
Equivalent Gumbel	0.29	0.05	0.18	0.24	0.08	0.32	0.27	0.07	0.26

terms of the influence on the variability of two criteria: the influence of the different model sets and the influence of the different strong wind generating mechanisms. Firstly, considering the strong wind generating mechanisms, it is seen from the results that the stations dominated by convective winds have a higher variability than the stations dominated by synoptic winds. This trend is reflected in the results for all three model sets. This increase in variability is not insignificant, and should be remembered when considering the final aim of this probabilistic model, i.e. to describe the total uncertainty of the characteristic free-field wind pressure selected at any position in the country using the South African wind loading standard.

When considering the results from the three model sets it is found that all three model sets give similar standard deviation values, however there is disparity between the mean value results. The model set consisting of the basic Gumbel models resulted in the lowest mean values in all cases, and the model set made up of the equivalent Gumbel distributions resulted the highest values in two of the three sets. Due to the low number of stations used in the EXP excluded model set, the results from that set should not be used directly. However, it is interesting and reassuring to note that with a significantly reduced dataset the final results obtained are very similar to those found using the full dataset. This serves as an indication of the robustness of the envelope methodology applied in this investigation.

In order to continue with the development of a free-field wind probabilistic model it is necessary to select from these nine possible distributions a single distribution as the representative prior of the free-field wind pressure uncertainty. As already mentioned above, the results from the EXP excluded model set are only to be considered as indicative findings. As the equivalent Gumbel model set is the closest representation of the final selected extreme wind prediction models used to develop the South African design wind speed map, it may be selected as the most representative model set. Finally, when considering the strong wind generating mechanisms, it stands to reason that by sampling values from all the stations combined the total variability calculated for the combined set encapsulates the uncertainty of both the higher

variability of convective winds and the lower variability of synoptic winds. Therefore, the final selected representative prior of South African free-field wind pressure is that obtained from the equivalent Gumbel model set with combined sampling from convective and synoptic stations.

4.3.3 Final representative distribution

In Sections 4.3.1 and 4.3.2 probability distributions were determined for the South African free-field wind systematic bias and variability. It should be reiterated that these distributions are regarded as prior distributions of independent random variables in a Bayesian hierarchical model in order to effectively combine uncertainties from multiple sources. Using this approach, the uncertainties due to the systematic bias introduced by the wind speed intervals used in the development of the design wind speed map were treated independently of the uncertainties due to variability of the extreme wind prediction models used. Using the Monte Carlo method developed in Section 3.5, these distributions were combined into a single posterior probability distribution representative of the South African free-field wind pressure.

The two input distributions used as well as the final representative distribution of free-field wind pressure are summarized in Table 4.6. Figure 4.12 shows the Monte Carlo histogram and probability density function of the representative distribution.

Table 4.6: Monte Carlo input distributions and resulting representative distribution of terrain roughness factors.

X	Distribution	μ_X	σ_X
Systematic bias	Normal	0.92	0.14
Standard deviation	Log-normal	0.27	0.07
50-year extremes of wind pressure	Gumbel	0.92	0.31

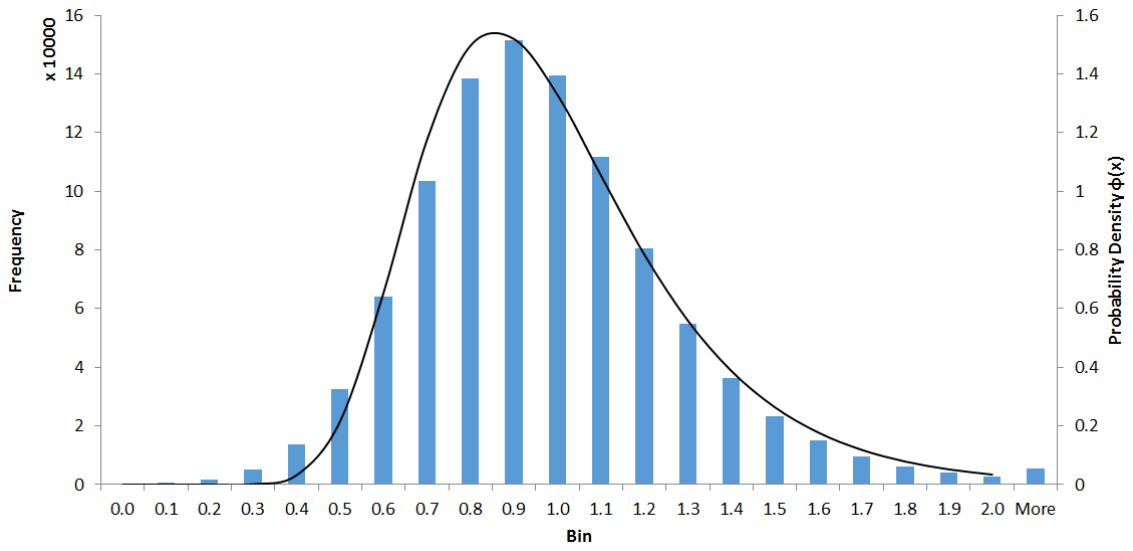

Figure 4.12: Monte Carlo histogram and probability density function of representative probability distribution of South African design wind pressure.

Chapter 5

Pressure Coefficients

The investigation of pressure coefficient uncertainties was the most challenging part of this investigation due to complexity of the underlying wind engineering models and the scope of possible pressure coefficients. As discussed in Section 2.2.4.2, these pressure coefficients are used to represent the aerodynamic influence of geometry of the structure. Pressure coefficients are subject to a multitude of uncertainties, both aleatoric and epistemic in nature. The two-pronged investigative methodology described in Section 3.4 was therefore employed in order to effectively use all available reliability data and information to quantify these uncertainties.

This chapter details the development of the pressure coefficient probabilistic model. Two investigations were undertaken to this end. In the first investigation the SANS pressure coefficient values were compared to results obtained from wind tunnel and full-scale tests. The second investigation consisted of a comparative investigation of the pressure coefficient values given in different international wind load standards using a parameter study of area-averaged pressure coefficient values across representative structures. These investigations are presented in detail in the following sections. The results from the investigations are then summarized and used to select a single representative distribution for the SANS pressure coefficient uncertainties.

5.1 Wind tunnel and full-scale test result comparison

It stands to reason that the most effective way to describe the probability distribution of the expected codified value of any wind load component normalized with respect to the observed values of that component is through a direct comparison of codified values and observed values.

Therefore, this is the first approach which is discussed in the overarching investigation of pressure coefficient uncertainties. Results were gathered from several representative wind tunnel and full-scale studies and compared with the SANS pressure coefficient values.

The studies considered in this investigation were selected based on how the results were presented and the reliability of the sources. The final selected studies which presented results from investigations of pressure coefficients on low-rise buildings were all published in the Journal of Wind Engineering and Industrial Aerodynamics or the Journal of Structural Engineering. In some of these studies the determination of pressure coefficients was not the final aim, but the wind tunnel and/or full-scale tests were an intermediate step in a larger investigation. Only studies in which pressure coefficient results were explicitly given and not only discussed qualitatively were considered. A conscious effort was made to ensure that the selected studies were reliable. Quality control was conducted based on three primary parameters: the number of third-party citations of a study in other peer-reviewed articles, the reputation and experience of the authors, and the transparency of the results given.

After a rigorous literature study, eleven studies were selected for this investigation. Each of the studies is briefly described in the following sections and the results from each study is compared to the equivalent SANS pressure coefficient value. In Section 5.1.8 the results from all the studies considered are summarized and used to determine a representative distribution of pressure coefficients based on direct comparison of codified values with observed values.

5.1.1 Texas Tech University experiment

The Wind Engineering Research Field Laboratory (WERFL) was a low-rise full-scale test building at Texas Tech University (TTU) which was built in 1991. The TTU experiment was arguably the most prolific full-scale wind engineering experiment of the last thirty years. The test setup, shown in Figure 5.1 was described by Levitan and Mehta (1992). The building was a $9.14 \times 13.72 \times 3.96$ m flat roofed structure located in an area with flat surrounding topography equivalent to SANS Terrain Category B. One of the noteworthy characteristics of the TTU building was that it was not directly anchored to the foundation. The structure was connected to a rigid frame undercarriage which was mounted on a circular rail, which allowed the building to be rotated a full 360°. This allowed researchers to control the wind angle of

Figure 5.1: Photo of the WERFL test building at TTU taken from Website (2015).

attack.

Numerous studies have been done using the results from the TTU experiment to investigate matters such as how well wind tunnel test results compare with full-scale test results, area-averaging of pressure coefficients and the effects of internal pressures on external pressures. In this investigation, the results from five of these studies is presented and compared to the pressure coefficients given in SANS.

The first three studies considered investigate the mean point pressure coefficient values along the central frame of the TTU building. Only the wind angle of attack in the plane of the frame is considered. The central frame geometry and wind direction considered are shown in Figure 5.2. The first study was done by Levitan *et al.* (1991) and presented the full-scale measurements on the TTU building. The second study by Surry (1991) presented the results from a boundary layer wind tunnel test at the University of Western Ontario (UWO) using a $1:100$ scale model. The final study by Endo *et al.* (2006) was conducted using a boundary layer wind tunnel at the Colorado State University (CSU) using a $1:50$ scale model.

The mean point pressure coefficients measured along the central frame of the TTU building

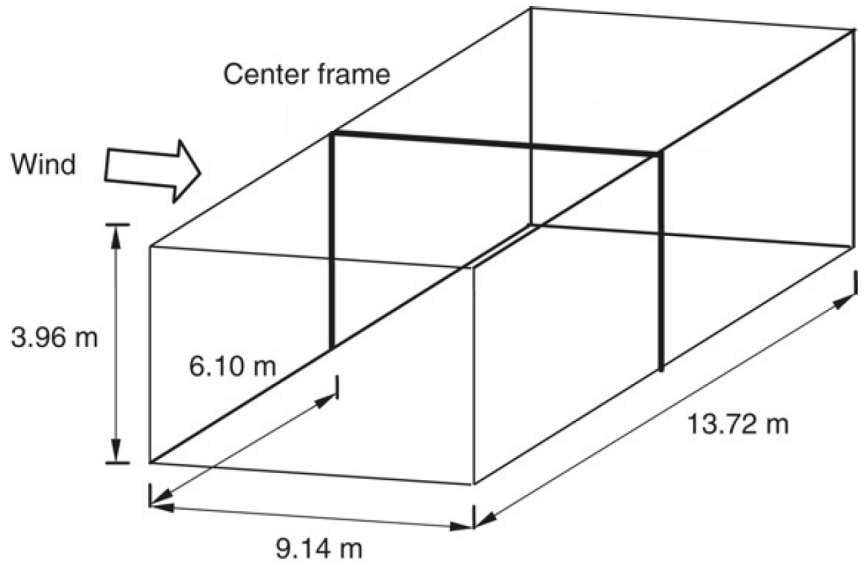

Figure 5.2: Central frame of TTU building as shown in Chen and Zhou (2007).

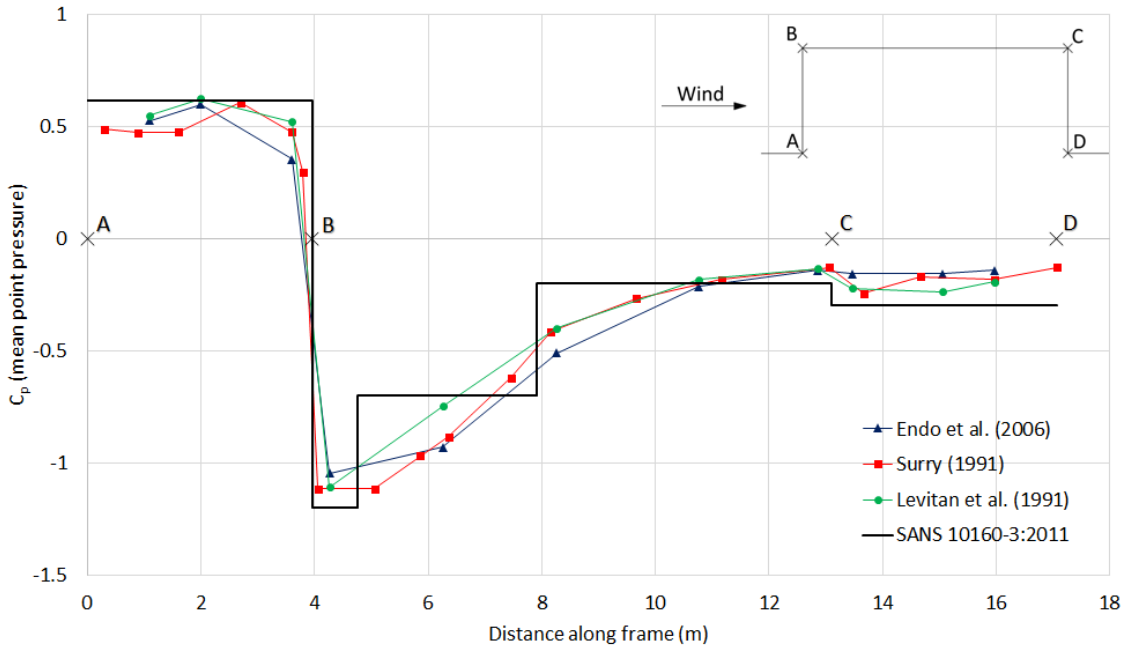

Figure 5.3: Mean point pressure coefficient results from wind tunnel and full-scale tests on central frame of TTU building.

in each of these three studies are shown in Figure 5.3. The results show good agreement between the wind tunnel and full-scale test results. The measured values also agree well with the SANS pressure coefficients values and the static pressure distribution pattern. On the walls of the structure (between A to B and C to D) the SANS pressure coefficients are greater than the observed values. However, on the roof (between B to C) the SANS values underestimate the observed values, especially near the windward edge.

Another study was done by Chen and Zhou (2007) at TTU and investigated equivalent

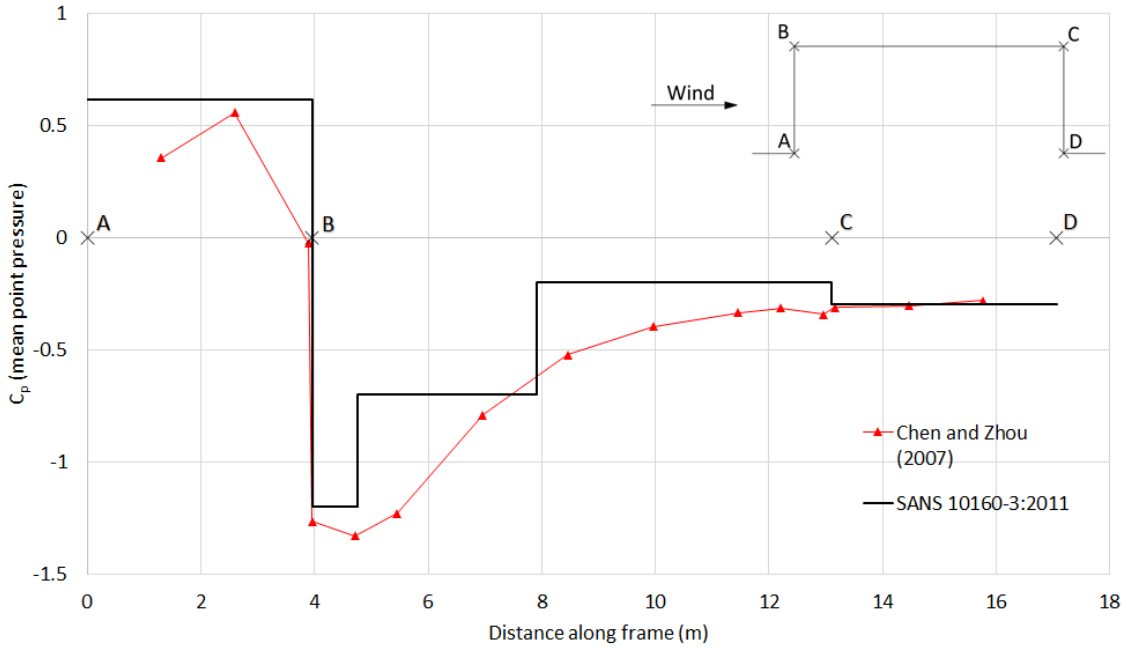

Figure 5.4: Mean area-averaged pressure coefficient results from full-scale test on central frame of TTU building.

static wind loads on low-rise buildings using the results from the TTU building. The pressure coefficients along the central frame as shown in Figure 5.2 were determined. However, unlike the previous three studies, the pressure coefficients were not point values, but were calculated using the area-average of 5 pressure taps distributed in the tributary area around each primary tap on the frame. The mean area-averaged pressure coefficients calculated in the study are shown in Figure 5.4. It is interesting to note that on the roof and leeward wall the area-averaged pressure coefficients are greater than the point pressure coefficients measured shown in Figure 5.3. The reason for this is unclear. It implies that the SANS pressure coefficients significantly underestimate the pressure on the leeward low-pressure area of the roof. The general trend observed in the first three studies of the SANS pressure coefficients is observed once again, with SANS overestimating wind pressure on the walls, with the exception of the leeward wall, and underestimating wind pressures on the roof.

The final study related to the TTU experiment which was considered in this investigation was done by Ginger and Letchford (1999) to investigate the net pressure coefficients, i.e. both the internal and external pressures, on low-rise buildings. As stated in Section 2.2.4 only the external pressure coefficients are considered for this investigation. Point pressure values were measured at numerous points across the WERFL building for two load cases, one in which the building was nominally sealed, and the second with a dominant 2% opening in the

windward wall of the structure. The mean pressure coefficients measured in the tests are given in Table 5.1. The SANS pressure coefficients are constant for each zone as codified external pressure coefficients are not dependant on the internal pressure. The measured external pressure coefficient values differ for the two cases. Nonetheless, the SANS values agree well with the measured coefficients, with the exception of the side wall value where the SANS pressure coefficient is more than double the values measured in both tests.

Table 5.1: External mean point pressure coefficient from TTU experiment for nominally sealed and 2% opening in windward wall cases.

Pressure Tap Position	SANS Pressure Zone	C_p (sealed)	C_p (2% opening)	SANS C_p
Windward wall center	D	0.70	0.62	0.62
Leeward wall center	E	-0.34	-0.43	-0.30
Side wall center	B	-0.29	-0.40	-0.80
Roof center	I	-0.27	-0.37	-0.20
Roof windward edge	G	-1.04	-1.28	-1.20

5.1.2 Jan Smuts Airport hanger experiment

At about the same time that the TTU experiment started in the USA, researchers in South Africa also conducted a full-scale experiment on a hangar at the Jan Smuts Airport (since renamed to O.R. Tambo International Airport). The study by Milford *et al.* (1992) compared full-scale and wind tunnel test results of the pressures measured in one corner of the roof of the hangar.

The hangar was a two-span duo-pitch roof structure with overall dimensions of 91.4 × 155.6 × 31.6 m and a roof pitch of 6°. A 39.6 × 38.9 m area on the corner of the roof was fitted with 25 pressure taps arrayed in 5 rows as shown in Figure 5.5. A section on the wall of the hangar was also fitted with pressure taps, however the measurements from these taps were not published. As the hangar was located at an airport, the terrain category was equivalent to SANS Terrain Category B with flat surrounding topography. The corresponding wind tunnel test was done at the Council for Scientific and Industrial Research (CSIR) boundary layer wind tunnel in Pretoria using a 1 : 300 scale model of the structure.

The mean point pressure coefficients measured in the full-scale and wind tunnel tests for two orthogonal wind attack directions, one perpendicular to the ridge of the structure and

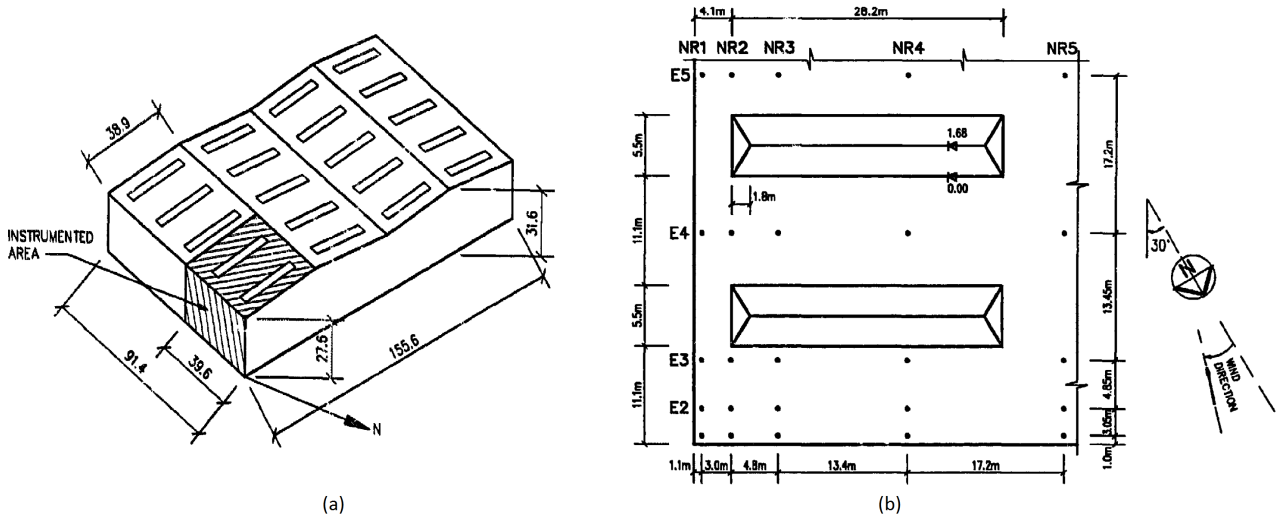

Figure 5.5: Jan Smuts experiment: (a) Hangar geometry, and (b) layout of roof pressure taps (taken from Milford *et al.* (1992)).

the other parallel to the ridge, are shown in Figure 5.6. The results are presented for each row of pressure taps perpendicular to the ridge. The study found good correlation between the trends observed in the full-scale and wind tunnel tests, however the full-scale pressures were consistently greater than those measured in the wind tunnel test. The wind tunnel test results agree well with the SANS pressure coefficients, but the codified pressure coefficients significantly underestimate the full-scale observations.

The discrepancy between the full-scale and SANS values is most apparent for the results of Row E5 with the wind direction of attack parallel to the ridge. For these results the measured full-scale pressure coefficients are up to five times greater than the SANS values. An explanation for this may be due to the interference in the wind flow of the two sky-lights upwind of these pressure taps as seen in Figure 5.5. The SANS stipulations are solely for flat roofs with no abnormal features, and as such do not take the effects of the sky-lights into account. Therefore, it has been decided to consider the results for row E5 with the wind direction of attack parallel to the ridge as outliers and to exclude them from this investigation.

5.1.3 Holmes low-rise building wind tunnel experiment

The determination of wind load effects on low-rise buildings was investigated in a study by Holmes and Best (1981). The paper described a new procedure for obtaining fluctuating and peak values of structural effects from wind tunnel test results. The procedure itself is not of interest in this investigation, but what is of interest are the area-averaged wind tunnel

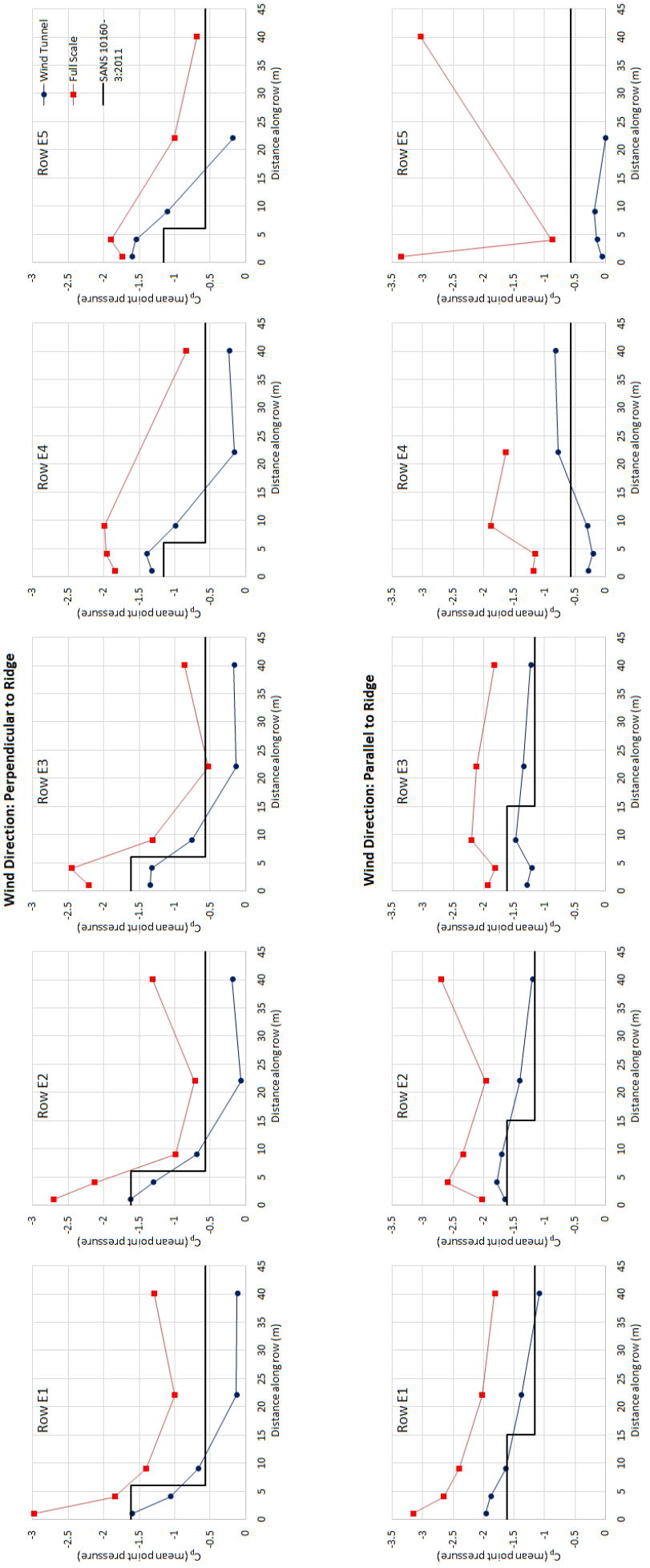

Figure 5.6: Mean point pressure coefficient results from wind tunnel and full-scale tests on Jan Smuts hangar.

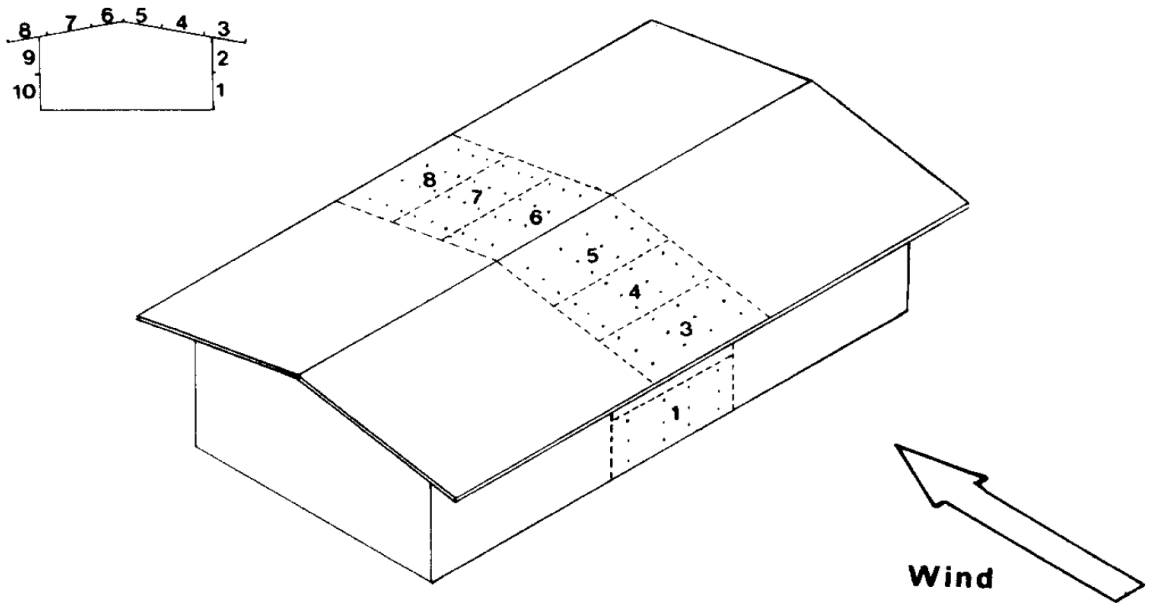

Figure 5.7: Holmes low-rise building experiment geometry and pressure tap panels (taken from Holmes and Best (1981)).

test results which were measured as an intermediate step in the study.

The low-rise building which was considered in the investigation was a small house with a 10° duo-pitch roof with overhung ends. The overall dimensions of the structure were 7.0 × 14.0 × 3.62 m. A 1 : 50 scale model of the structure was tested in a wind tunnel at the James Cook University of North Queensland. Pressures were measured over the central part of the building for a wind angle of attack perpendicular to the ridge of the building. Ten panels consisting of twelve pressure taps each were distributed over the central band of the building, as shown in Figure 5.7, and pressure coefficients were pneumatically averaged across each panel.

The mean area-averaged pressure coefficients measured in the study are shown in Figure 5.8. The wind tunnel values are slightly greater than the SANS pressure coefficients on the windward wall and roof in terms of absolute values, but significantly lower than the SANS values on the leeward faces. It was noted in the article that the area-averaged pressure coefficient values were about 10% lower than those measured from the individual pressure taps on each panel.

5.1.4 Silsoe Research Institute portal frame experiment

The use of the quasi-static design approach, as described in Section 2.2.4.1, was investigated by Hoxey (1991). The study consisted of a full-scale test on a portal frame structure at the Silsoe Research Institute. The study also considered the effects of curved and sharp eaves on

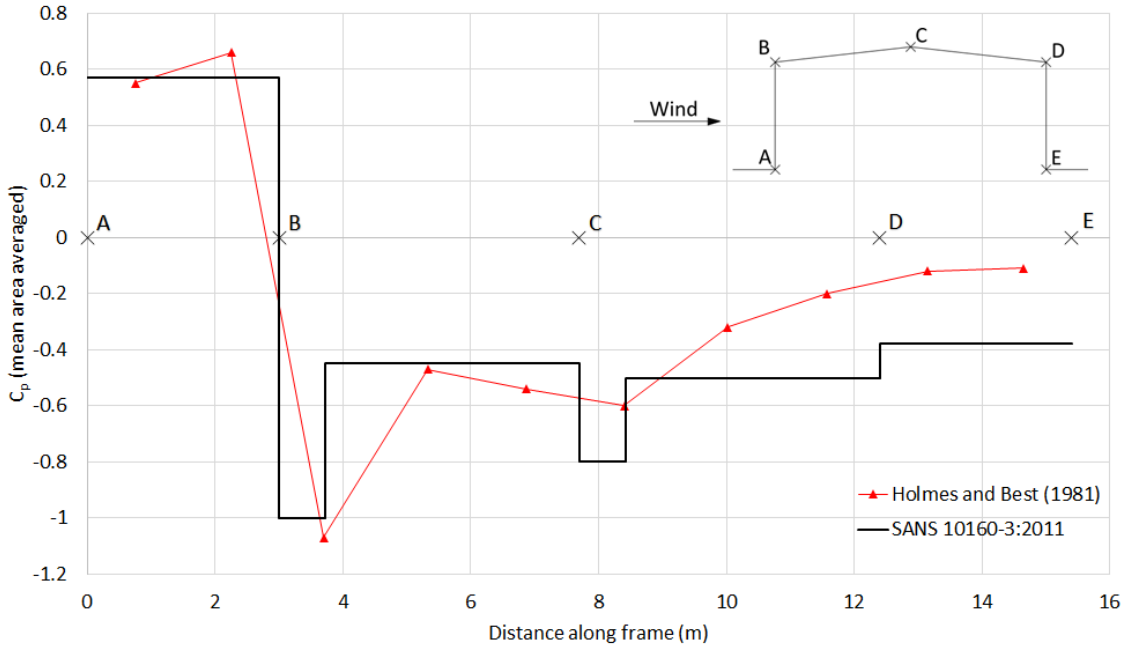

Figure 5.8: Mean area-averaged pressure coefficient results from Holmes wind tunnel test on low-rise building.

structural loads.

The Silsoe Structures Building was a steel framed and clad portal frame structure with overall dimensions of $12.9 \times 24.0 \times 5.5\ m$ and a roof pitch of $10°$. The building was situated in flat open country terrain corresponding to SANS Terrain Category B. Pressure measurements were taken on the central frame for the wind angle of attack perpendicular to the ridge of the structure. Two structural configurations were investigated, one with curved eaves and the second with sharp eaves.

The results from the Silsoe experiment are given in Figure 5.9. The pressure coefficients measured on the windward and leeward walls are approximately half the value of those given by SANS, indicating that the SANS wall pressure coefficients are overly conservative. The values measured on the windward roof and windward edge of the leeward roof, however, are consistently greater than the SANS values. It is interesting to note that on the windward edge of the windward roof the sharp eaves resulted in higher pressure coefficient values, as expected, but towards the leeward edge and across the entire leeward roof higher pressure coefficients were observed for the curved eaves. No distinction is made between roof pressure coefficients for sharp or curved eaves in SANS for angled roofs, however the results from this test indicate that the shape of the eaves does have a significant impact on the pressure coefficients.

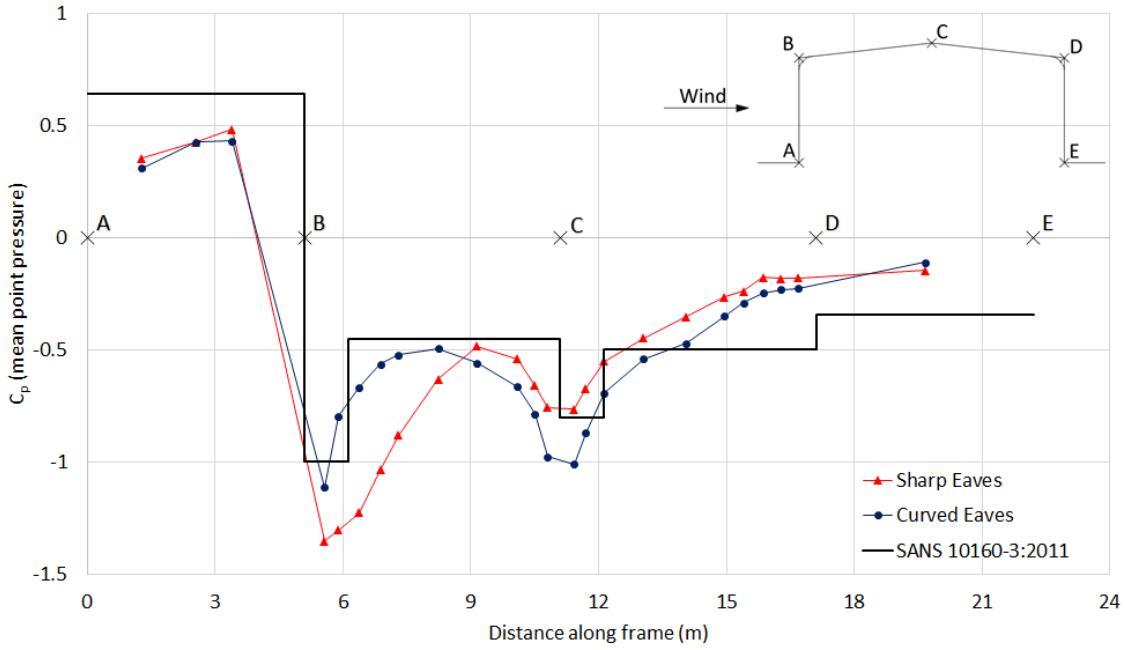

Figure 5.9: Mean point pressure coefficient results from full-scale tests on central frame of Silsoe Structures Building.

5.1.5 Fredericton low-rise building experiment

A full-scale test building was constructed in Fredericton, New Brunswick in order to investigate the pressure coefficients on low-rise structures. The full-scale test results were compared to wind tunnel tests conducted at Concordia University as well as the pressure coefficient provisions given in ASCE 7-05. The results of the study were published by Zisis and Stathopoulos (2009). Although the entire building was instrumented, the raw measured pressure coefficient values were only given on two of the building's walls in the article, and as such the results from those two pressure taps are the only results which are considered in this investigation.

The test building was a regular wooden duo-pitched roof structure with overall dimensions of $8.5 \times 16.8 \times 5.5\ m$ and a roof pitch of 18°. The surrounding terrain was a dense forestry area, equivalent to SANS Terrain Category C. The building was oriented with the longitudinal axis 20° from North. This investigation considers the measurements obtained from single pressure taps in the center of the Northern and Southern walls for all wind angles of attack.

The results from the study are shown in Figure 5.10. The wind tunnel and full-scale test results show good agreement. Only four values are given for SANS pressure coefficients which correspond to the four wind directions orthogonal to the structure. This is because unlike some of the other wind load standards considered in this investigation, SANS does not provide stipulations for other wind directions. The base assumption is that the maximum load effects

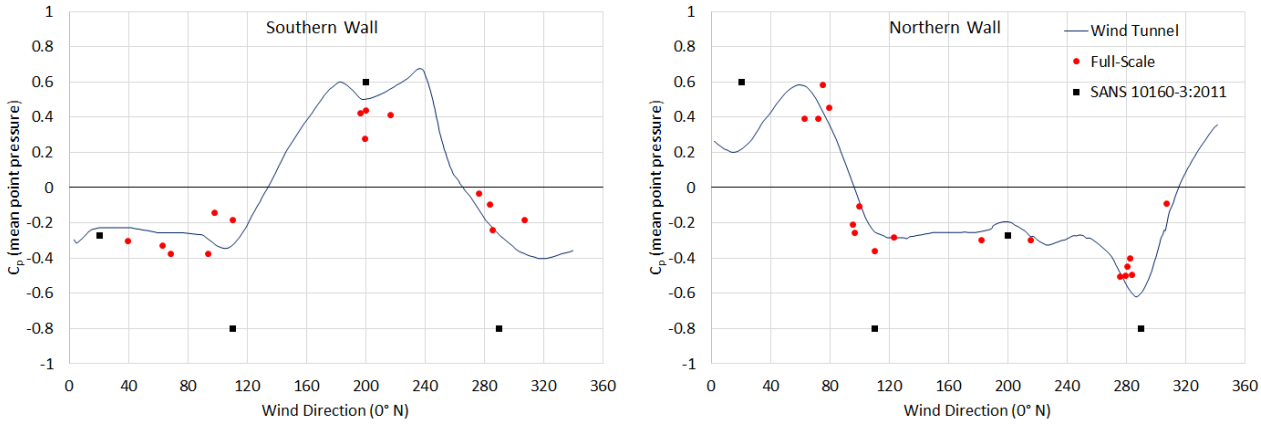

Figure 5.10: Mean point pressure coefficient results from full-scale and wind tunnel tests on Fredericton building.

will be sufficiently accounted for by designing for the orthogonal wind directions, as discussed in Section 2.2.6. Note that in most cases the peak pressure coefficients occur at these orthogonal directions and the base assumption holds true. A notable exception is seen when considering the positive pressure on the walls. For both the Northern and Southern pressure taps it may be seen that the maximum positive pressure occurs when the wind angle of attack is at approximately 40° to the angle of the windward wall, as seen at 240° for the Southern Wall and 60° for the Northern Wall. Nonetheless, the SANS pressure coefficients are consistently greater than both the wind tunnel and full-scale values, significantly so when the side wall pressure coefficients are considered.

5.1.6 Sainte-Foy light-frame wood building experiment

A comparison of full-scale and wind tunnel point pressure coefficients was done by Doudak *et al.* (2009). A low-rise industrial building in Sainte-Foy, Quebec was instrumented to measure full-scale pressures, and a 1 : 200 scale model of the structure was tested in a wind tunnel at Concordia University. Both mean and peak pressures were investigated, but for the purposes of this investigation only the mean pressure coefficients are considered.

The full scale building was a flat-roofed timber structure with overall dimensions of 8.0 × 15.0 × 5.1 m with a 0.5 m parapet. The building was oriented with the longitudinal axis 23° from North. Pressure taps were placed on the roof and three walls, but the NNE facing wall was not instrumented as it was adjacent to another structure of the same height. As such, the structure was investigated for wind angle of attack from all directions except for a 45° envelope around

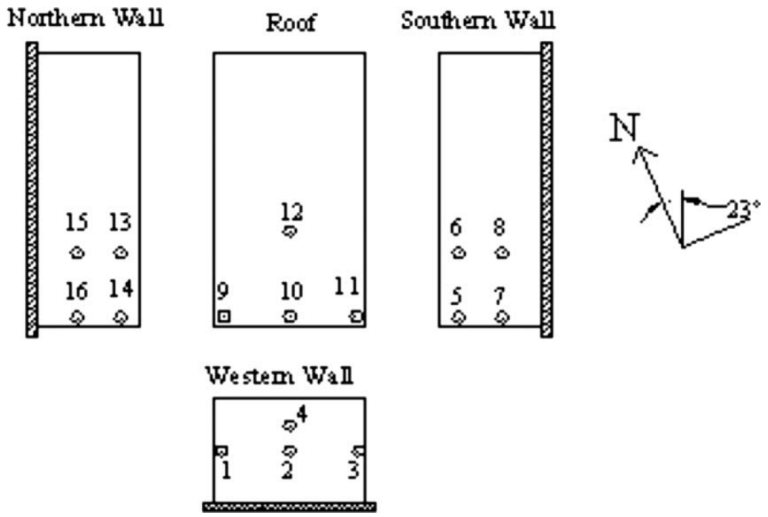

Figure 5.11: Position and numbers of pressure taps on Sainte-Foy building (taken from Doudak *et al.* (2009)).

the NNE direction. The position and numbers of the pressure taps are shown in Figure 5.11. The structure was surrounded by relatively flat topography, however there were a few buildings within the general vicinity of the structure.

The results from the wind tunnel and full-scale test for two pressure taps on each wall and on the roof of the structure are shown in Figure 5.12. SANS pressure coefficient values are given for the four orthogonal wind directions, including wind from the NNE which was not measured in the investigation. The results show good agreement between the wind tunnel and full-scale results, but a number of peculiarities are noted. Firstly, one would expect to see the same pressure coefficients pattern measured on all three, simply shifted by 90° or 180° depending on which wall is considered, but this is not the case. Secondly, there is a distinct lack of positive pressure values on the Northern and Southern walls, even when the wind angle of attack is acting orthogonally onto the wall (113° for the Northern wall and 293° for the Southern wall). The only explanation for this is that the peak negative pressures were great enough to reduce the mean pressure values to negative values. These extreme peaks may be as a result of the surrounding buildings. Comparison of the measured results with SANS values show that the SANS pressure coefficients generally agree well with the observed values. The exceptions are the cases when the Northern and Southern walls are the windward walls, and for the peak values observed on the roof.

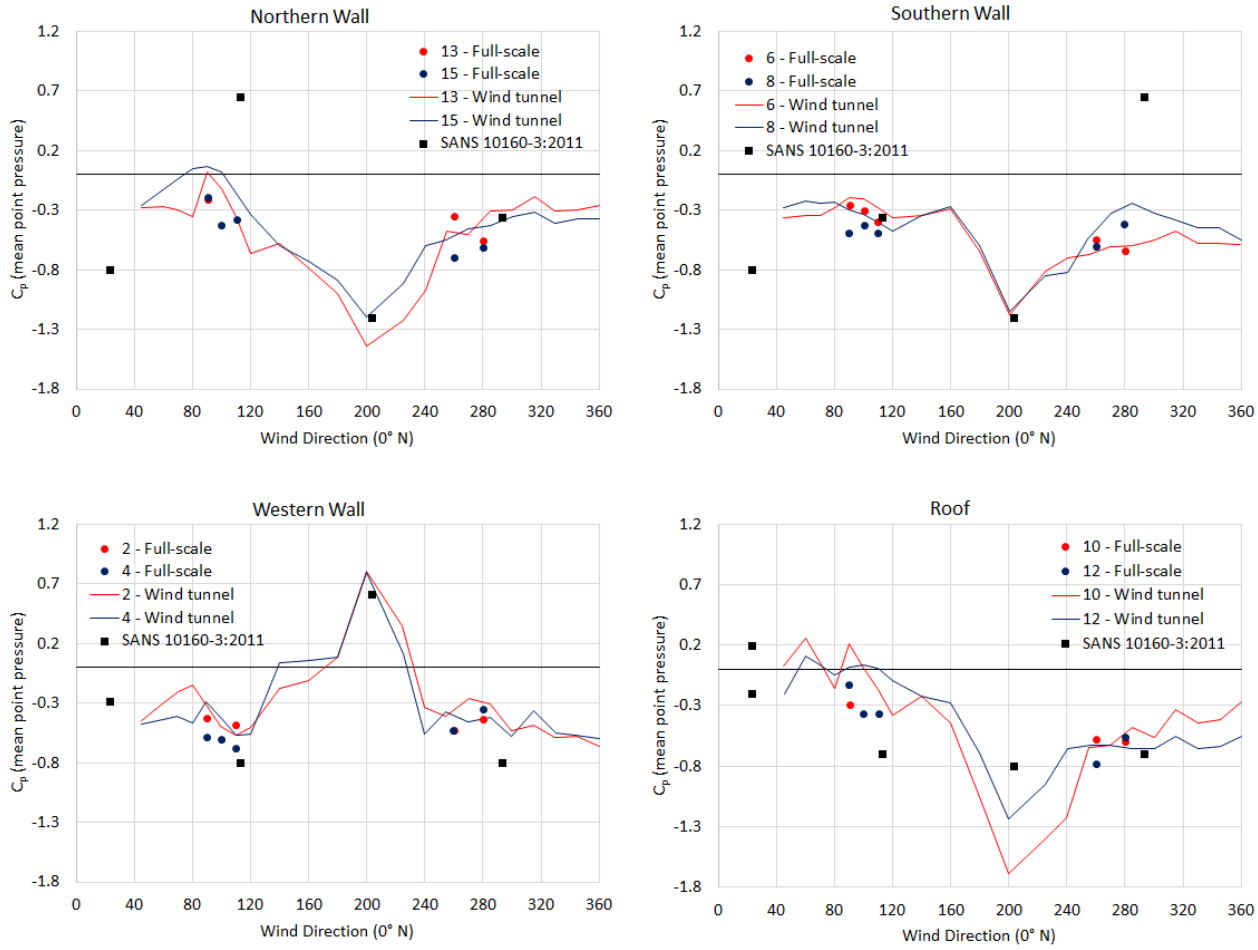

Figure 5.12: Mean point pressure coefficient results from full-scale and wind tunnel tests on Fredericton building on Sainte-Foy building.

5.1.7 Uematsu and Isyumov comparison of wind engineering studies

The final study considered in this investigation is not a wind tunnel or full-scale experiment of a single structure, but rather a summary of wind engineering papers related to pressure coefficients on low-rise buildings. Uematsu and Isyumov (1999) compared and presented results from more than two hundred research papers. These papers were obtained from the Journal of Wind Engineering and Industrial Aerodynamics, the Proceedings of the International Conference on Wind Engineering, and the Journal of Wind Engineering. The papers covered four primary topics, (i) full-scale measurements of wind pressures, (ii) wind tunnel tests of wind pressures, (iii) discussions of wind tunnel methodologies, and (iv) codification of wind pressure coefficients. Results from the papers were collected and a database of pressure coefficients was constructed. The study specifically investigated roof pressure coefficients for the critical areas

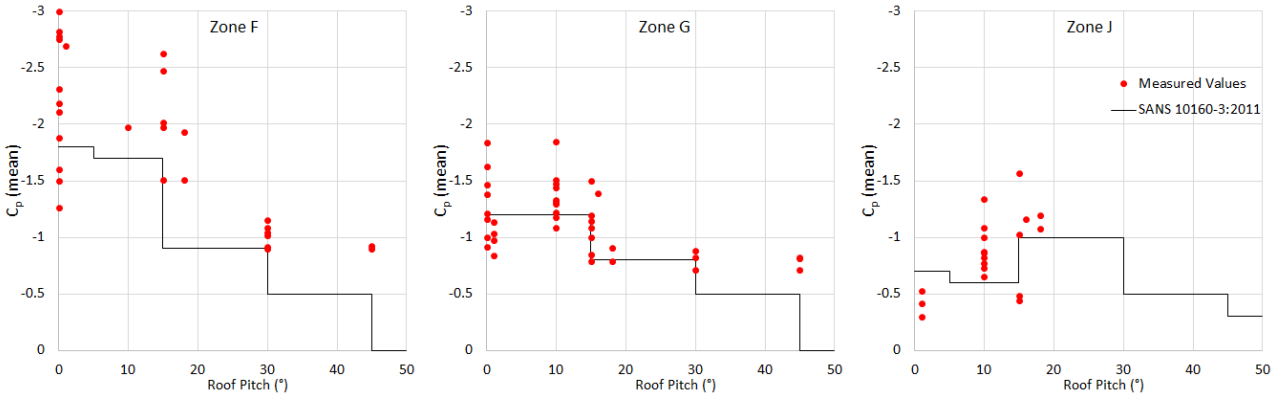

Figure 5.13: Mean pressure coefficient results from Uematsu and Isyumov comparison of wind engineering studies for roof pressure zones F, G and J.

along the windward eaves and ridge of duo-pitch roof structures. These areas correspond with Zones F, G and J in SANS.

The results presented by Uematsu and Isyumov (1999) are shown in Figure 5.13. The graph plots mean measured pressure coefficients from the selected studies against roof pitch. It is not made clear in the paper whether the measured values are point pressure coefficient values or area-averaged pressure coefficients. The SANS pressure coefficients are also plotted against roof pitch. It is noteworthy that although constant pressure coefficients are shown between roof pitch intervals, SANS 10160 does state that linear interpolation may be used between the specified intervals. However, as most of the observed values presented by Uematsu and Isyumov (1999) coincide with the SANS pressure coefficient intervals the use of linear interpolation has an insignificant impact in the calculation of bias values in this case.

It may be seen from the results that Zone F shows the greatest dispersion of values, with the measured values for Zones G and J showing relatively good agreement. It may be observed that the dispersion of measured values decreases as roof pitch increases. This indicates that wind pressures on flat roofs are more variable than pressures on steep roofs. Comparison with the SANS pressure values shows that the SANS values are consistently lower than the observed values for Zone F. The same is true for Zones G and J, however the SANS values are closer to the average observed values.

5.1.8 Summary of results

For each of the studies discussed above, both the observed values and the corresponding SANS pressure coefficient values at the position where the measurement was taken were given. It is

therefore possible to determine the systematic bias of the SANS pressure coefficients by taking the ratio of the observed values to the SANS values and then sampling those values to determine the representative statistical parameter of pressure coefficients. The methodology is described below.

In each of the studies considered, full-scale and/or wind tunnel tests were used to obtain measured pressure coefficients (m_i) obtained for a number (N) of observation points or pressure taps (p_i) on specific structures. The SANS pressure zones across the external face of the structure are then determined using the geometry of the specific structure. As each observation point falls within a specific pressure zone, the corresponding SANS pressure coefficient (c_i) is determined for each point. The systematic bias for each point (b_i) is then calculated using Equation 5.1.1. The overall mean (μ) and variance (σ^2) of the bias values for each study may then be calculated using Equations 5.1.2 and 5.1.3 respectively. As the process of determining bias values effectively normalizes all values, it allows comparison across all the studies.

$$b_i = \frac{m_i}{c_i} \tag{5.1.1}$$

$$\mu = \frac{1}{N}\sum_{i=1}^{N} b_i \tag{5.1.2}$$

$$\sigma^2 = \frac{1}{N-1}\sum_{i=1}^{N}(b_i - \mu)^2 \tag{5.1.3}$$

A summary of the mean and standard deviation of the calculated systematic bias values is given in Table 5.2 for each of the studies. The number of pressure measurements obtained from each study (n) is also shown in the table. The statistical parameters for each study were calculated separately by sampling the systematic bias values on the walls, roof and using all values measured across the structure. It is clear from the results that the SANS pressure coefficients generally underestimate the roof pressure coefficients, as only the study by Holmes resulted in a mean systematic bias of less than unity. This is not the case for wall pressure coefficients, however, as none of the studies considered resulted in a mean systematic bias of greater than unity when only considering the wall pressures.

The systematic bias values were averaged across all the studies for the roof, walls and overall values, as shown at the bottom of Table 5.2. In order to ensure unbiased sampling the

Table 5.2: Mean (μ) and standard deviation (σ) of SANS pressure coefficient systematic bias for each study considered in the investigation.

Study	n	**Roof**		**Walls**		**Overall**	
		μ	σ	μ	σ	μ	σ
Holmes and Best (1981)	10	0.85	0.31	0.68	0.44	0.78	0.35
Levitan *et al.* (1991)	11	1.06	0.14	0.83	0.13	0.97	0.17
Surry (1991)	19	1.15	0.19	0.68	0.10	0.96	0.29
Hoxey (1991)	48	1.10	0.55	0.57	0.15	1.01	0.55
Milford *et al.* (1992)	77	1.32	0.65	-	-	1.32	0.65
Ginger and Letchford (1999)	10	1.28	0.43	0.93	0.42	1.07	0.46
Uematsu and Isyumov (1999)	85	1.18	0.36	-	-	1.18	0.36
Endo *et al.* (2006)	11	1.21	0.30	0.66	0.08	0.99	0.39
Chen and Zhou (2007)	15	1.48	0.42	0.74	0.37	1.18	0.53
Doudak *et al.* (2009)	35	1.06	0.65	0.69	0.33	0.81	0.47
Zisis and Stathopoulos (2009)	31	-	-	0.57	0.23	0.57	0.23
All Studies	**11**	**1.17**	**0.43**	**0.71**	**0.28**	**0.99**	**0.43**

statistical parameters were determined by weighting each study equally and not according to the number of samples obtained from each study. By use of the central limit theorem the overall parameters were calculated using Equations 5.1.4 and 5.1.5 below. This process was repeated for the disaggregated wall and roof pressure coefficient datasets, however it is important to note that the number of samples obtained for wall pressure coefficients is significantly less than those obtained for roof pressure coefficients. As such the combined distributions for all studies as calculated for the disaggregated sets cannot be directly combined and compared in order to obtain the overall parameters, as that would imply equal weighting of the roof and wall pressure coefficient results. Nonetheless, the calculation of disaggregated distributions for roof and wall pressure coefficients do provide an idea of the general trends in those cases. From the results of this investigation it is clear that the SANS pressure coefficients generally overestimate wall pressures and underestimate roof pressures.

$$\mu_{all} = \frac{\sum_{i=1}^{N} \mu_i}{N} \tag{5.1.4}$$

$$\sigma_{all} = \sqrt{\frac{\sum_{i=1}^{N} \sigma_i^2}{N}} \tag{5.1.5}$$

Although it is possible to select separate distributions for the pressure coefficients on the roof and walls of the structure from this investigation, for the purposes of the overarching investigation only the combined distribution of all pressure coefficients across the structure is

required. Therefore, only the combined results taken across the entire structure are considered. It should be noted that the unconservative SANS values on the roof and overconservative values on the walls effectively cancel each other out when this approach is followed. The resulting overall mean is close to unity, and the disparity of the wall and roof bias values is reflected in a high variability. The final representative distribution of SANS pressure coefficients as calculated from a direct comparison with observed values may be selected as a normal distribution with a mean and standard deviation of 0.99 and 0.43 respectively.

5.1.9 Discussion

The results from this investigation may be regarded as an upper limit approximation of the SANS pressure coefficient uncertainty. Although a direct comparison of codified values and observed values does provide the closest approximation possible, additional uncertainties are included in this process.

Firstly, it is important to note that in this investigation the equivalent static pressure coefficients used in the quasi-static approach to wind loading were directly compared to observed point and area-averaged pressure coefficients. As explained in Section 2.2.4.2, the equivalent static pressure coefficients are applied over the entire structure simultaneously, whereas the observed pressure coefficients are transient and measured at specific locations. Due to the lack of spatial and temporal correlation between the observed pressure coefficients a direct comparison with static pressure coefficient results in a certain measure of conservatism when considering the systematic bias. A better comparison would be to compare load effects instead of pressure coefficient values. However, due to the complexity involved in such an analysis this falls outside of the scope of this investigation. As a first approximation of pressure coefficient uncertainties, however, direct comparison of pressure coefficients is sufficient.

A second source of uncertainty is due to the reliability of wind tunnel and full-scale tests themselves. This was discussed in detail in 2.2.4.2. The lack of standardization across wind tunnel and full-scale tests certainly affects the results obtained when comparing multiple studies. Additional variability may therefore be reflected in the results of this investigation which does not represent the true variability of pressure coefficients.

Finally, the investigation is limited by the number of studies considered. Due to the difficulty

of finding appropriate full-scale and wind tunnel results from reliable sources, as well as the time required to analyse these results, a relatively small number of studies were considered. This limited the scope of the investigation. The addition of further test results and comparison with SANS pressure coefficient would improve the approximation obtained from this investigation.

Considering these factors, it is safe to assume the normal distribution with a mean and standard deviation of 0.99 and 0.43 respectively as calculated in this investigation as an upper bound of the distribution of SANS pressure coefficient uncertainties.

5.2 Wind load standard pressure coefficient comparison

Having limited access to measured pressure coefficient data from wind tunnel and full-scale tests, another method is required to estimate the uncertainties inherent in codified pressure coefficients. As discussed in Chapter 3, one such method which may be used is the comparison of major international wind load standards. This section describes and presents the results from a direct comparison of codified pressure coefficients for the primary pressure zones on mono- and duo-pitch roofed low-rise structures. The principle and methodology behind the use of comparative investigations as a indicator of uncertainty is described broadly in Section 3.4.2. The application of the method specifically for investigating pressure coefficient uncertainties is described in the sections below.

A software package was written to automatically calculate design pressure coefficients and the pressure zones according to the stipulations of several international wind load standards. The software package called the Pressure Coefficient Calculation Program (PCCP) was developed in order to automatically calculate the design wind pressure zones across representative structures according to the stipulations of the various standards. In the following sections the development and use of the PCCP, the definition of the sampling space used in the investigation, and the results of the comparative parameter study of wind load standards are discussed.

5.2.1 Pressure Coefficient Calculation Program

The PCCP was written using the JAVA programming language. Using an object-oriented programming language allowed for a modular coding approach, which significantly decreased the time required to develop the program as code could be recycled and used in different modules.

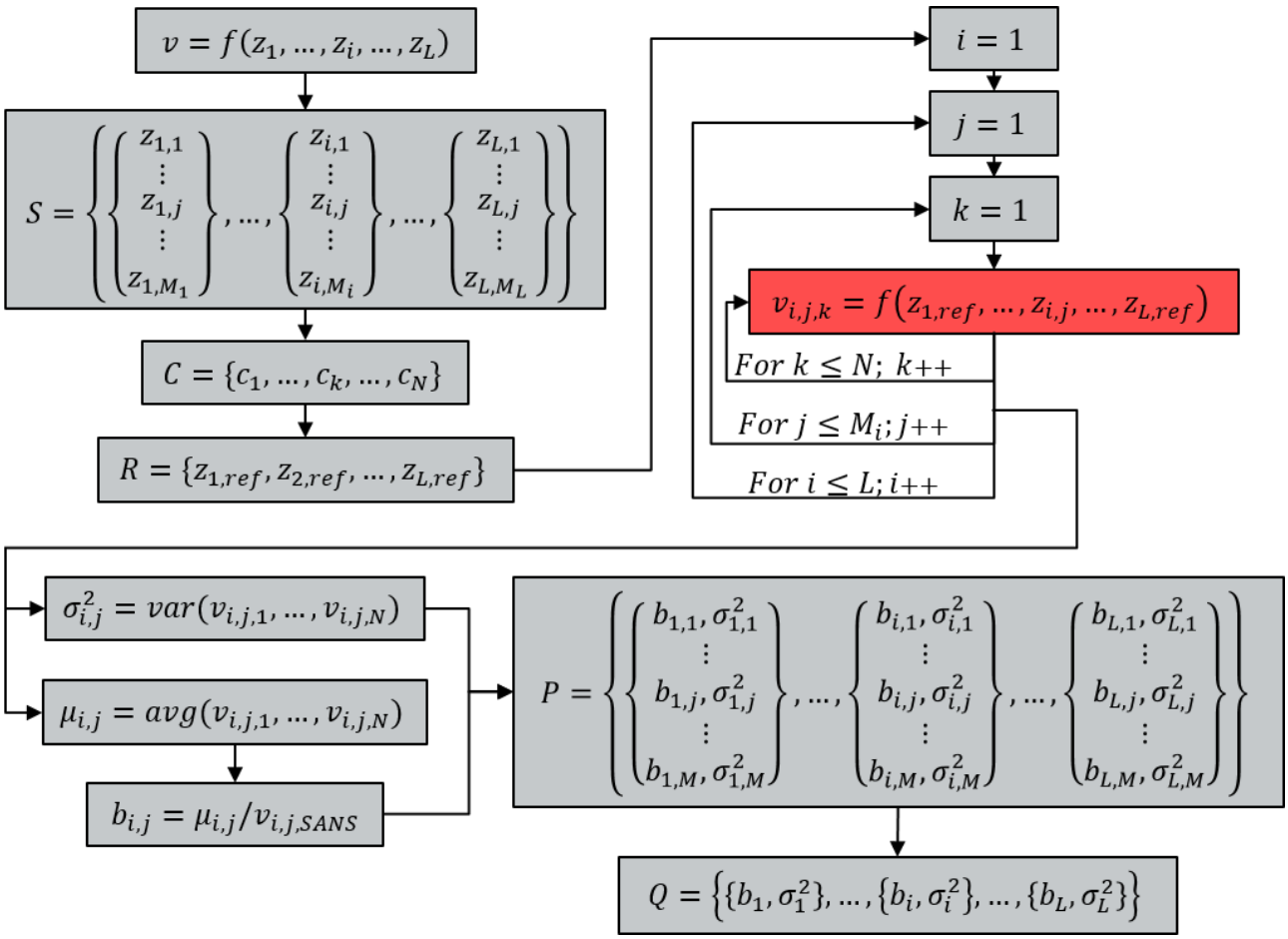

Figure 5.14: Algorithm for using comparison of design standards to estimate uncertainties.

This allowed for a greater scope of structures to be incorporated into the program. The purpose of the PCCP is twofold. Firstly, the program is used to easily generate external pressure distributions for a representative sample set of structures using the stipulations of various international wind load standards. The second purpose is to then use this generated data in a direct implementation of the comparative algorithm discussed in Section 3.4.2. The flow chart of the comparative algorithm is repeated here in Figure 5.14 for the sake of convenience.

To fully understand the way in which the PCCP functions it is necessary to consider the structure of the program, as shown in Figure 5.15. The top-level scripting module is used to define the structural and parameter study variables, control the flow of the analysis as the program cycles through the comparative algorithm, and to deal with the statistical treatment of the generated data. Effectively, the top-level module is a direct implementation of the algorithm shown in Figure 5.14.

The top-level module would however be useless without some way to implement the most important step in this algorithm, which is the calculation of the pressure coefficient distribution

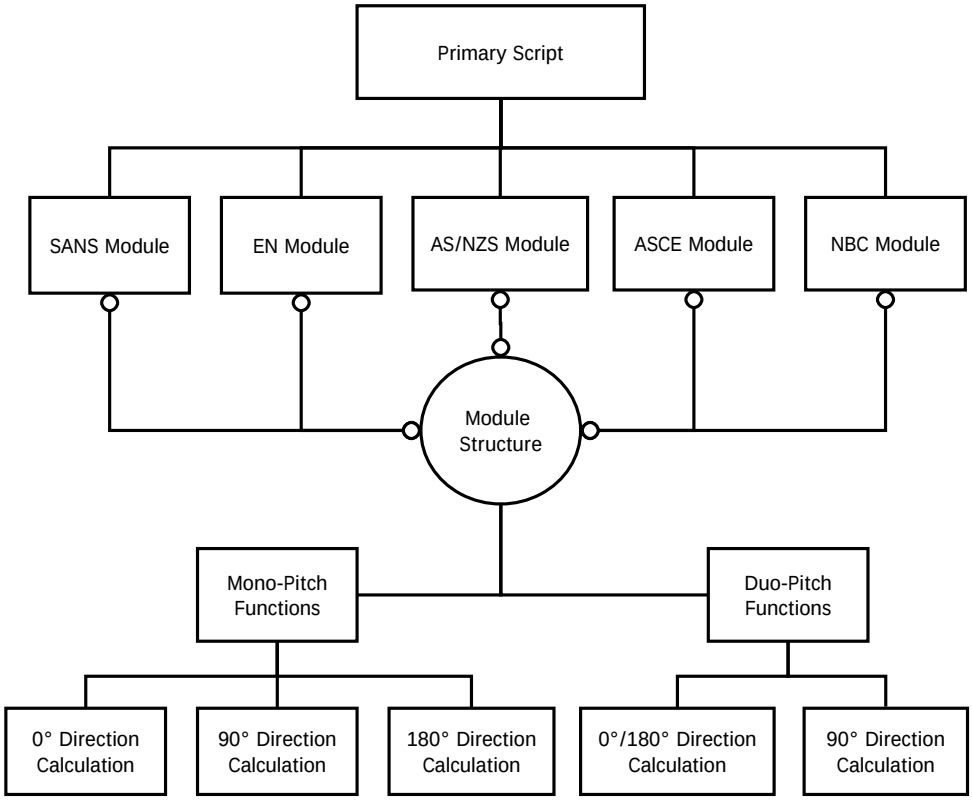

Figure 5.15: Pressure Coefficient Calculation Program structure.

across a given structure using various wind load standards. This step is represented in the flow diagram simply as $v_{i,j,k} = f(z_{1,ref}, ..., z_{i,j}, ..., z_{N,ref})$ and is highlighted in Figure 5.14 . The implementation of this calculation is carried out through the use of individual modules for each wind load standard. All wind load standard modules have the same structure, providing functions based on structure type and wind direction, however each module calculates the pressure coefficient distribution strictly according to the stipulations of the relevant design standard.

The set of design standards (C) which was selected for the comparative study consisted of SANS 10160-3 (South Africa), BS NA EN 1991-1-4 (United Kingdom), AS/NZS 1170-2 (Australia and New Zealand), ASCE 7-10 (USA), and NBCC 2010 (Canada). As the Eurocode pressure coefficients are identical to the SANS pressure coefficients, Eurocode is represented by the SANS pressure coefficients, and similarly the ISO pressure coefficients are represented by the AS/NZS values. As discussed in Section 2.2.4.2 and shown in Figure 2.8 there are three different primary zoning systems used in these wind load standards. These systems are briefly summarized below.

- **Eurocode Zoning System:** SANS 10160-3 and BS NA EN 1991-1-4 both use the Eu-

rocode zoning system, however with different pressure coefficient values. This zoning system is the most detailed of the three systems used in the considered wind load standards. On the windward roof face the system specifies small high pressure zones at the corners of the windward eave, with a reduced pressure zone along the rest of the eave and a low pressure zone across the remainder of the face. The leeward roof face is divided into a high pressure zone near the ridge of the roof and a low pressure zone for the rest of the face. Windward and leeward walls are defined as single pressure zones, with side walls divided into multiple pressure zones based on the cross-wind dimension and the height of the structure.

- **Directional Zoning System:** The directional zoning system is used in AS/NZS 1170-2 and ASCE 7-10. Although ASCE 7-10 does also make provision for the envelope zoning system, only its provisions for the directional system are considered in this investigation. The directional system is simpler than the Eurocode system, with the windward roof face and side walls divided into equally sized pressure zones of descending pressure with dimensions based on the height of the building. The leeward roof face, windward wall and leeward wall are all considered as single pressure zones.

- **Envelope Zoning System:** The envelope zoning system used in NBCC 2010 does not consider orthogonal wind directions but rather designates a single corner of a structure as subject to the primary load, with each corner taken in turn as the loaded corner. The windward faces of both the roof and walls are divided into a thin high pressure zone along the edge of the face with the rest of the face taken as a low pressure zone. Leeward and side walls are considered as single pressure zones. In order to allow a direct comparison with the loads from other zoning systems which use orthogonal wind loads, this system was implemented in the PCCP by considering the two corners on the windward face of the structure as loaded simultaneously.

Having established the set of standards to use, the next step in the development of the PCCP was to clearly define the target variable (v) and the parameters (z_i) which influence the target variable. In this case the target variables are external pressure coefficients (p) on regular low-rise structures. It should be noted that only pressure coefficients resulting in primary structural actions were considered, i.e. cladding and component pressure coefficients are not

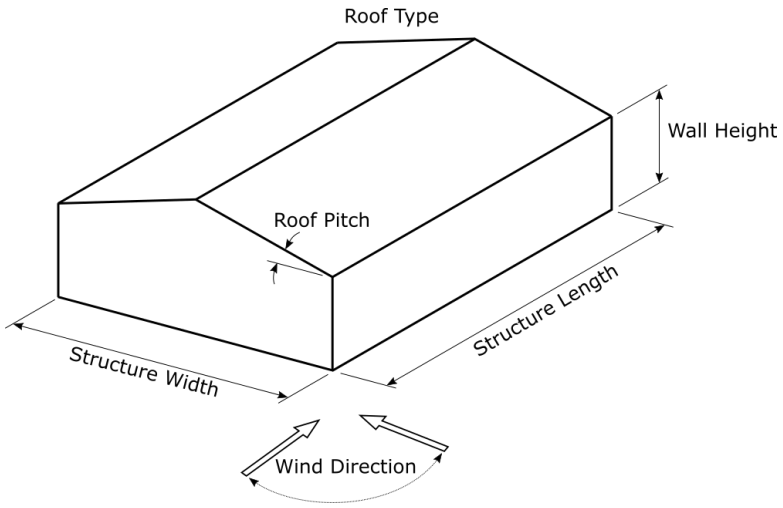

Figure 5.16: Structural and wind related parameters used in PCCP calculation process.

included in the investigation. External pressure coefficients are dependent on six structural and wind related parameters. These parameters were incorporated into the calculation procedure used by the PCCP. The parameters are defined below and shown in Figure 5.16.

- **Roof Type:** The PCCP allows for the investigation of pressure coefficients on three roof types, namely flat, mono-pitched and duo-pitched. The roof type may be defined as either mono- or duo-pitched, and the flat roof calculation module is automatically triggered if the roof pitch is below a given threshold.

- **Roof Pitch:** The roof pitch could be defined within the range of 0° to 60°. For structures with a roof pitch of less than 5°, flat roof procedures for calculating wind pressures were followed.

- **Wind Direction:** The program allowed the wind angle of attack from three orthogonal directions. 0° was defined as the wind direction perpendicular to the ridge of the structure blowing onto the low eave, 90° was defined as wind direction running parallel to the ridge of the structure, and 180° which is perpendicular to the ridge of the structure blowing onto the high eave. In the case of a duo-pitched or flat roofed structure, 0° and 180° cases result in the same pressure coefficient distribution.

- **Structure Width:** The width was defined as the plan dimension perpendicular to the ridge of the structure.

- **Structure Length:** The length was defined as the plan dimension parallel to the ridge of the structure.

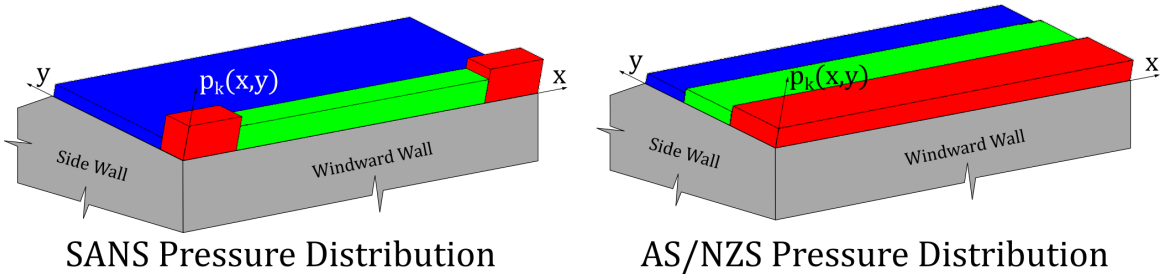

Figure 5.17: SANS and AS/NZS pressure coefficients on windward roof of example structure.

- **Wall Height:** The wall height was measured from ground level to eaves of the building. In the case of mono-pitched structures, this dimension was measured as the height up to the lowest eave. Using the other structural parameters defined, the peak roof height and its position is automatically calculated.

As the PCCP loops through the comparative algorithm the external pressure coefficients are calculated across the specific structure for each possible structural configuration within the sample set according to the stipulations of the five design standards considered. This process is most easily described by considering an example case. In this example only the windward roof of a duo-pitched roof structure with the wind blowing perpendicular to the ridge of the structure is considered. The external pressure coefficients for this case as calculated according to SANS 10130-3 and AS/NZS 1170-2 are shown in Figure 5.17.

The two pressure distributions shown in Figure 5.17 represent parts of two specific target variable cases ($p_{i,j,k}$ and $p_{i,j,k+1}$) in the comparative algorithm. Referring to Figure 5.14, these cases correspond to the j-th sampling value of the i-th parameter used in conjunction with the reference value of the other parameters to calculate the target variable value using the stipulations of two design standards considered (k and $k+1$). It should be clear that the pressure coefficient on all the other faces of the structure are included in the full target variable case, however for the sake of simplicity only the windward roof is considered here.

The pressure coefficients may be calculated at any point on the windward roof face for these cases ($p_k(x,y)$). As each wind load standard has different pressure coefficients and pressure zones, the pressure coefficients cannot simply be compared at arbitrary points on the face as such a comparison would not completely reflect the differences between the different cases. Comparison is therefore done by calculating the spatially averaged pressure coefficient (m_k) across the entire face for each of the faces of the structure using Equation 5.2.1. The best estimate of spatially averaged pressure coefficient ($\mu_{i,j}$) for this specific case (i,j) is then calcu-

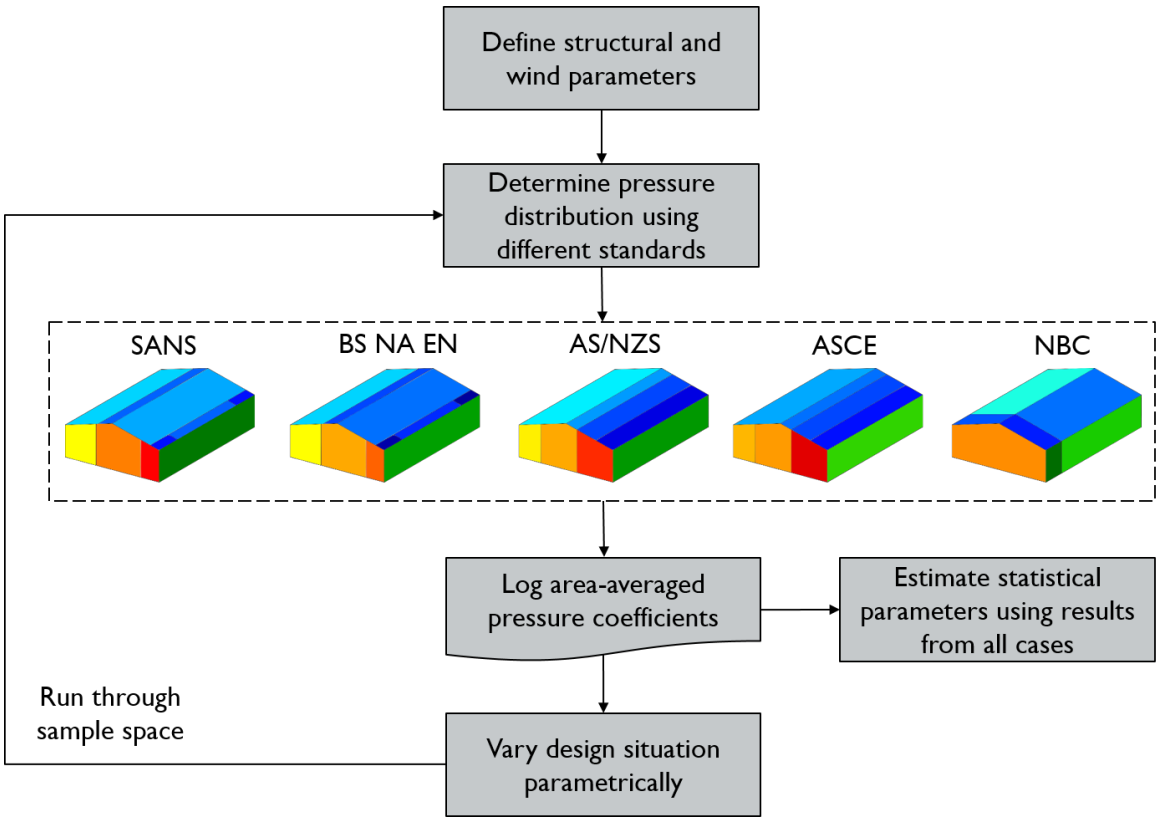

Figure 5.18: Simplified summary of PCCP calculation procedure.

lated by determining the average of the values calculated for the different design standards, as shown in Equation 5.2.2. The SANS systematic bias ($b_{i,j}$) is calculated using Equation 5.2.3. The variance of the pressure coefficients for this case is calculated using Equation 5.2.4. Finally the two statistical parameters of the pressure coefficients for the specific case are stored in a results array (P) and the process is repeated for the next case $(i, j+1)$. A simplified summary of this process is presented in the flow diagram in Figure 5.18.

$$m_k = \frac{1}{(b-a)(d-c)} \int_a^b \int_c^d p_k(x,y)dxdy \tag{5.2.1}$$

$$\mu_{i,j} = \frac{1}{N} \sum_k m_k \tag{5.2.2}$$

$$b_{i,j} = \frac{\mu_{i,j}}{m_{SANS}} \tag{5.2.3}$$

$$\sigma^2_{i,j} = \frac{1}{N-1} \sum_k (m_k - \mu_{i,j})^2 \tag{5.2.4}$$

The use of a parameter study to investigate pressure coefficients means that the influence of each parameter on the total uncertainty of the systematic bias and variability of pressure coef-

ficients may be determined using sensitivity factors. The sensitivity factor of a given parameter (S_i) is calculated as the ratio of the standard deviation of the values obtained by varying that parameter (σ_i) to total standard deviation of all the results in the results matrix (σ_p). These sensitivity factors allow the most critical parameters to be identified in terms of the epistemic uncertainty inherent in them.

5.2.2 Sampling space definition

The greatest benefit of using the PCCP is the ease and speed with which a large number of design situations may be investigated. However, this also presents the greatest challenge with using the program, as more data generated means that more data needs to be analysed. To provide a sense of scale, consider the following example.

Assuming a single parameter study is done which encompasses the entire scope of the SANS wind loading standard for mono- and duo-pitch roof structures, how many possible structural configurations would need to be investigated? The first problem would be to define the scope of SANS, but as this is only a theoretical example, the values given in Table 5.3 for the four primary structural parameters are assumed to be reasonable upper and lower limits. Next, the resolution of the parameter study would need to be defined by selecting the parameter intervals. For this example the parameter intervals are chosen to be 1° or 1 m, depending on the parameter. Finally, considering the two roof types and two orthogonal wind angles of attack (for the sake of simplicity the 180° wind direction on mono-pitched roofs is ignored), the total number of different structural configurations is the product of the number of possible values for each parameter, as calculated in Equation 5.2.5.

Table 5.3: Example parameter space of SANS scope.

Parameter	**Lower Limit**	**Upper Limit**
Roof Pitch (°)	0	45
Wall Height (m)	5	50
Width (m)	10	100
Length (m)	10	100

$$\begin{aligned} n_{total} &= n_{roof\ type} \times n_{wind\ dir.} \times n_{pitch} \times n_{wall} \times n_{width} \times n_{length} \\ &= (2) \times (2) \times (45 - 0) \times (50 - 5) \times (100 - 10) \times (100 - 10) \\ &= 65,610,000 \end{aligned} \tag{5.2.5}$$

Although a parameter study of this size could easily be done using the PCCP, the analysis of such a parameter study would prove to be futile. Not only is this number of configurations far too large to reasonably analyse, but there are also combinations of structural parameters that exist within this parameter space which are clearly unrealistic and would make the results from such a parameter study worthless. It is therefore critical that sampling space and parameter study methodology be selected in an intelligent fashion in order to provide meaningful results.

To best represent a large sampling space that is representative of pressure coefficients in general and does not include unrealistic structural configurations, a methodology based on the concept of representative structures was used. In this methodology, instead of simultaneously varying all parameters, a reference structure was selected and each parameter was varied in turn while the other parameters remained constant. This allowed for simple analysis and presentation of the results from the parameter study. Furthermore, varying each parameter independently allowed the influence of each parameter on the uncertainty of pressure coefficients to be investigated. The parameter ranges were selected within carefully selected limits so as to minimize the likelihood of unrealistic structural configurations. In order to counteract this restriction on the sampling space, multiple reference structures with different parameter ranges were used.

The three reference structures' dimensions and their parameter ranges as used in the final parameter study are given in Table 5.4. The choice of each reference value and parameter ranges for each parameter is explained below.

Roof Pitch

At first glance it may seem simplest to select a flat roof as the reference for each structure as the lower limit for all for reference structures is 0°. However, a different roof pitch is selected for each in order to avoid having results biased towards any one structural configuration. As the structures become larger, the reference value and parameter ranges for roof pitch decrease in order to avoid unrealistic structural configurations. Although most wind load standards provide pressure coefficients for greater pitch values, the upper limit value for Reference Structure 1 of

45° was selected as this was the highest value for which numerous wind tunnel and full-scale tests have been done, as reported by Uematsu and Isyumov (1999) (see Section 5.1.7).

Wall Height

As with roof height, the reference value across the three structures is varied in order to avoid results biased toward a specific value. As low-rise buildings were investigated, the upper limit values were selected in such a way that the ratio of wall height to building length would always be less than unity.

Building Width and Length

The pressure coefficients provided in wind load standards are all in some way dependent on the ratio of the building's plan dimensions and ratio of the crosswind dimension to the building height. As such, the building width and length were selected based on equal proportions for each of the reference structures. The reference dimensions were increased for each structure to investigate as large a parameter space as possible within reasonable limits. These values were based on a width to length ratio of 1:2 throughout. The width upper limit values were selected so that a ratio of 1:1 would be achieved with the reference length. The length lower limit values were based on the same ratio, and the length upper limit value was chosen so that a 1:4 ratio would be achieved. By selecting the values in this way the critical dimension ratios required by the wind load standards would be investigated for both primary wind angles of attack considered.

Table 5.4: Reference structures' dimensions and parameter ranges.

Parameter	Reference Structure 1			Reference Structure 2			Reference Structure 3		
	Ref.	Lower	Upper	Ref.	Lower	Upper	Ref.	Lower	Upper
Roof Pitch (°)	**20**	0	45	**10**	0	20	**0**	0	10
Wall Height (m)	**3**	3	15	**10**	5	25	**20**	10	40
Width (m)	**10**	5	20	**15**	10	30	**25**	20	50
Length (m)	**20**	10	40	**30**	15	60	**50**	25	100

Five combinations of the two roof types and three wind directions were used in the parameter study. As the results for duo-pitch roofs are the same for 0° and 180°, the logical sixth combination was not considered. The combinations are denoted as Mono 0, Mono 90, Mono 180, Duo 0 and Duo 90 in the results below, and are shown in Figure 5.19. For each of the representative structures the four primary parameters were varied independently and the SANS bias relative to the average value was recorded. The bias value results are presented in

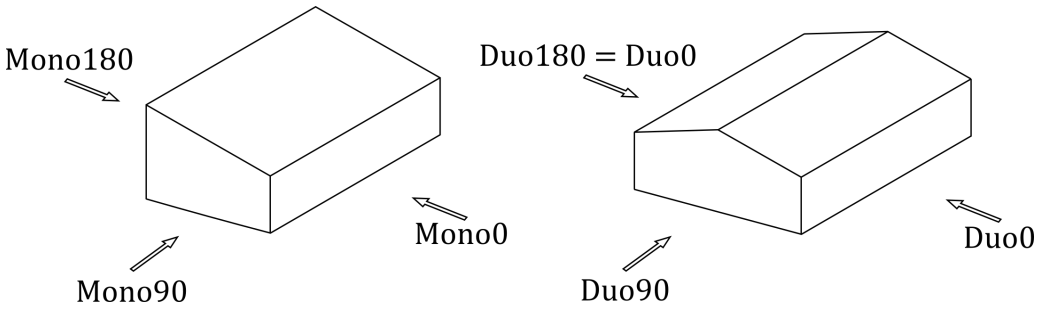

Figure 5.19: Combinations of wind direction and roof type considered in the parameter study.

Section 5.2.3.1. The variability of the pressure coefficient values given by the various wind load standards for each case were also calculated and are presented in Section 5.2.3.2.

5.2.3 Parameter study results

5.2.3.1 SANS bias

The SANS bias values calculated in the parameter study are shown in Figure 5.20. The results are given separately for each reference structure and primary varied parameter, with the bias values calculated for the five roof-direction combinations given in each case. The vertical black line on the graphs indicates the reference structure. The results are summarized in Table 5.5, wherein the mean and standard deviation of the SANS bias values are given for each case. It should be noted that in both Figure 5.20 and Table 5.5 results are not given for the mono-pitch roof case for Reference Structure 3 when wall height, width and length were varied. This is because the reference roof pitch for that structure is 0°, which means that the results for mono- and duo-pitch cases are the same. The sensitivity factors for each parameter related to their influence on the bias is given in Table 5.6.

Before the results of each varied parameter are discussed, consider the following general trends and observations. The first is the dispersion of the bias values for the five roof-direction combinations. In most cases, with the exception of the roof pitch parameter studies, the results of each roof-direction combination remain relatively constant. However, the different combinations all have notably different results. This is reflected in the values given Table 5.5, where it may be seen that the standard deviation for the individual cases are 0.02 on average for each roof-direction combination individually, but the average combined standard deviation of all combinations is 0.07. It is also interesting to note that the combinations remain in the same order relative to each other, with the Mono 0 case consistently having the highest SANS

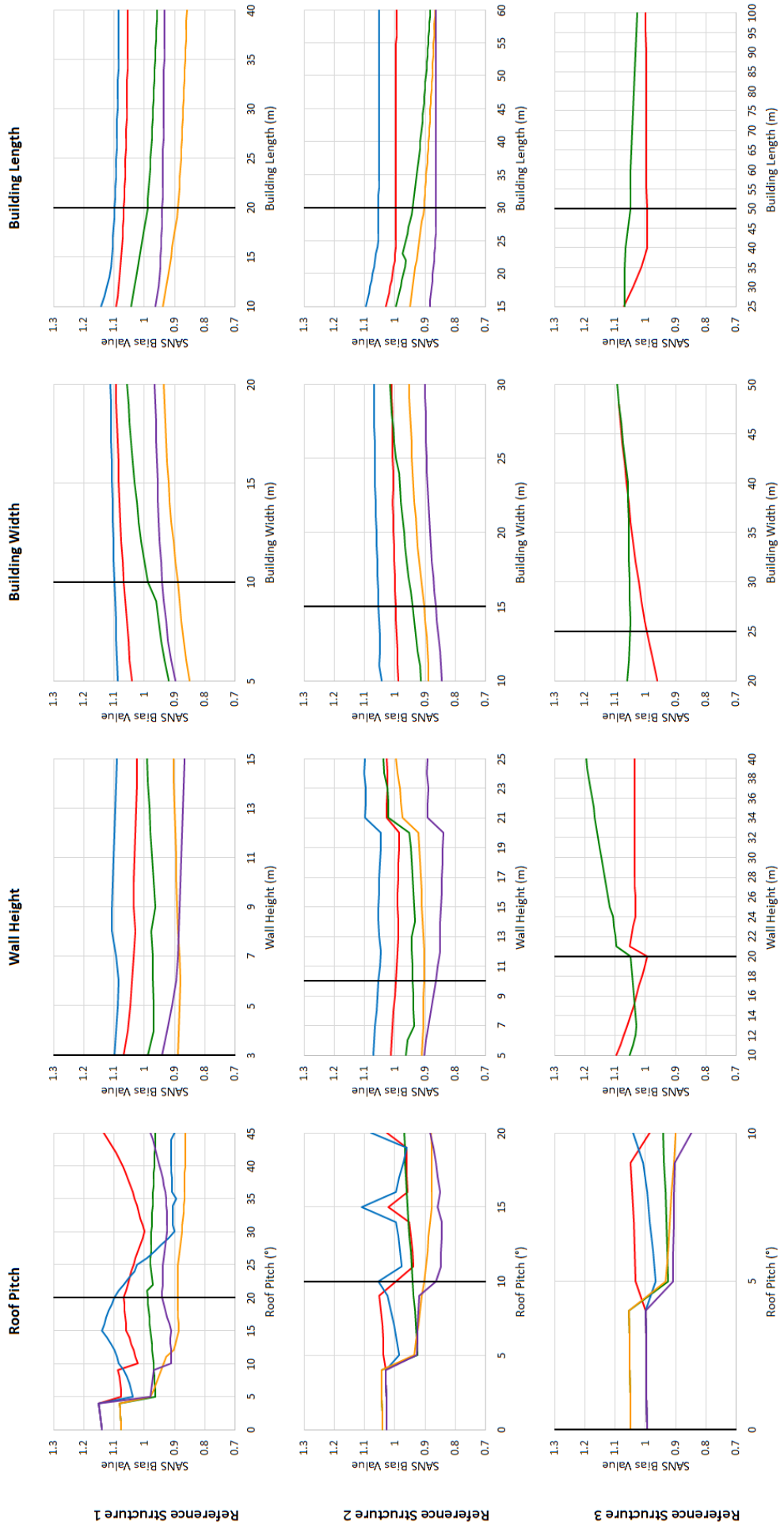

Figure 5.20: SANS bias values calculated in parameter study.

Table 5.5: Mean and standard deviation of SANS bias values calculated in parameter study.

Roof/Direction		Roof Pitch		Wall Height		Width		Length	
		Mean	Std Dev	Mean	Std Dev	Mean	Std Dev	Mean	Std Dev
Ref Struct 1	Duo0	1.06	0.04	1.04	0.01	1.07	0.02	1.07	0.01
	Duo90	0.99	0.03	0.98	0.01	1.00	0.05	0.99	0.03
	Mono0	1.02	0.10	1.10	0.01	1.10	0.01	1.10	0.01
	Mono90	0.91	0.07	0.89	0.01	0.90	0.03	0.89	0.02
	Mono180	0.96	0.07	0.89	0.02	0.94	0.02	0.94	0.01
	All	0.99	0.08	0.98	0.08	1.00	0.08	1.00	0.08
Ref Struct 2	Duo0	1.00	0.04	1.00	0.02	1.00	0.01	1.00	0.01
	Duo90	0.97	0.04	1.01	0.06	0.97	0.03	0.93	0.03
	Mono0	1.01	0.04	1.07	0.02	1.06	0.01	1.06	0.01
	Mono90	0.93	0.07	0.93	0.03	0.92	0.02	0.90	0.02
	Mono180	0.91	0.07	0.87	0.02	0.88	0.02	0.87	0.01
	All	0.97	0.06	0.97	0.07	0.97	0.07	0.95	0.07
Ref Struct 3	Duo0	1.02	0.02	1.04	0.02	1.04	0.04	1.01	0.02
	Duo90	0.99	0.06	1.11	0.06	1.06	0.01	1.05	0.01
	Mono0	1.00	0.02	-	-	-	-	-	-
	Mono90	0.98	0.07	-	-	-	-	-	-
	Mono180	0.94	0.05	-	-	-	-	-	-
	All	0.98	0.05	1.07	0.06	1.05	0.03	1.03	0.03

Table 5.6: Bias sensitivity factors of parameters used to determine pressure coefficients.

Variable (z_i)	Sensitivity Factor (S_i)
Roof Pitch	0.550
Wall Height	0.249
Length	0.173
Width	0.226
Roof Type	0.429
Wind Direction	0.609

bias and the Mono 180 case having the lowest.

Variation of the roof pitch shows the most erratic results for all three reference structures. For the most part this may be explained by the difference in intervals used to specify roof pressure coefficients in the different wind load standards. Each standard specifies pressure coefficients for specific roof pitch values and allows for linear interpolation between these values. The difference is that the specified pitch values and intervals are not the same. SANS specifies pressure coefficient values for 5° and then at 15° intervals, ASCE and AS/NZS specify pressure coefficient at 5° intervals between 10° and 45°, and finally NBC provides pressure coefficients for 5°, 20°, 30° and 45°. These overlapping intervals result in sharp jumps in the SANS bias, which is most clearly seen in the roof pitch parameter study for Reference Structure 2.

The wall height parameter studies showed a relatively constant SANS bias for low wall heights with a sharp jump at a wall height of 20 m, followed by a steady rise in the SANS bias for the wind direction parallel to the ridge of the structure. The jump at 20 m is due to the fact that it is the limit used by all the standards considered for high walls, and once this limit is exceeded the windward wall is divided into different pressure zones along its height. The rise in SANS bias after this limit is a result of the ratio of the building height to the along-wind dimension of the structure increasing, which is used to determine the pressure coefficients on the roof in ASCE, AS/NZS and ISO but not in SANS.

Finally, the building length parameter study shows that the SANS relative bias remains fairly constant for wind directions perpendicular to the ridge of the structure and a general decrease as the building length increases for wind directions parallel to the ridge. This trend is mirrored in the results of the building length study, showing a general increase in the SANS bias as the building width increases for wind directions parallel to the ridge. These trends are explained by the way in which pressure zones are defined in the different standards. SANS and NBC use zone definitions which change in proportion to the dimensions of the structure, and therefore the zone area ratios remain relatively constant. The other standards use set zone sizes based on the reference height for the high-pressure zones on the structure, with the remaining part of the structure classified using low-pressure zones. Consider the building length parameter study. When calculating the wind load using ASCE or AS/NZS for the wind direction parallel to the building ridge, the low-pressure zone on the leeward side of the roof increases in area and has a larger influence on the total wind load on the structure as the building length increases. As the total average wind load decreases, the SANS wind load becomes more conservative relative to these standards, resulting in the lower relative bias. From the building width parameter study the inverse is found, as expected, with an increase in the relative bias as the building width increases for the wind direction parallel to the building ridge. This is due to the fact that the ASCE and AS/NZS wind loads do not decrease as the structure width decreases, but the SANS loads do decrease.

The final step in the process was to reduce the results matrix to a set of independent values in order to find a single representative distribution for the distribution of the pressure coefficient systematic bias. A total of 2,512 cases were considered in the parameter study. However, as certain parameters such as structure width and length have large parameter ranges with many

individual cases, the results would be biased towards the values obtained for those parameters if all values were sampled. The combined bias was therefore determined for each combination of the four structural parameters, the three reference structures, and five roof type and wind direction combinations. This resulted in a set of 60 values for the bias that were treated as independent. The representative systematic bias distribution of pressure coefficients for the total sampling space was determined from this set. The mean and standard deviation were calculated as 0.98 and 0.08 respectively. As the samples were independent, the bias was normally distributed by the central limit theorem.

5.2.3.2 Variability

The SANS variability values calculated in the parameter study are shown in Figure 5.21. The results are given in the same format as the SANS bias results, and the mean and standard deviation values calculated are summarized in Table 5.7. The sensitivity factors for each parameter related to their influence on the variability is given in Table 5.8. This variability is the calculated coefficient of variation of the pressure coefficients as stipulated by the various wind load standards. It describes the dispersion of the values and is indicative of the epistemic variability inherent in pressure coefficients. Furthermore, in the calculation procedure all values were normalised with respect to the average value. The mean value is therefore equal to unity which means that the standard deviation and coefficient of variation are equal. As the variability is considered as a random variable its mean and standard deviation is calculated in this section. The variability is referred to as the coefficient of variation of pressure coefficients to avoid ambiguity.

It stands to reason that many of the same general trends observed in the bias results are also observed when considering the variability results and that these trends are due to the same reasons. Examples of these trends are the erratic results seen in the pressure coefficient parameter study due to the overlap of pressure coefficient intervals, the sudden jump in values seen in the wall height parameter study at 20 m due to the high wall cutoff limit, and the general increase in variability as the building width and length increases due to the different ways in which wind load standards define pressure zones. These trends are therefore not discussed again in this section. It is important, however, that the interpretation of the variability results is made clear.

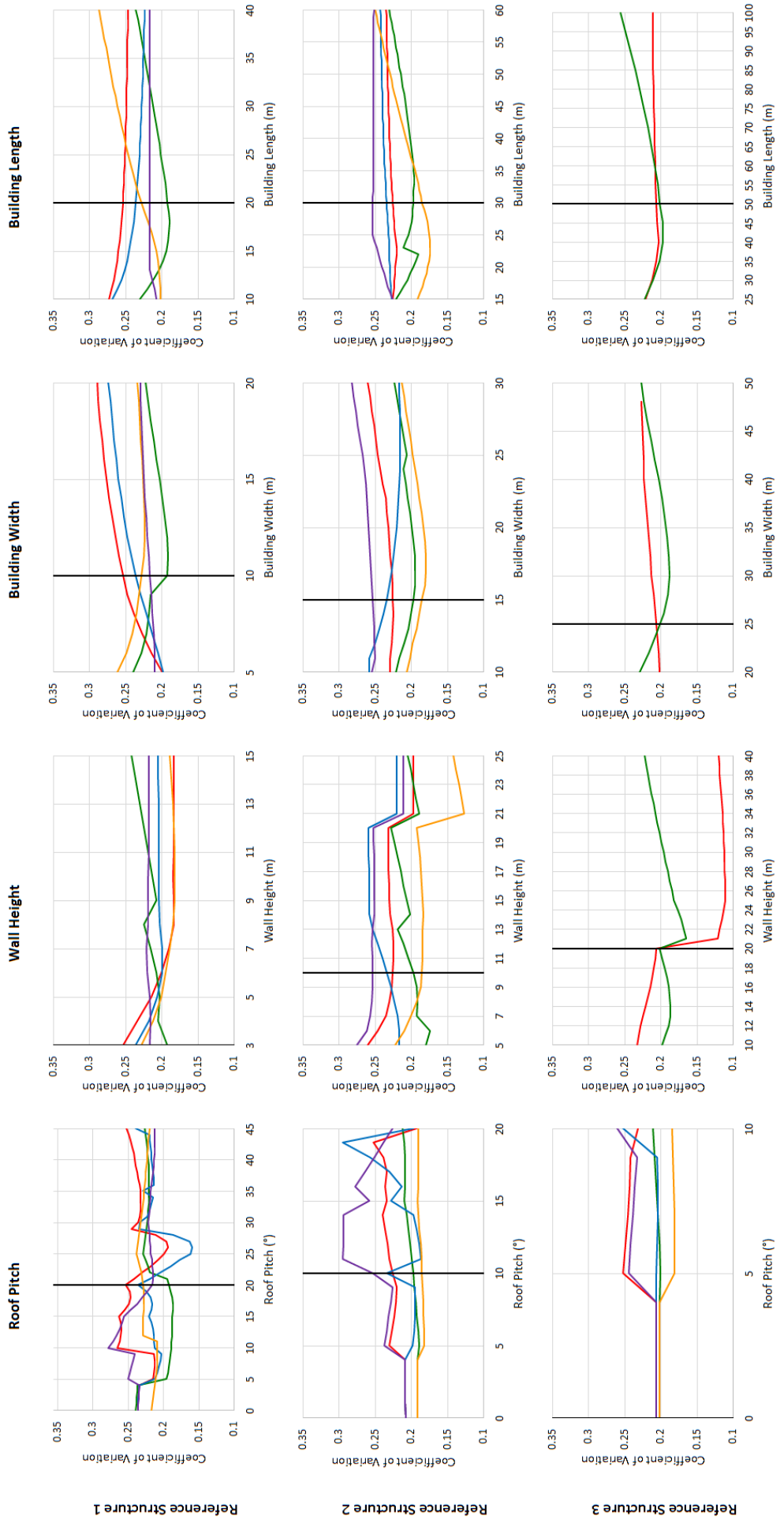

Figure 5.21: Coefficient of variation of wind load standard pressure coefficients calculated in the parameter study.

Table 5.7: Mean and standard deviation of the pressure coefficient variability calculated in parameter study.

Roof/Direction		Roof Pitch		Wall Height		Width		Length	
		Mean	Std Dev	Mean	Std Dev	Mean	Std Dev	Mean	Std Dev
Ref Struct 1	Duo0	0.24	0.02	0.20	0.02	0.26	0.03	0.25	0.01
	Duo90	0.21	0.02	0.22	0.01	0.21	0.01	0.21	0.01
	Mono0	0.21	0.02	0.21	0.01	0.24	0.02	0.24	0.01
	Mono90	0.22	0.01	0.19	0.01	0.23	0.01	0.24	0.03
	Mono180	0.23	0.02	0.22	0.00	0.22	0.01	0.22	0.00
	All	0.22	0.02	0.21	0.02	0.23	0.02	0.23	0.02
Ref Struct 2	Duo0	0.22	0.01	0.22	0.02	0.24	0.01	0.23	0.00
	Duo90	0.20	0.01	0.22	0.02	0.21	0.01	0.21	0.01
	Mono0	0.21	0.03	0.24	0.02	0.23	0.01	0.24	0.00
	Mono90	0.19	0.00	0.18	0.03	0.19	0.01	0.21	0.02
	Mono180	0.25	0.03	0.24	0.02	0.26	0.01	0.25	0.01
	All	0.21	0.03	0.22	0.03	0.23	0.03	0.23	0.02
Ref Struct 3	Duo0	0.23	0.02	0.15	0.05	0.22	0.01	0.21	0.00
	Duo90	0.20	0.00	0.20	0.01	0.21	0.01	0.22	0.02
	Mono0	0.21	0.01	-	-	-	-	-	-
	Mono90	0.19	0.01	-	-	-	-	-	-
	Mono180	0.23	0.02	-	-	-	-	-	-
	All	0.21	0.02	0.17	0.04	0.21	0.01	0.21	0.01

Table 5.8: Variability sensitivity factors of parameters used to determine pressure coefficients.

Variable (z_i)	Sensitivity Factor (S_i)
Roof Pitch	0.375
Wall Height	0.470
Length	0.278
Width	0.326
Roof Type	0.389
Wind Direction	0.552

For the SANS bias values in the previous section, the results are fairly straightforward. Where a value of greater than unity is observed it is clear that in that case the SANS pressure coefficient stipulations result in lower values than those given in the other standards considered, and where a value of less than unity is observed the SANS values are greater than those given in other standards. Care needs to be taken when interpreting the variability, however, as these values do not specifically reflect the variability of the SANS pressure coefficients, but rather the variability of all the pressure coefficients calculated for a specific case. A lower variability indicates good agreement between the wind load standards, such as seen in the Duo 0 case for Reference Structure 3 when considering wall height. Higher variability values, as observed for Reference Structure 2 when considering roof pitch, indicate that for those cases there is a high

dispersion of pressure coefficient values.

As in the bias investigation, the final step in the process was to reduce the results matrix to a set of independent values in order to find a single representative distribution for the distribution of the pressure coefficient variability. The total of 2,512 cases were reduced to a set of 60 values for the bias that were treated as independent. The representative variability distribution of pressure coefficients for the total sampling space were determined from this set. The mean and standard deviation were calculated as 0.22 and 0.03 respectively. As with the bias values, it may be assumed that by the central limit theorem the variability is also normally distributed. However, as the variability cannot be negative, the normal distribution is undesirable. Therefore, the log-normal distribution which is bounded at 0 on the lower end was used.

5.2.3.3 Combined distribution

By regarding the statistical parameters of a given distribution as random variables themselves, it is possible to determine distributions for the parameters and combine them into a single representative distribution which encompasses the total uncertainty. This principle was discussed in Section 3.5 through the use of hierarchical Bayesian models. The Monte Carlo method developed in that section was used to combine the prior distributions of the SANS bias and the pressure coefficient variability as calculated in the parameter study above into a single representative posterior predictive distribution describing the uncertainty of the SANS pressure coefficients.

It should be noted that the probability distributions obtained from this parameter study are not representative of the intrinsic natural uncertainty of pressure coefficients, but rather the uncertainty in the models used to represent pressure coefficients. As mentioned in the general methodology of the comparison of wind load standards as a method for determining pressure coefficients uncertainty (see Section 3.4.2), in the absence of observed or measured values each wind load standard is assumed to be equally reliable. The uncertainty quantified using the comparison of these standards is therefore representative of the uncertainty of the stipulations of wind load standards. In other words, the epistemic uncertainty of the pressure coefficients is quantified as opposed to the aleatoric uncertainty.

The Monte Carlo method developed in Section 3.5 was applied using one million simula-

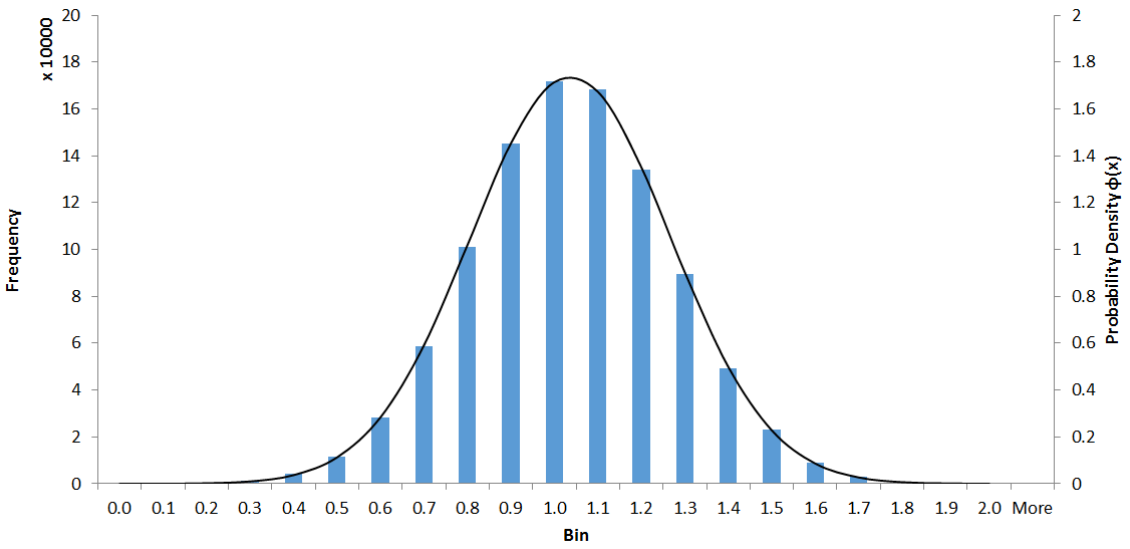

Figure 5.22: Monte Carlo histogram and probability density function of representative probability distribution of SANS pressure coefficients.

tions. The two input distributions used as well as the final representative distribution of SANS pressure coefficients are given in Table 5.9. To reiterate, although the variability has been referred to as the coefficient of variation throughout the discussion above, it was added to the hierarchical Bayesian model as the distribution of the pressure coefficient standard deviation. This was possible as the coefficient of variation and the standard deviation are equal, and the standard deviation is necessary in order to accurately combine the two prior distributions using the Monte Carlo method. Figure 5.22 shows the Monte Carlo generated histogram and probability density function of the representative distribution.

Table 5.9: Monte Carlo input distributions and resulting representative distribution of SANS pressure coefficients.

X	Distribution	μ_X	σ_X
Systematic Bias	Normal	0.98	0.08
Standard Deviation	Log-normal	0.22	0.03
SANS Pressure Coefficient	Normal	0.98	0.23

5.3 Summary and discussion

The investigations described above represent two different approaches of representing pressure coefficient uncertainties. The comparison of SANS pressure coefficients with test results provides a direct comparison of codified values and observed values. However, due to the limited

number of test results available it provides a very limited scope. The limited scope and the addition of artificial uncertainties introduced because of measurement procedures results in the method providing an upper limit approximation of pressure coefficient uncertainties. Comparison of the SANS pressure coefficients with the pressure coefficient values found in other wind load standards allows for a much larger scope to be investigated. However, as the codified values are not anchored to observed values, the method provides an approximation of uncertainties which are predominantly due to modeling of pressure coefficients (epistemic uncertainties). It may be safely assumed that wind load standards aim to represent pressure coefficients as accurately as possible, and as such it is clear that a significant measure of the inherent aleatoric uncertainty is nonetheless quantified through the process. Therefore the procedure does not result in a strictly lower bound approximation of pressure coefficients, but rather an "upper" lower bound approximation.

Table 5.10 provides a summary of the representative probability distributions of SANS pressure coefficients calculated in each of the investigations. As already mentioned it should be noted that although these two studies were used to quantify predominantly different types of uncertainties, i.e. aleatoric and epistemic uncertainties, the results from neither study completely excludes the other type of uncertainty. The distributions obtained are not purely independent and cannot be combined to obtain a final representative distribution. Rather, the true wind representative wind load model lies somewhere between the bounds of these two models. As it is not clear where the true model lies within the range - even though it may be argued that the lower bound is closer to the true target than the upper bound - it was decided to conservatively select the parameters of the final representative distribution from precisely the middle of these upper and lower bound limits. This was done by calculating the geometric mean of the values of the parameters of the two distributions. In doing so the results from both studies are effectively regarded as equally reliable and are therefore weighted equally.

Table 5.10: Summary of representative distributions of SANS pressure coefficients

Investigation	Distribution	Mean	Std Dev
Observed value comparison	Normal	0.99	0.43
Codified value comparison	Normal	0.98	0.23
Final distribution	Normal	0.99	0.31

Chapter 6

Terrain Roughness Factors

The final independent wind load component to be investigated in this study is terrain roughness factors (c_r). Terrain roughness factors are primarily subject to epistemic uncertainties due to the use of terrain categories and the subjective way in which representative terrain categories are selected. It should be noted that, as explained in Section 2.2.3, topographical effects are not included and this investigation is only concerned with the reduction in wind speed with height above ground level due to surface roughness. Terrain roughness factors are used to affect the reduction on the total wind load, with some formulations applying a reduction factor to the wind speed and others applying a reduction to the wind pressure. In this investigation of terrain roughness uncertainties all factors are converted to a reduction on the pressure.

This chapter details the development of the SANS terrain roughness factor probabilistic model. Firstly, a baseline model which has been tested using both wind tunnel and full-scale results is described. Two investigations are then undertaken to determine the representative probabilistic distribution of terrain roughness factors. These investigations were used to determine statistical distributions of the systematic bias and the variability independently. Through the use of hierarchical Bayesian models and the Monte Carlo method developed in Section 3.5 these distributions were then combined into a single representative distribution of terrain roughness factor uncertainties.

6.1 Baseline model

For the purposes of this investigation, a baseline model needed to be defined and accepted as theoretically correct in order to quantify the terrain roughness factor uncertainties. This proved to be challenging due to the subjective nature of terrain categories and how they may be selected and defined. It was decided that the theoretical model used needed to provide clear descriptions of terrain categories which could be compared to the terrain categories used in international wind load standards, and the velocity profiles needed to be verified using both wind tunnel and full-scale test results.

The exposure model developed by Wang and Stathopoulos (2007) was selected as the baseline model for this investigation. The Wang-Stathopoulos model is based on the power law and was specifically developed to incorporate the effects of multiple zones, or patches, of different roughnesses upwind of the site under consideration. The model is used to determine piecewise defined boundary layer profiles composed of Internal Boundary Layers (IBLs), as illustrated in Figure 6.1, based on the number of roughness changes in the wind's fetch. Equations 6.1.1 to 6.1.4 are used to define the boundary layer profile. For the purposes of this investigation, only homogenous terrain using one roughness patch and no terrain change is considered. For this simplified case Equation 6.1.3 does not apply and Equation 6.1.1 reduces to the ordinary power law function as given in Equation 2.2.6. Changing terrain roughness is an example of a special case for which reliability should conform to the basic case investigated here, as mentioned in Section 2.1.

$$(U)(z) = U(g_n(x))\left(\frac{z}{z_{g_n}}\right)^{\alpha_n}, (g_{n+1} < z < g_n; n = 0, ..., N; g_{N+1} = 0) \tag{6.1.1}$$

$$g_0(x) = G, (n = 0) \tag{6.1.2}$$

$$g_n(x) = 0.5 z_{0,(n,n-1)}^{0.2} x_n^{0.8}, (n = 1, 2, ..., N) \tag{6.1.3}$$

$$z_{0,(n,n-1)} = max(z_{0,(n)}, z_{0,(n-1)}) \tag{6.1.4}$$

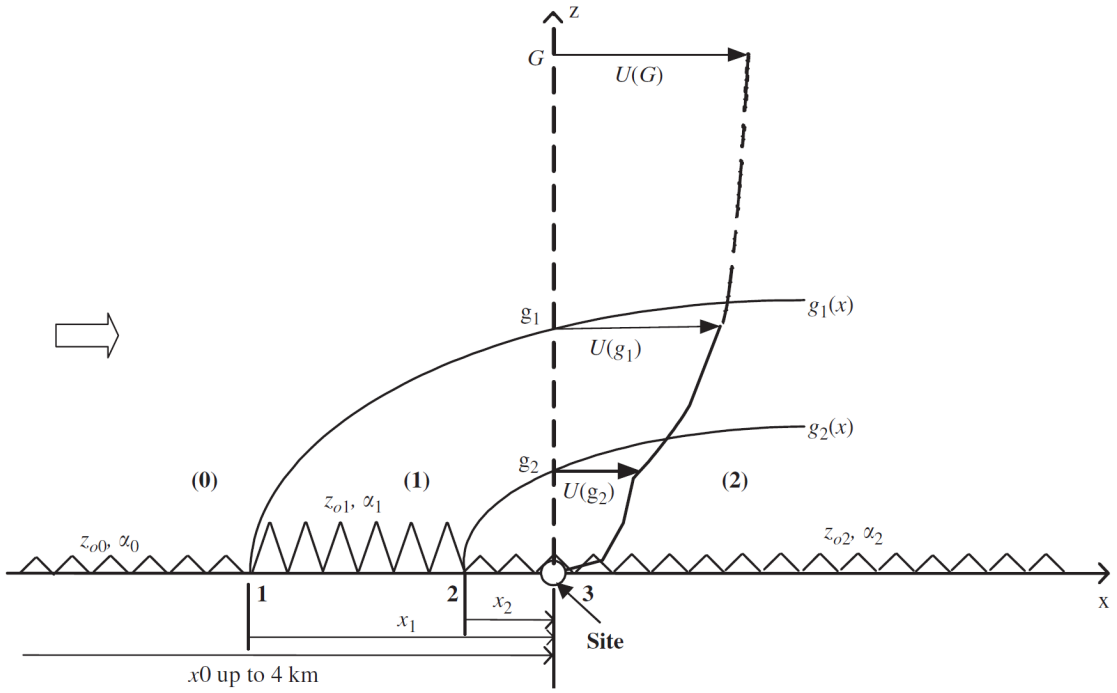

Figure 6.1: Schematic boundary layer above a fetch with two roughness changes using Wang-Stathopoulos model. (Taken from Wang and Stathopoulos (2007))

where, n is the patch number

N is the patch number of the site

$g_0(x)$ is the gradient height

$g_n(x)$ is the depth of the nth IBL

x_n is the distance from the nth roughness change to the site

$z_{0,n}$ is the surface roughness of the nth patch

α_n is the power law exponent of the nth patch

Table 6.1: Wang-Stathopoulos terrain roughness classification and power law parameters.

Terrain Category	z_0 (m)	α	G (m)
1. Sea	0.0002	0.090	213
2. Smooth	0.005	0.125	213
3. Open Country (OC)	0.03	0.150	274
4. Roughly Open	0.1	0.200	274
5. Suburban (Rough)	0.25	0.250	366
6. Very Rough	0.5	0.300	366
7. Urban (Closed)	1	0.330	366

The reason the Wang-Stathopoulos model was selected as the baseline model for this investigation is not the ability to incorporate the effects of different terrain types, but rather

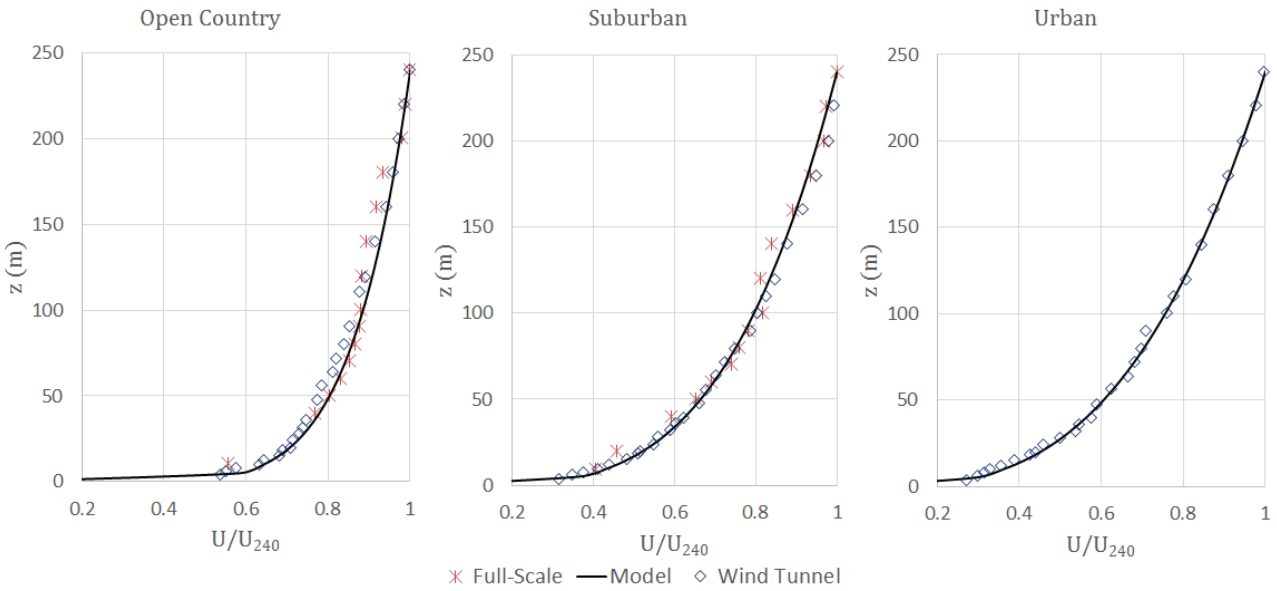

Figure 6.2: Wang-Stathopoulos wind velocity profiles for OC, Suburban and Urban terrain categories with wind tunnel and full-scale test results.

because of the roughness classification system it uses. The model uses a modified roughness classification from Davenport *et al.* (2000), as shown in Table 6.1. The original Davenport roughness classification specified eight terrain categories, however the highest roughness grade (Class 8, Chaotic, $z_0 > 2$ m) was combined within Urban (Closed). The original roughness lengths were maintained, however the power law exponents were adjusted by best fit of data from numerous wind tunnel and full-scale tests. Figure 6.2 shows the speed profile for the typical Open Country (OC), Suburban and Urban homogeneous terrain categories. Wind tunnel measurements are given for all three cases, and full-scale results from Tamura *et al.* (2001) are given for the OC and Suburban terrain categories. There is good agreement between the model and the observed values, validating the use of the Wang-Stathopoulos model as a theoretically accurate baseline model of terrain roughness factors.

Using the Wang-Stathopoulos velocity profiles, terrain roughness factor equations for each category were determined by normalizing the equations by a reference velocity. As with SANS, the reference velocity was taken at a height of 10 m in the OC terrain category. Equation 6.1.5 gives the Wang-Stathopoulos terrain roughness equation, and Figure 6.3 shows the roughness factor profiles of the Wang-Stathopoulos and SANS models. It is clear that at lower elevations the SANS roughness factors are less conservative than the Wang-Stathopoulos values, but at higher elevations the Wang-Stathopoulos values are exceeded.

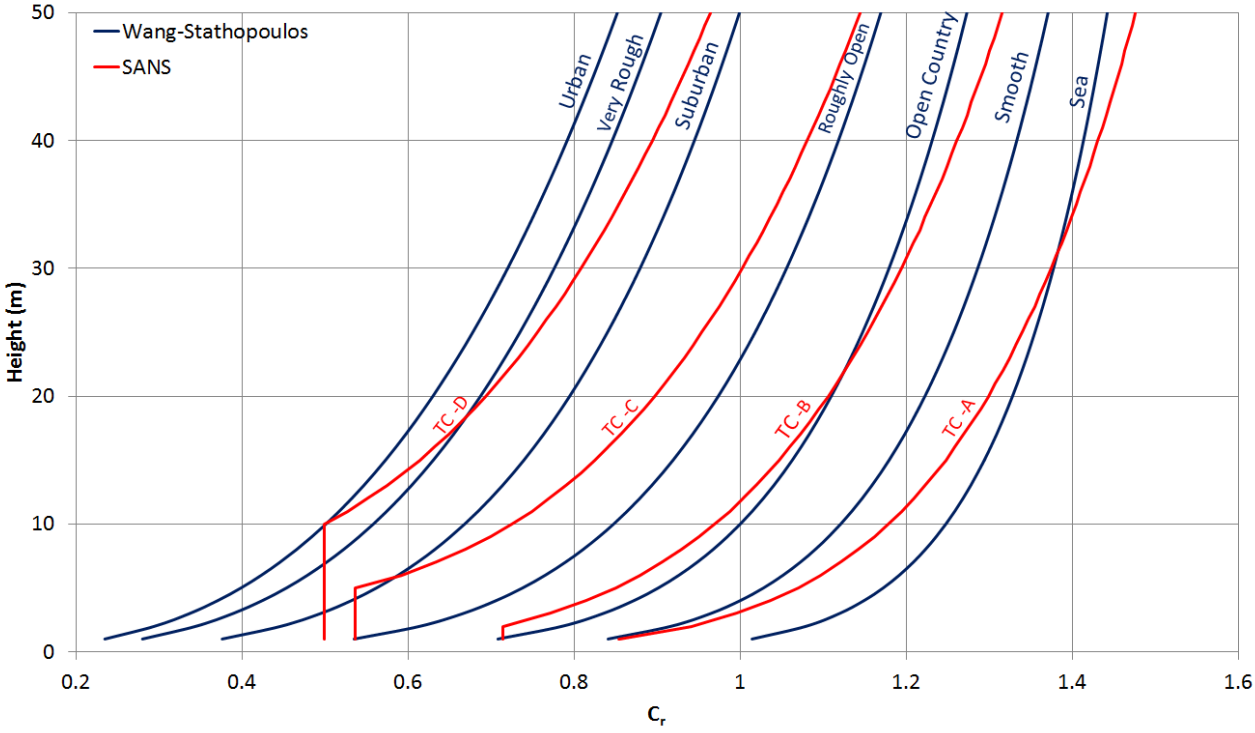

Figure 6.3: Wang-Stathopoulos and SANS terrain roughness factor profiles.

$$c_r = 1.64 \left(\frac{z}{z_g} \right)^{\alpha} \tag{6.1.5}$$

6.2 Systematic bias

As discussed in Section 2.2.3.1, the general wind load standard representation of terrain roughness factors is inherently conservative due to the use of terrain categories. This section of the investigation aims to quantify the systematic bias of the terrain roughness factors used in the South African wind load standard. It should be noted that this is not a general representation of the systematic bias of terrain roughness factors, but only of the systematic bias of the SANS stipulations.

The surface roughness length of the terrain surrounding a structure may have any positive value. The surface roughness creates a boundary layer, which represents the reduction of the reference wind speed over height. A continuum of possible values exists for all values of the structure's height and terrain roughness length. As it is not practical to provide terrain roughness factors for every possible value of the roughness length, and considering that it is often not possible to accurately measure the terrain roughness length, wind load standards

make use of terrain categories. Terrain categories divide the continuum into distinct zones, and the upper limit value of each zone is used to determine the appropriate terrain roughness factor when designing a structure. This process intuitively results in a conservative bias, since the upper limit is used for design purposes rather than a "best estimate" mid-interval value.

Furthermore, the SANS terrain roughness factor bias is also dependent on the comparison with the Wang-Stathopoulos baseline model selected for this investigation. The terrain category limits of the SANS and Wang-Stathopoulos models differ, with the SANS model giving lower values at low elevations and greater values at higher elevations. As such, the average bias is smaller at lower elevations and increases with elevation. The maximum height cutoff value selected may have a significant impact on the calculated systematic bias, and should be selected in such a way that the sampling space is the best possible representation of typical design situations.

A method was developed to determine the statistical distribution of the terrain roughness factor systematic bias across the continuum of structure height and terrain roughness length values. As the SANS and Wang-Stathopoulos models do not use the same terrain category definitions, the first step was to determine which categories were to be selected as being equivalent. Although this may seem trivial, inspection of Figure 6.3 shows that for the higher terrain categories there are more than one possible equivalent profiles if selection is based purely on which profiles are most similar. Selection of the correct equivalent profiles is crucial as it has a significant impact on the final results of the analysis. Therefore, the equivalent profiles were selected based on a combination of the roughness length values and the qualitative descriptions used to define the terrain categories. The selected equivalent categories are given in Table 6.1.

Table 6.2: Equivalent SANS and Wang-Stathopoulos terrain categories and roughness lengths as given by Retief and Dunaiski (2009) and Wang and Stathopoulos (2007).

Equivalent TC (SANS/W-S)	SANS z_0 (m)	W-S z_0 (m)
A / 1	0.02	0.0002
B / 3	0.05	0.03
C / 5	0.35	0.25
D / 6	0.6	0.5

The parameter limits of the investigation were defined as follows. It was decided that the roughness profiles would be considered on the height range between 1 m and 50 m. Furthermore,

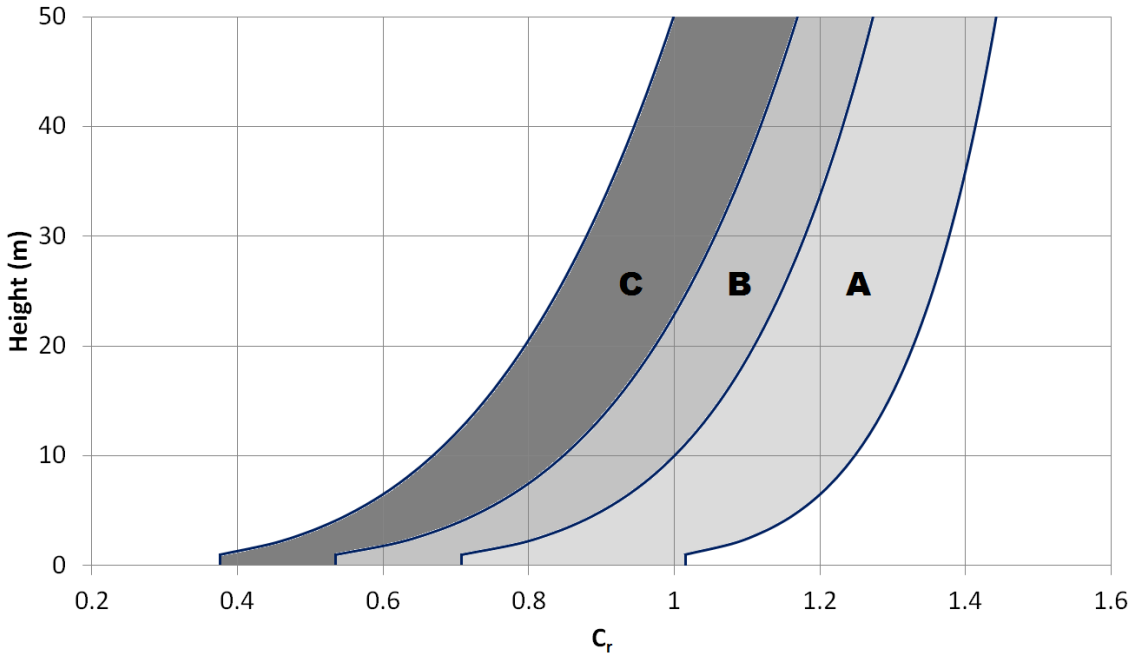

Figure 6.4: Bounded parameter space and subdivided zones for terrain roughness factor systematic bias investigation.

only values bounded by the equivalent SANS Terrain Categories A and D would be considered as the roughness factor values greater than those given in Terrain Category A are unlikely to occur as this exposure category effectively represents a flat plane with no obstructions, and any values less than those given for Terrain Category D would imply that the structure is not in an area in which it will be subjected to high wind loads. The bounded area was then divided into three zones, denoted A, B, and C, based on the upper limit terrain category which bounded the zone as specified using the Wang-Stathopoulos model, as shown in Figure 6.4.

The distribution of the systematic bias of each zone may then be calculated by integrating over the area of each zone. First, the upper limit roughness factor function and lower limit function are defined. As the best available approximation of these limits is the classification used in the modified Davenport model which has been experimentally validated, the equivalent Wang-Stathopoulos model profiles are used to define these limits. The average roughness factor function for the zone is then determined using the upper and lower limits. The systematic bias at a differential point may then be found as the ratio of the average roughness factor to the roughness factor values specified in SANS for that point ($t(z)$). A function for the systematic bias may then be calculated as shown in Equation 6.2.1. The mean and variance of the bias function may then be determined by integrating over the height of the parameter space using Equations 6.2.2 and 6.2.3. This method is then repeated for each zone in order to determine the

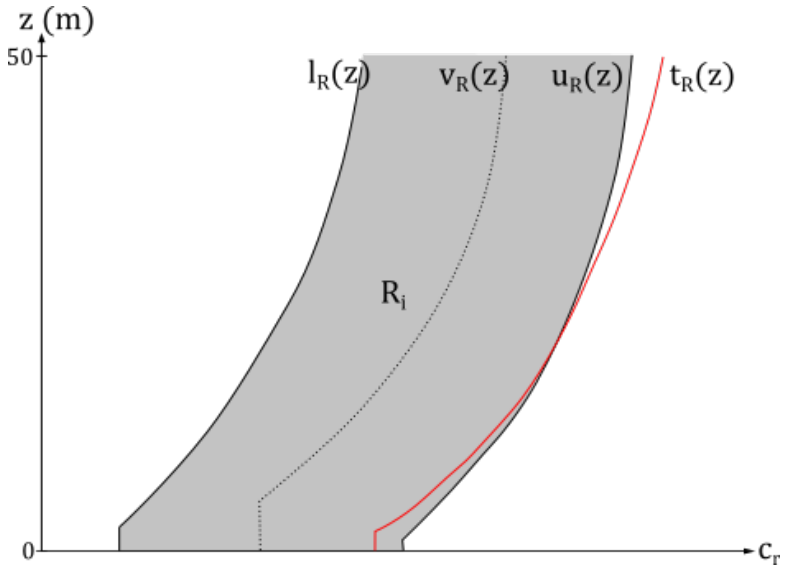

Figure 6.5: Functions used to determine mean and variance of systematic bias for a given zone.

representative terrain roughness factor systematic bias distribution. As the same height interval is used for all the profiles, the values may be sampled directly without having biased results.

$$s(z) = \frac{v(z)}{t(z)} = \frac{0.5(u(z) + l(z))}{t(z)} \tag{6.2.1}$$

$$\mu = \frac{1}{b-a}\int_a^b s(z)dz \tag{6.2.2}$$

$$\sigma^2 = \frac{1}{b-a}\int_a^b (s(z) - \mu)^2 dz \tag{6.2.3}$$

where, z is the elevation above the ground

$s(z)$ is the average systematic bias function

$v(z)$ is the average roughness factor function of the zone

$u(z)$ is the upper limit roughness factor function of the zone

$l(z)$ is the lower limit roughness factor function of the zone

$t(z)$ is the SANS roughness factor function

μ is the mean value of the systematic bias

σ^2 is the variance of the systematic bias

The method described above was used to determine the statistical parameters for Zones A, B and C as shown in Figure 6.4. The results are given in Table 6.3, as well as the statistical parameters for all three zones combined. The final combined mean value indicates an overall conservatism of terrain roughness factors, as expected.

Table 6.3: Terrain roughness factor systematic bias statistical parameters.

Zone	Mean (μ)	Standard Deviation (σ)
A	0.93	0.02
B	0.86	0.01
C	0.83	0.03
Combined	0.88	0.05

6.3 Variability

Having quantified the systematic bias of the terrain roughness factors, the variability of these factors needed to be determined. The systematic bias investigation clearly revealed the inherent variability in the terrain category method of selecting the upper limit value from a continuum. There is, however, another source of uncertainty which affects terrain roughness factors, namely defining the representative profiles. From comparison of the SANS and Wang-Stathopoulos roughness factor profiles it is clear that the representative terrain categories are significantly different. One approach would be to assume that as the Wang-Stathopoulos model is accepted as being theoretically correct for this investigation, the SANS profiles are simply incorrect and any variability is adequately represented in the systematic bias distribution. However, further investigation reveals that no two major international wind load standards use the same terrain roughness factor profiles or exposure category models. Lacking proper background and testing information, it may be assumed that the terrain roughness stipulations given in these standards were all based on data from trustworthy or reliable sources. This infers that there are epistemic uncertainties which affect terrain roughness factors, as discussed in Section 8.2.1, beyond the inherent variability of the terrain category method.

The simplest method for quantifying this epistemic uncertainty is to conduct a comparative investigation of wind load standards. As the Wang-Stathopoulos model has been assumed to be correct for this investigation, comparison of the different roughness factor profiles used in wind load standards does not provide an indication of the systematic bias of the SANS roughness profile. It does, however, provide an indication of the additional variability inherent in the use of the terrain category method by quantifying the variability of the representative terrain roughness profiles. As with the pressure coefficient investigation, the general principle of using comparative investigations as an indication of uncertainty as described in Section 3.4.2 was used. The methodology used for terrain roughness factors is described below.

The wind load standards which were selected for the comparative study were the SANS 10160-3 (South Africa), EN 1991-1-4 (Europe), AS/NZS 1170-2 (Australia and New Zealand), ASCE 7-10 (USA), NBCC 2010 (Canada) and ISO 4354. The primary concerns with comparing different wind load standards is that they use different profile laws to describe the velocity profile and provide different terrain categories. Eurocode and AS/NZS use the logarithmic law, whereas SANS, ASCE, NBCC and ISO use the power law. Each code has between three and five different terrain categories. For the purposes of this investigation, three representative terrain categories were chosen. These categories and their descriptions were taken from SANS and are given in Table 6.4. The equivalent terrain categories for the other standards are given in Table 6.5.

Table 6.4: Representative exposure categories used in comparative study of terrain roughness factors.

Category	Description	Roughness Length (m)
A	Flat horizontal terrain with negligible vegetation and without any obstacles (for example, coastal areas exposed to open sea or large lakes)	0.02
B	Area with low vegetation such as grass and isolated obstacles (for example trees and buildings) with separations of at least 20 obstacle heights	0.05
C	Area with regular cover of vegetation or buildings or with isolated obstacles with separations of maximum 20 obstacle heights (such as villages, light urban suburban terrain and permanent forest)	0.4

Table 6.5: Equivalent terrain categories for each wind load standard considered in the terrain roughness factor variability investigation

SANS	EN	AS/NZ	ASCE	ISO	NBCC
A	I	1	D	1	A
B	II	2	C	2	Intermediate
C	III	3	B	3	B

Another concern with comparing terrain roughness factors used in different wind load standards is taking into consideration when terrain roughness factors are applied in the wind load formulation procedure. Four of the wind load standards considered, namely SANS, Eurocode, AS/NZS and ISO, apply the terrain roughness factor to the free-field wind velocity before squaring the velocity to determine the peak pressure. As such, the influence of the terrain

roughness factors is squared as well. ASCE and NBCC, on the other hand, apply the terrain roughness factor to peak pressure directly. In order to effectively compare the roughness factor profiles the values used in the standards where the factors are applied to the velocity needed to be squared. The equivalent roughness factor profile for each representative terrain category after squaring the appropriate values are shown in Figure 6.6. As with the systematic bias investigation, the roughness profiles are only considered up to a height of 50 m.

Graphical comparison of the terrain roughness factor profiles shows that for Terrain Categories A and B the Eurocode roughness factors are significantly more conservative than the other wind load standards considered, and for Terrain Categories B and C the NBCC profiles are unconservative relative to the other standards. SANS, AS/NZS, ACSE and ISO show good agreement across all three terrain categories. It is interesting to note that the standards which show good agreement do not all share similar attributes, i.e. power law profiles or squared roughness factor values. This is a good indiction that the type of profile and where the roughness factors are applied during the wind load formulation procedure do not have a significant effect on the uncertainty, as different combinations may still result in similar answers.

Having established equivalent terrain roughness profiles, the terrain roughness factor for a given standard (c_k) may be calculated at any height within the sample set ($z \leq 50$ m) for a given terrain category. The values at each height ($c_{k,z}$) are then normalized with respect to the calculated average roughness factor at that height (μ_z) for the terrain category. This allows direct comparison of the roughness factors across the entire height and all three terrain categories. The variability of the terrain roughness factors at that height (σ_z^2) may be calculated using Equations 6.3.1 and 6.3.2 below. The representative statistical parameters for the terrain roughness variability are determined by sampling the calculated variability at each height for the different terrain categories. As in the systematic bias analysis, the number of points measured on each profile are the same, so all the values could be sampled to obtain the combined representative parameters without having biased results. The results are given in Table 6.6.

$$\mu_z = \frac{1}{N}\sum_k c_k \tag{6.3.1}$$

$$\sigma_z^2 = \frac{1}{N-1}\sum_k \left(\frac{c_k}{\mu_z} - 1\right)^2 \tag{6.3.2}$$

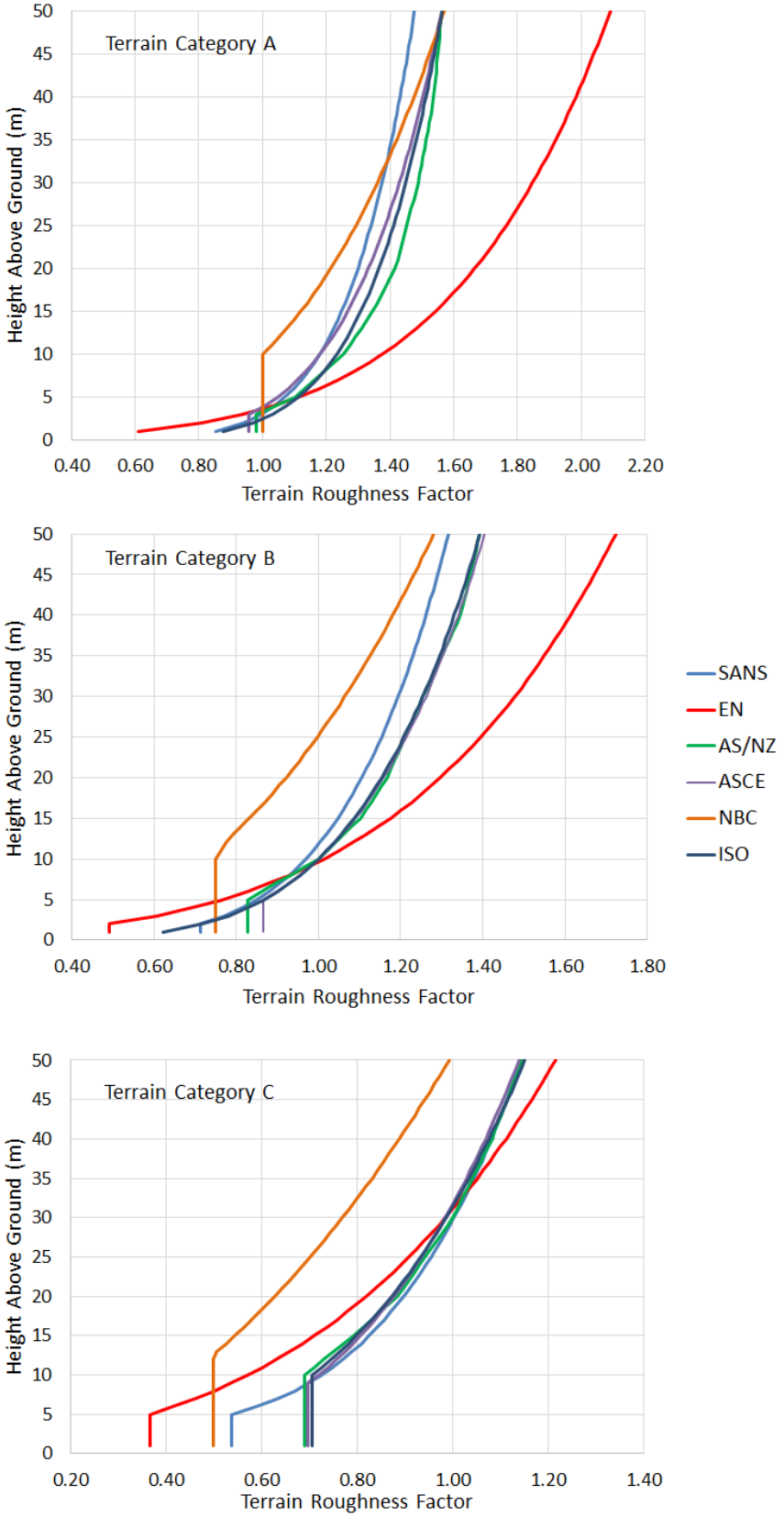

Figure 6.6: Wind load standard terrain roughness factors for equivalent terrain categories.

As in the systematic bias investigation, the mean and variance were calculated for each terrain category and for all three categories combined. The terrain roughness factor variability is shown to decrease for the higher terrain categories, with an approximately deterministic result shown for Terrain Category C as indicated by a very low standard deviation. Once again, as the variation cannot be negative, a log-normal distribution was selected for the model. The final representative distribution of the terrain roughness variability due to the epistemic uncertainties inherent in selecting the terrain roughness profiles was therefore selected as a log-normal distribution with a mean and standard deviation of 0.15 and 0.09 respectively. It is critical to emphasize that this distribution is not representative of the total uncertainty of terrain roughness factors, but rather representative of the probability of the degree to which the terrain roughness factors may vary. In other words, where the mean value of terrain roughness factors was the random variable under consideration in the systematic bias investigation, here the standard deviation of the terrain roughness factors distribution is the random variable.

Table 6.6: Terrain roughness factor epistemic variability statistical parameters.

Zone	Mean (μ)	Standard Deviation (σ)
A	0.23	0.10
B	0.15	0.05
C	0.08	0.01
Combined	0.15	0.09

6.4 Combined Distribution

In Sections 6.2 and 6.3 statistical distributions were determined in order to quantify the uncertainties inherent in terrain roughness factors due to the systematic bias of the terrain category method and the epistemic variability which exists when selecting terrain roughness profiles. In these distributions the terrain roughness factor was not the random variable being described, but rather the statistical parameters of the terrain roughness factor probability distribution were described. Using a Bayesian hierarchical model framework and the Monte Carlo method developed in Section 3.5 these prior distributions were combined into the posterior probability distribution representative of the SANS terrain roughness factors.

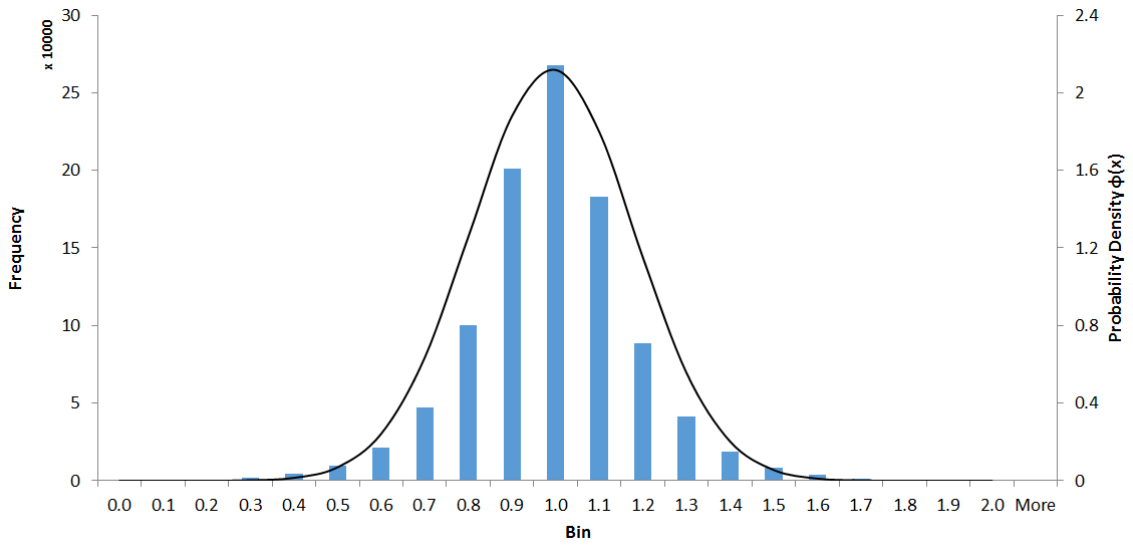

Figure 6.7: Monte Carlo histogram and probability density function of representative probability distribution of terrain roughness factors.

The Monte Carlo method was applied using one million simulations. Using this number of simulations stabilized the results obtained on subsequent iterations. The two input distributions used as well as the final representative distribution of terrain roughness factors are given in Table 6.7. Figure 6.7 shows the Monte Carlo generated histogram and probability density function of the representative distribution.

Table 6.7: Monte Carlo input distributions and resulting representative distribution of terrain roughness factors.

X	Distribution	μ_X	σ_X
Systematic Bias	Normal	0.88	0.05
Standard Deviation	Log-normal	0.15	0.09
Roughness Factor	Normal	0.88	0.18

Chapter 7

Preliminary Reliability Assessment of SANS 10160

In the previous three chapters the uncertainties inherent in the three primary wind load components, namely free-field wind, pressure coefficients and terrain roughness factors, were investigated and quantified. In doing so a primary goal of this dissertation was achieved by developing probabilistic models of those components. In this chapter the influence of these new probabilistic models on the total reliability of the South African design wind loads is determined through a preliminary reliability assessment of SANS 10160. The three models in isolation are however not sufficient to investigate the formulation of design wind loads on low-rise structures, nor can these models be combined and directly compared to existing probabilistic models, as the remaining factors which affect wind loading need to be taken into consideration as well.

A summary of the three primary wind load component models and a comparison of these with the corresponding distributions from existing probabilistic wind load models are presented at the start of this chapter. The development of full probabilistic wind load models using the three primary models and engineering judgement based distributions for the other wind load factors, as well as using Bayesian updating of the existing probabilistic models is then discussed. Using the full models allowed a preliminary reliability assessment of SANS 10160-3 to be performed. It should be noted that the purpose of this reliability assessment was not to serve as a comprehensive reliability assessment of SANS 10160, but rather to perform simple analyses in order to obtain an indication of the effect that the new probabilistic model may have on the reliability performance of the wind load standard. Finally, the combined influence

of the incorporation of the new wind map and the potential updating of the partial factor for wind loads on the total wind loading on low-rise structures in South Africa is presented.

7.1 Summary of wind load component models

The probabilistic wind load component models developed in this investigation differ from the corresponding component models in the existing probabilistic models not only in terms of their distribution parameters but also in their form. From the outset of this study it has been made clear that a serious problem with the existing models is the lack of clear background information detailing how the uncertainties were quantified and what sources were used to do so. In response to this the new models have not only been developed using transparent sources, but the nature of the models has been changed. These models were not simply regarded as single distributions representing a combined total uncertainty inherent in a given component. Instead, the distributions were broken down to their basic components through the use of Bayesian hierarchical models.

Although the final models may still be represented as a single probability distribution, as in the existing wind load models, the use of hierarchical models allows for a more detailed level of approximation of the models. Using this approach allowed different sources of uncertainty inherent in the components to be identified and investigated separately. Furthermore, as the structure of the models is more transparent, the models may easily be updated in future when new or better information becomes available to quantify the wind load component uncertainties.

The following sections present a brief summary of each of the three primary wind load component probabilistic models developed in this study. The final representative distribution of each is compared to the corresponding component distributions in the existing wind load models. Such a comparison has a two-fold purpose by aiding in identifying and understanding the deficiencies in the existing models, while simultaneously using the existing models as a benchmark to identify which components of the new models require further investigation. Although this may seem counterintuitive, it is important to remember that neither the existing models nor the new models are perfectly representative of wind load uncertainties. The new models may be regarded as the next iteration in an updating process. The differences between the new models and the existing ones may be used as an indication of which areas require further

research for further iteration of the process. Continuing this process is the most effective way of ultimately closing the gap between the true wind load uncertainties and the models of those uncertainties.

7.1.1 Free-field wind pressure model

A summary of the new probabilistic model of the South African free-field wind pressure is given in Figure 7.1. The summary is given in terms of the prior and posterior distributions of the Bayesian hierarchical model used. In the investigation of free-field wind pressure uncertainties in Chapter 4, two primary sources of uncertainty were identified, each affecting the variability and the systematic bias of the free-field wind pressure independently.

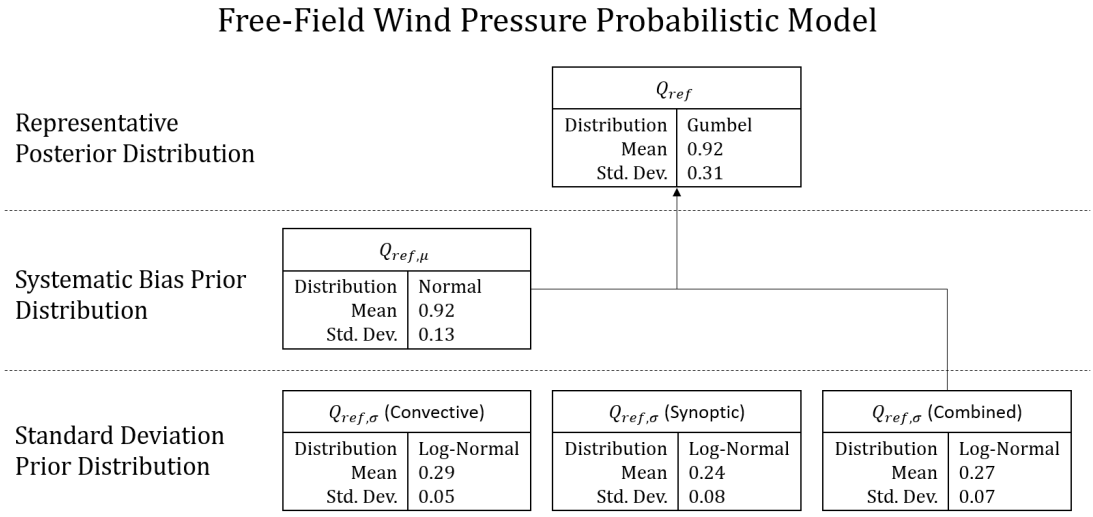

Figure 7.1: Summary of new free-field wind pressure probabilistic model.

The first source of uncertainty which affects the variability of the free-field wind pressure was the natural aleatoric uncertainty of wind loads across a large region due to different strong wind generating mechanisms and macroclimatic conditions. These uncertainties were quantified by comparison of the extreme wind prediction models for wind measurement stations across South Africa as developed by Kruger (2011). As shown in Figure 7.1, three variability priors were developed by disaggregating the stations based on their dominant strong wind generating mechanisms, namely synoptic events and convective events, as well as using all stations to develop a combined distribution representative of the uncertainty across the entire country. This combined distribution was selected as the representative prior for the variability.

The second source of uncertainty was the influence of the wind map on the systematic bias of the free-field wind pressure. The use of wind speed intervals results in a built-in conservatism. The bias prior of the distribution was obtained by comparing the characteristic free-field wind pressure as calculated using the predictive models at each of the stations across the country to the specified design value for that location as given on the new South African wind map.

The final representative posterior distribution of the free-field wind pressure was obtained as a combination of the uncertainties of the prior distributions. An important point to remember when considering this distribution is the *a priori* assumption that the Gumbel distribution would be used to model free-field wind pressure. Although there is historical precedent for the decision, it was shown in this investigation that the basic assumption of a Gumbel distribution to model wind speeds does not imply that a Gumbel distribution should be used to model wind pressure, due to a change in the skewness of the distribution when the basic variable is squared. As such, the use of a Gumbel distribution may be slightly unconservative. However, given the lack of sufficient data to accurately estimate the skewness of the extreme wind speed distribution, the practical advantages of using the Gumbel distribution outweigh the potential loss in accuracy from doing so.

Comparison of free-field wind pressure models should be done carefully as the free-field wind pressures of different regions vary quite significantly. As stated by Ellingwood and Tekie (1999) in the development of the ASCE 7-95 model, free-field wind pressure uncertainties are entirely site specific. As such, comparison of the South African model with the European models provides more information about the differences in wind climates of the two regions than it does about the probabilistic modeling of the uncertainties of the wind pressure. It should also be noted that the new free-field wind pressure model is based on gust wind pressure values, whereas most of the existing models are based on 10 minute mean pressure values. The gust factor probability distribution therefore needs to be included in the free-field wind distributions for the models based on 10 minute mean values. The gust factor has little influence on the normalized probabilistic model, however, as the existing probabilistic models of gust factors have a systematic bias of unity and a value of 0.1 for the standard deviation.

Table 7.1 summarizes the final representative free-field wind pressure distributions from this investigation and the existing wind load probabilistic models investigated in Section 3.3.2. It should be noted that the gust factor distributions are included in the international existing

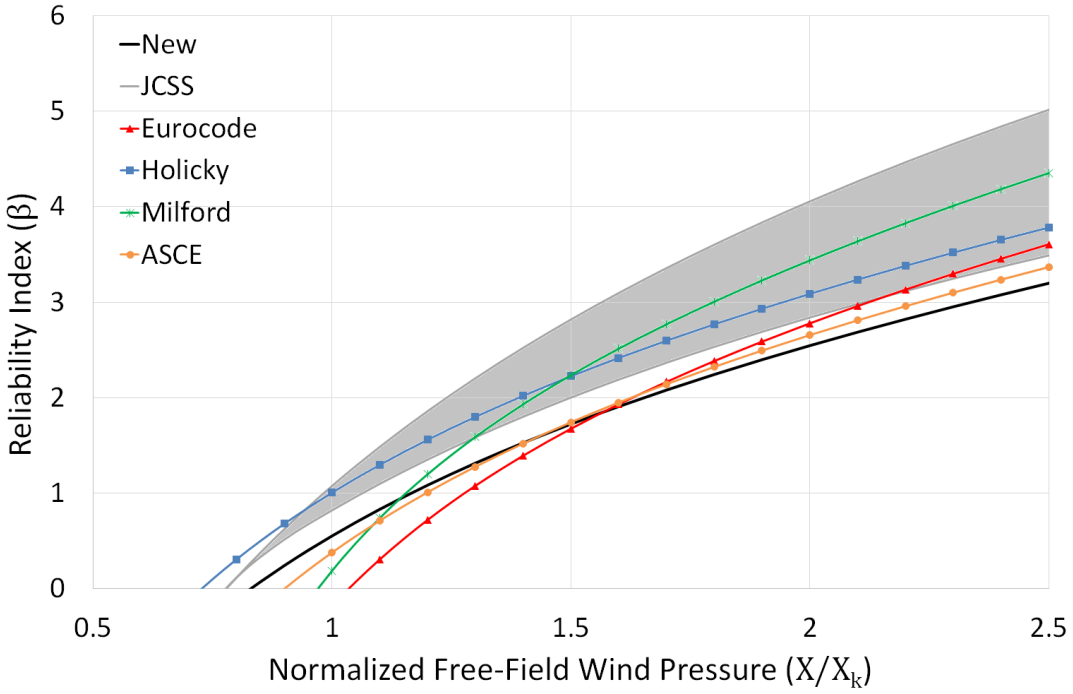

Figure 7.2: Comparison of new free-field wind pressure probabilistic model with existing models.

models' distributions. The tail-end reliability indices of these distributions are shown in Figure 7.2. It should be noted that higher variability results in a flatter curve, therefore a larger design value is required to achieve a target level of reliability. The new model has a higher standard deviation than the existing models, resulting in the highest required design values at high levels of reliability. As the relative mean shifts the entire curve up or down, the mid-range mean value of the new model offsets the reliability requirement somewhat, especially for lower reliability levels.

Table 7.1: New and existing free-field wind pressure probabilistic models.

Model	Distribution	Relative Mean $[\mu_X/X_k]$	Standard Deviation $[\sigma_X/X_k]$	Coefficient of Variation $[w_X]$
New	Gumbel	0.92	0.31	0.34
JCSS (upper)	Log-normal	0.80	0.28	0.35
JCSS (lower)	Log-normal	0.80	0.19	0.24
Eurocode	Gumbel	1.10	0.22	0.20
Holický	Gumbel	0.80	0.25	0.31
ASCE 7-95	Gumbel	0.98	0.27	0.28
Milford	Gumbel	1.02	0.17	0.17

As the comparison of free-field wind pressure distributions for different regions is not directly applicable, the most important result from this analysis is the comparison of the new model

and the previous South African model developed by Milford (1985*b*). It is seen that the new model is significantly different from the Milford model, with a lower systematic bias and higher variability. The higher variability results from the large dispersion of free-field wind variability values around the "mean variability" as discussed in Section 4.3.2.3 and shown in Figure 4.11. The differences between the models may therefore be attributed to the improved data used to develop the new wind map and by extension this new model. It is worth noting again that the previous version of the South African wind map and the information which Milford used in the development of the previous model were based on data from only 14 weather stations across South Africa. It therefore stands to reason that different and improved distribution parameters would be obtained when using the increased data from 76 stations across the country.

7.1.2 Pressure coefficient model

A summary of the new probabilistic model of pressure coefficients as developed in Chapter 5 is given in Figure 7.3. The new model is not a single model but three separate models consisting of lower and upper bound approximations and an average distribution selected from the range between the limits. As such, even though a single distribution is used in the remainder of this investigation, it is important to note that the final results of this investigation should not be viewed as a single distribution of pressure coefficient uncertainties but rather as an envelope of possible values that may be narrowed through future research.

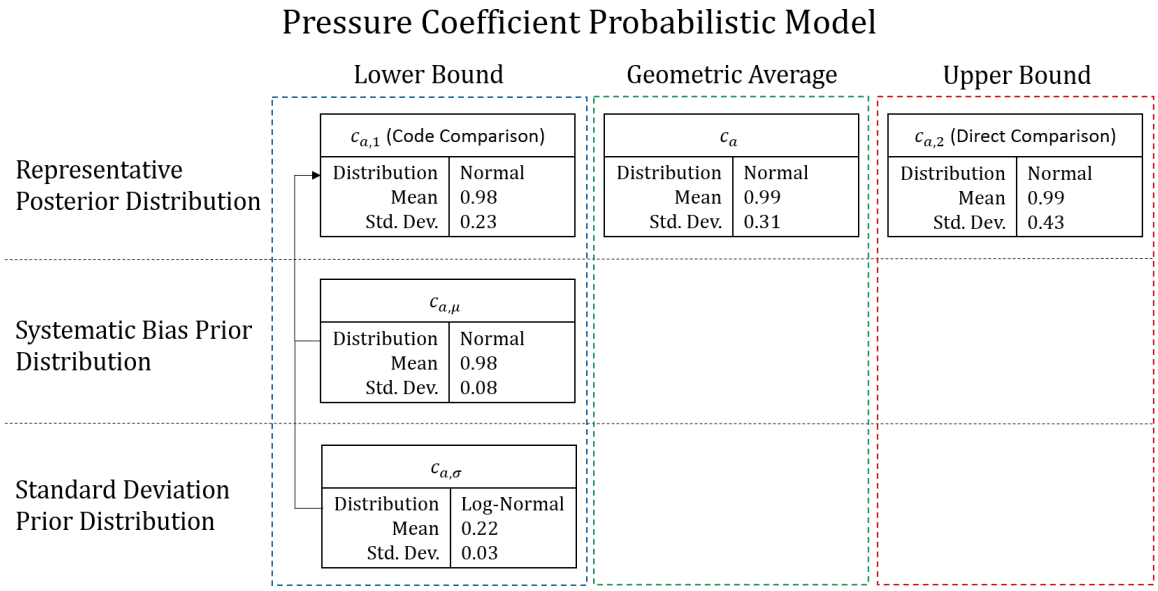

Figure 7.3: Summary of pressure coefficient probabilistic model.

The lower bound model was developed as a Bayesian hierarchical model with the comparison of wind load standards used to quantify the bias and variability priors of the distribution. This distribution is a lower bound approximation as the comparison of wind load standards does not fully incorporate the inherent aleatoric uncertainty of pressure coefficients but is dominated by the epistemic uncertainty in modeling pressure coefficients. The upper bound model is a single representative distribution which was obtained by sampling directly from the results of several wind tunnel and full-scale tests. The upper bound model may easily be improved in future through the addition of pressure coefficient studies to the sample space considered. This is an upper limit approximation as it incorporates not only the inherent aleatoric uncertainty of the pressure coefficients but also additional "artificial" uncertainty due to the lack of standardization of testing procedures. With no clear evidence as to whether the lower or upper bound is the closest approximation of the true uncertainty, the average distribution was selected by taking the geometric average between the posterior distributions of the upper and lower limits to be used as the best representation of the envelope of possible values.

Table 7.2 summarizes the final representative pressure coefficient distributions from this investigation and the existing wind load probabilistic models. The tail-end reliability indices of these distributions are shown in Figure 7.4. All three new distributions defining the pressure coefficient uncertainty envelope are included in the figure.

Table 7.2: New and existing pressure coefficient probabilistic models.

Model	Distribution	Relative Mean $[\mu_X/X_k]$	Standard Deviation $[\sigma_X/X_k]$	Coefficient of Variation $[w_X]$
New (upper)	Normal	0.99	0.43	0.43
New (average)	Normal	0.99	0.31	0.31
New (lower)	Normal	0.98	0.23	0.23
JCSS (upper)	Log-normal	1.00	0.30	0.30
JCSS (lower)	Log-normal	1.00	0.10	0.10
Eurocode	Normal	1.00	0.10	0.10
Holický	Normal	1.00	0.20	0.20
ASCE 7-95	Normal	1.00	0.12	0.12
Milford	Normal	0.70	0.14	0.20

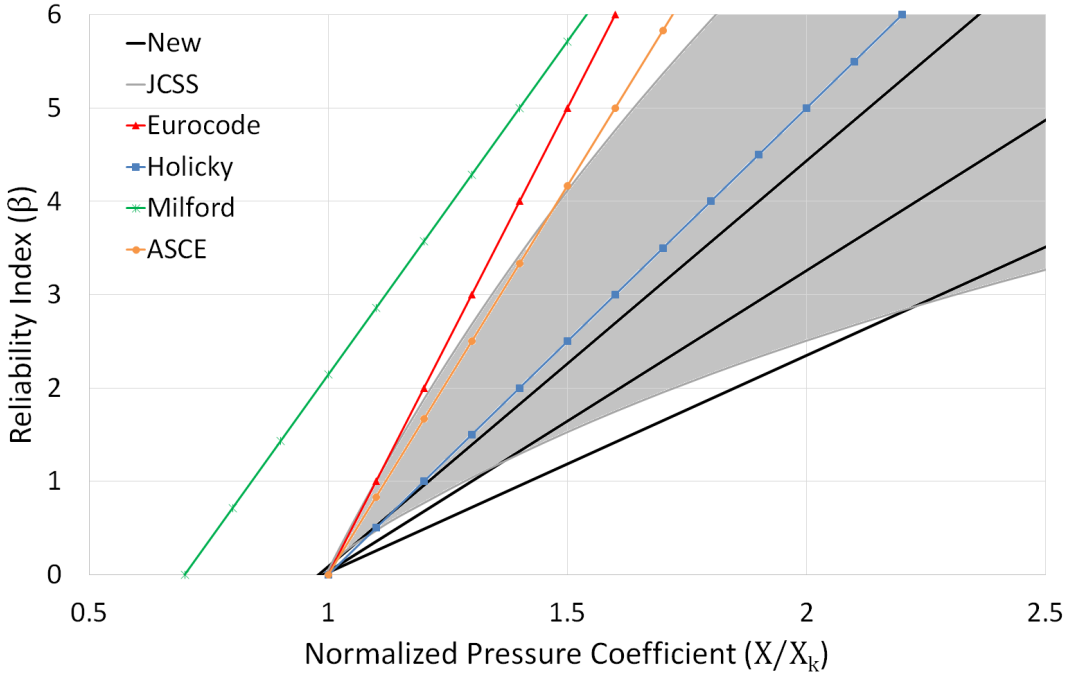

Figure 7.4: Comparison of new pressure coefficient probabilistic model with existing models.

The comparison of the existing pressure coefficient models leads to an interesting finding. When considering the JCSS model and the Eurocode model it is interesting to note the influence due to the change of distribution type. Even though the bias and standard deviations used in the Eurocode model were selected from the JCSS model, the decision to use a normal distribution instead of log-normal distribution means that the tail-end of the distribution no longer falls within the envelope of recommended values as stipulated by JCSS (2001-2002).

It is also interesting to note that with the exception of the Milford model, all the models have the same bias value, with a large spread in the variability values. The new models have a significantly greater variability than most of the existing models, resulting in a flatter distribution with lower reliability indices at higher pressure coefficient values. Nonetheless, the region bounded by the new model falls within the JCSS envelope of recommended values for the most part. Although the sources used to develop the JCSS models are not clear, this result is encouraging as it confirms that the high variability obtained for pressure coefficients in this investigation is reasonable. The comparison of the new model with the Milford and ASCE 7-95 models shows that those models have significantly lower variability values. It should be noted, however, that those models are not based on the same pressure coefficient scheme as used in Eurocode and SANS 10160-3 and are therefore not directly comparable.

7.1.3 Terrain roughness factor model

A summary of the new probabilistic model of terrain roughness factors is given in Figure 7.5. The terrain roughness factor model developed in Chapter 6 is the simplest of the new models, consisting of a single three level Bayesian hierarchical model as shown in Figure 3.7.

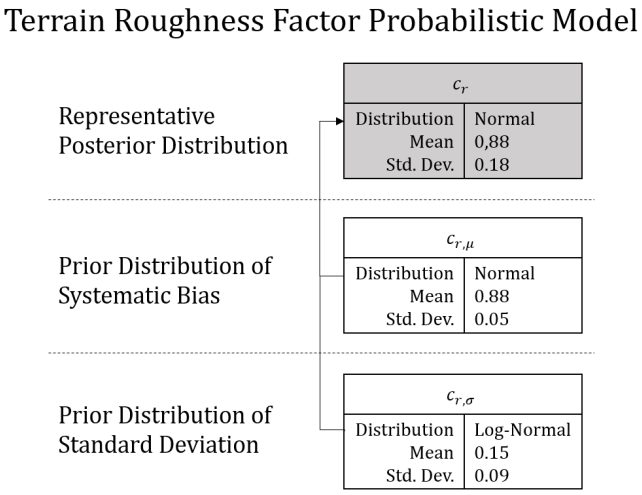

Figure 7.5: Summary of terrain roughness factor probabilistic model.

As with the other two models, the sources of uncertainty in terrain roughness factors were identified and investigated independently in order to quantify the prior distributions. The first source of uncertainty considered was due to the use of terrain categories, which causes a certain amount of conservatism in terrain roughness factors. The bias prior was developed by comparing the SANS terrain categories to an experimentally tested baseline model. The baseline model selected was the Wang and Stathopoulos (2007) power law model using a modified Davenport roughness classification. Terrain roughness factor variability is primarily due to the epistemic uncertainty of defining terrain category limits. As such, the variability prior was developed by comparing the terrain categories of several major wind load standards. The prior distributions were then combined into a single representative distribution using the Monte Carlo method.

The final representative terrain roughness factor distributions from this investigation and the existing wind load probabilistic models are given in Table 7.3. The tail-end reliability indices of these distributions are shown in Figure 7.6. The new model shows lower reliability indices than most of the existing models due to a higher bias and variability. However, of all three primary wind load components investigated, the terrain roughness factor model is the

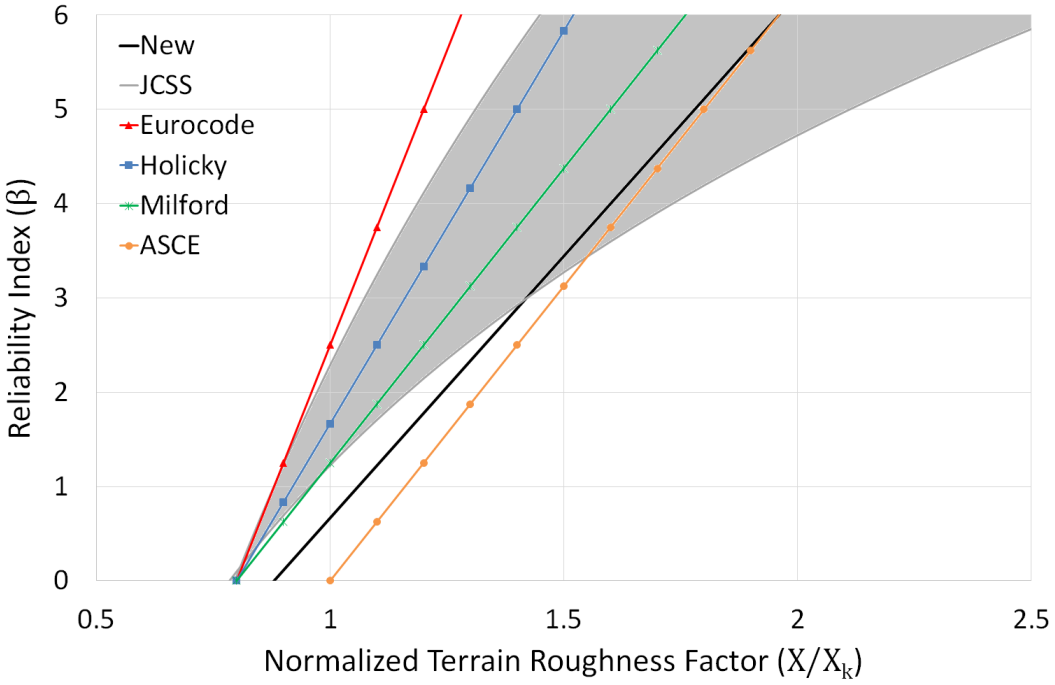

Figure 7.6: Comparison of new terrain roughness factor probabilistic model with existing models.

closest to the existing models. The new model corresponds well with the ASCE 7-95 model and falls within the JCSS envelope at higher reliability indices, albeit close to the upper limit.

Table 7.3: New and existing terrain roughness factor probabilistic models.

Model	Distribution	Relative Mean $[\mu_X/X_k]$	Standard Deviation $[\sigma_X/X_k]$	Coefficient of Variation $[w_X]$
New	Normal	0.88	0.18	0.20
JCSS (upper)	Log-normal	0.80	0.16	0.20
JCSS (lower)	Log-normal	0.80	0.08	0.10
Eurocode	Normal	0.80	0.08	0.10
Holický	Normal	0.80	0.12	0.15
ASCE 7-95	Normal	1.00	0.16	0.16
Milford	Normal	0.80	0.16	0.20

7.2 Full probabilistic wind load model

Although this investigation resulted in the development of probabilistic models for the three primary wind load components, the uncertainties inherent in other factors which influence wind loads were only briefly covered in Chapter 2 as they did not fall within the scope of the investigation. Those factors include gust factors, the effect of surrounding topography and

		Wind Load Components				
		Free-Field Wind	Pressure Coefficients	Terrain Roughness Factors	Model Uncertainty	Wind Directionality
Full Models	Judgement Based	New Model	New Model	New Model	Conservative Assumption	Literature
	Updated Eurocode	New Model	Bayesian Updating	Bayesian Updating	Unchanged	-
	Updated Holický	New Model	Bayesian Updating	Bayesian Updating	-	-
	Updated Milford	New Model	Bayesian Updating	Bayesian Updating	Unchanged	Unchanged

Figure 7.7: Summary of the development of full probabilistic models.

wind directionality effects. The three primary component models cannot be used for reliability assessment of the South African wind loading standard without incorporating the effects of these factors. As such, before the preliminary reliability assessment could be done a full probabilistic wind load model needed to be developed.

The ultimate aim of the preliminary reliability assessment presented in this chapter is not to develop a final full probabilistic model, but rather to determine the influence that the new component models have on the total reliability performance of design wind loads. To this end two different approaches were employed. The first was to simply select judgement based distributions for the unknown components using the information gathered in Chapter 2. The second approach was to perform Bayesian updating of the existing European and South African probabilistic models using the new component models. These methods are discussed in detail in the following sections. The outcome of this study was therefore not a single final probabilistic model, but rather multiple models derived from different sources. A summary of how the models were established is shown in Figure 7.7, and each of the models is described in more detail in the following sections.

7.2.1 Engineering judgement based model

The engineering judgement based model was based on the three primary component models and information regarding additional wind load factors from the background investigation presented in Chapter 2. The distributions selected for the model were chosen to conservatively represent the influence of the additional factors on total wind load uncertainty. The full model

is summarized in Table 7.4.

Table 7.4: Engineering judgement based full probabilistic wind load model.

Variable	Distribution	Relative Mean $[\mu_X/X_k]$	Standard Deviation $[\sigma_X/X_k]$	Coefficient of Variation $[w_X]$	Source
50-year extremes of wind pressure	Gumbel	0.92	0.31	0.34	Chapter 4
Pressure coefficient	Normal	0.99	0.31	0.31	Chapter 5
Roughness factor	Normal	0.88	0.18	0.20	Chapter 6
Directional factor	Deterministic	0.85	-	-	Chapter 2
Model coefficient	Normal	0.95	0.10	0.11	Engineering judgement
Design wind load	Gumbel	0.71	0.39	0.55	FORM analysis

The free-field wind pressure distribution was chosen as the posterior distribution from the primary model based on the variability prior using the combined data from all wind stations. As the new model is based on gust wind speed values, there was no need to include a gust factor variable. The pressure coefficient distribution was selected as the geometric average distribution taken between the upper and lower limit models. Finally, the terrain roughness factor distribution was simply taken directly as the posterior distribution from the primary terrain roughness factor model.

From the summary of wind directionality effects presented in Section 2.2.6, the approach used in the ASCE 7-95 model was selected for the judgement based model. Wind directionality effects were included in the model as a deterministic variable with a value of 0.85. This follows directly from the results obtained from the studies by Ellingwood and Tekie (1999) and Rigato *et al.* (2001). Although wind directionality certainly has an inherent variability, not enough information was available to estimate the variability. Judging from existing probabilistic models such as the Milford (1985*b*) model, the variability is almost negligible in comparison to the variability of the other wind load components. As such, the decision to include the factor as a deterministic variable was deemed to be reasonable.

Other wind load uncertainties such as the lack of both spatial and temporal correlation of wind pressures across the structure and topographical effects were included in the model through the use of a model uncertainty factor. These factors reduce the systematic bias of wind loads, however it is difficult to quantify this influence. An upper limit approximation based solely on engineering judgement was made by selecting a normal distribution with a bias value of 0.95 and a nominal standard deviation value of 0.10. The true influence of these factors will almost certainly decrease the bias even further, however as this decision is primarily subjective it is difficult to defend a model uncertainty factor with a bias of less than a nominal 5% bias reduction.

A multivariate parametric FORM analysis as done in Section 3.3.2 was performed using the full model. The component distributions were combined into a single representative distribution of the design wind load by fitting a Gumbel distribution to the tail-end of the results from the FORM analysis. This is the basis for the design wind load distribution as given in Table 7.4. The representative distribution is required for the reliability assessment of SANS 10160 to follow. The results of the FORM analysis are presented in Section 7.2.3 together with the results from the other full models considered in this investigation.

7.2.2 Bayesian updating of existing models

The second approach used to determine a full probabilistic model of design wind loads was to perform Bayesian updating of the existing probabilistic models using the new information obtained in this investigation. This process suits the overall investigative philosophy of this study by not excluding the existing models and simply replacing them with the new models, but rather treating the existing models as an additional source of information which may be used to obtain a better approximation of the final model of wind load uncertainties.

For each of the existing models which was updated, namely the Eurocode, Holický, and Milford models, the free-field wind pressure component model was replaced with the new primary free-field model obtained in this investigation. This was due to the fact that the new model was developed using the most recent region-specific data available. As such, it is safe to assume that the new model is the closest representation of the South African free-field pressure uncertainties available. This decision also lead to gust factors being excluded from the models

as the new model is based on gust wind speed data.

The pressure coefficient and terrain roughness factor models in the existing models were updated using Bayesian updating of the entire models and not only of the bias. The updated probability distributions were calculated by taking linear combinations of the prior models and the new models, as shown in Equation 7.2.1. This process was done using standard combination rules for normally distributed random variables as given in Holický (2009). The equations for calculating the mean and standard deviation of the posterior distribution are given in Equations 7.2.2 and 7.2.3 respectively. It was decided to weight the existing models and new models equally, with weighting factors chosen as $a = b = 0.5$.

$$Z = aX + bY \tag{7.2.1}$$

where, Z is the posterior variable

X is the prior variable

Y is the new information variable

a and b are weighting factors with $a + b = 1$

$$\mu_Z = a\mu_X + b\mu_Y \tag{7.2.2}$$

$$\sigma_Z = \sqrt{a^2\sigma_X^2 + b^2\sigma_Y^2} \tag{7.2.3}$$

All other wind load component distributions in the existing distributions remained unchanged. The models are summarized in Tables 7.5, 7.6 and 7.7 below. As with the judgement based model, parametric FORM analyses were performed in order to determine a single representative distribution of the design wind load. The results of the FORM analysis and comparison of all the full models are presented in the section below.

7.2.3 Full model comparison

As done for the comparison of the existing probabilistic models in Section 3.3.2, a parametric FORM analysis was used to compare the judgement based model and the updated existing models. The analysis was performed using the multivariate limit state function of each model by varying the normalized design wind load (w_d) between 0.5 and 2.5. This allowed the tail-end

Table 7.5: Updated Eurocode full probabilistic wind load model.

Variable	Distribution	Relative Mean $[\mu_X/X_k]$	Standard Deviation $[\sigma_X/X_k]$	Coefficient of Variation $[w_X]$	Source
50-year extremes of wind pressure	Gumbel	0.92	0.31	0.34	Chapter 4
Pressure coefficient	Normal	1.00	0.16	0.16	Updated
Roughness factor	Normal	0.84	0.10	0.12	Updated
Model coefficient	Normal	0.80	0.16	0.20	Eurocode model
Design wind load	Gumbel	0.65	0.32	0.49	FORM analysis

Table 7.6: Updated Holický full probabilistic wind load model.

Variable	Distribution	Relative Mean $[\mu_X/X_k]$	Standard Deviation $[\sigma_X/X_k]$	Coefficient of Variation $[w_X]$	Source
50-year extremes of wind pressure	Gumbel	0.92	0.31	0.34	Chapter 4
Pressure coefficient	Normal	1.00	0.19	0.19	Updated
Roughness factor	Normal	0.84	0.11	0.13	Updated
Design wind load	Gumbel	0.81	0.34	0.43	FORM analysis

of the resulting design wind load distribution to be obtained. A Gumbel distribution was then fitted to the tail-end distribution for each of the full models, as shown in Figure 7.8, in order to obtain the representative design wind load distributions as given at the bottom of Tables 7.4 to 7.7.

Table 7.7: Updated Milford full probabilistic wind load model.

Variable	Distribution	Relative Mean $[\mu_X/X_k]$	Standard Deviation $[\sigma_X/X_k]$	Coefficient of Variation $[w_X]$	Source
50-year extremes of wind pressure	Gumbel	0.92	0.31	0.34	Chapter 4
Pressure coefficient	Normal	0.85	0.17	0.20	Updated
Roughness factor	Normal	0.84	0.12	0.14	Updated
Directional factor	Normal	0.80	0.08	0.10	Milford model
Model coefficient	Normal	1.00	0.15	0.15	Milford model
Design wind load	Gumbel	0.62	0.32	0.51	FORM analysis

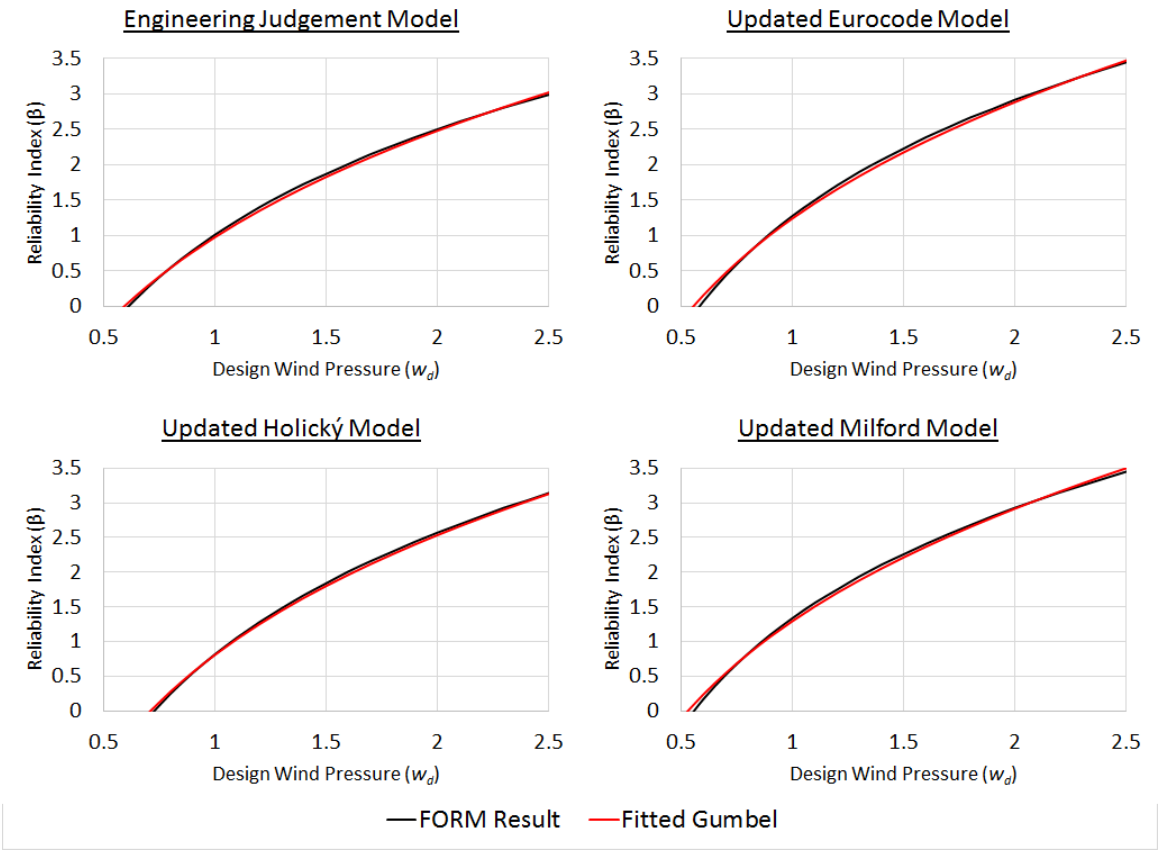

Figure 7.8: Fitting of Gumbel distributions to tail-end of FORM analysis results for full probabilistic models.

Due to the normalization, w_d can be interpreted as the partial factor that will achieve the corresponding reliability index according to the relevant probability model, denoted as γ_w. The

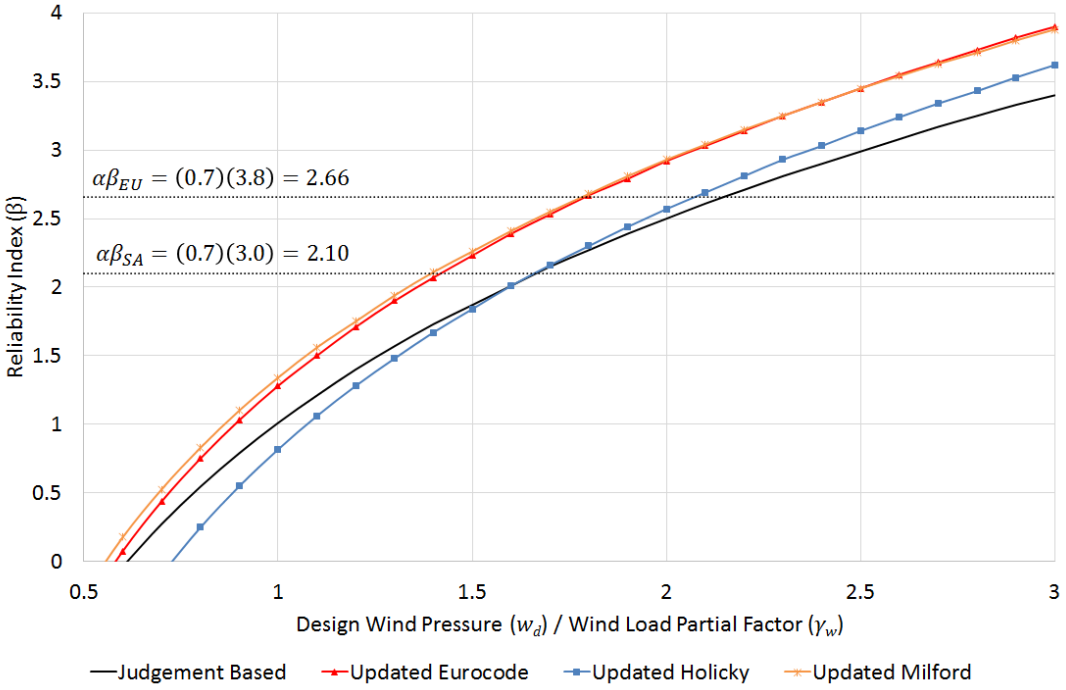

Figure 7.9: Results from multivariate FORM analysis of new models.

combined results of the FORM analyses for the four full models are shown in Figure 7.9. The normalized design wind pressure or partial factor required to obtain the South African and European target reliability indices for loading was then found for each of the models. These values are given in Table 7.8.

Table 7.8: Required normalized design wind pressure (partial factor) to achieve target reliability indices using new models.

Model	w_d ($\alpha\beta = 2.10$)	w_d ($\alpha\beta = 2.66$)
Engineering Judgement	1.66	2.15
Updated Eurocode	1.42	1.79
Updated Holický	1.66	2.08
Updated Milford	1.39	1.78

Another outcome of a multivariate FORM analysis is the calculation of sensitivity factors for the different components. The sensitivity factors obtained from the analysis of the judgement based model are shown in Figure 7.10. These sensitivity factors are direction cosines normal to the failure boundary at a given design point. In more practical terms, these factors are a measure of the relative contribution of each component to the overall uncertainty of the formulation. The sum of the squares of sensitivity factors always equals unity, and as such the squared sensitivity factor for a given component is indicative of the fraction of the total uncertainty which that component contributes. The results show that for the applicable range

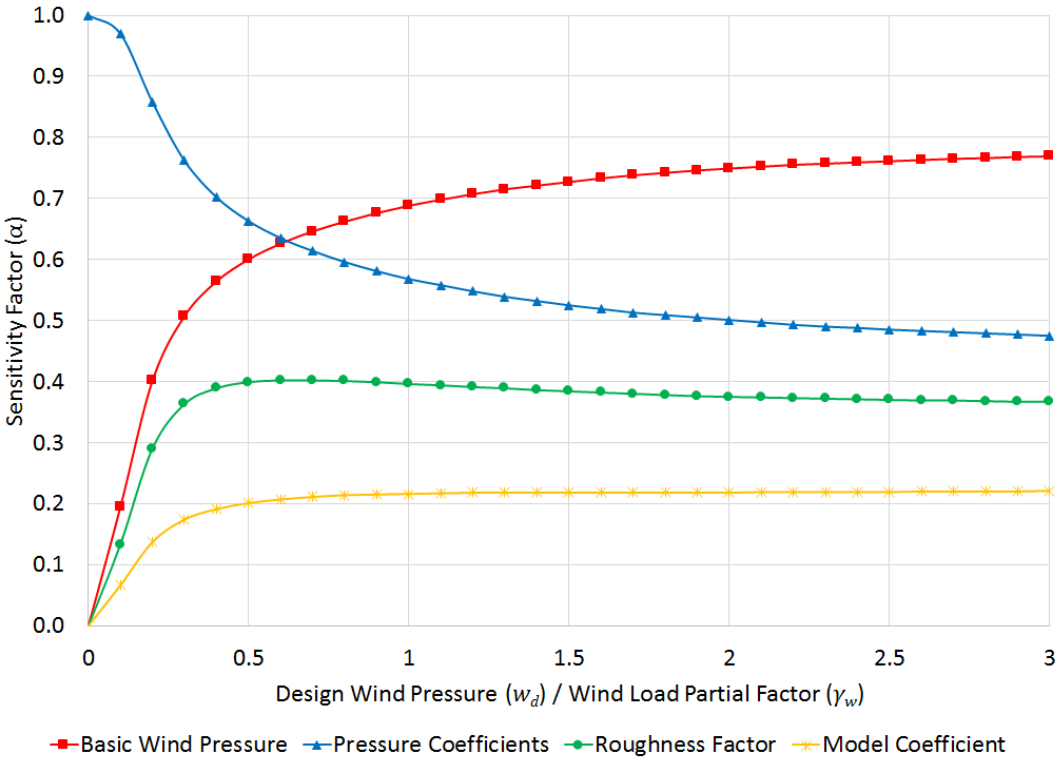

Figure 7.10: Sensitivity obtained from multivariate FORM analysis of the engineering judgement based model.

of design wind pressure values - which corresponds with the range of positive β values obtained in Figure 7.9 - the free-field wind pressure uncertainty is dominant. These sensitivity factors are a useful tool in the identification where the most valuable contribution may be added through further research of a component.

The aim of this analysis was not to select one of the models as the final full wind load probabilistic model. Instead, by comparing different models a sensitivity study of sorts may be used to determine the influence of the new wind load component models on the total wind load uncertainty. As the different models have different levels of approximation and varying levels of specificity, a better impression of the true wind load uncertainty may be obtained by comparing and contrasting the models than by simply investigating a single model.

Initial inspection of the results shows that the four models are grouped into two pairs of corresponding models. The updated Eurocode and Milford models correspond well, whereas the judgement based model and the updated Holický model show less agreement but have consistently lower reliability index values. Further inspection of the models shows that these corresponding pairs may be regarded as upper and lower bound approximations of the total wind load uncertainty.

Considering the upper limit first, the results show that the judgement based model requires the highest partial factor value for both the South African and Eurocode target reliability values. This is expected as the new component models used in the judgement based model have significantly higher variabilities than the existing models. Furthermore, the conservative estimates of the additional wind load factors' uncertainties used in the model imply that lower reliability indices would result from use of the model. Inspection of the updated Holický model shows that the model includes no model uncertainty factor or allowance for any uncertainties other than those inherent in the three primary wind load components. Considering that the additional wind load factors typically result in a reduction of the total systematic bias of wind loads, it stands to reason that the model results in conservative estimates of the total wind load reliability. Both of these models may therefore be regarded as upper bound approximations, as using a more realistic approximation of the reduction in the systematic bias due to the additional factors would result in a lower required partial factor.

The updated Eurocode and Milford models result in almost identical required partial factor values. Both of the models include model uncertainty factors, and the Milford model also incorporates the uncertainty due to wind directionality. In the updating process these additional factor distributions were not modified from the original distributions in the existing models. However, it is reasonable to assume that by using Bayesian updating of the primary wind load components some of the uncertainties which were originally incorporated in the model uncertainty factors are now accounted for in the updated primary models. The use of the original model uncertainty distributions therefore results in a certain measure of redundancy. The effects of this redundancy are different when considering the two statistical parameters. In terms of the systematic bias, such a redundancy would lead to an underestimation of total reliability, whereas redundancy in terms of the variability would result in overestimation of the total uncertainty. As the bias has a more significant impact on total reliability than the variability, it is safe to assume that these distributions are closer to a lower bound approximation of the total uncertainties than an upper bound approximation. Furthermore, the results from the investigations presented in Chapters 5 and 6 suggest that the existing models significantly underestimate the time invariant wind load components' uncertainty, and as such Bayesian updating of the existing models still results in an underestimation of the total uncertainty.

Clearly all four final distributions considered here have some form of deficiency, and any

one can not easily be singled out as a better approximation of design wind load uncertainties than the others. By considering all four models, however, it is possible to develop an indicative range of values of where the true wind load uncertainty model exists. It is also noteworthy that when compared to the initial comparison of existing wind load models in Figures 3.3 and Table 3.9, this range of possible values is significantly narrower than a similar range defined by the existing models.

7.3 Reliability assessment

A preliminary reliability assessment of SANS 10160 was performed using the full probabilistic wind load models discussed in the previous section. Through the use of multiple probabilistic wind load models this reliability assessment may be regarded as a sensitivity study in which the influence of the wind load uncertainty on the reliability performance of the South African loading code's design functions is determined. The aim of the assessment is not to be used for calibration of the standard, however the results may provide an indication of the potential changes of future reliability calibrations.

The methodology used for the reliability assessment is the same as used by Retief and Dunaiski (2009) in the previous reliability calibration of the standard. The method was outlined by Ter Haar and Retief (2001) and consists of the determination of a single graph which represents the global safety factor (GSF) required to achieve a target level of reliability. Design functions are then assessed through comparison with the GSF to ensure acceptable reliability performance. The methodology is based on a reliability performance function, as given in Equation 7.3.1, in which the limit state is expressed as a simple linear combination of the basic variables, namely the structural resistance (R), permanent actions (G) and variable actions (W). For this preliminary assessment only wind loads were included as variable actions, ignoring combination with other variable actions due to the complexity involved. A summary of the probabilistic models for the basic variables as used by Retief and Dunaiski (2009) as well as the wind load models used in this investigation is given in Table 7.9. It should be noted that the resistance coefficient of variation is parametrically varied in 5% increments in order to determine the reliability requirement for different construction materials.

$$g(X) = R - (G + W) = 0 \tag{7.3.1}$$

Table 7.9: Probability models for representative basic variables.

Variable	Source	Distribution	Relative Mean $[\mu_X/X_k]$	Standard Deviation $[\sigma_X/X_k]$	Coefficient of Variation $[w_X]$
Resistance	Retief and Dunaiski (2009)	Log-normal	1.00	0.10 0.15 0.20 0.25	0.10 0.15 0.20 0.25
Permanent Load	Retief and Dunaiski (2009)	Normal	1.05	0.11	0.10
Wind Load	Judgement Based Updated Eurocode Updated Holický Updated Milford	Gumbel Gumbel Gumbel Gumbel	0.71 0.65 0.81 0.62	0.39 0.32 0.35 0.32	0.55 0.49 0.43 0.51

The reliability requirement against which design functions are assessed is found by obtaining an inverse FORM solution to Equation 7.3.1 for a given target reliability. From the results the GSF is obtained as the ratio of the characteristic values of the resistance and the combined permanent and variable actions, as shown in Equation 7.3.2. By parametrically varying the ratio of variable actions to total actions (χ) as defined in Equation 7.3.3, the reliability requirement is obtained for the full range of permanent and variable action combinations.

$$GSF = \frac{R_k}{G_k + W_k} \tag{7.3.2}$$

$$\chi = \frac{W_k}{G_k + W_k} \tag{7.3.3}$$

Using the general target reliability of $\beta = 3.0$ for the South African loading standard the GSF reliability requirement may be determined. Figure 7.11 shows the reliability requirements obtained using the new wind load models as well as the SABS model, using a coefficient of variation of resistance of $w_R = 0.15$ throughout which is representative of typical reinforced concrete structures. A clear disparity is seen in the reliability requirements obtained using the new models and the SABS model. As stated in the introduction to this dissertation, the low reliability requirement obtained using the SABS model led to the adequacy of the model

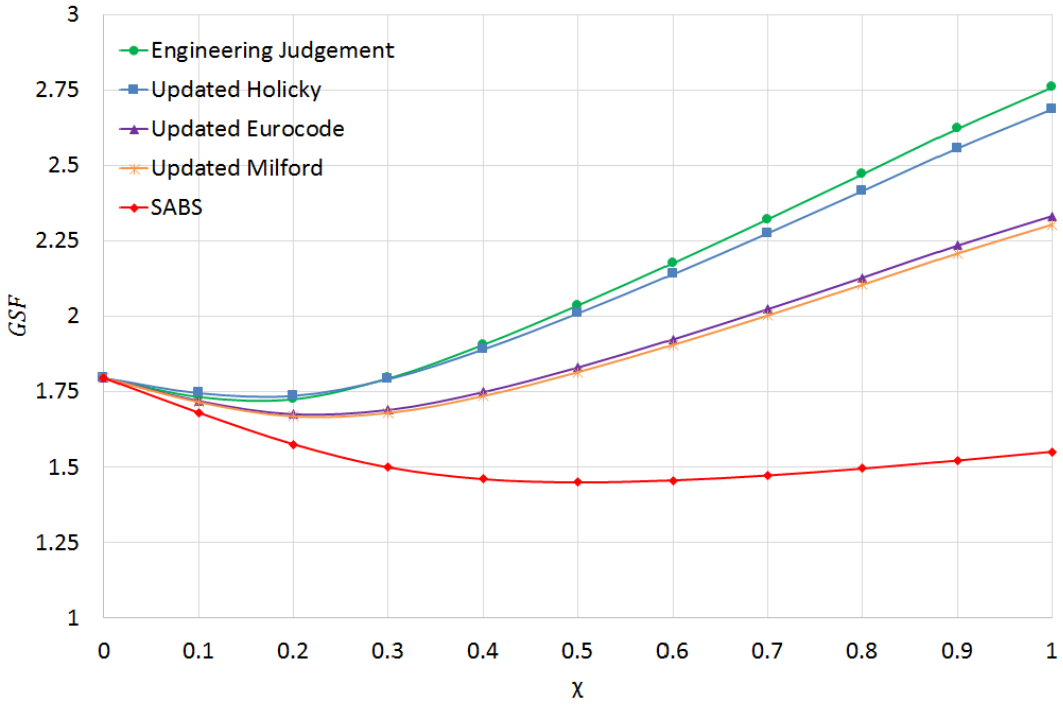

Figure 7.11: Reliability requirement for $\beta = 3.0$ for different models using a coefficient of variation of resistance $w_R = 0.15$.

being questioned. In fact, this questioning served as the primary motivation for the present investigation. The subsequent investigation of the model presented in Section 3.3.1.4 found that an error in the SABS model was the cause of the low reliability requirement. The results shown in Figure 7.11 clearly illustrate the influence of this error, and once again serve as motivation for the need for new reliability models and reassessment of the South African loading code reliability performance.

As the reliability requirements of the new wind load models are all different, testing design functions against all four reliability requirements provides a good indication of how the uncertainty of the wind load affects the total reliability performance of the standards. The general equation for the design functions ($f(X)$) used in SANS 10160 is given in Equation 7.3.4 in terms of the dimensionless ratio χ. The SANS 10160 scheme for the combination of permanent and variable actions uses more than one performance function, each of which are only acceptable over a portion of the full range of load ratios. Each performance function uses different partial factors for the same basic variables, excluding resistance (γ_G, γ_W), resulting in different linear graphs. The performance function which results in the most stringent reliability requirement for any given design situation is selected as the controlling load case in design verification. By calibrating the partial factors a piecewise defined reliability performance scheme may be

established.

$$f(X) = \gamma_R((1-\chi)\gamma_G + \chi\gamma_W) \tag{7.3.4}$$

In this assessment only the two primary SANS 10160-1 performance functions were used, namely the STR and STR-P design functions. The STR-P function results in the most unfavourable action effect in situations where the permanent load is dominant, i.e. for low values of χ. The STR expression should apply for other cases. The SANS partial factors for the basic variables for these functions as well as the resistance factors are present in Table 7.10. The resistance factor corresponds with a target level of reliability for resistance $\beta_R = (0.8)(3.0) = 2.4$, and as such the factor varies for different values of the coefficient of variation of resistance.

Table 7.10: SANS (2011*a*) basic variable partial factors

Variable		Partial Factor
Resistance	$w_R = 0.10$	1.26
	$w_R = 0.15$	1.42
	$w_R = 0.20$	1.59
	$w_R = 0.25$	1.79
STR	Permanent Load	1.20
	Wind Load	1.30
STR-P	Permanent Load	1.35
	Wind Load	1.00

As stated above, a reliability assessment was performed using each of the new wind load models in turn. The reliability requirements obtained are shown in Figure 7.12. The SANS design functions were plotted over these reliability requirements, with the STR partial factor for wind loads $\gamma_{W,STR}$ varied parametrically in increments of 0.3.

It is immediately clear that the design function using the existing partial factor is not acceptable for the required reliability performance using any of the full wind load models. Considering the reliability requirements of the four models and the summary of the models given in the previous sections, it is reasonable to assume that the appropriate reliability requirement lies between the Updated Eurocode and the Updated Holický curves. The STR-P function has sufficient reliability performance for values of χ between 0.0 and 0.3, however the STR function using a 1.3 partial factor does not meet the required reliability performance. It is therefore recommended that $\gamma_{W,STR}$ be adjusted.

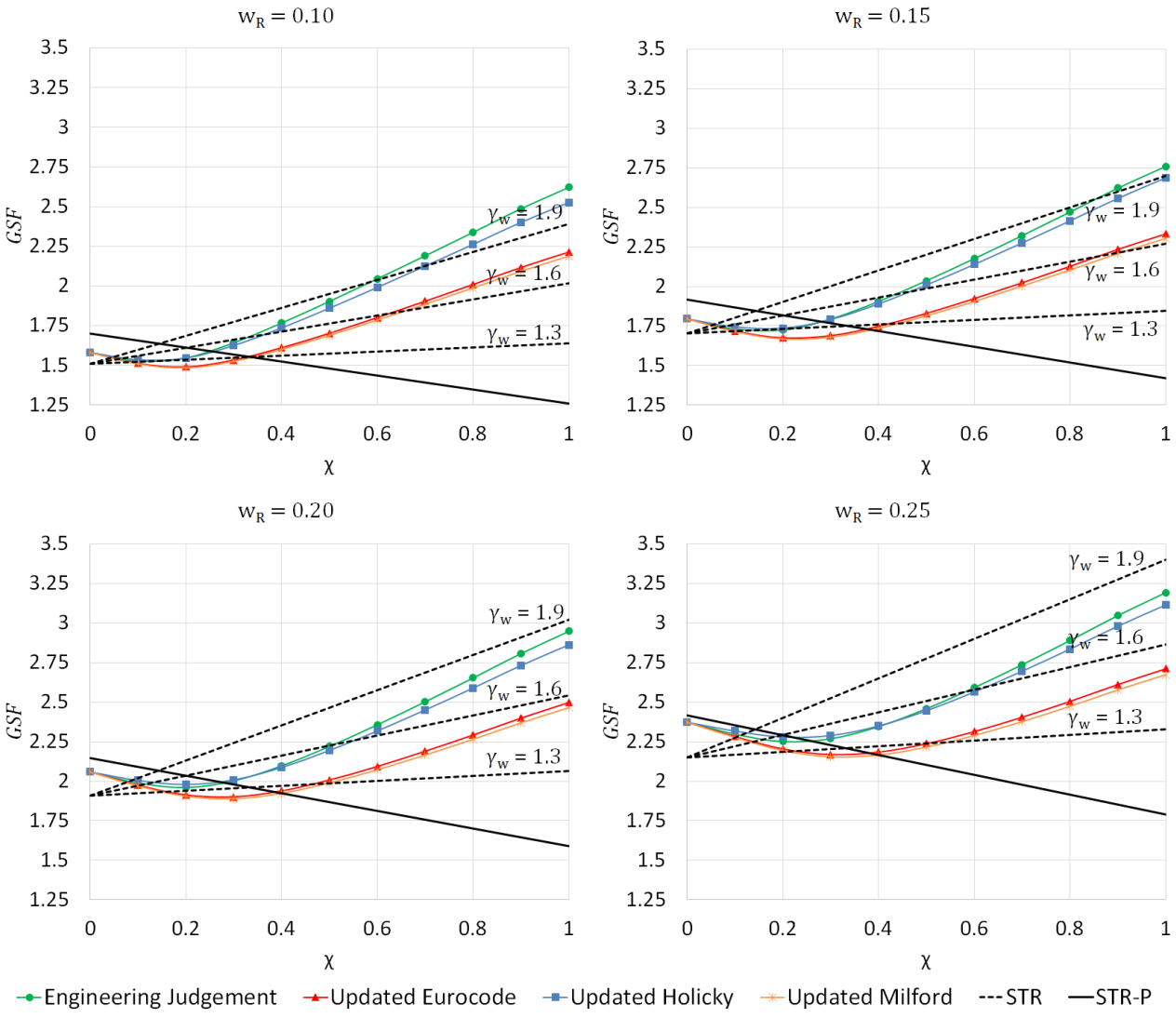

Figure 7.12: Reliability performance of SANS 10160 design function for $\beta = 3.0$ across parametric range of resistances.

Holický (2005) stated that a realistic range of χ for typical design situations is between 0.1 and 0.6. This preliminary reliability assessment shows that a partial wind load factor value of 1.6 would result in acceptable reliability performance of the SANS 10160 design functions across this range, although for structures with a coefficient of variation of resistance of 0.15 only the lower bound reliability requirement estimates are met. The 1.6 partial factor value also corresponds well with the partial factor values obtained from the direct FORM analysis of the wind load models as summarized in Table 7.8. It is clear from the results, however, that for light wind sensitive structures with load ratios of $\chi > 0.6$, a partial factor of 1.6 would not be adequate. Further investigation is required in order to develop the most efficient way to treat the reliability performance of these types of structures.

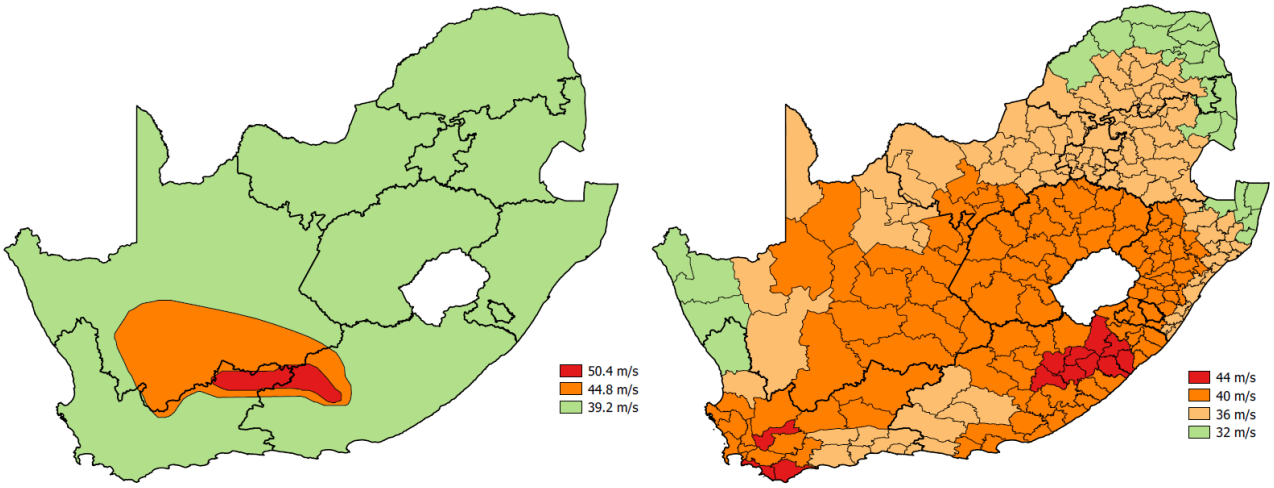

Figure 7.13: Old (left) and new (right) characteristic gust wind speed maps for South Africa.

7.4 Influence of changes to SANS 10160

The influence of the incorporation of the new wind map into the South African wind loading standard is not well defined. Furthermore, potential updating of the partial factor for wind loads will also impact the design wind loads across the country. This section aims to quantify the influence of these changes on the total design wind load across the country. As with the reliability assessment presented in the previous section, this investigation is theoretical and does not aim to propose specific changes to the standard. However, the investigation may serve as a useful resource during future updating of the code.

The development of the new characteristic gust wind speed map for South Africa was discussed in Section 4.2. For the sake of convenience the maps are shown here in Figure 7.13. It should be noted that the wind speeds shown on the old wind map include the "gust conversion factor" of 1.4 stipulated in the code. From inspection it is clear that the new wind map will lead to a significant reduction in wind loads across a large part of the country when compared to the old wind map. In order to precisely quantify this reduction it is necessary to convert the gust wind speeds to gust wind pressures. As the stipulations for pressure coefficients and terrain roughness are constant multiplication factors which are not affected by changing the wind map, the influence on the ultimate wind loads on structures due to the change of the map may be directly calculated from the change in gust wind pressure.

The equation for the calculation of gust wind pressure (Q_g) is repeated here in Equation 7.4.1. Two variables are required for the calculation, namely gust wind speed (v_g) and air density (ρ). The gust wind speed may be read off directly from the wind map. Air density is

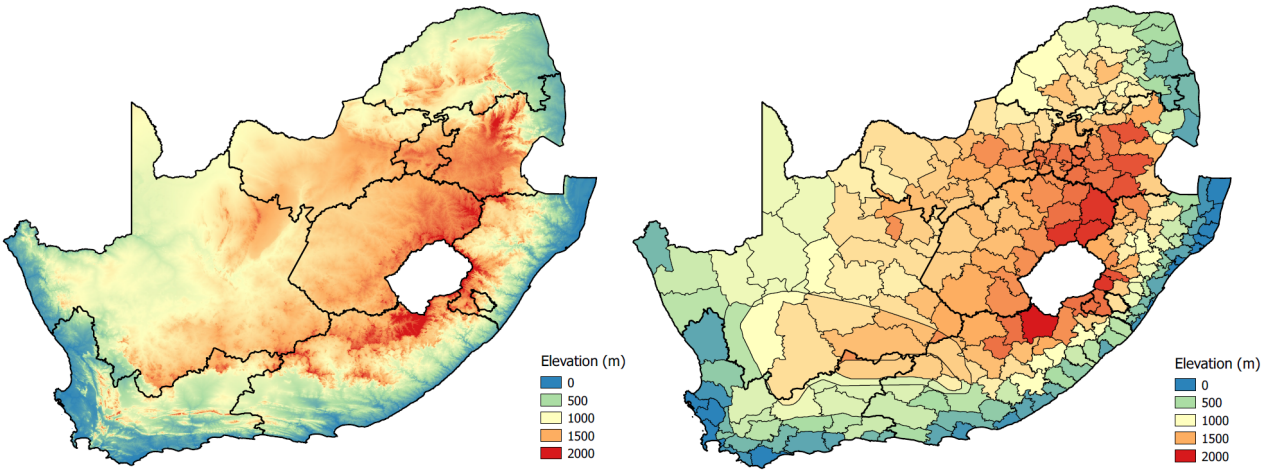

Figure 7.14: South Africa elevation map from GeoCommunity (2016) (left) and region averaged elevation map (right).

dependent on the altitude above sea level. Table 7.11 is taken from SANS 10160-3 and specifies air density values for a temperature of $20°C$ at various altitudes. The code allows linear interpolation between the values given in the table.

$$Q_g = 0.5 \times \rho \times v_g^2 \tag{7.4.1}$$

Table 7.11: Air density as a function of altitude as specified in SANS (2011*b*).

Altitude above sea level (m)	Air density ρ (kg/m^3)
0	1.20
500	1.12
1000	1.06
1500	1.00
2000	0.94

Raster data of South African elevation was obtained from GeoCommunity (2016). A regional map of South Africa was then developed using the QGIS software package by overlaying the municipal regions used to define the new wind speed map and the three zone wind regions from the old wind map. This regional map was overlaid onto the elevation raster data and the average elevation of each region was calculated. The raster elevation map and the region averaged elevation map are shown in Figure 7.14. Using linear interpolation of the values given in Table 7.11 the average air density was then calculated for each of the regions.

Using the gust wind speed values and the average air density calculated above, the gust wind pressure was calculated for each region using the old and new wind speed maps, as shown in Figures 7.15 and 7.16 respectively. The systematic bias of the peak wind load averaged

across each region was calculated by taking the ratio of the new pressures to the old pressures for each of the regions using Equation 7.4.2. The regional bias values mapped across South Africa are shown in Figure 7.17, and the regional parameters used in the calculation are given in Appendix C. Finally, the area-averaged bias value for the entire country was calculated using Equation 7.4.3.

$$b_i = \frac{Q_{g,i}^{new}}{Q_{g,i}^{old}} \tag{7.4.2}$$

where, b_i is the systematic bias for region i

$Q_{g,i}^{new}$ is the gust wind pressure from the new wind map for region i

$Q_{g,i}^{old}$ is the gust wind pressure from the old wind map for region i

$$b_{total} = \frac{\sum_{i=1}^{n} b_i A_i}{\sum_{i=1}^{n} A_i} \tag{7.4.3}$$

where, b_{total} is the area-averaged systematic bias for the entire country

A_i is the total area of region i

The area-averaged bias across the entire country was calculated to be 0.90. The incorporation of the new wind map into the South African wind load standard will therefore result a total wind load reduction of 10% on average. From Figure 7.17 it is seen that this bias is not evenly distributed across the country. Certain areas, specifically the Free State and large portions of the Northern Cape, Western Cape and Eastern Cape, show a slight increase in the total wind load with a bias value of approximately 1.04. Certain regions in central Eastern Cape and Western Cape show a significant increase with a bias value of up to 1.26. This increase is however offset by significant decreases in the average wind load across the remainder of the country, with reductions of between 15% and 35% in the Northern parts of the country and a reduction of up to 50% in areas near Beaufort West.

This analysis of the influence of the new wind map on the average wind load on structures across the country also provides an opportunity to investigate the influence of an updated partial factor for wind loads. As shown in the previous section, the current SANS 10160 wind load partial factor for the STR design function does not meet the required reliability performance when using the new probabilistic models developed in this dissertation. To determine the influence of an updated partial factor the area-averaged bias as calculated above may simply

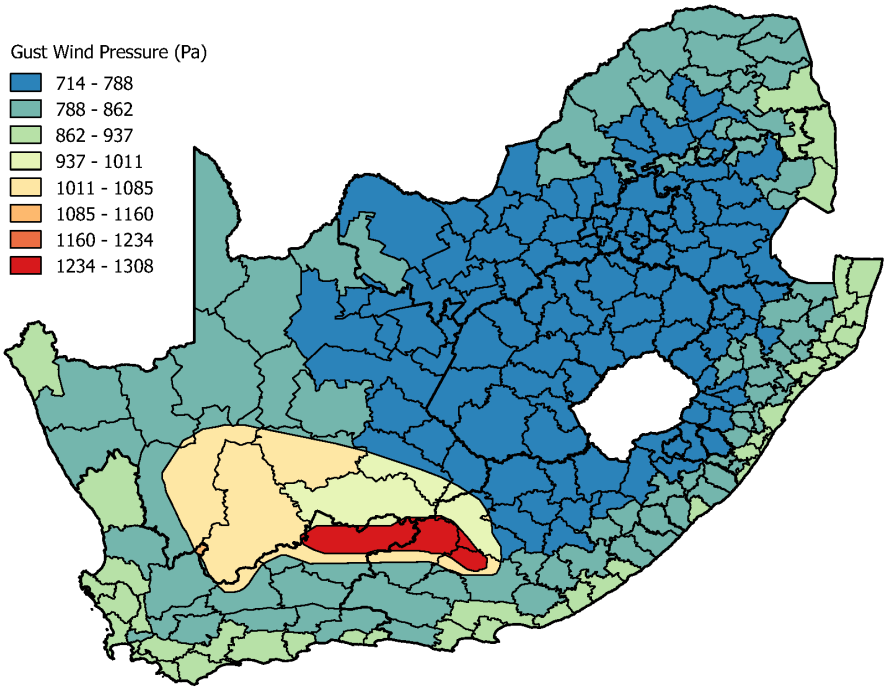

Figure 7.15: Average gust wind pressure across South Africa calculated using the old wind map.

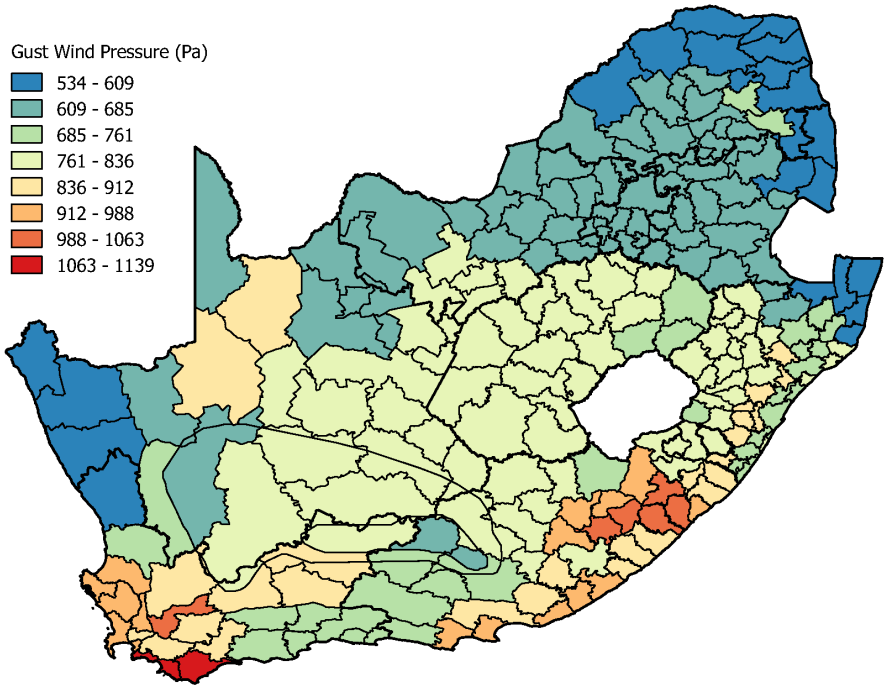

Figure 7.16: Average gust wind pressure across South Africa calculated using the new wind map.

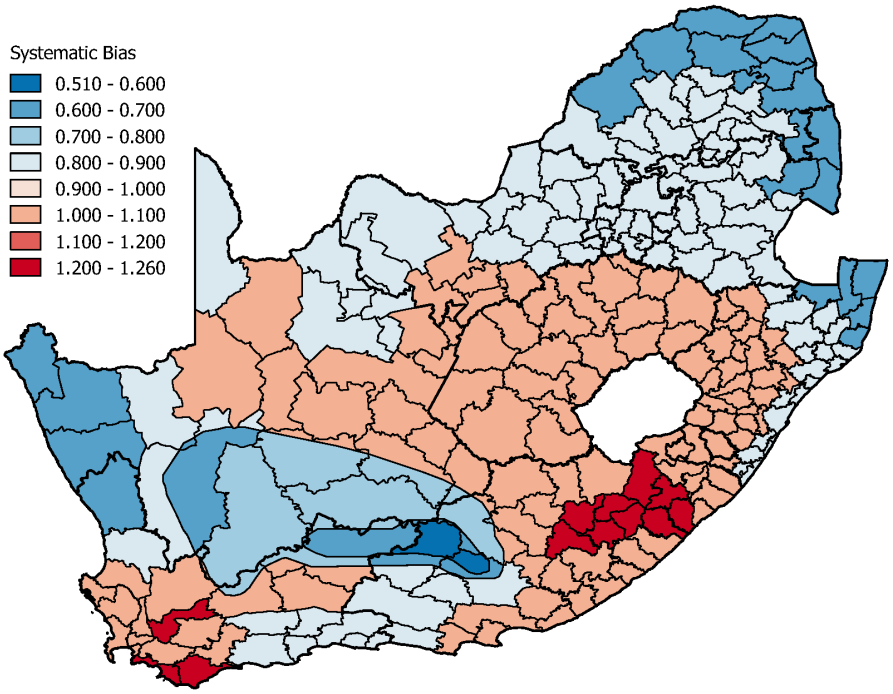

Figure 7.17: Regional systematic bias of total design wind loads across South Africa.

be multiplied by the ratio of the new partial factor to the old partial factor. The result is a linear increase in the systematic bias as the partial factor increases, as shown in Figure 7.18. An updated partial factor of 1.45 would result in a bias value of 1.0, effectively negating the average reduction in wind loads due to the new wind map. Using a partial factor of 1.6 or higher in order to ensure adequate reliability performance of the code as calculated in Section 7.3 would result in area-averaged bias values of 1.11 or higher. A summary of the factored area-averaged bias values for the provinces of South Africa and across the entire country for different partial factor values is presented in Table 7.12.

Table 7.12: Area-averaged bias values of total wind load across South Africa for different partial wind load factors γ_W.

Province	$\gamma_W = 1.30$	$\gamma_W = 1.45$	$\gamma_W = 1.60$	$\gamma_W = 1.75$	$\gamma_W = 1.90$
Eastern Cape	0.99	1.11	1.22	1.33	1.45
Free State	1.04	1.16	1.28	1.40	1.52
Gauteng	0.84	0.94	1.04	1.14	1.23
KwaZulu-Natal	0.92	1.03	1.14	1.24	1.35
Limpopo	0.76	0.84	0.93	1.02	1.11
Mpumalanga	0.80	0.89	0.98	1.07	1.16
North West	0.89	0.99	1.10	1.20	1.30
Northern Cape	0.87	0.97	1.07	1.17	1.28
Western Cape	0.92	1.03	1.14	1.24	1.35
Entire Country	0.90	1.01	1.11	1.21	1.32

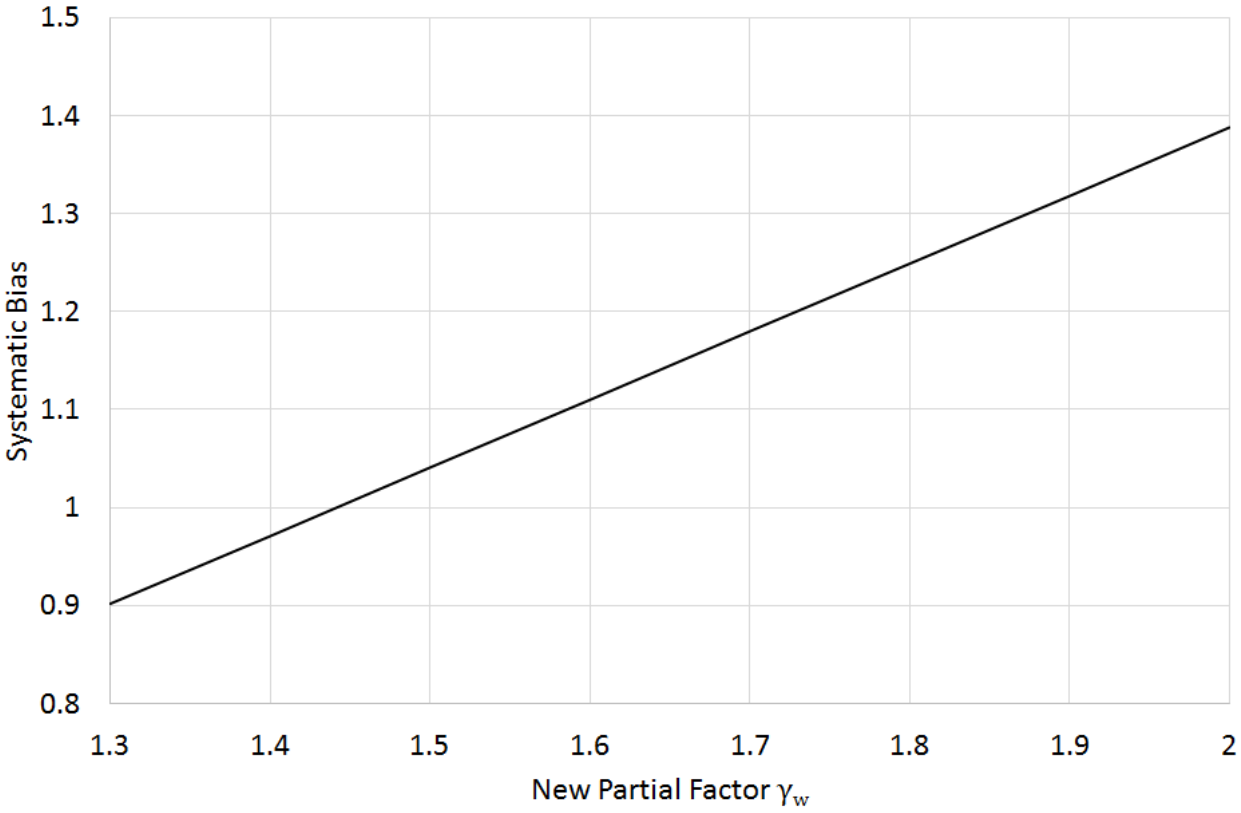

Figure 7.18: Area-averaged systematic bias of South African wind loads with new wind map and an updated wind load partial factor.

Chapter 8

Conclusions

This study described the investigation of the uncertainties and probabilistic models of the South African design wind load formulation. Although the primary focus of the study has been on South African wind loads, wind load formulations from across the globe have been investigated in an attempt to characterise and quantify wind load uncertainties, with the ultimate goal of developing a new probabilistic wind load model. As a result, the insights gained from the investigation are not only applicable to the South African environment, but relate to the fundamental principles of the physical process of wind loading and the wind engineering models used to describe that process.

8.1 Assessment of the reliability basis and methodology of the investigation

An underlying theme throughout this dissertation has been the efficient and transparent use of information. A reliability model is only as good as the data upon which it is based, and throughout this study the recurring challenge has been the lack of readily available data. Effective reliability treatment of the limited data and information was a necessity, and it was achieved through the development and implementation of reliability methods to maximise the value added by each source of information. Specifically, these reliability methods were: the use of hierarchical Bayesian models for wind load component uncertainties, the development of the comparative algorithm for wind load standards, and the use of Bayesian updating of existing models to develop full probabilistic models.

Critical self-evaluation, not only of the final results obtained but also during the implementation of the reliability methods, was performed throughout the investigation to ensure accurate, unbiased and transparent results. In keeping with this self-evaluation, assessments of the two novel reliability methodologies developed in this dissertation - namely the use of hierarchical Bayesian models for wind load components and the comparative algorithm for wind load standards - are presented in the following sections. Bayesian updating is a well-established reliability method which was implemented without modification, and as such is not be assessed here. Nonetheless, the implementation of Bayesian updating of the existing models serves as a critical example of how all available information, both new and old, was used in this investigation.

8.1.1 Hierarchical Bayesian models

The fundamental principle of the traditional method for probabilistic modeling of wind loads is that each wind load component is independent and subject to its own uncertainties described by a representative probability distribution. The combination of the probability distributions of the various components provides the means by which the total uncertainty of the wind load formulation may be quantified. This approach describes the system level reliability treatment of wind load uncertainties. The investigation expanded upon the traditional method through the use of rational reliability treatment of the component level of the wind load formulation.

In Section 3.5 the process by which the representative probability distribution for a given component is developed was reformulated. Instead of directly developing a single probability distribution, hierarchical Bayesian models were used to allow the different sources of uncertainty inherent in each component to be quantified independently. In doing so the same rational methodology applied at system level was extended to the component level, allowing for a better level of approximation of each component and more accurate quantification of the wind load uncertainties.

The framework provided by the combination of the traditional system level approach and the hierarchical Bayesian model component level approach is the most novel contribution of this investigation. By using this framework to investigate and quantify wind load uncertainties, the probabilistic model developed is on a fundamentally higher level of rationality than the existing

wind load models. Unlike the existing models, the framework is transparent and accessible. The information used to develop the model is readily available and well-documented, and any part of the model may easily be updated or changed with the addition of better information.

8.1.2 Comparative algorithm for wind load standards

This investigation directly followed the investigation by Kruger (2011) of the South African strong wind climatology and the development of a new characteristic wind speed map, which provided the information required to quantify the South African free-field wind pressure uncertainties. Careful treatment and assessment of the information was required, but the information itself was from a trustworthy and readily accessible source. Unfortunately this was not true for the two time invariant components considered, pressure coefficients and terrain roughness factors. In the investigation of these components the theme of effective use of limited information was most apparent, as one of the greatest challenges of investigating the components was finding sources of information. In the search for data relating to these components, wind load standards were identified as a potential source of information. By using an expert opinion analysis approach in which the wind load standards are considered as experts (or even bodies of experts), the comparison of the standards could be used as an indicator of wind load uncertainties.

As discussed in Chapter 3, the use of wind load standards in reliability analyses is not without precedent. Furthermore, expert opinion analysis is a well-established and accepted reliability technique in situations where limited observed data is available but experts with empirical knowledge may be consulted. Herein lies the greatest defense of the methodology. Wind load standards are developed by wind engineering experts using the best available information at the time of development. It therefore stands to reason that the wind load standard itself is representative of the empirical and theoretical knowledge from all sources used in its development. By accepting that wind load standards may effectively be regarded as “experts”, the natural conclusion is that differences between the stipulations of different wind load standards are indicative of the uncertainty in the wind load formulation.

There are a number of weaknesses in the use of comparison of standards as a reliability technique. These weaknesses are a result of uncertainties in the codification process of the

standards, such as the simplification of the formulation to allow for operational models which accommodate a large scope of design situations, and potential conservatism built into components in order to achieve a desired total wind load from the overall formulation of the standard. There is therefore a certain amount of "model uncertainty" in the results obtained using this method that cannot be quantified without detailed information about the codification process, which is not available in most cases. Certain measures were taken during the implementation of the method in order to counteract these weaknesses and ensure that the most accurate results possible were obtained. To this end the comparative algorithm was specifically developed to ensure unbiased sampling, verification was done that the wind load standards considered were completely independent and did not share the same background information, and the comparison was done across a large scope of design situations in order to smooth out any specific discrepancies between the standards and obtain results representative of the general case.

Using the comparison of wind load standards did have several significant advantages. First and foremost is the amount of data which becomes available with the acceptance of wind load standards as a valid source of information. Furthermore, the operational nature of the stipulations in the standards makes them conducive to automation, which allows a far larger scope of design situations to be investigated than possible with manual comparisons. This is illustrated best in the pressure coefficient investigation, in which over 3.5 million individual comparisons were performed on 60 independent structural configurations using a software package which was developed to perform a parametric investigation of pressure coefficients.

8.2 Achievement of research objectives

In the introductory chapter of this dissertation three questions were posed in order to define the problem statement of the investigation. These questions were:

1. What are the uncertainties inherent in the South African wind load formulation?
2. How can these uncertainties be quantified?
3. What influence do these uncertainties have on the reliability performance of the South African wind load standard?

It is only fitting that the conclusion to this investigation directly address the issues raised in these questions.

8.2.1 Wind load uncertainties

In the background investigation presented in Chapter 2 the sources of uncertainty in the wind load formulation of the three primary components were identified, as summarized in Table 8.1. Not all the sources of uncertainties which were identified were quantified, however those uncertainties which were deemed to have the greatest influence on the reliability of wind loads were investigated and quantified in the subsequent chapters relating to the respective components.

Table 8.1: Sources of uncertainty identified in the formulation of the primary wind load components.

Component	Identified Sources of Uncertainty
Free-field wind	• Inherent variability of free-field wind pressures. • Different types of strong wind generating mechanisms across the country, i.e. synoptic and convective winds. • Short record periods for South African wind speeds. • The representation of the variability of local wind climate across the country in a single model. • The use of wind speed intervals in a characteristic wind speed map.
Pressure coefficients	• Inherent variability of pressure coefficients. • Lack of sufficiently standardized experimental methods in wind tunnel and full-scale tests. • The use of wind tunnel models to investigate full-scale behaviour. • The representation of dynamic and temporally variable pressures using equivalent static load distributions. • The representation of pressure coefficient uncertainties for a large scope of design situations in a single model. • Model uncertainty due to reliability methods used to quantify pressure coefficient uncertainties.
Terrain roughness factors	• Inherent variability of surface roughness effects. • Subjective selection of representative terrain categories. • Difficulty in quantifying terrain roughness length. • “Rounding up” of terrain roughness factors due to the use of terrain categories. • The potential nullification of terrain roughness categories due to thunderstorm downbursts.

It has became clear through the investigation that in many cases - such as the free-field wind bias due to the use of wind speed intervals or the variability inherent in the selection of terrain category parameters - the epistemic uncertainty of wind load components is more

dominant than the aleatoric uncertainty. The positive aspect of epistemic uncertainty is that it may be reduced through the improvement of engineering models. Such improvement may not be warranted or required in all cases, especially where the total uncertainty of a component is already relatively low. Nonetheless, the identification of these uncertainties serves as a reference in order to determine areas for future research which would yield the most valuable contributions in terms of the reliability of a wind load component.

The final representative probability distribution for each of the three primary components is given in Table 8.2 below. These distributions encompass the combined component level uncertainties which were investigated as quantified using hierarchical Bayesian models. Using these distributions it is possible to quantitatively determine which components, and by implication which sources of uncertainty, have the greatest impact on the total uncertainty of the wind load formulation. The average sensitivity factors calculated using the component models above in combination with a nominal model uncertainty factor are presented in Table 8.3, as determined in Section 7.2.3. From these factors it is clear that free-field wind uncertainty dominates the design wind load formulation. Of the time invariant components, pressure coefficients have a significantly higher contribution to the total uncertainty than terrain roughness factors or the model uncertainty factor. These results are a useful tool in the identification of future research, as it is possible to determine where the greatest contribution may be made.

Table 8.2: Representative probability distributions for primary wind load components.

Variable	Distribution	Relative Mean $[\mu_X/X_k]$	Standard Deviation $[\sigma_X/X_k]$	Coefficient of Variation $[w_X]$	Source
50-year extremes of wind pressure	Gumbel	0.92	0.31	0.34	Chapter 4
Pressure coefficient	Normal	0.99	0.31	0.31	Chapter 5
Roughness factor	Normal	0.94	0.19	0.20	Chapter 6

8.2.2 Probabilistic wind load models

At the outset of this investigation the goal was to develop a single probabilistic model of South African wind loads. The outcome of the investigation was not one model, but four models which

Table 8.3: Average sensitivity factors calculated using combined component uncertainty distributions.

Component	Sensitivity Factor
Free-field wind	0.74
Pressure coefficient	0.51
Roughness factor	0.38
Model factor	0.22

describe the best available upper and lower limit approximations of wind load uncertainties. It has been made clear throughout the investigation that there simply is not enough information available to properly quantify wind load uncertainties at this time. By using rational reliability techniques an envelope of possible reliability models was defined as opposed to specifying a single model which itself is subject to significant uncertainties. This approach mirrors the one followed in the JCSS Probabilistic Model Code, which serves as the primary reference for the existing probabilistic wind load models. The upper and lower limit distributions of the developed probabilistic model are given in Table 8.4, and Figure 8.1 shows the model ranges for the new model and the JCSS model.

Table 8.4: Upper and lower limits of representative probabilistic model of design wind pressure for South Africa.

Variable	Symbol	Distribution	Relative mean $[\mu_X/X_k]$	Standard Deviation $[\sigma_X/X_k]$	Coefficient of Variation $[w_X]$
Lower limit	$W_{ref,l}$	Gumbel	0.65	0.33	0.50
Upper limit	$W_{ref,u}$	Gumbel	0.75	0.41	0.55

The results show that the reliability envelope defined in this investigation is significantly narrower than the envelope defined by the JCSS model. Compared to the disparate results obtained from the existing models as illustrated in Figure 3.3, it is clear that the new model is a significant improvement. The new model is not a perfect representation of wind load uncertainties, but it is the most accurate representation of those uncertainties available at this time. The narrowing of the probabilistic range is an iterative process, and future investigations may lead to further narrowing of the range defined in this investigation. Nonetheless, the new model and the information obtained during this investigation are valuable tools for assessment and potential calibration of the South African wind load standard.

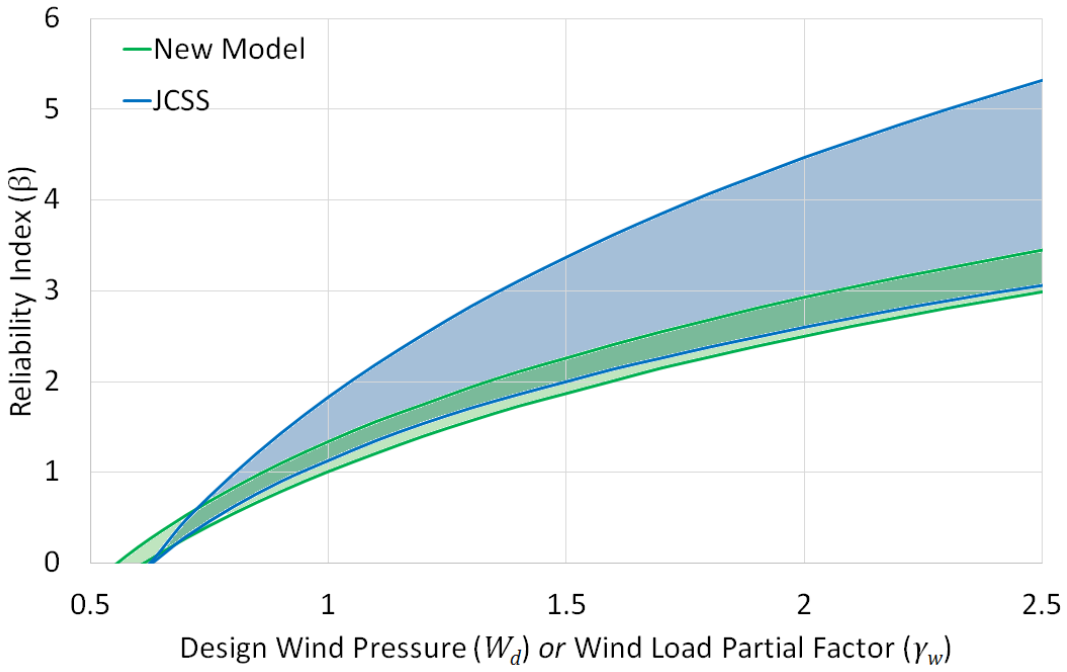

Figure 8.1: Envelope of reliability models of design wind pressure developed in the investigation.

It should be noted that the most important difference between the new model and the existing models is not the quantitative difference between them, but rather the difference in the basis of the models. This is illustrated best by considering the events which ultimately led to this investigation. In the previous reliability assessment of the South African loading code, the results obtained using the existing SANS probabilistic wind load model were called into question by Retief and Dunaiski (2009). However, due to the lack of background information there was no way to assess or verify the accuracy of the results obtained using the model. No information was available regarding independent wind load component uncertainties, only a single representative distribution for design wind loads was given. Similarly, it was not possible to establish what background information was used to develop the European models. In contrast, the new model presented in this dissertation was developed to be transparent on a fundamental level. An example of this is the relatively direct manner in which time invariant uncertainties can be extended to any other design standards; together with the time variant uncertainties that should be based on the local strong wind climate models. Unlike any of the existing models, the results obtained using the new model are rationally defensible. This is the greatest strength of the new model.

8.2.3 Reliability implications for South African wind loads

Multiple reliability assessments were performed using the new models to investigate the reliability performance of the South African wind load formulation. This included reliability assessments in which the wind load was considered in isolation and assessments in which the effects of other basic variables such as structural resistance and the combination with permanent loads were considered. The effects of wind loads on different types of structural materials was also included by parametrically varying the probabilistic model of resistance used. The results of all analyses performed showed that the reliability performance of the design functions using a wind load partial factor of 1.3 is inadequate.

It is clear from the reliability assessments performed that the reliability requirements across the scope of design situations within the loading code is not constant. More stringent reliability requirements are obtained for structures with lower variability of resistance, such as steel structures, and for lightweight structures in which wind loads are significantly greater than the own weight of the structure. This makes selection of a single partial factor value for wind loads particularly challenging. Two options are available: either a partial factor must be selected which ensures adequate reliability performance for all structures, albeit resulting in rather conservative requirements for most typical buildings; or a lower partial factor value must be selected which ensures adequate reliability performance for typical structures, with special requirement formulated for wind-sensitive structures. The goal of this thesis is not to answer the question of what partial factor value is required for wind loads in South Africa, but rather to provide the appropriate tools with which that question may be answered. It is however strongly recommended that the partial factor value be updated, as it is clearly shown that the current partial factor is inadequate.

8.2.4 Secondary objectives

In addition to the primary objectives of this research as discussed above, a number of potential secondary goals were identified in the introduction of this dissertation. These goals were achieved indirectly through the application of the logical methodology used to meet the primary objectives, but they are nonetheless unique academic contributions.

The first of these goals was to conduct a comprehensive study of the relevant existing

probabilistic wind load models. This was done in Section 3.3.1, in which five probabilistic wind load models from South Africa, Europe and the United States of America were investigated. In the case of the South African model, previously undiscovered errors in the model were found and an explanation for the questionable results obtained in the previous reliability assessment of SANS 10160 by Retief and Dunaiski (2009) was given. Furthermore, the comparison of these models, specifically the overall lack of consensus on wind load uncertainties shown in the models, served as additional motivation for this investigation.

The next three secondary goals were: the identification of readily available sources of data and information relating to wind load uncertainties, the identification and potential development of a methodology in which all readily available data is used to quantify uncertainties, and the investigation of available statistical and reliability techniques for the treatment of processes subject to multiple sources of uncertainty. These three goals were simultaneously fulfilled through the development of the reliability methodology used in this investigation, as discussed in Section 8.1 above.

In the final section of the previous chapter the last secondary goal was achieved, namely an investigation of the influence of changes to the South African wind load standard on the design wind loads across the country. The combined effect of the implementation of the new characteristic wind speed map and a potentially updated wind load partial factor was quantified. This was done using an area-averaged systematic bias calculation for municipal regions, provinces, and across the entire country. It was found that the implementation of the new wind map would result in an average decrease of the design wind load across the country of 10%. An updated partial factor would result in a linear overall increase on the average design wind load which was directly proportional to the ratio of the updated partial factor to the existing partial factor with a value of 1.3. A partial factor of 1.6, which is similar to the partial factors for other variable actions, would result in a bias of $(0.9) \times (1.6/1.3) = 1.11$, which indicates a net increase in wind loading of 11%.

8.3 Future research

Through the investigation of wind load uncertainties and probabilistic models several topics have been identified which require further investigation. These topics are briefly summarized

as follows:

- Detailed reliability investigation of secondary wind load factors such as wind directionality and the effects of topography, leading to updating of the secondary factor models used in this investigation.
- Extension of the pressure coefficient model developed in this investigation through the addition of more wind tunnel and full-scale test results using standardized test protocols.
- Development of a better model uncertainty factor for the new probabilistic model presented in this dissertation. Such a model is required to encapsulate all the presently unidentified uncertainties in the wind load formulation.
- Investigation of the reliability effects of winds from different strong wind generating mechanisms, specifically convective winds (thunderstorms), and the formulation of wind loads caused by those mechanisms.
- Investigation of the use of the Gumbel distribution for modeling design wind pressures, considering the conversion of free-field wind speed models to pressure models and combination with normal distributions used to describe time-invariant components.
- Updating of the South African partial factor value using the new probabilistic wind load model. Careful consideration of the scope of design situations covered in the new models is required for such a calibration exercise.

List of References

Ang, A. and Tang, W. (1984). *Probability concepts in engineering planning and design.* John Wiley & Sons.

AS-NZS (2011). *1170-2 - Structural design actions - Part 2: Wind actions.* Standards Australia Limited/Standards New Zealand.

ASCE (1995). *7-95 - Minimum Design Loads for Buildings and Other Structures.* American Society of Civil Engineers.

ASCE (2010). *7-10 - Minimum Design Loads for Buildings and Other Structures.* American Society of Civil Engineers.

Baker, C. (2007). Wind engineering - Past, present and future. *Journal of Wind Engineering and Industrial Aerodynamics*, vol. 95, no. 9, pp. 843–870.

Bashor, R., Kareem, A. and Moran, R. (2009 November). Comparitive Study of Major International Standards. In: *Proceedings of the Seventh Asia-Pacific Conference on Wind Engineering.*

Botha, J., Retief, J., Holický, M. and Viljoen, C. (2014 June). Development of probabilistic wind load model for South Africa. *Proceedings of the Thirteenth Conference of the Italian Association for Wind Engineering.*

BS-NA-EN (2010). *BS NA EN 1991-1-4 - UK National Annex to Eurocode 1: Actions on structures, Part 1-4: General actions - Wind actions.* British Standards Institute.

Chay, M. (2001 August). *Physical modeling of thunderstorm downbursts for wind engineering applications.* Ph.D. thesis, Texas Tech University.

Chen, X. and Zhou, N. (2007). Equivalent static wind loads on low-rise buildings based on full-scale pressure measurements. *Engineering Structures*, vol. 29, no. 10, pp. 2563–2575.

Choi, E. (2004). Field measurement and experimental study of wind speed profile during thunderstorms. *Journal of Wind Engineering and Industrial Aerodynamics*, vol. 92, pp. 275 – 290.

Choi, E. and Hidayat, F. (2002). Gust factors for thunderstorm and non-thunderstorm winds. *Journal of Wind Engineering and Industrial Aerodynamics*, vol. 90, pp. 1683 – 1696.

Cook, N. (1985). The Designer's Guide to Wind Loading of Building Structures. Part I: Background, Damage Survey, Wind Data and Structural Classification. *Building Research Establishment Report, London, Butterworths.*

Cook, N. and Mayne, J. (1979). A novel working approach to the assessment of wind loads for equivalent static design. *Journal of Wind Engineering and Industrial Aerodynamics*, vol. 4, no. 2, pp. 149–164.

Davenport, A. (1983). The relationship of reliability to wind loading. *Journal of Wind Engineering and Industrial Aerodynamics*, vol. 13, no. 1, pp. 3–27.

Davenport, A. (2002). Past, present and future of wind engineering. *Journal of Wind Engineering and Industrial Aerodynamics*, vol. 90, no. 12, pp. 1371–1380.

Davenport, A., Grimmond, S., Oke, T. and Wieringa, J. (2000). The revised Davenport roughness classification for cities and sheltered country, 3rd Symp. *On the Urban Environment*, pp. 14–18.

Davenport, A.G. (1960). Rationale for determining design wind velocities. *ASCE Journal of the Structural Division*, vol. 86, no. 5, pp. 39–68.

Davenport, A.G. (1961). The application of statistical concepts to the wind loading of structures. *Proceedings of the Institution of Civil Engineers*, vol. 19, no. 4, pp. 449–472.

De Haan, L. and Ferreira, A. (2007). *Extreme value theory: an introduction.* Springer Science & Business Media.

De Wit, M. (1999). Uncertainty in wind pressure coefficients for low-rise buildings. *HERON, vol. 44 (1), 1999.*

Der Kiureghian, A. and Ditlevsen, O. (2009). Aleatory or epistemic? does it matter? *Structural Safety*, vol. 31, no. 2, pp. 105–112.

Doudak, G., McClure, G., Smith, I. and Stathopoulos, T. (2009). Comparison of field and wind tunnel pressure coefficients for a light-frame industrial building. *Journal of Structural Engineering*, vol. 135, no. 10, pp. 1301–1304.

Dyrbye, C. and Hansen, S. (1996). *Wind loads on structures*. John Wiley & Sons. ISBN 978-0-471-95651-8.

Ellingwood, B., Galambos, T.V., MacGregor, J.G. and Cornell, A.C. (1980). *Development of a probability based load criterion for American National Standard A58: Building code requirements for minimum design loads in buildings and other structures*, vol. 13. US Department of Commerce, National Bureau of Standards.

Ellingwood, B.R. and Tekie, P.B. (1999). Wind load statistics for probability-based structural design. *Journal of Structural Engineering*, vol. 125, no. 4, pp. 453–463.

Endo, M., Bienkiewicz, B. and Ham, H. (2006). Wind-tunnel investigation of point pressure on TTU test building. *Journal of Wind Engineering and Industrial Aerodynamics*, vol. 94, no. 7, pp. 553–578.

Fink, D. (1997). A compendium of conjugate priors. Available online at www.leg.ufpr.br/lib/exe/fetch.php/projetos:mci:tabelasprioris.pdf.

Fishman, G. (2013). *Monte Carlo: Concepts, Algorithms, and Applications*. Springer Science & Business Media.

Gamerman, D. and Lopes, H. (2006). *Markov chain Monte Carlo: stochastic simulation for Bayesian inference*. CRC Press.

GeoCommunity (2016). GIS Data for South Africa. Available online at http://data.geocomm.com/catalog/SF/datalist.html.

Ginger, J. and Holmes, J. (2003). Effect of building length on wind loads on low-rise buildings with a steep roof pitch. *Journal of Wind Engineering and Industrial Aerodynamics*, vol. 91, no. 11, pp. 1377–1400.

Ginger, J. and Letchford, C. (1999). Net pressures on a low-rise full-scale building. *Journal of Wind Engineering and Industrial Aerodynamics*, vol. 83, no. 1, pp. 239–250.

Goliger, A. (2012 October). Wind Actions in SANS 10160:2010 Part 3. In: *SANS 10160:2011 Induction Seminar Lecture Notes*.

Goliger, A. (2015 March). Personal Communication.

Goliger, A.M. (2002). *Development of a wind damage and disaster risk model for South Africa*. Ph.D. thesis, Stellenbosch: Stellenbosch University.

Goliger, A.M. (2005). South African sports stadia–from the perspective of the 2010 FIFA World Cup. *Bautechnik*, vol. 82, no. 3, pp. 174–178.

Goliger, A.M.W. (2016 March). Wind Engineering Science and its Role in Optimising the Design of the Built Environment. D.Eng. thesis, Stellenbosch University.

Gomes, L. and Vickery, B. (1978). Extreme wind speeds in mixed wind climates. *Journal of Wind Engineering and Industrial Aerodynamics*, vol. 2, no. 4, pp. 331–344.

Gulvanessian, H. and Holický, M. (2005 August). Eurocodes: using reliability analysis to combine action effects. *Structures and Buildings*, pp. 243 – 252.

Hansen, S. and Sørensen, E. (1986). The Aylesbury experiment. Comparison of model and full-scale tests. *Journal of Wind Engineering and Industrial Aerodynamics*, vol. 22, no. 1, pp. 1–22.

Hansen, S.O., Pedersen, M.L. and Sørensen, J.D. (2015). Probability based calibration of pressure coefficients. In: *Icwe14 Conference Proceedings*.

Ho, T., Surry, D. and Davenport, A. (1991). Variability of low building wind loads due to surroundings. *Journal of Wind Engineering and Industrial Aerodynamics*, vol. 38, no. 2, pp. 297–310.

Holický, M. (2005). New load combinations for equal safety of structural members. *ICOSSAR 2005, Millpress, Roterdam*, pp. 641–645.

Holický, M. (2009). *Reliability analysis for structural design*. AFRICAN SUN MeDIA.

Holický, M., Retief, J.V., Diamantidis, D. and Viljoen, C. (2015 July). On standardization of the reliability basis of structural design. In: *12th International Conference on Applications of Statistics and Probability in Civil Engineering*.

Holmes, J. and Best, R. (1981). An approach to the determination of wind load effects on low-rise buildings. *Journal of Wind Engineering and Industrial Aerodynamics*, vol. 7, no. 3, pp. 273–287.

Holmes, J. and Syme, M. (1994). Wind loads on steel-framed low-rise buildings. *Steel Construct*, vol. 28, pp. 2–12.

Holmes, J.D. (2015). *Wind loading of structures*. 3rd edn. CRC Press.

Hoxey, R. (1991). Structural response of a portal framed building under wind load. *Journal of Wind Engineering and Industrial Aerodynamics*, vol. 38, no. 2, pp. 347–356.

Isyumov, N., Ho, E. and Case, P. (2014). Influence of wind directionality on wind loads and responses. *Journal of Wind Engineering and Industrial Aerodynamics*, vol. 133, pp. 169–180.

JCSS (2001-2002). *Probabilistic Model Code, Parts 1 to 4*. Joint Committee on Structural Safety.

Kemp, A., Milford, R. and Laurie, J. (1987 September). Proposals for a comprehensive limit states formulation for South African structural codes. *The Civil Engineer in South Africa*, pp. 351 – 360.

Kruger, A. (2011 March). *Wind climatology of South Africa relevant to the design of the built environment*. Ph.D. thesis, University of Stellenbosch.

Kruger, A., Retief, J. and Goliger, A. (2013). Strong winds in South Africa - Part 1: Application of estimation methods, Part 2: Mapping of updated statistics. *Journal of the South African Institution of Civil Engineering*, vol. 55, no. 2, pp. 29–58.

Letchford, C., Mans, C. and Chay, M. (2002). Thunderstorms - their importance in wind engineering. *Journal of Wind Engineering and Industrial Aerodynamics*, vol. 90, pp. 1415 – 1433.

Levitan, M.L. and Mehta, K.C. (1992). Texas Tech field experiments for wind loads Part 1: building and pressure measuring system, Part II: meteorological instrumentation and terrain parameters. *Journal of Wind Engineering and Industrial Aerodynamics*, vol. 43, no. 1, pp. 1565–1588.

Levitan, M.L., Mehta, K.C., Vann, W. and Holmes, J. (1991). Field measurements of pressures on the Texas Tech building. *Journal of Wind Engineering and Industrial Aerodynamics*, vol. 38, no. 2, pp. 227–234.

Marshall, R.D. (1977). *The measurement of wind loads on a full-scale mobile home*. US Department of Commerce, National Bureau of Standards.

Melchers, R.E. (1999). *Structural reliability analysis and prediction*. John Wiley & Son Ltd. ISBN 0-471-98771-9.

Mendis, P., Ngo, T., Haritos, N., Hira, A., Samali, B. and Cheung, J. (2007). Wind loading on tall buildings. *EJSE Special Issue: Loading on Structures*, vol. 3, pp. 41–54.

Milford, R. (1985*a*). Development of load factors for inclusion in SABS 0160 (the general procedures and loadings to be adopted for the design of buildings). Tech. Rep., CSIR.

Milford, R. (1985*b*). Extreme value analysis of South African gust speed data. *Unpublished Internal Report, CSIR*, vol. 85, no. 4.

Milford, R., Goliger, A. and Waldeck, J. (1992). Jan Smuts experiment - Part 1: Details of full-scale experiment, Part 2: comparison of full-scale and wind-tunnel results. *Journal of Wind Engineering and Industrial Aerodynamics*, vol. 43, no. 1, pp. 1693–1716.

Montgomery, D.C. and Runger, G.C. (2010). *Applied statistics and probability for engineers*. John Wiley & Sons.

Murphy, K.P. (2007). Conjugate Bayesian analysis of the Gaussian distribution. *def*, vol. 1, no. $2\sigma 2$, p. 16.

Nowak, A.S. and Collins, K.R. (2000). *Reliability of structures*. McGraw-Hill. ISBN 0-07-116354-9.

Palutikof, J., Brabson, B., Lister, D. and Adcock, S. (1999). A review of methods to calculate extreme wind speeds. *Meteorological applications*, vol. 6, no. 02, pp. 119–132.

Peterka, J.A. and Cermak, J.E. (1975). Wind pressures on buildings-probability densities. *Journal of the structural division*, vol. 101, no. 6, pp. 1255–1267.

Retief, J., Barnardo-Viljoen, C. and Holický, M. (2013). Probabilistic models for design of structures against wind loads. *Research and Applications in Structural Engineering, Mechanics and Computation*, p. 237.

Retief, J. and Dunaiski, P. (2009). *Background to SANS 10160*. SUN MeDIA.

Retief, J., Kruger, A. and Goliger, A. (2015 March). Personal Communication.

Rigato, A., Chang, P. and Simiu, E. (2001). Database-assisted design, standardization, and wind direction effects. *Journal of Structural Engineering*, vol. 127, no. 8, pp. 855–860.

SANS (2011*a*). *SANS 10160-1 - Basis of structural design and actions for buildings and industrial structures, Part 1: Basis of structural design*. South African Bureau of Standards.

SANS (2011*b*). *SANS 10160-3 - Basis of structural design and actions for buildings and industrial structures, Part 3: Wind actions*. South African Bureau of Standards.

Schneider, J. (2006). *Introduction to safety and reliability of structures*, vol. 5. Iabse.

Simiu, E., Sadek, F., Whalen, T.M., Jang, S., Lu, L.-W., Diniz, S.M., Grazini, A. and Riley, M.A. (2003). Achieving safer and more economical buildings through database-assisted, reliability-based design for wind. *Journal of Wind Engineering and Industrial Aerodynamics*, vol. 91, no. 12, pp. 1587–1611.

Sinharay, S. and Stern, H. (2003). Posterior predictive model checking in hierarchical models. *Journal of Statistical Planning and Inference*, vol. 111, no. 1, pp. 209–221.

Stathopoulos, T. (1980). Pdf of wind pressures on low-rise buildings. *Journal of the Structural Division*, vol. 106, no. 5, pp. 973–990.

Stathopoulos, T. (2003). Wind loads on low buildings: in the wake of Alan Davenport's contributions. *Journal of Wind Engineering and Industrial Aerodynamics*, vol. 91, no. 12, pp. 1565–1585.

Stathopoulos, T., Wang, K. and Wu, H. (2000). Proposed new Canadian wind provisions for the design of gable roofs. *Canadian Journal of Civil Engineering*, vol. 27, no. 5, pp. 1059–1072.

Surry, D. (1991). Pressure measurements on the Texas Tech building: wind tunnel measurements and comparisons with full scale. *Journal of Wind Engineering and Industrial Aerodynamics*, vol. 38, no. 2, pp. 235–247.

Szewczuk, S. and Prinsloo, F. (2010). Wind Atlas for South Africa (WASA): Project overview and current status.

Tamura, Y., Suda, K., Sasaki, A., Miyashita, K., Iwatani, Y., Maruyama, T., Hibi, K. and Ishibashi, R. (2001). Simultaneous wind measurements over two sites using doppler sodars. *Journal of Wind Engineering and Industrial Aerodynamics*, vol. 89, no. 14, pp. 1647–1656.

Ter Haar, T. and Retief, J. (2001 March). A Methodology for Structural Code Calibration. In: *Proceedings of the International Conference on Safety, Risk and Reliability.*

Uematsu, Y. and Isyumov, N. (1999). Wind pressures acting on low-rise buildings. *Journal of Wind Engineering and Industrial Aerodynamics*, vol. 82, no. 1, pp. 1–25.

Wang, K. and Stathopoulos, T. (2007). Exposure model for wind loading of buildings. *Journal of Wind Engineering and Industrial Aerodynamics*, vol. 95, no. 9, pp. 1511–1525.

Website, T.T.U. (2015). Wind engineering research field laboratory. File: WERFL1-lg.jpg. Available at: `http://www.depts.ttu.edu/nwi/facilities/WERFL.php`

Wieringa, J. (1992). Updating the Davenport roughness classification. *Journal of Wind Engineering and Industrial Aerodynamics*, vol. 41, no. 1, pp. 357–368.

Wieringa, J. (2001). New revision of Davenport roughness classification. *Proc., 3EACWE, Eindhoven, The Netherlands*, pp. 285–292.

Zisis, I. and Stathopoulos, T. (2009). Wind-induced cladding and structural loads on low-wood building. *Journal of Structural Engineering*, vol. 135, no. 4, pp. 437–447.

Appendices

Appendix A

Design Wind Speed Quantiles

Table A.1: Design wind speed quantiles calculated using the selected extreme wind estimation model shown for stations across South Africa.

Station Name	Selected Distribution	X_{50} [m/s]	X_{100} [m/s]	X_{500} [m/s]
Struisbaai	EXP	34.7	36.1	39.3
Strand	Mixed	36.6	38.3	42.1
Hermanus	EXP	36.6	38.1	41.6
Tygerhoek	EXP	37.3	39.3	44.0
Stilbaai	EXP	30.3	31.4	34.0
George	EXP	33.3	34.7	37.9
Knysna	Gumbel	28.5	29.5	31.9
Plettenbergbaai	Gumbel	31.1	32.5	35.6
Tsitsikamma	EXP	31.6	32.9	35.9
Robbeneiland	EXP	28.7	29.8	32.3
Cape Town	Mixed	38.7	41.0	46.3
Paarl	Mixed	26.1	27.1	29.2
Worcester	EXP	41.5	43.4	48.0
Patensie	Mixed	30.5	32.7	37.8
Uitenhage	Mixed	33.8	36.0	41.8
Port Elizabeth	EXP	40.4	42.1	45.9
Geelbek	EXP	28.8	30.0	32.8
Malmesbury	Mixed	28.8	30.1	33.1
Porterville	EXP	32.9	34.9	39.3

Station Name	Selected Distribution	X_{50}	X_{100}	X_{500}
Grahamstown	Mixed	34.0	36.4	42.2
East London	EXP	36.1	37.8	41.7
Langebaanweg	Mixed	33.1	35.3	40.5
Fort Beaufort	Mixed	37.2	39.6	45.2
Lambertsbaai	EXP	27.9	29.1	31.8
Beaufort-Wes	EXP	39.0	40.7	44.7
Graaff-Reinet	Mixed	31.9	33.3	36.6
Queenstown	EXP	37.1	38.8	42.8
Umtata	Mixed	41.9	44.7	51.2
Calvinia	EXP	33.4	34.9	38.4
Noupoort	EXP	37.4	39.0	42.8
Jamestown	EXP	31.9	33.5	37.0
Elliot	EXP	44.2	46.8	52.8
Port Edward	EXP	32.6	34.2	37.7
De Aar	EXP	42.3	44.8	50.7
Paddock	Mixed	30.5	32.2	36.3
Margate	Gumbel	30.8	32.1	35.3
Koingnaas	Mixed	27.6	28.8	31.6
Brandvlei	EXP	35.2	37.0	41.2
Prieska	EXP	33.9	35.6	39.4
Pietermaritzburg	EXP	29.1	30.8	34.5
Oribi Airport	Mixed	35.4	37.7	43.0
Durban	Gumbel	33.3	34.8	38.3
Virginia	Gumbel	31.1	32.8	36.7
Bloemfontein	EXP	36.3	38.2	42.5
Alexanderbaai	EXP	32.1	33.2	35.7
Kimberley	EXP	37.7	39.6	44.1
Ladysmith	Mixed	37.3	39.4	44.3
Mtunzini	Mixed	29.8	30.9	33.5
Upington	Gumbel	37.4	39.6	44.6
Postmasburg	EXP	32.7	34.3	38.0
Bethlehem	Mixed	29.1	30.1	32.4

Station Name	Selected Distribution	X_{50}	X_{100}	X_{500}
Ulundi	EXP	32.9	34.7	38.7
Charters Creek	Mixed	25.9	27.2	30.1
Kathu	EXP	33.3	35.0	39.0
Taung	EXP	36.9	39.0	43.8
Bloemhof	Mixed	32.3	34.2	38.7
Welkom	EXP	40.0	42.2	47.2
Newcastle	EXP	38.2	40.2	44.9
Pongola	EXP	31.2	33.0	37.0
Vereeniging	EXP	33.4	35.0	38.8
Standerton	Gumbel	34.4	36.3	40.7
Lichtenburg	Gumbel	33.0	34.9	39.1
Johannesburg	Gumbel	34.0	35.9	40.5
Ermelo	EXP	32.1	33.5	36.7
Mafikeng	EXP	33.0	34.5	38.0
Rustenburg	Gumbel	29.1	30.7	34.4
Irene	EXP	33.6	35.3	39.3
Witbank	EXP	31.5	33.1	36.7
Komatidraai	Gumbel	30.9	32.8	37.1
Pilanesberg	EXP	32.4	34.1	38.3
Graskop	Gumbel	31.2	33.1	37.7
Hoedspruit	Mixed	31.9	34.0	39.0
Ellisras	Mixed	28.7	30.4	34.4
Marken	Mixed	30.6	32.8	37.8
Pietersburg	EXP	35.0	37.0	41.6
Thohoyandou	EXP	29.0	30.4	33.9

Appendix B

Free-Field Wind Pressure Systematic Bias

Table B.1: Exposure corrected design wind speed 2% quantiles from Kruger (2011) and new wind map converted to pressure values and used to calculate the free-field wind systematic bias.

Station Name	Predictive Models		New Wind Map		Bias
	Speed [m/s]	Pressure [Pa]	Speed [m/s]	Pressure [Pa]	
Struisbaai	43.9	963.6	44	968	1.00
Strand	41.0	840.5	40	800	1.05
Hermanus	44.2	976.8	44	968	1.01
Tygerhoek	38.7	748.8	40	800	0.94
Stilbaai	31.1	483.6	36	648	0.75
George	34.0	578.0	36	648	0.89
Knysna	35.7	637.2	36	648	0.98
Plettenbergbaai	32.6	531.4	36	648	0.82
Tsitsikamma	29.2	426.3	36	648	0.66
Robbeneiland	29.4	432.2	40	800	0.54
Cape Town	39.5	780.1	40	800	0.98
Paarl	32.6	531.4	40	800	0.66
Worcester	42.6	907.4	40	800	1.13
Patensie	35.4	626.6	40	800	0.78
Uitenhage	42.5	903.1	40	800	1.13
Port Elizabeth	41.1	844.6	40	800	1.06

Station Name	Predictive Models		New Wind Map		Bias
	Speed [m/s]	Pressure [Pa]	Speed [m/s]	Pressure [Pa]	
Geelbek	29.8	444.0	40	800	0.56
Malmesbury	35.2	619.5	40	800	0.77
Porterville	41.0	840.5	40	800	1.05
Grahamstown	36.8	677.1	40	800	0.85
East London	36.7	673.4	40	800	0.84
Langebaanweg	36.2	655.2	40	800	0.82
Fort Beaufort	41.4	857.0	40	800	1.07
Lambertsbaai	28.7	411.8	36	648	0.64
Beaufort-Wes	40.3	812.0	40	800	1.02
Graaff-Reinet	33.7	567.8	36	648	0.88
Queenstown	44.5	990.1	44	968	1.02
Umtata	45.0	1012.5	44	968	1.05
Calvinia	34.3	588.2	36	648	0.91
Noupoort	38.6	745.0	40	800	0.93
Jamestown	39.2	768.3	40	800	0.96
Elliot	44.7	999.0	44	968	1.03
Port Edward	33.8	571.2	36	648	0.88
De Aar	43.8	959.2	40	800	1.20
Paddock	38.4	737.3	36	648	1.14
Margate	36.6	669.8	36	648	1.03
Koingnaas	29.1	423.4	32	512	0.83
Brandvlei	36.6	669.8	36	648	1.03
Prieska	35.0	612.5	40	800	0.77
Pietermaritzburg	35.2	619.5	40	800	0.77
Oribi Airport	40.0	800.0	40	800	1.00
Durban	34.9	609.0	36	648	0.94
Virginia	33.0	544.5	40	800	0.68
Bloemfontein	37.3	695.6	40	800	0.87
Alexanderbaai	32.5	528.1	32	512	1.03
Kimberley	38.8	752.7	40	800	0.94
Ladysmith	39.4	776.2	40	800	0.97

Station Name	Predictive Models		New Wind Map		Bias
	Speed [m/s]	Pressure [Pa]	Speed [m/s]	Pressure [Pa]	
Mtunzini	36.1	651.6	36	648	1.01
Upington	39.8	792.0	40	800	0.99
Postmasburg	34.0	578.0	36	648	0.89
Bethlehem	38.2	729.6	40	800	0.91
Ulundi	33.9	574.6	36	648	0.89
Charters Creek	30.4	462.1	32	512	0.90
Kathu	34.3	588.2	36	648	0.91
Taung	38.0	722.0	40	800	0.90
Bloemhof	38.8	752.7	40	800	0.94
Welkom	40.9	836.4	40	800	1.05
Newcastle	39.3	772.2	40	800	0.97
Pongola	32.0	512.0	32	512	1.00
Vereeniging	34.3	588.2	36	648	0.91
Standerton	37.0	684.5	36	648	1.06
Lichtenburg	35.0	612.5	36	648	0.95
Johannesburg	36.3	658.8	36	648	1.02
Ermelo	32.8	537.9	36	648	0.83
Mafikeng	34.1	581.4	36	648	0.90
Rustenburg	31.0	480.5	36	648	0.74
Irene	34.7	602.0	36	648	0.93
Witbank	32.4	524.9	36	648	0.81
Komatidraai	32.6	531.4	32	512	1.04
Pilanesberg	33.8	571.2	36	648	0.88
Graskop	33.9	574.6	36	648	0.89
Hoedspruit	34.3	588.2	36	648	0.91
Ellisras	30.5	465.1	32	512	0.91
Marken	32.7	534.6	32	512	1.04
Pietersburg	36.4	662.5	36	648	1.02
Thohoyandou	29.3	429.2	32	512	0.84

Appendix C

Regional Total Wind Load Systematic Bias

The regions used in the investigation of the influence of the new characteristic wind speed map for South Africa were delineated using the superposition of the regions used in the old wind map and the new wind map. As the new wind map uses municipal boundaries, certain municipalities were divided into multiple regions in cases where the old wind map region boundaries crossed through the municipalities. As such, there are apparent "duplicates" in the table of regional properties given below, however these are simply different regions which fall within the same municipality.

Table C.1: Regional properties used to calculate the total wind load systematic bias across South Africa.

Municipality Name	Old Speed (m/s)	New Speed (m/s)	Average Elevation $(masl)$	Area (km^2)	Air Density (kg/m^3)	New Pressure (Pa)	Old Pressure (Pa)	Bias
Buffalo City	39.2	40	297	2445	1.14	916	879	1.04
Camdeboo	50.4	36	1283	5316	1.00	651	1276	0.51
Camdeboo	44.8	36	837	2732	1.06	688	1065	0.65
Camdeboo	39.2	36	815	3855	1.06	690	818	0.84
Blue Crane Route	39.2	36	635	6315	1.09	706	838	0.84

Municipality Name	Old Speed (m/s)	New Speed (m/s)	Average Elevation $(masl)$	Area (km^2)	Air Density (kg/m^3)	New Pressure (Pa)	Old Pressure (Pa)	Bias
Blue Crane Route	50.4	36	1074	2109	1.03	668	1308	0.51
Blue Crane Route	44.8	36	853	2200	1.06	686	1063	0.65
Ikwezi	39.2	36	570	4403	1.10	713	845	0.84
Makana	39.2	40	450	4233	1.12	895	860	1.04
Ndlambe	39.2	40	176	1786	1.17	933	896	1.04
Sundays River Valley	39.2	40	361	5816	1.13	907	871	1.04
Baviaans	39.2	36	764	11293	1.07	694	823	0.84
Kouga	39.2	40	233	2602	1.16	925	888	1.04
Ngquza Hill	39.2	40	546	2345	1.10	883	848	1.04
Kou-Kamma	39.2	36	531	3549	1.11	717	850	0.84
Mbhashe	39.2	40	464	3029	1.12	893	858	1.04
Mnquma	39.2	40	565	3133	1.10	881	846	1.04
Great Kei	39.2	40	355	1669	1.13	908	872	1.04
Amahlathi	39.2	40	958	4625	1.05	836	803	1.04
Ngqushwa	39.2	40	234	2167	1.16	924	888	1.04
Nkonkobe	39.2	40	688	3490	1.08	866	832	1.04
Nxuba	39.2	40	1038	2624	1.03	828	795	1.04
Inxuba Yethemba	50.4	40	1291	960	1.00	803	1274	0.63
Inxuba Yethemba	39.2	40	1150	2139	1.02	817	784	1.04
Inxuba Yethemba	44.8	40	1291	7233	1.00	803	1007	0.80

Municipality Name	Old Speed (m/s)	New Speed (m/s)	Average Elevation $(masl)$	Area (km^2)	Air Density (kg/m^3)	New Pressure (Pa)	Old Pressure (Pa)	Bias
Inxuba Yethemba	39.2	40	1319	783	1.00	800	768	1.04
Tsolwana	44.8	40	1098	130	1.03	822	1031	0.80
Tsolwana	39.2	40	1367	5670	0.99	795	764	1.04
Inkwanca	39.2	40	1602	3403	0.97	773	743	1.04
Lukanji	39.2	44	1161	3642	1.02	987	783	1.26
Intsika Yethu	39.2	44	1006	2586	1.04	1006	798	1.26
Emalahleni	39.2	44	1364	3276	0.99	963	764	1.26
Engcobo	39.2	44	954	2363	1.05	1012	803	1.26
Sakhisizwe	39.2	44	1410	2234	0.99	957	760	1.26
Elundini	39.2	44	1543	4779	0.97	942	748	1.26
Senqu	39.2	40	1922	6913	0.93	743	714	1.04
Maletswai	39.2	40	1580	4116	0.97	775	745	1.04
Gariep	39.2	40	1468	8414	0.98	786	755	1.04
Port St Johns	39.2	40	296	1226	1.14	916	879	1.04
Nyandeni	39.2	44	620	2351	1.09	1058	839	1.26
Mhlontlo	39.2	44	1012	2675	1.04	1005	798	1.26
King Sabata Dalindyebo	39.2	44	693	2882	1.08	1047	831	1.26
Matatiele	39.2	40	1630	4083	0.96	771	740	1.04
Umzimvubu	39.2	40	1260	2428	1.01	806	774	1.04
Mbizana	39.2	40	654	2281	1.09	870	836	1.04
Ntabankulu	39.2	40	947	1308	1.05	837	804	1.04
Nelson Mandela Bay	39.2	40	145	1907	1.17	937	900	1.04
Letsemeng	39.2	40	1225	9132	1.01	809	777	1.04

Municipality Name	Old Speed (m/s)	New Speed (m/s)	Average Elevation $(masl)$	Area (km^2)	Air Density (kg/m^3)	New Pressure (Pa)	Old Pressure (Pa)	Bias
Kopanong	39.2	40	1403	14624	0.99	792	761	1.04
Mohokare	39.2	40	1507	8222	0.98	782	751	1.04
Naledi	39.2	40	1513	3191	0.98	782	751	1.04
Masilonyana	39.2	40	1387	6271	0.99	793	762	1.04
Tokologo	39.2	40	1258	8593	1.01	806	774	1.04
Tswelopele	39.2	40	1299	5989	1.00	802	770	1.04
Matjhabeng	39.2	40	1372	4730	0.99	795	763	1.04
Nala	39.2	40	1290	3775	1.00	803	771	1.04
Setsoto	39.2	40	1555	5503	0.97	778	747	1.04
Dihlabeng	39.2	40	1748	4492	0.95	760	729	1.04
Nketoana	39.2	40	1634	5141	0.96	770	740	1.04
Maluti a Phofung	39.2	40	1765	3991	0.95	758	728	1.04
Phumelela	39.2	40	1749	7486	0.95	759	729	1.04
Mantsopa	39.2	40	1565	3978	0.97	777	746	1.04
Moqhaka	39.2	40	1405	7238	0.99	792	760	1.04
Ngwathe	39.2	40	1490	6432	0.98	784	753	1.04
Metsimaholo	39.2	40	1488	1560	0.98	784	753	1.04
Mafube	39.2	40	1574	3620	0.97	776	745	1.04
Mangaung	39.2	40	1391	5827	0.99	793	762	1.04
Ekurhuleni	39.2	36	1603	1784	0.97	626	742	0.84
Emfuleni	39.2	36	1488	875	0.98	635	753	0.84
Midvaal	39.2	36	1543	1561	0.97	631	748	0.84
Lesedi	39.2	36	1612	1343	0.97	626	742	0.84
Mogale City	39.2	36	1511	1210	0.98	633	751	0.84
Randfontein	39.2	36	1633	429	0.96	624	740	0.84

Municipality Name	Old Speed (m/s)	New Speed (m/s)	Average Elevation $(masl)$	Area (km^2)	Air Density (kg/m^3)	New Pressure (Pa)	Old Pressure (Pa)	Bias
Westonaria	39.2	36	1594	579	0.97	627	743	0.84
Merafong City	39.2	36	1520	1475	0.98	633	750	0.84
City of Johannesburg	39.2	36	1589	1485	0.97	627	744	0.84
City of Tshwane	39.2	36	1335	5662	1.00	647	767	0.84
eThekwini	39.2	36	293	2138	1.15	742	880	0.84
Vulamehlo	39.2	36	359	899	1.13	735	871	0.84
Umdoni	39.2	36	106	236	1.18	764	906	0.84
Umzumbe	39.2	36	411	1183	1.13	729	865	0.84
uMuziwabantu	39.2	40	852	1025	1.06	848	814	1.04
Ezingoleni	39.2	36	471	610	1.12	723	857	0.84
Hibiscus Coast	39.2	36	187	791	1.16	754	894	0.84
uMshwathi	39.2	40	893	1689	1.05	843	810	1.04
uMngeni	39.2	40	1300	1457	1.00	802	770	1.04
Mpofana	39.2	40	1469	1688	0.98	786	755	1.04
Impendle	39.2	40	1676	1422	0.96	766	736	1.04
The Msunduzi	39.2	40	944	591	1.05	838	804	1.04
Mkhambathini	39.2	40	621	832	1.09	874	839	1.04
Richmond	39.2	40	881	1173	1.06	844	811	1.04
Emnambithi / Ladysmith	39.2	40	1222	2730	1.01	809	777	1.04
Indaka	39.2	40	1002	914	1.04	832	799	1.04
Umtshezi	39.2	40	1093	1825	1.03	822	790	1.04
Okhahlamba	39.2	40	1411	3668	0.99	791	760	1.04
Imbabazane	39.2	40	1556	1322	0.97	777	747	1.04

Municipality Name	Old Speed (m/s)	New Speed (m/s)	Average Elevation $(masl)$	Area (km^2)	Air Density (kg/m^3)	New Pressure (Pa)	Old Pressure (Pa)	Bias
Endumeni	39.2	40	1242	1480	1.01	807	775	1.04
Nqutu	39.2	40	1142	1805	1.02	817	785	1.04
Msinga	39.2	40	1019	2308	1.04	830	797	1.04
Umvoti	39.2	40	1011	2330	1.04	831	798	1.04
Newcastle	39.2	40	1421	1698	0.99	790	759	1.04
Emadlangeni	39.2	40	1479	3236	0.98	785	754	1.04
Dannhauser	39.2	40	1314	1391	1.00	800	769	1.04
eDumbe	39.2	36	1126	1774	1.02	663	786	0.84
uPhongolo	39.2	32	510	2958	1.11	568	852	0.67
Abaqulusi	39.2	36	1057	3833	1.03	669	793	0.84
Nongoma	39.2	36	463	2000	1.12	724	858	0.84
Ulundi	39.2	36	735	2988	1.08	697	827	0.84
Umhlabuya-lingana	39.2	32	66	3611	1.19	608	912	0.67
Jozini	39.2	32	191	3140	1.16	596	894	0.67
The Big 5 False Bay	39.2	32	53	1942	1.19	609	914	0.67
Hlabisa	39.2	36	257	1429	1.15	746	885	0.84
Mtubatuba	39.2	32	70	1600	1.19	607	911	0.67
Mfolozi	39.2	36	82	1116	1.18	767	909	0.84
uMhlathuze	39.2	36	53	733	1.19	771	914	0.84
Ntambanana	39.2	36	265	999	1.15	745	884	0.84
uMlalazi	39.2	36	317	2048	1.14	739	877	0.84
Mthonjaneni	39.2	36	719	1002	1.08	699	828	0.84
Nkandla	39.2	40	893	1687	1.05	843	810	1.04
Mandeni	39.2	36	113	506	1.18	763	905	0.84

Municipality Name	Old Speed (m/s)	New Speed (m/s)	Average Elevation $(masl)$	Area (km^2)	Air Density (kg/m^3)	New Pressure (Pa)	Old Pressure (Pa)	Bias
KwaDukuza	39.2	36	134	683	1.17	761	902	0.84
Ndwedwe	39.2	36	493	1016	1.11	721	854	0.84
Maphumulo	39.2	40	470	830	1.12	893	857	1.04
Ingwe	39.2	40	1273	1846	1.01	804	773	1.04
Kwa Sani	39.2	40	1753	1727	0.95	759	729	1.04
Greater Kokstad	39.2	40	1636	2513	0.96	770	740	1.04
Ubuhlebezwe	39.2	40	860	1503	1.06	847	813	1.04
Umzimkhulu	39.2	40	1173	2284	1.02	814	782	1.04
Greater Giyani	39.2	32	435	3684	1.12	574	862	0.67
Greater Letaba	39.2	32	702	1672	1.08	553	830	0.67
Greater Tzaneen	39.2	36	780	2874	1.07	693	822	0.84
Ba-Phalaborwa	39.2	32	385	6610	1.13	578	868	0.67
Maruleng	39.2	36	561	2886	1.10	714	846	0.84
Musina	39.2	32	611	6646	1.09	560	840	0.67
Mutale	39.2	32	520	3412	1.11	567	851	0.67
Thulamela	39.2	32	500	5136	1.11	569	854	0.67
Makhado	39.2	32	885	7311	1.05	540	811	0.67
Blouberg	39.2	32	875	8143	1.06	541	812	0.67
Aganang	39.2	36	1177	1664	1.02	659	782	0.84
Molemole	39.2	36	1093	2959	1.03	666	790	0.84
Polokwane	39.2	36	1314	3340	1.00	648	769	0.84

Municipality Name	Old Speed (m/s)	New Speed (m/s)	Average Elevation $(masl)$	Area (km^2)	Air Density (kg/m^3)	New Pressure (Pa)	Old Pressure (Pa)	Bias
Lepele-Nkumpi	39.2	36	1120	3079	1.02	664	787	0.84
Thabazimbi	39.2	36	1011	9971	1.04	673	798	0.84
Lephalale	39.2	32	981	12201	1.04	534	801	0.67
Mookgopong	39.2	36	1122	5069	1.02	664	787	0.84
Modimolle	39.2	36	1354	4165	1.00	645	765	0.84
Bela-Bela	39.2	36	1148	3045	1.02	662	784	0.84
Mogalakwena	39.2	36	1108	5465	1.03	665	788	0.84
Ephraim Mogale	39.2	36	982	1797	1.04	675	801	0.84
Elias Motsoaledi	39.2	36	1246	3326	1.01	654	775	0.84
Makhudu-thamaga	39.2	36	1203	1871	1.01	657	779	0.84
Fetakgomo	39.2	36	949	983	1.05	678	804	0.84
Greater Tubatse	39.2	36	1066	4104	1.03	668	792	0.84
Albert Luthuli	39.2	36	1463	5014	0.98	637	755	0.84
Msukaligwa	39.2	36	1661	5445	0.96	622	737	0.84
Mkhondo	39.2	36	1284	4439	1.00	651	772	0.84
Pixley Ka Seme	39.2	36	1706	4758	0.95	618	733	0.84
Lekwa	39.2	36	1600	4165	0.97	626	743	0.84
Dipaleseng	39.2	36	1585	2375	0.97	628	744	0.84
Govan Mbeki	39.2	36	1629	2674	0.96	624	740	0.84
Victor Khanye	39.2	36	1567	1415	0.97	629	746	0.84

Municipality Name	Old Speed (m/s)	New Speed (m/s)	Average Elevation $(masl)$	Area (km^2)	Air Density (kg/m^3)	New Pressure (Pa)	Old Pressure (Pa)	Bias
Emalahleni	39.2	36	1543	2414	0.97	631	748	0.84
Steve Tshwete	39.2	36	1568	3580	0.97	629	746	0.84
Emakhazeni	39.2	36	1696	4255	0.96	619	734	0.84
Thembisile	39.2	36	1344	2140	1.00	646	766	0.84
Dr JS Moroka	39.2	36	1015	1268	1.04	672	797	0.84
Thaba Chweu	39.2	36	1451	5117	0.98	638	756	0.84
Mbombela	39.2	32	724	4837	1.08	552	828	0.67
Umjindi	39.2	36	1018	1570	1.04	672	797	0.84
Nkomazi	39.2	32	319	4298	1.14	584	876	0.67
Bushbuckridge	39.2	32	391	9134	1.13	578	867	0.67
Moretele	39.2	36	1057	1235	1.03	669	793	0.84
Madibeng	39.2	36	1125	3445	1.02	663	787	0.84
Rustenburg	39.2	36	1240	3078	1.01	654	776	0.84
Kgetlengrivier	39.2	36	1369	3574	0.99	644	764	0.84
Moses Kotane	39.2	36	1101	5120	1.03	665	789	0.84
Ratlou	39.2	36	1227	4406	1.01	655	777	0.84
Tswaing	39.2	36	1401	5407	0.99	642	761	0.84
Mafikeng	39.2	36	1348	3331	1.00	646	766	0.84
Ditsobotla	39.2	36	1498	5834	0.98	634	752	0.84
Ramotshere Moiloa	39.2	36	1158	6443	1.02	661	783	0.84
Naledi	39.2	40	1284	6304	1.00	803	772	1.04
Mamusa	39.2	40	1338	3293	1.00	798	767	1.04
Greater Taung	39.2	40	1314	5147	1.00	800	769	1.04
Lekwa-Teemane	39.2	40	1273	3366	1.01	804	773	1.04

Municipality Name	Old Speed (m/s)	New Speed (m/s)	Average Elevation $(masl)$	Area (km^2)	Air Density (kg/m^3)	New Pressure (Pa)	Old Pressure (Pa)	Bias
Kagisano / Molopo	39.2	36	1137	21504	1.02	662	785	0.84
Ventersdorp	39.2	36	1492	3402	0.98	635	752	0.84
Tlokwe City Council	39.2	36	1412	2426	0.99	641	760	0.84
City of Matlosana	39.2	36	1420	3233	0.99	640	759	0.84
Maquassi Hills	39.2	40	1353	4231	1.00	797	765	1.04
Richtersveld	39.2	32	365	8877	1.13	580	870	0.67
Nama Khoi	39.2	32	676	16730	1.08	555	833	0.67
Kamiesberg	39.2	32	620	13336	1.09	559	839	0.67
Hantam	44.8	36	995	19268	1.04	674	1044	0.65
Hantam	39.2	36	635	11806	1.09	707	838	0.84
Hantam	39.2	36	935	2048	1.05	679	805	0.84
Hantam	39.2	36	872	1009	1.06	685	812	0.84
Karoo Hoogland	39.2	40	782	223	1.07	855	821	1.04
Karoo Hoogland	50.4	40	1374	111	0.99	795	1262	0.63
Karoo Hoogland	44.8	40	1204	30356	1.01	811	1018	0.80
Khâi-Ma	44.8	36	902	338	1.05	682	1056	0.65
Khâi-Ma	39.2	36	898	15142	1.05	682	809	0.84
Ubuntu	50.4	40	1291	331	1.00	803	1274	0.63
Ubuntu	50.4	40	1244	146	1.01	807	1282	0.63
Ubuntu	44.8	40	1364	18854	0.99	796	998	0.80

Municipality Name	Old Speed (m/s)	New Speed (m/s)	Average Elevation $(masl)$	Area (km^2)	Air Density (kg/m^3)	New Pressure (Pa)	Old Pressure (Pa)	Bias
Umsobomvu	44.8	40	1538	957	0.97	779	977	0.80
Umsobomvu	39.2	40	1391	5473	0.99	793	762	1.04
Emthanjeni	44.8	40	1307	6213	1.00	801	1005	0.80
Emthanjeni	39.2	40	1198	6469	1.01	812	780	1.04
Kareeberg	44.8	40	1135	14371	1.02	818	1026	0.80
Kareeberg	39.2	40	1036	2270	1.04	828	795	1.04
Renosterberg	39.2	40	1299	5181	1.00	802	770	1.04
Thembelihle	39.2	40	1121	7480	1.02	819	787	1.04
Siyathemba	39.2	40	1058	13718	1.03	826	793	1.04
Siyancuma	39.2	40	1171	15510	1.02	814	782	1.04
Mier	39.2	36	911	20336	1.05	681	808	0.84
Kai !Garib	39.2	40	854	24400	1.06	847	814	1.04
//Khara Hais	39.2	40	918	19927	1.05	840	807	1.04
!Kheis	39.2	40	960	10308	1.04	836	803	1.04
Tsantsabane	39.2	36	1197	16825	1.01	658	780	0.84
Kgatelopele	39.2	36	1489	2278	0.98	635	753	0.84
Sol Plaatjie	39.2	40	1137	2905	1.02	818	785	1.04
Dikgatlong	39.2	40	1271	6722	1.01	805	773	1.04
Magareng	39.2	40	1170	1417	1.02	814	782	1.04
Phokwane	39.2	40	1160	764	1.02	816	783	1.04
Joe Morolong	39.2	36	1094	18317	1.03	666	790	0.84
Ga-Segonyana	39.2	36	1430	4107	0.99	639	758	0.84
Gamagara	39.2	36	1207	2395	1.01	657	779	0.84
City of Cape Town	39.2	40	134	2383	1.17	939	902	1.04
Matzikama	39.2	32	300	12293	1.14	586	879	0.67

Municipality Name	Old Speed (m/s)	New Speed (m/s)	Average Elevation $(masl)$	Area (km^2)	Air Density (kg/m^3)	New Pressure (Pa)	Old Pressure (Pa)	Bias
Cederberg	39.2	36	471	7663	1.12	723	857	0.84
Bergrivier	39.2	40	208	4242	1.16	928	891	1.04
Saldanha Bay	39.2	40	57	1945	1.19	951	913	1.04
Swartland	39.2	40	131	3589	1.17	940	902	1.04
Witzenberg	39.2	40	801	10061	1.07	853	819	1.04
Witzenberg	44.8	40	645	308	1.09	871	1093	0.80
Drakenstein	39.2	40	320	1494	1.14	912	876	1.04
Stellenbosch	39.2	40	432	810	1.12	897	862	1.04
Breede Valley	39.2	44	728	3722	1.08	1042	827	1.26
Langeberg	39.2	40	594	4398	1.10	877	842	1.04
Theewaterskloof	39.2	40	375	3159	1.13	905	869	1.04
Overstrand	39.2	44	189	1675	1.16	1126	894	1.26
Cape Agulhas	39.2	44	118	3403	1.18	1139	904	1.26
Swellendam	39.2	40	374	3744	1.13	905	869	1.04
Kannaland	39.2	36	541	4622	1.10	716	849	0.84
Hessequa	39.2	36	231	5604	1.16	749	888	0.84
Mossel Bay	39.2	36	253	1963	1.15	747	885	0.84
George	39.2	36	758	5048	1.07	695	824	0.84
Oudtshoorn	39.2	36	622	3436	1.09	708	839	0.84
Bitou	39.2	36	357	967	1.13	735	871	0.84
Knysna	39.2	36	334	1081	1.14	737	874	0.84
Laingsburg	44.8	40	1090	1796	1.03	823	1032	0.80
Laingsburg	39.2	40	875	6689	1.06	845	812	1.04
Prince Albert	39.2	40	775	7871	1.07	856	822	1.04
Beaufort West	50.4	40	1258	9492	1.01	806	1279	0.63

Municipality Name	Old Speed (m/s)	New Speed (m/s)	Average Elevation $(masl)$	Area (km^2)	Air Density (kg/m^3)	New Pressure (Pa)	Old Pressure (Pa)	Bias
Beaufort West	44.8	40	888	4155	1.05	844	1058	0.80
Beaufort West	44.8	40	1478	1065	0.98	785	984	0.80
Beaufort West	44.8	40	1257	908	1.01	806	1011	0.80
Beaufort West	39.2	40	805	5359	1.07	853	819	1.04